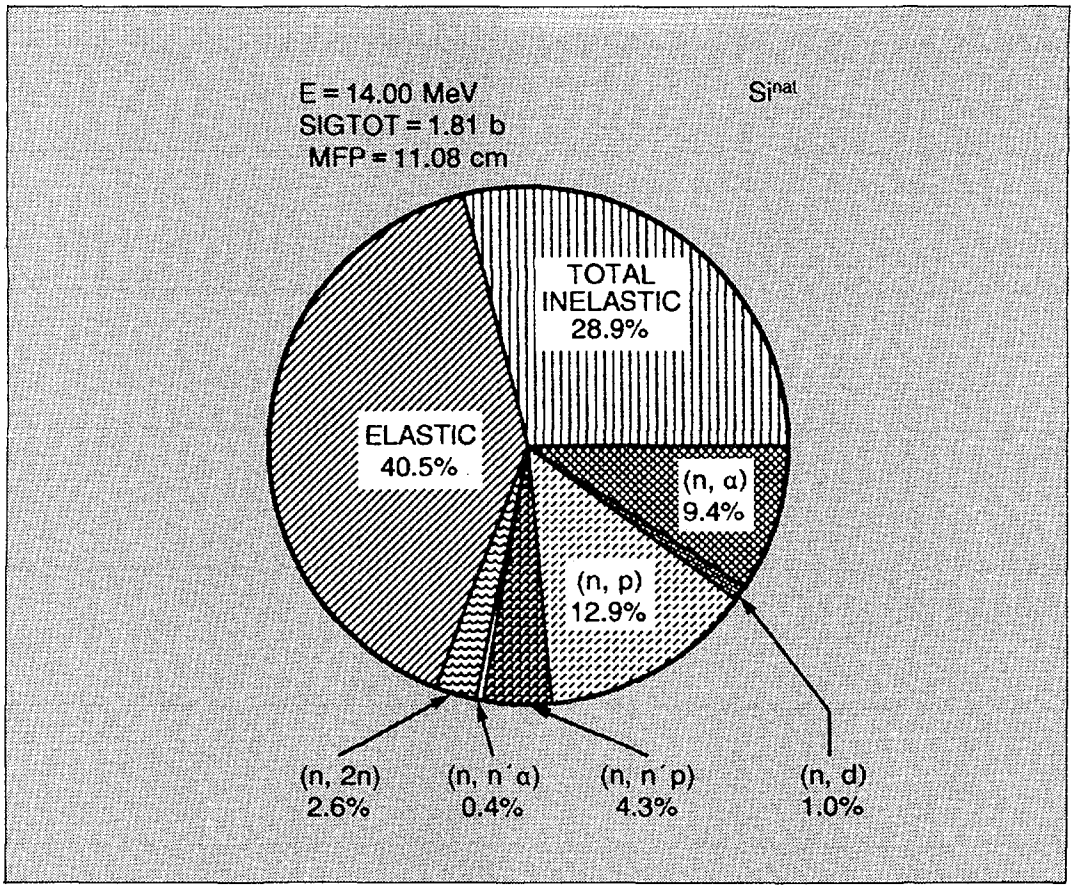

TECHNICAL REPORTS SERIES No. **357**

Handbook on Nuclear Data for Borehole Logging and Mineral Analysis

INTERNATIONAL ATOMIC ENERGY AGENCY, VIENNA, 1993

HANDBOOK ON NUCLEAR DATA FOR BOREHOLE LOGGING AND MINERAL ANALYSIS

The following States are Members of the International Atomic Energy Agency:

AFGHANISTAN
ALBANIA
ALGERIA
ARGENTINA
AUSTRALIA
AUSTRIA
BANGLADESH
BELARUS
BELGIUM
BOLIVIA
BRAZIL
BULGARIA
CAMBODIA
CAMEROON
CANADA
CHILE
CHINA
COLOMBIA
COSTA RICA
COTE D'IVOIRE
CROATIA
CUBA
CYPRUS
DEMOCRATIC PEOPLE'S REPUBLIC OF KOREA
DENMARK
DOMINICAN REPUBLIC
ECUADOR
EGYPT
EL SALVADOR
ESTONIA
ETHIOPIA
FINLAND
FRANCE
GABON
GERMANY
GHANA
GREECE
GUATEMALA
HAITI
HOLY SEE
HUNGARY
ICELAND
INDIA
INDONESIA
IRAN, ISLAMIC REPUBLIC OF
IRAQ
IRELAND
ISRAEL
ITALY
JAMAICA
JAPAN
JORDAN
KENYA
KOREA, REPUBLIC OF
KUWAIT
LEBANON
LIBERIA
LIBYAN ARAB JAMAHIRIYA
LIECHTENSTEIN
LUXEMBOURG
MADAGASCAR
MALAYSIA
MALI
MAURITIUS
MEXICO
MONACO
MONGOLIA
MOROCCO
MYANMAR
NAMIBIA
NETHERLANDS
NEW ZEALAND
NICARAGUA
NIGER
NIGERIA
NORWAY
PAKISTAN
PANAMA
PARAGUAY
PERU
PHILIPPINES
POLAND
PORTUGAL
QATAR
ROMANIA
RUSSIAN FEDERATION
SAUDI ARABIA
SENEGAL
SIERRA LEONE
SINGAPORE
SLOVENIA
SOUTH AFRICA
SPAIN
SRI LANKA
SUDAN
SWEDEN
SWITZERLAND
SYRIAN ARAB REPUBLIC
THAILAND
TUNISIA
TURKEY
UGANDA
UKRAINE
UNITED ARAB EMIRATES
UNITED KINGDOM OF GREAT BRITAIN AND NORTHERN IRELAND
UNITED REPUBLIC OF TANZANIA
UNITED STATES OF AMERICA
URUGUAY
VENEZUELA
VIET NAM
YUGOSLAVIA
ZAIRE
ZAMBIA
ZIMBABWE

The Agency's Statute was approved on 23 October 1956 by the Conference on the Statute of the IAEA held at United Nations Headquarters, New York; it entered into force on 29 July 1957. The Headquarters of the Agency are situated in Vienna. Its principal objective is "to accelerate and enlarge the contribution of atomic energy to peace, health and prosperity throughout the world".

Printed by the IAEA in Austria
August 1993
STI/DOC/010/357

TECHNICAL REPORTS SERIES No. 357

HANDBOOK ON NUCLEAR DATA FOR BOREHOLE LOGGING AND MINERAL ANALYSIS

INTERNATIONAL ATOMIC ENERGY AGENCY
VIENNA, 1993

VIC Library Cataloguing in Publication Data

Handbook on nuclear data for borehole logging and mineral analysis.
— Vienna : International Atomic Energy Agency, 1993.
p. ; 24 cm. — (Technical reports series, ISSN 0074-1914 ; 357)
STI/DOC/10/357
ISBN 92-0-102393-6
Includes bibliographical references.

1. Radiation well logging — Handbooks, manuals, etc. 2. Mineralogy, Determinative — Handbooks, manuals, etc. 3. Isotope geology — Techniques. I. International Atomic Energy Agency. II. Series: Technical reports series (International Atomic Energy Agency) ; 357.

VICL 93-00063

FOREWORD

In April 1986 the International Atomic Energy Agency convened a meeting on Nuclear Data for Applied Nuclear Geophysics at its Headquarters in Vienna. The meeting was attended by specialists in nuclear geochemistry and nuclear geophysics, and by other nuclear data experts from seven countries. From discussions at this meeting it became evident that a major effort was needed to produce a Handbook and an associated database to fulfil the nuclear data requirements of the nuclear geophysics and geochemistry community. The participants identified the most pressing requirements in microscopic cross-section and decay data (the Proceedings of this meeting were published by the IAEA as Report INDC(NDS)-184, issued in 1987). The contents of this Handbook follows the recommendations of this meeting.

The Handbook is divided into seven chapters. Chapter 1 is the introduction, Chapters 2 to 4 contain decay data and Chapters 5 to 7 contain neutron source spectra and neutron cross-section data.

The preparation of such a Handbook requires a number of compromises that may not be universally acceptable. To ensure that the length of the Handbook remained within acceptable limits, it was necessary to omit some material from the original nuclear decay data tables. Owing to such omissions, in the table of prompt γ rays from thermal neutron capture (Chapter 3) only γ rays with intensities higher than 2% are cited. In Chapter 4 (nuclear decay γ rays) only γ rays with intensities higher than 5% are cited. It is believed that γ rays with intensities below these limits are rarely usable for practical purposes and therefore these omissions will not usually cause any inconvenience to users. It should also be mentioned that it was not possible to include all the existing references in the figures in Chapter 6, and, in many cases, only the most recent results were quoted.

While every effort has been made to ensure consistency and uniformity of presentation between the different parts of this Handbook, there may still remain some inconsistencies concerning the standard reference values of some half-life, abundance or branching ratio data. The user is therefore requested to refer to Chapter 2 for the recommended values of these quantities.

It should be emphasized that the data contained in Chapters 5 and 6 of this Handbook have been assembled in a special computer file, the International Nuclear Geophysics Database-90 (INGD-90), in order to present the data in greater detail and facilitate their updating in the future. This computer database can be obtained from the IAEA Nuclear Data Section upon request, together with the documenting Report INDC(NDS)-127. This database is recommended for the computer treatment of experimentally measured results.

The Agency wishes to thank all the contributors and also those who have critically reviewed the original manuscript, especially J. Schweitzer, C. Clayton, P. Ekstroem, J.K. Tuli and M.A. Lone. The IAEA officer responsible for the overall co-ordination and compilation of this Handbook was N.P. Kocherov (Division of Physical and Chemical Sciences).

EDITORIAL NOTE

CONTENTS

Chapter 1

INTRODUCTION

1.1. GENERAL REMARKS

The use of nuclear data in the design of nuclear reactors and reactor shielding is well understood and well established. In general, the problems encountered are characterized by man-made materials of precise composition and by well defined geometrical configurations. The relevant nuclear data are widely available, although there are many examples of requirements for more accurate and detailed information.

In nuclear geophysics, an extension of the nuclear data available for reactor and shielding calculations is required. In general, the problems and the methods of attack are the same, but in nuclear geophysics the environment is earth materials, with virtually all the natural elements in the Periodic Table involved, although not at the same time.

In addition, the geometrical configurations encountered in nuclear geophysics are very different from those associated with reactor and shielding design, and they can impose a different demand on the required accuracy of the nuclear data and on the dependence on the calculational approach.

Borehole logging is a very good example, since an experimental investigation aimed at varying only one parameter (e.g. moisture content) whilst keeping all the others constant in a geologically complex system that effectively exhibits 'infinite geometry' for neutrons and γ rays is virtually impossible. Calculation, coupled with one or two critical experiments, is the only realistic route to success. A deterministic approach may be adequate in particular situations, but, for complex strata and complex geometrical configurations, and for a full account of the influence of detector materials and their disposition, Monte Carlo methods are strongly preferred and are generally the only option. However, whatever the calculational approach, the final result depends critically on the validity of the nuclear data.

Although emphasis has been placed on the derivation of the required data, there is an equal need for knowledge of the associated uncertainties and confidence limits.

An increasingly important area of nuclear geophysics is the on-line analysis of natural materials such as coal (e.g. C, H, O, Al, Si, Ca, Fe, Cl, S, N), the raw materials of the cement industry (S, Na, K, Al, Si, Ca, Fe, Mn, Ti, P, Mg, F, O), and mined ores of Fe, Al, Mn, Cu, Ni, Ag and Au, amongst others. A significant number of these elements are secondary in nuclear reactor and shielding design, so that more detailed and reliable data are required for nuclear geophysics to ensure accurate calculations and to guarantee effective designs for analytical systems for

laboratory, field and on-line applications. In calculations relating to the exploration, mining or processing of metalliferous minerals, it is equally important to have data available for the gangue minerals, and these are likely to include a wide range of elements not encountered in the nuclear energy industry. The requirement for new and extended nuclear data can be significant for evaporite deposits, but it is even more important for porphyritic and disseminated deposits.

A similar situation exists in oil well logging, where one of the outstanding requirements is for an early, accurate interpretation of the formation mineralogy. Whilst this can be achieved from borehole cores (with some degree of spatial misrepresentation), it is clearly an advantage in time and cost to derive this information early in an exploration programme from borehole logging. Success in achieving this objective has recently been demonstrated by measuring the concentrations of about ten elements. From these data, formation properties such as total clay content, cation exchange capacity, grain density and porosity can be deduced. However, in order to validate the results obtained experimentally for the concentration of each element, very substantial Monte Carlo computations are required to ensure that perturbations in the spatial neutron and γ ray flux distributions relevant to the calculations of the concentration of each element can be properly accounted for.

Whereas, in borehole logging, variations in the geometrical configuration (the source–rock–detector system) mainly relate to the diameter of the borehole and the probe and the position of the probe within the borehole, in on-line measurements large variations in source–detector separation and in the mass and profile of the mineral are possible. An experimental approach to parametrize this situation is extremely difficult and tedious, so that resort to calculation is strongly preferred, if this is possible. At the time of writing, there is a very significant requirement for adequate nuclear data in this area of nuclear geophysics.

From what has been stated above, it is apparent that a very significant amount of data are required for a very large number of elements. The neutron cross-sections relevant to deterministic and Monte Carlo calculations in nuclear geophysics are as follows:

(a) Total cross-section: $\sigma\ (E)$;

(b) Cross-sections for elastic scattering:
  (i) Total cross-sections: $\sigma_n(E)$,
  (ii) Angular distributions of elastically scattered neutrons: $\sigma_n(E,\theta)$;

(c) Cross-sections for inelastic scattering:
  (i) Total cross-sections: $\sigma'_n(E)$,
  (ii) Energy distributions of the scattered neutrons: $\sigma'_n(E;E';\theta)$;

(d) Cross-sections for neutron multiplicative processes:
  (i) Fission cross-section: $\sigma_f(E)$,
  (ii) Cross-sections for the reaction (n, 2n): $\sigma_{2n}(E)$, $\sigma_{2n}(E;E')$;

(e) Cross-sections for processes in which the neutron disappears:
  (i) Radiative capture: σ_γ,
  (ii) Charged particle reactions, e.g. (n, p), (n, d), (n, α).

Apart from microscopic cross-section data, there is a variety of macroscopic data that must be evaluated in order to make progress with the more effective use of nuclear methods in the geosciences. In this category we can include the use of neutron migration lengths as link parameters in the design of porosity probes in oil well logging and the use of λ_0 values (λ_0 is the total epithermal neutron flux per unit lethargy interval per unit thermal flux) to describe the shape of the neutron spectrum in different types of rock.

As an introduction to this Handbook, we give a brief summary of the most important techniques, with illustrative examples of typical applications.

This first edition of the Handbook is an initial presentation of evaluated microscopic nuclear data for applications in nuclear geophysics. It is anticipated that new and improved data will be presented as they become available and as new applications, instruments and techniques increase the demand for such data.

1.2. RADIATION SOURCES IN NUCLEAR GEOPHYSICS

It is clear that the requirements for nuclear data depend not only on the mineral content of the formation (consolidated in borehole logging, fragmented in on-line measurements) but also on the choice of radiation source.

In borehole logging applications and on-line measurements, the principal neutron sources are ^{252}Cf and ^{241}Am–Be, and the source spectra, shown in Figs 1.1 and 1.2, respectively, indicate the highest neutron energies for which nuclear data are required when using these sources. ^{239}Pu–Be sources are occasionally used and their neutron spectra are similar to those for ^{241}Am–Be.

The choice of isotopic neutron source is partly dictated by the threshold energies of the required reactions, by the radiation shielding and by safety considerations, and this is particularly true for on-line measurements. For example, although the oxygen concentration is fundamental in on-line coal analysis, it can only be measured directly by the ^{16}O(n, n′γ) reaction ($E_{\gamma\,\mathrm{thresh}}$ = 6.129 MeV), which requires a ^{241}Am–Be neutron source. However, the substantial shielding required for ^{241}Am–Be compared with that for ^{252}Cf has resulted in the latter source being adopted and the oxygen content being derived indirectly (and not very accurately) or diagnosed.

Apart from isotopic sources, 14 MeV neutron tubes based on the D(T, n)^{4}He reaction are widely used in oil field exploration and, to a smaller extent, in other applications where high energy neutrons or pulsed sources are required. Neutron

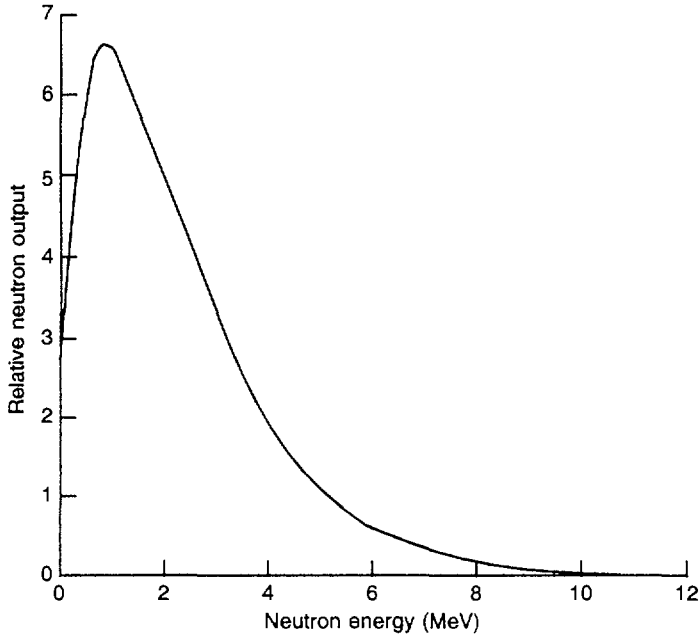

FIG. 1.1. Neutron energy spectrum of the ^{252}Cf source.

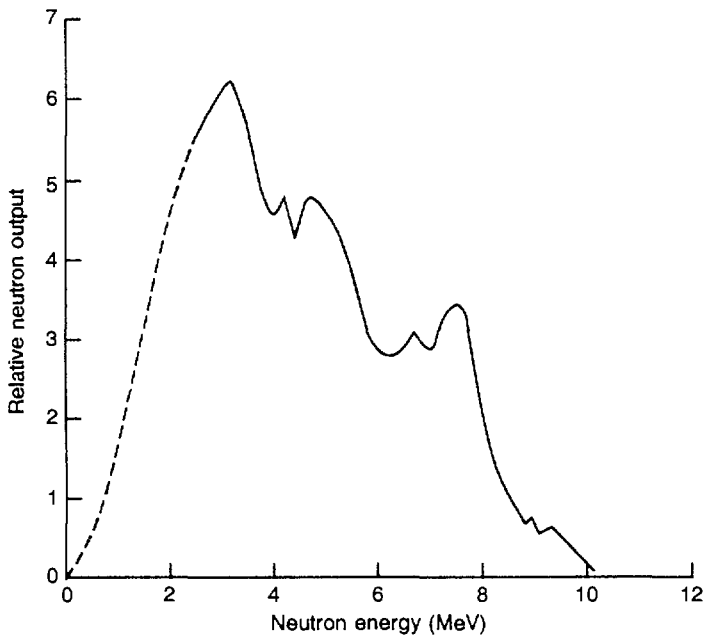

FIG. 1.2. Neutron energy spectrum of the ^{241}Am–Be source.

tubes have the advantage that they can be switched off (and pulsed), but beam monitoring is required if they are used for activation analysis.

Both circular (cyclotron and microtron) and linear accelerators have been investigated as potential neutron and γ ray sources for mineral analysis, but neither are believed to be in significant routine use at the present time. Circular accelerators have been mainly used as bremsstrahlung sources with photon energies up to about 20 MeV. The dearth of reliable data for (γ, n) reactions in a wide range of elements, as well as the low availability of circular accelerators, have contributed to a limited interest in this method.

The development of the radiofrequency quadrupole (RFQ) structure for proton acceleration at low energies and high currents has opened up the possibility of energy selective activation analysis being carried out at exploration sites, mines and mineral processing plants. Lithium is the most frequently used target for neutron production via the reaction $^{7}Li(p,n)^{7}Be$, which beta decays to ^{7}Li with a half-life of 53 d. Typically, for 1 mA beam current and 4.5 MV acceleration, a yield of 2.6×10^{12} n/s with a maximum energy of 2.85 MeV can be obtained.

Small linear electron accelerators with an energy in the range of 5–15 MeV and an average beam current between 100 and 1000 μA are now available commercially. With a suitable combination target, such as W–Be for the (e^-, γ), (γ, n) reactions, and with a target surrounded by an efficient moderator, small linear accelerators provide a means of generating an intense thermal neutron flux over a substantial volume of rock, which is several orders of magnitude greater than the thermal neutron flux available from acceptable radioisotope sources. Spatial neutron flux distributions over a range of 'standard rocks' are required to pursue this option with confidence.

So far, only man-made sources have been mentioned, but a significant area of nuclear geophysics is concerned with natural radioactivity: with measurements underground, at the ground surface and above ground, and by airborne radiometry. However, the basic data for most of these applications are now available.

1.3. IMPORTANT TECHNIQUES AND APPLICATIONS IN NUCLEAR GEOPHYSICS AND THEIR RELEVANCE TO NUCLEAR DATA REQUIREMENTS

1.3.1. Neutron interaction methods

1.3.1.1. Neutron activation γ ray analysis

Techniques based on the (n_{th}, γ) reaction have their most important application in the field of laboratory analysis. Except for product nuclides of very short half-life, the use of this reaction in borehole logging and on-line analysis is limited because of the time required to achieve a reasonable activity in the product nucleus.

The (n_{fast}, x) reaction has a limited use, but the measurement of the oxygen concentration by the $^{16}O(n,p)^{16}N$ reaction and of fluorine by the (n,α) and (n,p) reactions are two of the limited number of important candidates.

The cross-sections for the (n,γ) and (n,x) reactions up to 14 MeV are required for transport calculations.

1.3.1.2. Neutron induced prompt γ ray analysis

Measurement of the intensities of prompt γ rays from neutron capture from isotopic neutron sources is probably the most important factor for measurements of elemental concentrations in borehole logging and in on-line analysis.

However, as has been emphasized previously, accurate data are also required for the variation of the cross-section with energy of all the elements that will probably be encountered during neutron transport.

1.3.1.3. Neutron inelastic and elastic scattering

The $(n,n'\gamma)$ reaction is used in the on-line analysis of the concentrations of several elements, the most important being silicon, which is measured by the reaction $^{28}Si(n,n'\gamma)$ (E_{thresh} = 1.78 MeV), oxygen by the reaction $^{16}O(n,n'\gamma)$ (E_{thresh} = 6.1 MeV) and carbon by the reaction $^{12}C(n,n'\gamma)$ (E_{thresh} = 4.44 MeV). In the analysis of coal, the silicon concentration can also be determined by thermal neutron capture, whilst oxygen can only be obtained by the fast neutron reaction.

Neutron inelastic scattering leading to an isomeric state, as in the $^{197}Au(n,n'\gamma)^{197}Au^{m}$ reaction, is the basis of a method of sorting lumps of rock containing gold ($\geq$ 1 ppm Au) from waste rock.

In oil well logging the measurement of (scattered) neutrons from a fast neutron source is used to determine the hydrogen, or fluid, content of rocks by measuring the resultant thermal or epithermal neutron fluxes. At the neutron source energy, the primary interaction mechanism is elastic scattering, the mean free path in rocks being about 8 cm and independent of water content. The effect of hydrogen becomes apparent at lower energies. For example, at 100 keV the mean free path varies between 4 cm in pure limestone and about 2 cm in limestone of 40% porosity that is totally saturated with water.

Neutron transport depends on two processes: the loss of energy from the source energy to thermal energies, and the diffusion of neutrons at thermal energies until they are captured. The epithermal neutron flux from a point source can be characterized by an exponential dependence on the distance from the source, with a length parameter, the slowing down length, L_s. A simple model based on diffusion theory yields an epithermal neutron flux, Φ_{epi}, at a distance r from the source, of

$$\Phi_{\text{epi}} \propto \frac{\exp(-r/L_s)}{D_{\text{epi}}\, r} \tag{1}$$

where D_{epi} is an epithermal diffusion coefficient related to the transport mean free path.

For thermal neutrons, there is a comparable length parameter, the diffusion length, L_d, such that the thermal neutron flux can be represented as

$$\Phi_{\text{th}} \propto \frac{L_d^2}{D\,(L_s^2 - L_d^2)} \frac{\exp(-r/L_s) - \exp(-r/L_d)}{r} \tag{2}$$

where D is the thermal diffusion coefficient. D can be calculated from the thermal neutron cross-sections of the elements in the material and is related to L_d by $D = L_d^2 \Sigma$, where Σ is the macroscopic thermal neutron absorption cross-section for the material.

The preceding discussion indicates that a calculable parameter, L_s, will be adequate to represent the flux distribution in the formation for the case of a point source in an infinite medium. While this is not the true description of neutron scattering in rock formations, which are also affected by the fluid composition, salinity, rock type, geometry and other factors, it illustrates the underlying philosophy of the measurement and the types of nuclear data that are needed to calculate an accurate response.

1.3.1.4. Detection of neutron induced fission neutrons

The measurement of neutron induced fission neutrons has been used to explore for uranium. The measurement of neutron intensities has an advantage over the measurement of γ rays from uranium daughters, since the latter have long half-lives so that geological processes can transport uranium to regions that are separated from the daughters, thus leading to erroneous indications of uranium presence and to missing regions that contain uranium. This problem can be avoided by measurements of the prompt fission neutrons or the delayed neutrons produced by the decay of fission products. Measurements of delayed neutrons are made by using a pulsed accelerator and by determining the neutron intensity after the neutrons produced by the accelerator have been absorbed. Alternatively, an isotopic source can be used, with the detector being moved into the measurement region after the source neutrons have been absorbed. These techniques require a knowledge of all neutron interaction cross-sections, in particular the energy dependent fission cross-section for uranium.

1.3.1.5. Thermal neutron decay time

The macroscopic thermal neutron absorption cross-section Σ is the total capture cross-section per unit volume. For a molecule $A_\alpha B_\beta$, $\sigma_{mol} = \alpha\sigma_A + \beta\sigma_B$, where σ_A (or σ_B) is the microscopic thermal neutron absorption cross-section for a nucleus A (or B). For a collection of molecules, the macroscopic cross-section is given by

$$\Sigma = \sum_i \frac{V_i \rho_i \sigma_{mol(i)} N_A}{M_i} \tag{3}$$

where M_i is the molecular weight of the 'i-th' type of molecule with volume fraction V_i. The main use of this type of measurement is in borehole logging, for determining the water fraction of the total fluid, since the presence of NaCl in water, or of impurities such as boron, both of which are particularly common in subsurface formations, leads to a rapid rise in the water cross-section compared with that of oil. The measured value of Σ also depends on the chemical constituents of the rock.

Since the value of Σ is obtained by measuring the time dependence of thermal neutron capture γ rays, a pulsed neutron source is used with a γ ray detector (typically NaI(Tl)). The source of 14 MeV neutrons is pulsed for a brief period (≈ 200 μs), forming a cloud of high energy neutrons in the borehole and formation and this cloud becomes thermalized through repeated collisions. The neutrons are captured at a rate that depends on the thermal neutron absorption cross-section. The decay of the capture γ ray counting rate reflects the decay of the neutron population.

The reaction rate for thermal neutron absorption is given by the product of Σ and the velocity of the neutron, v. The number of neutrons remaining at time t is

$$N(t) = N(0) \exp(-\Sigma v t) \tag{4}$$

This simple analysis of the time dependence of the captured γ rays does not take account of an important aspect of the actual measurements: the thermal neutron diffusion effect. At any observation point, the local thermal neutron density decreases because the neutrons are diffusing as well as being captured. The time dependent diffusion equation is required to quantify the diffusion effect on the local decay time constant.

The apparent decay time of the local neutron population in an infinite medium has two components:

$$\frac{1}{\tau_a} = \frac{1}{\tau_{int}} + \frac{1}{\tau_{diff}} \tag{5}$$

where τ_{int} is the intrinsic formation decay time (i.e. that expected from absorption alone) and τ_{diff} is the diffusion time, which depends on the distance from the source and the thermal diffusion coefficient. The apparent Σ value of a formation is greater than the intrinsic value owing to the diffusion rate of thermal neutrons near the detector.

In the simple case of a single mineral, the measured formation Σ, after correcting for borehole and diffusion effects, consists of three components — one from the rock matrix, one from the water and one from the hydrocarbon content:

$$\Sigma = (1 - \phi)\,\Sigma_{ma} + \phi S_w \Sigma_w + \phi\,(1 - S_w)\,\Sigma_h \tag{6}$$

which can be used to determine the water saturation, S_w (i.e. the fraction of the pore volume ϕ containing water). Since the value of Σ_h for oil is nearly the same as that for fresh water, this measurement distinguishes hydrocarbon from water by the water salinity, which makes Σ_w significantly larger than Σ_h. The presence of certain minerals, which may contain thermal absorbers such as boron, seriously affects this simple analysis by making a priori knowledge of Σ_{ma} questionable; however, several methods for dealing with this problem have been developed.

The primary nuclear data required to understand this measurement are accurate thermal neutron capture cross-sections and γ ray production rates and energies. Neutron scattering cross-sections are important for calculations involving thermal neutron diffusion effects.

1.3.1.6. Epithermal neutron decay time

Previously described neutron scattering measurements have been based on a measurement of the slowing down length. Recently, a neutron scattering measurement based on the determination of the time taken for neutrons to slow down to epithermal energies has been proposed. This measurement requires a pulsed source of neutrons. To determine the number of epithermal neutrons, a 0.635 cm diameter, 10 atm (10^6 Pa) ^{3}He detector is used, which is surrounded by a thin (0.0152 cm) gadolinium foil to absorb the thermal neutrons.

The motivation for measuring the fall-off rate of epithermal neutrons is to obtain a quantity that correlates more strongly with the hydrogen concentration. Measurements of the slowing down length depend mostly on the distance travelled during the first few collisions of high energy neutrons, where elements other than hydrogen have a significant impact. Measurement of the fall-off rate is dominated by the last few neutron interactions at low energies. At these energies, the interactions depend more strongly on the hydrogen content.

1.3.1.7. Gamma–gamma scattering and energy dispersive X ray fluorescence

The γ–γ scattering technique is the basis of a well established method for measuring the bulk density or moisture content of rocks and ores in the exploration and mining of minerals. In general, ^{137}Cs (662 keV) or ^{60}Co (1173 and 1332 keV) sources are used with a NaI(Tl) detector with an energy threshold of about 200 keV to ensure that only Compton scattered γ rays are recorded.

For calculational purposes, the Klein–Nishina formulas are adequate; errors in the technique are associated principally with bound hydrogen concentrations when moisture is required, or with an unknown moisture content when the rock hydrogen concentrations are to be determined.

Energy dispersive X ray fluorescence is mainly used in a range of important instruments for the analysis of mineral samples in the laboratory and in on-stream applications, for which the data available at present are quite adequate for calculational purposes.

1.4. CONCLUSIONS

Accurate information about the spatial distribution of mineralization is an essential requirement in the development of an economic route in the exploration, extraction and processing of a wide range of minerals.

The scientific and technical developments that have already taken place in nuclear geophysics have made a profound impact on the exploration and extraction of oil and gas, and are becoming increasingly important in the coal industry and in a number of metalliferous and non-metalliferous industries worldwide.

Although many of the recent advances can be attributed to improved neutron sources, to more reliable and improved detectors, to fast electronics and to advances in computerized data processing, the critical requirement is the accuracy of the information that can be extracted.

With the complex situations with which much of nuclear geophysics is now concerned, an experimental approach to the development of new technologies is neither convenient nor possible. The calculational approach is crucial and the Monte Carlo method is at present dominant. The availability and accuracy of nuclear data is the ultimate key to success.

This Handbook and the associated computer files present evaluated nuclear data for applications in nuclear geophysics.

Chapter 2

TABLE OF NUCLIDES*

2.1. INTRODUCTION

The table presents the half-life, the abundance and the decay modes for all known nuclides and some of their isomeric states. The nuclides for which none of these three properties are known have been omitted. The data given here are from the adopted properties of the various nuclides as given in the Evaluated Nuclear Structure Data File (ENSDF) [1]. The data in ENSDF are based on experimental results as reported in Nuclear Data Sheets for A = 45 to 263 [2] and in Nuclear Physics for A < 45 [3, 4]. For those nuclides for which either there are no data in ENSDF or more recent data are available, the half-life and decay modes are taken from the Chart of the Nuclides, 14th Edition [5]. The isotopic abundances are those of Holden [6].

For other references, experimental data and information on the data measurements, please refer to the original evaluations [2–4].

2.2. EXPLANATION OF THE TABLE

Column 1, isotope (Z, El, A):

The nuclides are listed in the order of increasing atomic number (Z) and are subordered by increasing mass number (A). Included are all isotopic species, all isomers with a half-life of ≥ 1 s, and other selected well known isomers. The nuclides for which neither the half-life nor the decay modes are known have been omitted. The ^{235}U fission products with fractional yields of $> 10^{-6}$ are italicized.

Isomeric states are denoted by the symbol m after the mass number and are given in the order of increasing excitation energy. More than one entry for a nuclide, without the symbol m for any, indicates that their relative excitation energies are not known.

---

* The nuclear properties given here are based upon the author's pocket size handbook Nuclear Wallet Cards (1990), published and distributed by the National Nuclear Data Center, Brookhaven National Laboratory, Upton, NY, USA. Other quantities contained in the Nuclear Wallet Cards and not presented here are spin, parity, mass excess, instructions for computer access to databases maintained by the National Nuclear Data Center, and a number of useful appendices.

This research was supported by the Office of Basic Energy Sciences, United States Department of Energy, Washington, DC, USA.

The symbols Rf (rutherfordium) and Ha (hahnium) have been used for elements with Z=104 and 105, respectively. These, however, have not been accepted internationally owing to conflicting claims of their discovery.

Column 2, half-life or abundance:

The half-life and the abundance are given, followed by units (symbol % in the case of abundance), which are followed by the uncertainty in *italics*. The uncertainty given is in the last significant figures. For example, 8.1 s *10* means $T_{1/2}$ = 8.1 ± 1.0 s. For some very short lived nuclei, level widths rather than half-lives are given. There also, the width is followed by the units (eV, keV or MeV), which are followed by the uncertainty in *italics*.

Column 3, decay mode:

Decay modes are given, followed by the per cent branching, if known (w indicates a weak branch). The decay modes are given in decreasing strength from left to right. The percentage branching is omitted where there is no competing mode of decay.

The various modes of decay are given below:

$\beta-$	$\beta-$ decay
ϵ	ϵ (electron capture), or $\epsilon+\beta+$, or $\beta+$ decay
IT	isomeric transition (through γ decay or conversion-electron decay)
n, p, α, ...	neutron, proton, alpha, ... decay
SF	spontaneous fission
$2\beta-$, 3α, ...	double $\beta-$ decay ($\beta-\beta-$), decay through emission of three alphas, ...
β-n, β-p, $\beta-\alpha$, ...	delayed n, p, α, ... emission following $\beta-$ decay
ϵp, $\epsilon\alpha$, ϵSF, ...	delayed p, α, SF, ... decay following ϵ or $\beta+$ decay

REFERENCES

[1] US NATIONAL NUCLEAR DATA CENTER, Evaluated Nuclear Structure Data File, a computer file of evaluated experimental nuclear structure data maintained by the National Nuclear Data Center, Brookhaven National Laboratory, Upton, NY (1991).

[2] Nuclear Data Sheets, Evaluations published by mass number for A = 45 to 263, Academic Press, New York, Vol. 27 (1979) to Vol. 67 (1992).

[3] AJZENBERG-SELOVE, F., Evaluations for A = 5 to 20:
A = 5–10: Nucl. Phys., A **413** (1984) 1;
A = 11–12: Nucl. Phys., A **433** (1985) 1;
A = 13–15: Nucl. Phys., A **449** (1986) 1;
A = 16–17: Nucl. Phys., A **460** (1986) 1;
A = 18–20: Nucl. Phys., A **475** (1987) 1.

[4] ENDT, P.M., Energy levels of A = 21–44 nuclei (VII), Nucl. Phys., A **521** (1990) 1.

[5] WALKER, F.W., PARRINGTON, J.R., FEINER, F., Chart of the Nuclides, 14th edn, Knolls Atomic Power Laboratory, operated by General Electric Co., San José, CA (1988).

[6] HOLDEN, N.E., Table of Isotopes, CRC Handbook of Chemistry and Physics, 71st edn, CRC Press, Boca Raton, FL (1990) 11–33.

TABLE OF NUCLIDES

Isotope Z	El	A	T1/2 or Abundance	Decay Mode
0	n	1	10.4 m *2*	β-
1	H	1	99.985% *1*	
		2	0.015% *1*	
		3	12.33 y 6	β-
2	He	3	0.000137% *3*	
		4	99.999863% *3*	
		5	0.80 MeV *2*	α, n
		6	806.7 ms *15*	β-
		7	160 keV *30*	n
		8	119.0 ms *15*	β-, β-n 16%
		9	very short	n
3	Li	5	≈1.5 MeV	α, p
		6	7.5% *2*	
		7	92.5% *2*	
		8	838 ms *6*	β-, β-2α
		9	178.3 ms *4*	β-, β-n 49.5%, β-n2α
		10	1.2 MeV *3*	n
		11	8.7 ms *1*	β-, β-nα 0.027%, β-n
4	Be	6	92 keV *6*	2p, α
		7	53.29 d *7*	ε
		8	6.8 eV *17*	2α
		9	100%	
		10	1.51×10^6 y *6*	β-
		11	13.81 s *8*	β-, β-α 3.1%
		12	24.4 ms *30*	β-, β-n<1%
		13		n
		14	4.2 ms *7*	β-
5	B	7	1.4 MeV *2*	α, p
		8	770 ms *3*	εα, ε, ε2α
		9	0.54 keV *21*	2α, p
		10	19.9% *2*	
		11	80.1% *2*	
		12	20.20 ms *2*	β-, β-3α 1.58%
		13	17.36 ms *16*	β-, β-n 0.28%
		14	16.1 ms *12*	β-
		15	8.8 ms *6*	β-, β-n
		16		n
		17		β-
6	C	8	230 keV *50*	α, p
		9	126.5 ms *9*	ε, εp, ε2α
		10	19.255 s 53	ε
		11	20.385 m *20*	ε
		12	98.90% *3*	
		13	1.10% *3*	
		14	5730 y *40*	β-
		15	2.449 s *5*	β-
		16	0.747 s *8*	β-, β-n≥98.8%
		17	202 ms *17*	β-
		18	66 ms *20*	β-, β-n
		20		β-
7	N	11	0.74 MeV *10*	p
		12	11.000 ms *16*	ε, ε3α 3.44%
		13	9.965 m *4*	ε
		14	99.63% *2*	
		15	0.37% *2*	
		16	7.13 s *2*	β-, β-α 0.0012%
		17	4.173 s *4*	β-, β-n 95%
		18	624 ms *12*	β-, β-α, β-n
		19	290 ms *90*	β-, β-n
		20	100 ms *25*	β-, β-n
		21	95 ms *13*	β-n 84%, β-
		22	24 ms *7*	β-n 35%, β-
8	O	12	400 keV *250*	p
		13	8.90 ms *20*	ε, εp
8	O	14	70.606 s *18*	ε
		15	122.24 s *16*	ε
		16	99.76% *1*	
		17	0.038% *3*	
		18	0.20% *1*	
		19	26.91 s *8*	β-
		20	13.57 s *10*	β-
		21	3.42 s *10*	β-
		22	2.25 s *15*	β-
		23	82 ms *37*	β-, β-n 31%
		24	61 ms *26*	β-, β-n 58%
9	F	14		p
		15	1.0 MeV *2*	p
		16	40 keV *20*	p
		17	64.49 s *16*	ε
		18	109.77 m *5*	ε
		19	100%	
		20	11.00 s *2*	β-
		21	4.158 s *20*	β-
		22	4.23 s *4*	β-
		23	2.23 s *14*	β-
		24	340 ms *80*	β-
10	Ne	16	122 keV *37*	2p
		17	109.0 ms *10*	ε, εp
		18	1.672 s *8*	ε
		19	17.22 s *2*	ε
		20	90.48% *3*	
		21	0.27% *1*	
		22	9.25% *3*	
		23	37.24 s *12*	β-
		24	3.38 m *2*	β-
		25	602 ms *8*	β-
		26	230 ms *60*	β-
11	Na	18		p
		19	0.03 s ?	p
		20	447.9 ms *23*	ε, εα 21%
		21	22.48 s *3*	ε
		22	2.6088 y *14*	ε
		23	100%	
		24	14.9590 h *12*	β-
		24m	20.20 ms *7*	IT, β-≈0.05%
		25	59.1 s *6*	β-
		26	1.072 s *9*	β-
		27	301 ms *6*	β-, β-n 0.13%
		28	30.5 ms *4*	β-, β-n 0.58%
		29	44.9 ms *12*	β-, β-n 22%
		30	48 ms *2*	β-, β-n 30%, β-2n 1.17%, β-α 0.0055%
		31	17.0 ms *4*	β-, β-n 37%, β-2n 0.9%
		32	13.2 ms *4*	β-, β-n 39%, β-2n 1.2%
		33	8.2 ms *4*	β-, β-n 52%, β-2n 12%
		34	5.5 ms *10*	β-, β-n, β-2n
		35	1.5 ms *5*	β-, β-n
12	Mg	20	0.1 s	ε, εp
		21	122 ms *3*	ε, εp 32%
		22	3.857 s *9*	ε
		23	11.317 s *11*	ε
		24	78.99% *3*	
		25	10.00% *1*	
		26	11.01% *2*	
		27	9.462 m *11*	β-
		28	20.91 h *3*	β-
		29	1.30 s *12*	β-

TABLE OF NUCLIDES (cont.)

Isotope Z El	A	T1/2 or Abundance	Decay Mode
12 Mg	30	335 ms *17*	β-
	31	0.23 s *2*	β-
	32	120 ms *20*	β-, β-n 2.4%
	33	90 ms *20*	β-, β-n 17%
	34	20 ms *10*	β-, β-n
13 Al	22	70 ms *45*	ε, εp, ε2p
	23	0.47 s *3*	ε, εp
	24	2.053 s *4*	ε, εα 0.035%
	24m	131.3 ms *25*	IT 82%, ε 18%, εα 0.028%
	25	7.183 s *12*	ε
	26	7.4×10^5 y *3*	ε
	26m	6.3452 s *19*	ε
	27	100%	
	28	2.2414 m *12*	β-
	29	6.56 m *6*	β-
	30	3.60 s *6*	β-
	31	0.644 s *25*	β-
	32	33 ms *4*	β-
	34	60 ms *18*	β-, β-n 27%
	35	0.15 s *5*	β-, β-n 40%
	22	6 ms *3*	ε, εp
	24	102 ms *35*	ε, εp
	25	220 ms 3	ε, εp
	26	2.234 s *13*	ε
	27	4.16 s *2*	ε
	28	92.23% *1*	
14 Si	29	4.67% *1*	
	30	3.10% *1*	
	31	157.3 m *3*	β-
	32	172 y *4*	β-
	33	6.18 s *18*	β-
	34	2.77 s *20*	β-
	35	0.78 s *12*	β-
	36	0.45 s *6*	β-n<10%, β-
15 P	26	≈20 ms	ε, εp, ε2p
	27	0.26 s *8*	ε, εp
	28	270.3 ms *5*	ε
	29	4.140 s *14*	ε
	30	2.498 m *4*	ε
	31	100%	
	32	14.262 d *14*	β-
	33	25.34 d *12*	β-
	34	12.43 s *8*	β-
	35	47.3 s *7*	β-
	36	5.6 s *3*	β-
	37	2.31 s *13*	β-
	38	0.64 s *14*	β-
	39	≈160 ms	β-, β-n 41%
	40	0.26 s *8*	β-, β-n 30%
	41	0.12 s *2*	β-, β-n 30%
	42	0.11 s *3*	β-, β-n 50%
16 S	28	125 ms *10*	ε, εp
	29	0.187 s *4*	εp 47%, ε
	30	1.178 s *5*	ε
	31	2.572 s *13*	ε
	32	95.02% *9*	
	33	0.75% *1*	
	34	4.21% *8*	
	35	87.51 d *12*	β-
	36	0.02% *1*	
	37	5.05 m *2*	β-
	38	170.3 m *7*	β-
	39	11.5 s *5*	β-
	40	8.8 s *22*	β-
17 Cl	31	150 ms *25*	ε, εp
	32	298 ms *1*	ε, εα 0.09%, εp 0.026%
	33	2.511 s *3*	ε
	34	1.5264 s *14*	ε
	34m	32.00 m *4*	ε 53.4%, IT 46.6%
	35	75.77% *5*	
	36	3.01×10^5 y *2*	β- 98.2%, ε 1.8%
	37	24.23% *5*	
	38	37.24 m *5*	β-
	38m	715 ms *3*	IT
	39	55.6 m *2*	β-
	40	1.35 m *2*	β-
	41	38.4 s *8*	β-
	42	6.8 s *3*	β-
	43	3.3 s *2*	β-
18 Ar	32	98 ms *2*	εp 43%, ε
	33	173 ms *2*	ε, εp 31%
	34	844.5 ms *35*	ε
	35	1.775 s *3*	ε
	36	0.337% *3*	
	37	35.04 d *4*	ε
	38	0.063% *1*	
	39	269 y *3*	β-
	40	99.600% *3*	
	41	1.822 h *2*	β-
	42	32.9 y *11*	β-
	43	5.37 m *6*	β-
	44	11.87 m *5*	β-
	45	21.48 s *15*	β-
	46	8.4 s *6*	β-
19 K	35	190 ms *30*	ε, εp 0.37%
	36	342 ms *2*	ε, εp 0.05%, εα 0.003%
	37	1.226 s *7*	ε
	38	7.636 m *18*	ε
	38m	923.9 ms *6*	ε
	39	93.2581% *30*	
	40	1.277×10^9 y *8*	β- 89.33%,
		0.0117% *1*	ε 10.67%
	41	6.7302% *30*	
	42	12.360 h *3*	β-
	43	22.3 h *1*	β-
	44	22.13 m *19*	β-
	45	17.3 m *6*	β-
	46	105 s *10*	β-
	47	17.5 s *3*	β-
	48	6.8 s *2*	β-
	49	1.26 s *5*	β-, β-n 86%
	50	472 ms *4*	β-, β-n 29%
	51	365 ms *5*	β-, β-n 68%
	52	105 ms *5*	β-, β-n>88%
	53	30 ms *5*	β-, β-n 85%
	54	10 ms *5*	β-, β-n
20 Ca	35	0.05 s *3*	ε, ε2p
	36	100 ms *65*	ε, εp
	37	175 ms *3*	ε 24%, εp
	38	440 ms *8*	ε
	39	859.6 ms *14*	ε
	40	96.941% *13*	
	41	1.03×10^5 y *4*	ε
	42	0.647% *3*	
	43	0.135% *3*	
	44	2.086% *5*	
	45	163.8 d *18*	β-
	46	0.004% *3*	

TABLE OF NUCLIDES (cont.)

Isotope Z El	A	T1/2 or Abundance	Decay Mode
20 Ca	47	4.536 d *2*	β-
	48	>6×10^18 y 0.187% *3*	
	49	8.715 m *23*	β-
	50	13.9 s *6*	β-
	51	10.0 s *8*	β-
	51	10 s	β-n?
	52	4.6 s *3*	β-
	53	90 ms *15*	β-, β-n>30%
21 Sc	40	182.3 ms *7*	ε, εp 0.44%, εα 0.017%
	41	596.3 ms *17*	ε
	42	681.3 ms *7*	ε
	42m	1.028 m *7*	ε
	43	3.891 h *12*	ε
	44	3.927 h *8*	ε
	44m	2.442 d *4*	IT 98.8%, ε 1.2%
	45	100%	
	45m	0.32 s *1*	IT
	46	83.810 d *10*	β-
	46m	18.75 s *4*	IT
	47	3.345 d *3*	β-
	48	43.7 h *1*	β-
	49	57.2 m *2*	β-
	50	102.5 s *5*	β-
	50m	0.35 s *4*	IT>97.5%, β-<2.5%
	51	12.4 s *1*	β-
	52	8.2 s *2*	β-
22 Ti	40	50 ms *15*	ε, εp
	41	80 ms *2*	ε, εp
	42	199 ms *6*	ε
	43	509 ms *5*	ε
	44	49 y *3*	ε
	45	3.08 h *1*	ε
	46	8.0% *1*	
	47	7.3% *1*	
	48	73.8% *1*	
	49	5.5% *1*	
	50	5.4% *1*	
	51	5.76 m *1*	β-
	52	1.7 m *1*	β-
	53	32.7 s *9*	β-
23 V	44	90 ms *25*	ε, εα
	45	539 ms *18*	ε
	46	422.37 ms *20*	ε
	47	32.6 m *3*	ε
	48	15.974 d *3*	ε
	49	338 d *5*	ε
	50	1.4×10^17 y +4-3	ε 83%,
		0.250% *2*	β- 17%
		0.250% *2*	
	51	99.750% *2*	
	52	3.75 m *1*	β-
	53	1.61 m *4*	β-
	54	49.8 s *5*	β-
	55	6.54 s *15*	β-
24 Cr	45	50 ms *6*	ε, εp≈25%
	46	0.26 s *6*	ε
	47	508 ms *10*	ε
	48	21.56 h *3*	ε
	49	42.3 m *1*	ε
	50	>1.8×10^17 y 4.345% *9*	
	51	27.702 d *4*	ε
	52	83.79% *1*	
24 Cr	53	9.50% *1*	
	54	2.365% *5*	
	55	3.497 m *3*	β-
	56	5.94 m *10*	β-
	57	21.1 s *10*	β-
	58	7.0 s *3*	β-
	59	1.0 s *4*	β-
	60	0.57 s *6*	β-
25 Mn	46		ε, εp
	47		ε, εp
	48	0.15 s *1*	ε, εp
	49	384 ms *17*	ε
	50	283.1 ms *4*	ε
	50m	1.75 m *3*	ε, IT<7.4%
	51	46.2 m *1*	ε
	52	5.591 d *3*	ε
	52m	21.1 m *2*	ε 98.25%, IT 1.75%
	53	3.74×10^6 y *4*	ε
	54	312.12 d *10*	ε, β-<0.001%
	55	100%	
	56	2.5785 h *2*	β-
	57	87.2 s *8*	β-
	58	65.3 s *7*	β-
	58m	3.0 s *1*	β-
	59	4.6 s *1*	β-
	60	51 s *6*	β-
	60m	1.77 s *2*	β-, IT
	61	0.71 s *1*	β-
	62	0.88 s *15*	β-
	63	0.25 s *4*	β-
26 Fe	48		ε, εp
	49	75 ms *10*	ε, εp≤60%
	50		ε, εp
	51	310 ms *5*	ε
	52	8.275 h *8*	ε
	52m	45.9 s *6*	ε
	53	8.51 m *2*	ε
	53m	2.58 m *4*	IT
	54	5.9% *2*	
	55	2.73 y *3*	ε
	56	91.72% *15*	
	57	2.1% *1*	
	58	0.28% *2*	
	59	44.496 d *7*	β-
	60	1.5×10^6 y *3*	β-
	61	5.98 m *6*	β-
	62	68 s *2*	β-
	63	6.1 s *6*	β-
	64	2.0 s *2*	β-
27 Co	50		ε, εp
	51		ε, εp
	52		ε, εp
	53	240 ms *20*	ε
	53m	247 ms *12*	ε≈98.5%, p≈1.5%
	54	193.24 ms *14*	ε
	54m	1.48 m *2*	ε
	55	17.53 h *3*	ε
	56	77.12 d *7*	ε
	57	271.80 d *5*	ε
	58	70.82 d *3*	ε
	58m	9.15 h *10*	IT
	59	100%	
	60	5.2714 y *5*	β-
	60m	10.47 m *4*	IT 99.76%, β- 0.24%

TABLE OF NUCLIDES (cont.)

Isotope Z El	A	T1/2 or Abundance	Decay Mode
27 Co	61	1.650 h *5*	β-
	62	1.50 m *4*	β-
	62m	13.91 m *5*	β->99%, IT<1%
	63	27.4 s *5*	β-
	64	0.30 s *3*	β-
	65	1.25 s *5*	β-
	66	0.23 s *2*	β-
	67	0.42 s *7*	β-
28 Ni	51		ε, εp
	52		ε, εp
	53	45 ms *15*	ε
	54		ε
	55	189 ms *5*	ε
	56	6.10 d *2*	ε
	57	35.65 h *5*	ε
	58	68.077% *5*	
	59	7.5×10^4 y *13*	ε
	60	26.223% *5*	
	61	1.140% *1*	
	62	3.634% *1*	
	63	100.1 y *20*	β-
	64	0.926% *1*	
	65	2.520 h *1*	β-
	66	54.6 h *4*	β-
	67	21 s *1*	β-
	68	19 s *5*	β-
	69	11.4 s *3*	β-
29 Cu	55		ε, εp
	56		ε, εp
	57	233 ms *16*	ε
	58	3.204 s *7*	ε
	59	81.5 s *5*	ε
	60	23.7 m *4*	ε
	61	3.347 h *12*	ε
	62	9.74 m *2*	ε
	63	69.17% *2*	
	64	12.700 h *2*	ε 61%, β- 39%
	65	30.83% *2*	
	66	5.10 m *1*	β-
	67	61.92 h *9*	β-
	68	31.1 s *15*	β-
	68m	3.75 m *5*	IT 84%, β- 16%
	69	2.85 m *15*	β-
	70	4.5 s *10*	β-
	70m	47 s *5*	β-
	71	19.5 s *16*	β-
	72	6.6 s *1*	β-
	73	3.9 s *3*	β-
	75	1.3 s *1*	β-, β-n 3.5%
	76	0.61 s *10*	β-, β-n
30 Zn	57	40 ms *10*	ε, εp≥65%
	58		ε
	59	183.7 ms *23*	ε, εp
	60	2.38 m *5*	ε
	61	89.1 s *2*	ε
	62	9.186 h *13*	ε
	63	38.50 m *8*	ε
	64	48.6% *3*	
	65	243.9 d *1*	ε
	66	27.9% *2*	
	67	4.1% *1*	
	68	18.8% *4*	
	69	56.4 m *9*	β-
	69m	13.76 h *2*	IT 99.97%, β- 0.03%
	70	$>5\times10^{14}$ y 0.6% *1*	2β-?

Isotope Z El	A	T1/2 or Abundance	Decay Mode
30 Zn	71	2.45 m *10*	β-
	71m	3.96 h *5*	β-, IT≤0.05%
	72	46.5 h *1*	β-
	73	23.5 s *10*	β-
	73m	5.8 s *8*	β-, IT
	74	96 s *1*	β-
	75	10.2 s *2*	β-
	76	5.7 s *3*	β-
	77	2.08 s *5*	β-
	77m	1.05 s *10*	β-<50%, IT>50%
	78	1.47 s *15*	β-
	79	1.0 s *1*	β-
	80	0.55 s *3*	β-
31 Ga	62	116.12 ms *23*	ε
	63	32.4 s *5*	ε
	64	2.630 m *11*	ε
	65	15.2 m *2*	ε
	66	9.49 h *7*	ε
	67	3.261 d *1*	ε
	68	67.629 m *24*	ε
	69	60.108% *6*	
	70	21.14 m *3*	β- 99.59%, ε 0.41%
	71	39.892% *6*	
	72	14.10 h *2*	β-
	73	4.86 h *3*	β-
	74	8.12 m *12*	β-
	74m	9.5 s *10*	IT 75%, β-<50%
	75	126 s *2*	β-
	76	29.1 s *7*	β-
	77	13.2 s *2*	β-
	78	5.09 s *5*	β-
	79	3.00 s *9*	β-, β-n 0.1%
	80	1.66 s *2*	β-, β-n 0.84%
	81	1.23 s *1*	β-, β-n 12%
	82	0.602 s *6*	β-, β-n 19.8%
	83	0.31 s *1*	β-, β-n 43%
32 Ge	61	40 ms *15*	ε, εp
	64	63.7 s *25*	ε
	65	30.9 s *7*	ε, εp 0.013%
	66	2.26 h *5*	ε
	67	18.7 m *5*	ε
	68	270.82 d *27*	ε
	69	39.05 h *10*	ε
	70	21.23% *4*	
	71	11.43 d *3*	ε
	71m	20.40 ms *17*	IT
	72	27.66% *3*	
	73	7.73% *1*	
	73m	0.499 s *11*	IT
	74	35.94% *2*	
	75	82.76 m *4*	β-
	75m	47.7 s *5*	IT 99.97%, β- 0.03%
	76	7.44% *2*	
	77	11.30 h *1*	β-
	77m	52.9 s *6*	β- 79%, IT 21%
	78	88 m *1*	β-
	79	19.1 s *3*	β-
	79m	39.0 s *10*	β- 96%, IT 4%
	80	29.5 s *4*	β-
	81	7.6 s *6*	β-
	81m	7.6 s *6*	β-
	82	4.60 s *35*	β-
	83	1.9 s *4*	β-
	84	1.2 s *3*	β-

TABLE OF NUCLIDES (cont.)

Isotope Z El	A	T1/2 or Abundance	Decay Mode
33 As	66	95.77 ms *23*	ε
	67	42.5 s *12*	ε
	68	151.6 s *8*	ε
	69	15.2 m *2*	ε
	70	52.6 m *3*	ε
	71	65.28 h *15*	ε
	72	26.0 h *1*	ε
	73	80.30 d *6*	ε
	74	17.77 d *2*	ε 66%, β- 34%
	75	100%	
	76	26.32 h *7*	β-, ε<0.02%
	77	38.83 h *5*	β-
	78	90.7 m *2*	β-
	79	9.01 m *15*	β-
	80	15.2 s *2*	β-
	81	33.3 s *8*	β-
	82	19.1 s *5*	β-
	82m	13.6 s *4*	β-
	83	13.4 s *3*	β-
	84	5.5 s *3*	β-, β-n 0.08%
	84m	0.65 s	β-
	85	2.028 s *12*	β-, β-n 23%
	86	0.9 s *2*	β-, β-n 12%
	87	0.73 s *6*	β-, β-n 44%
34 Se	68	1.6 m *4*	ε
	69	27.4 s *2*	ε, εp 0.05%
	70	41.1 m *3*	ε
	71	4.74 m *5*	ε
	72	8.40 d *8*	ε
	73	7.15 h *8*	ε
	73m	39.8 m *13*	IT 72.6%, ε 27.4%
	74	0.89% *2*	
	75	119.779 d *4*	ε
	76	9.36% *12*	
	77	7.63% *5*	
	77m	17.36 s *5*	IT
	78	23.78% *15*	
	79	≤6.5×10⁴ y	β-
	79m	3.91 m *5*	IT
	80	49.61% *31*	
	81	18.45 m *12*	β-
	81m	57.28 m *5*	IT 99.95%, β- 0.05%
	82	1.4×10²⁰ y *4* 8.73% *6*	2β-
	83	22.3 m *3*	β-
	83m	70.1 s *4*	β-
	84	3.1 m *1*	β-
	85	31.7 s *9*	β-
	86	15.3 s *9*	β-
	87	5.85 s *15*	β-, β-n 0.18%
	88	1.52 s *3*	β-, β-n 0.94%
	89	0.41 s *4*	β-, β-n 5%
	91	0.27 s *5*	β-, β-n 21%
35 Br	70	80.2 ms *8*	ε
	70m	2.2 s *2*	ε
	71	21.4 s *6*	ε
	72	78.6 s *24*	ε
	72m	7.2 s *5*	εp
	72m	10.6 s *3*	ε?, IT
	73	3.4 m *3*	ε
	74	25.4 m *3*	ε
	74m	46 m *2*	ε
	75	96.7 m *13*	ε
	76	16.2 h *2*	ε
	76m	1.31 s *2*	IT>99.4%, ε<0.6%
35 Br	77	57.036 h *6*	ε
	77m	4.28 m *10*	IT
	78	6.46 m *4*	ε≥99.99%, β-≤1×10⁻²%
	79	50.69% *5*	
	79m	4.86 s *4*	IT
	80	17.68 m *2*	β- 91.7%, ε 8.3%
	80m	4.42 h *1*	IT
	81	49.31% *5*	
	82	35.30 h *2*	β-
	82m	6.13 m *5*	IT 97.6%, β- 2.4%
	83	2.40 h *2*	β-
	84	31.80 m *8*	β-
	84m	6.0 m *2*	β-
	85	2.90 m *6*	β-
	86	55.1 s *4*	β-
	87	55.60 s *15*	β-, β-n 2.57%
	88	16.5 s *1*	β-, β-n 6.4%
	89	4.40 s *3*	β-, β-n 13%
	90	1.71 s *14*	β-, β-n 23%
	91	0.541 s *5*	β-, β-n 18.3%
	92	0.365 s *7*	β-, β-n 21%
	93		β-, β-n
	94		β-, β-n
36 Kr	71	97 ms *9*	ε
	72	17.2 s *3*	ε
	73	27.0 s *12*	ε, εp 0.68%
	74	11.50 m *11*	ε
	75	4.3 m *2*	ε
	76	14.8 h *1*	ε
	77	74.4 m *6*	ε
	78	0.35% *2*	
	79	35.04 h *10*	ε
	79m	50 s *3*	IT
	80	2.25% *2*	
	81	2.13×10⁵ y *21*	ε
	81m	13 s *1*	IT 99.99%, ε 0.01%
	82	11.6% *1*	
	83	11.5% *1*	
	83m	1.83 h *2*	IT
	84	57.0% *3*	
	85	10.756 y *18*	β-
	85m	4.480 h *8*	β- 78.6%, IT 21.4%
	86	17.3% *2*	
	87	76.3 m *6*	β-
	88	2.84 h *3*	β-
	89	3.15 m *4*	β-
	90	32.32 s *9*	β-
	91	8.57 s *4*	β-
	92	1.85 s *1*	β-, β-n 0.03%
	93	1.29 s *1*	β-, β-n 3.2%
	94	0.20 s *1*	β-, β-n 5.7%
	95	0.78 s *3*	β-, β-n
	97?	<0.1 s	β-
37 Rb	74	64.9 ms *5*	ε
	75	19.0 s *12*	ε
	76	39.1 s *6*	ε
	77	3.75 m *8*	ε
	78	17.66 m *8*	ε
	78m	5.74 m *6*	ε 90%, IT 10%
	79	22.9 m *5*	ε
	80	34 s *4*	ε
	81	4.576 h *5*	ε
	81m	30.49 m *29*	IT 97.7%, ε 2.3%
	82	1.273 m *2*	ε

TABLE OF NUCLIDES (cont.)

Isotope Z El A	T1/2 or Abundance	Decay Mode
37 Rb 82m	6.472 h *6*	ε, IT<0.33%
83	86.2 d *1*	ε
84	32.77 d *14*	ε 96.2%, β- 3.8%
84m	20.26 m *4*	IT
85	72.17% *1*	
86	18.631 d *18*	β- 99.99%, ε 0.0052%
86m	1.017 m *3*	IT
87	4.75×10^{10} y *4*	β-
	27.83% *1*	
88	17.78 m *11*	β-
89	15.15 m *12*	β-
90	153 s *3*	β-
90m	258 s *5*	β- 95.7%, IT 4.3%
91	58.4 s *4*	β-
92	4.50 s *2*	β-, β-n 0.012%
93	5.7 s *1*	β-, β-n 2.5%
94	2.702 s *5*	β-, β-n 10.4%
95	384 ms *6*	β-, β-n 9.1%
96	0.199 s *3*	β-, β-n 13%
97	171.8 ms *16*	β-, β-n 24.6%
98	0.114 s *5*	β-, β-n 15.9%, β-2n
99	59 ms *1*	β-, β-n 15%
100	51 ms *8*	β-, β-n 6%
102?	90 ms *20*	β-, β-n
38 Sr 77	9.0 s *2*	ε, εp<0.25%
78	2.5 m *3*	ε
79	2.25 m *10*	ε
80	106.3 m *15*	ε
81	22.3 m *4*	ε
82	25.55 d *15*	ε
83	32.41 h *3*	ε
83m	4.95 s *12*	IT
84	0.56% *1*	
85	64.84 d *2*	ε
85m	67.63 m *4*	IT 86.6%, ε 13.4%
86	9.86% *1*	
87	7.00% *1*	
87m	2.803 h *3*	IT 99.7%, ε 0.3%
88	82.58% *1*	
89	50.53 d *7*	β-
90	29.1 y *3*	β-
91	9.63 h *5*	β-
92	2.71 h *1*	β-
93	7.423 m *24*	β-
94	75.1 s *7*	β-
95	25.1 s *2*	β-
96	1.06 s *4*	β-
97	420 ms *30*	β-, β-n 0.27%
98	0.65 s *3*	β-, β-n 0.8%
99	0.271 s *4*	β-, β-n 0.32%
100	202 ms *3*	β-, β-n 0.73%
101	115 ms *1*	β-, β-n
102	68 ms *8*	β-, β-n
39 Y 80	33.8 s *6*	ε
81	72.4 s *13*	ε
82	9.5 s *3*	ε
83	7.08 m *6*	ε
83m	2.85 m *2*	ε
84	4.6 s *2*	ε
84m	40 m *1*	ε
85	2.68 h *5*	ε
85m	4.86 h *13*	ε, IT<2.0×10^{-3}%
86	14.74 h *2*	ε
86m	48 m *1*	IT 99.31%, ε 0.69%
39 Y 87	79.8 h *3*	ε
87m	13.37 h *3*	IT 98.43%, ε 1.57%
88	106.65 d *4*	ε
89	100%	
89m	16.06 s *4*	IT
90	64.1 h *1*	β-
90m	3.19 h *1*	IT, β- 0.002%
91	58.51 d *6*	β-
91m	49.71 m *4*	IT, β-<1.5%
92	3.54 h *1*	β-
93	10.10 h *16*	β-
93m	0.82 s *4*	IT
94	18.7 m *1*	β-
95	10.3 m *2*	β-
96	6.2 s *2*	β-
96m	9.6 s *2*	β-
96n	2.3 m *1*	β-
97	3.76 s *2*	β-, β-n 0.06%
97m	1.21 s *2*	β-, IT<0.7%
98	0.59 s *4*	β-, β-n 0.3%
98m	2.13 s *12*	β-
99	1.47 s *2*	β-, β-n 0.96%
100	735 ms *7*	β-, β-n 0.81%
100m	0.94 s *3*	β-
101	431 ms *7*	β-, β-n
102	0.36 s *4*	β-, β-n
40 Zr 81	15 s *5*	ε, εp
82	32 s *5*	ε
83	44 s *1*	ε
83m	7 s *2*	ε
84	25.9 m *8*	ε
85	7.86 m *4*	ε
85m	10.9 s *3*	IT≤92%, ε>8%
86	16.5 h *1*	ε
87	1.68 h *1*	ε
87m	14.0 s *2*	IT
88	83.4 d *3*	ε
89	78.41 h *12*	ε
89m	4.18 m *1*	IT 93.77%, ε 6.23%
90m	809.2 ms *20*	IT
91	11.22% *3*	
92	17.15% *2*	
93	1.53×10^{6} y *10*	β-
94	17.38% *3*	
95	64.02 d *4*	β-
96	>3.56×10^{17} y	
	2.80% *1*	
97	16.90 h *5*	β-
98	30.7 s *4*	β-
99	2.1 s *1*	β-
100	7.1 s *4*	β-
101	2.1 s *3*	β-
102	2.9 s *2*	β-
103	1.3 s *1*	β-
104	1.2 s *1*	β-
41 Nb 84	12 s *3*	ε, εp
85	20.9 s *7*	ε
86	88 s *1*	ε
87	2.6 m *1*	ε
87m	3.7 m *1*	ε
88	14.5 m *1*	ε
88m	7.8 m *1*	ε
89	1.18 h *10*	ε
89m	1.9 h *2*	ε
90	14.60 h *5*	ε

TABLE OF NUCLIDES (cont.)

Isotope Z	El	A	T1/2 or Abundance	Decay Mode
41	Nb	90m	18.8 s *1*	IT
		91	6.8×10^{2} y *13*	ε
		91m	60.86 d *22*	IT 93%, ε 7%
		92	3.5×10^{7} y *3*	ε
		92m	10.15 d *2*	ε
		93	100%	
		93m	16.1 y *2*	IT
		94	2.03×10^{4} y *16*	β-
		94m	6.26 m *1*	IT 99.5%, β- 0.5%
		95	34.97 d *3*	β-
		95m	3.61 d *3*	IT 94.4%, β- 5.6%
		96	23.35 h *5*	β-
		97	1.227 h *5*	β-
		97m	58.1 s *5*	IT
		98	2.86 s *6*	β-
		98m	51.3 m *4*	β-
		99	15.0 s *2*	β-
		99m	2.6 m *2*	β-, IT<2.5%
		100	1.5 s *2*	β-
		100m	2.99 s *11*	β-
		101	7.1 s *3*	β-
		102	1.3 s *2*	β-
		102	4.3 s *4*	β-
		103	1.5 s *2*	β-
		104	0.91 s *10*	β-
		104	4.8 s *4*	β-
		105	2.95 s *6*	β-
		106	1.02 s *5*	β-
42	Mo	87	13.4 s *4*	ε, εp>0%
		88	8.0 m *2*	ε
		89	2.04 m *11*	ε
		89m	190 ms *15*	IT
		90	5.67 h *5*	ε
		91	15.49 m *1*	ε
		91m	65.0 s *7*	IT 50.1%, ε 49.9%
		92	14.84% *4*	
		93	3.5×10^{3} y *7*	ε
		93m	6.85 h *7*	IT 99.88%, ε 0.12%
		94	9.25% *2*	
		95	15.92% *4*	
		96	16.68% *4*	
		97	9.55% *2*	
		98	24.13% *6*	
		99	65.94 h *1*	β-
		100	9.63% *2*	
		101	14.6 m *1*	β-
		102	11.3 m *2*	β-
		103	67.5 s *15*	β-
		104	60 s *2*	β-
		105	35.6 s *16*	β-
		106	8.4 s *5*	β-
		107	3.5 s *5*	β-
		108	1.5 s *4*	β-
43	Tc	90	8.3 s	ε
		90	49.2 s	ε
		91	3.14 m *2*	ε
		91m	3.3 m *1*	ε, IT<1%
		92	4.4 m *3*	ε
		93	2.75 h *5*	ε
		93m	43.5 m *10*	IT 77.8%, ε 22.2%
		94	293 m *1*	ε
		94m	52.0 m *10*	ε, IT<0.1%
		95	20.0 h *1*	ε
		95m	61 d *2*	ε 96%, IT 4%
		96	4.28 d *6*	ε
		96m	51.5 m *10*	IT 98%, ε 2%
43	Tc	97	2.6×10^{6} y *4*	ε
		97m	90.5 d *10*	IT
		98	4.2×10^{6} y *3*	β-
		99	2.111×10^{5} y *12*	β-
		99m	6.01 h *1*	IT, β- 0.004%
		100	15.8 s *1*	β-
		101	14.2 m *1*	β-
		102	5.28 s *15*	β-
		102m	4.35 m *7*	β-≈98%, IT≈2%
		103	54.2 s *8*	β-
		104	18.3 m *3*	β-
		105	7.6 m *1*	β-
		106	36 s *1*	β-
		107	21.2 s *2*	β-
		108	5.17 s *7*	β-
		109	1.4 s *4*	β-
		110	0.83 s *4*	β-
		111	0.30 s *3*	β-
44	Ru	91	9 s *1*	ε
		91m	7.6 s *8*	IT, ε>0%, εp>0%
		92	3.65 m *5*	ε
		93	59.7 s *6*	ε
		93m	10.8 s *3*	ε 77.8%, IT 22.2%, εp 0.03%
		94	51.8 m *6*	ε
		95	1.64 h *1*	ε
		96	5.54% *2*	
		97	2.9 d *1*	ε
		98	1.86% *2*	
		99	12.7% *1*	
		100	12.6% *1*	
		101	17.1% *1*	
		102	31.6% *2*	
		103	39.26 d *2*	β-
		104	18.6% *2*	
		105	4.44 h *2*	β-
		106	373.59 d *15*	β-
		107	3.75 m *5*	β-
		108	4.55 m *5*	β-
		109	34.5 s *10*	β-
		110	14.6 s *10*	β-
		111	2.12 s *7*	β-
		112	1.75 s *7*	β-
		113	0.80 s *5*	β-
		114	0.5 s	β-
45	Rh	94m	25.8 s *2*	ε
		94m	70.6 s *6*	ε
		95	5.02 m *10*	ε
		95m	1.96 m *4*	IT 88%, ε 12%
		96	9.6 m	ε
		96m	1.51 m *2*	IT 60%, ε 40%
		97	31.1 m *8*	ε
		97m	44.3 m *8*	ε 95.1%, IT 4.9%
		98	8.7 m *2*	ε
		98m	3.5 m *3*	ε
		99	16.1 d *2*	ε
		99m	4.7 h *1*	ε, IT<0.16%
		100	20.8 h *1*	ε
		100m	4.6 m *2*	IT≈98.3%, ε≈1.7%
		101	3.3 y *3*	ε
		101m	4.34 d *1*	ε 92.3%, IT 7.7%
		102	≈2.9 y	ε
		102m	207 d *3*	ε 75%, β- 20%, IT 5%
		103	100%	
		103m	56.12 m *1*	IT

TABLE OF NUCLIDES (cont.)

Isotope Z El A	T1/2 or Abundance	Decay Mode
45 Rh 104	42.3 s *4*	β- 99.55%, ε 0.45%
104m	4.34 m *5*	IT 99.87%, β- 0.13%
105	35.36 h *6*	β-
105m	≈40 s	IT
106	29.80 s *8*	β-
106m	130 m *2*	β-
107	21.7 m *4*	β-
108m	16.8 s *5*	β-
108n	6.0 m *3*	β-
109	80 s *2*	β-
110	3.2 s *2*	β-
110	28.5 s *15*	β-
111	11 s *1*	β-
112m	3.8 s *6*	β-
112n	6.8 s *2*	β-
113	2.72 s *22*	β-
114	1.85 s *5*	β-
114m	1.85 s *5*	β-
115	0.99 s *5*	β-
116	0.68 s *6*	β-
116	0.9 s *4*	β-
46 Pd 94	9.0 s *5*	ε
95m	13.3 s *3*	εp>0.93%, ε
96	2.03 m *3*	ε
97	3.1 m *1*	ε
98	17.7 m *3*	ε
99	21.4 m *2*	ε
100	3.63 d *9*	ε
101	8.47 h *6*	ε
102	1.02% *1*	
103	16.991 d *19*	ε
104	11.14% *8*	
105	22.33% *8*	
106	27.33% *3*	
107	6.5×10^{6} y *3*	β-
107m	21.3 s *5*	IT
108	26.46% *9*	
109	13.7 h *1*	β-
109m	4.69 m *1*	IT
110	11.72% *9*	
111	23.4 m *2*	β-
111m	5.5 h *1*	IT 73%, β- 27%
112	21.03 h *5*	β-
113	93 s *5*	β-
113m	≥100 s	
114	2.42 m *6*	β-
115	47 s *2*	β-
116	12.4 s *5*	β-
117	5.0 s *+5-7*	β-
118	2.4 s *4*	β-
47 Ag 96	5.1 s *4*	εp 8%, ε
97	21 s *3*	ε
98	47 s *1*	ε, εp>0%
99	124 s *3*	ε
99m	10.5 s *5*	IT
100	2.01 m *9*	ε
100m	2.24 m *13*	ε, IT
101	11.1 m *3*	ε
101m	3.10 s *10*	IT
102	12.9 m *3*	ε
102m	7.7 m *5*	ε 51%, IT 49%
103	65.7 m *7*	ε
103m	5.7 s *3*	IT
104	69.2 m *10*	ε
104m	33.5 m *20*	ε 67%, IT 33%
47 Ag 105	41.29 d *7*	ε
105m	7.23 m *16*	IT 99.66%, ε 0.34%
106	23.96 m *4*	ε 99.5%, β-<1%
106m	8.46 d *10*	ε
107	51.839% *5*	
107m	44.3 s *2*	IT
108	2.37 m *1*	β- 97.15%, ε 2.85%
108m	127 y *21*	ε 91.3%, IT 8.7%
109	48.161% *5*	
109m	39.6 s *2*	IT
110	24.6 s *2*	β- 99.7%, ε 0.3%
110m	249.76 d *4*	β- 98.64%, IT 1.36%
111	7.45 d *1*	β-
111m	64.8 s *8*	IT 99.3%, β- 0.7%
112	3.130 h *9*	β-
113	5.37 h *5*	β-
113m	68.7 s *16*	IT≈80%, β-≈20%
114	4.6 s *1*	β-
115	20.0 m *5*	β-
115m	18.0 s *7*	β-, IT
116	2.68 m *1*	β-
116m	10.4 s *8*	β- 98%, IT 2%
117m	5.34 s *5*	β-
117n	72.8 s *+20-7*	β-
118	3.76 s *15*	β-
118m	2.0 s *2*	β- 59%, IT 41%
119	2.1 s *1*	β-
120	1.23 s *3*	β-
120m	0.32 s *4*	β-≈63%, IT≈37%
121	0.78 s *1*	β-, β-n
122	0.56 s *3*	β-, β-n
122m	1.5 s *5*	β-, β-n
123	0.31 s *2*	β-, β-n
124	0.22 s *3*	β-, β-n
48 Cd 97	3 s *+4-2*	ε, εp
98	≈8 s	ε, εp?
99	16 s *3*	ε, εp 0.17%, εα<1×10^{-4}%
100	49.1 s *5*	ε
101	1.2 m *2*	ε
102	5.5 m *5*	ε
103	7.3 m *1*	ε
104	57.7 m *10*	ε
105	55.5 m *4*	ε
106	1.25% *4*	
107	6.50 h *2*	ε
108	0.89% *2*	
109	462.0 d *6*	ε
110	12.49% *12*	
111	12.80% *8*	
111m	48.54 m *5*	IT
112	24.13% *14*	
113	9.3×10^{15} y *19*	β-
	12.22% *8*	
113m	14.1 y *5*	β- 99.86%, IT 0.14%
114	28.73% *28*	
115	53.46 h *10*	β-
115m	44.6 d *3*	β-
116	7.49% *12*	
117	2.49 h *4*	β-
117m	3.36 h *5*	β-
118	50.3 m *2*	β-
119	2.69 m *2*	β-

TABLE OF NUCLIDES (cont.)

Isotope Z El A	T1/2 or Abundance	Decay Mode
48 Cd *119m*	2.20 m *2*	β-
120	50.80 s *21*	β-
121	13.5 s *3*	β-
121m	8 s	β-
122	5.3 s *1*	β-
123	2.09 s *3*	β-
123m	1.9 s *1*	β-
124	1.24 s *5*	β-
125	0.68 s *5*	β-
125m	0.66 s *3*	β-
126	0.52 s *4*	β-
127	0.4 s *1*	β-
128	0.28 s *4*	β-
129	0.27 s *4*	β-
130	0.20 s *4*	β-, β-n≈4%
49 In 100		ε, εp
102	23 s *4*	ε
103	65 s *7*	ε
104	1.84 m *5*	ε
104m	15.7 s *5*	IT
105	5.07 m *7*	ε
105m	48 s *6*	IT
106	6.2 m *1*	ε
106m	5.2 m *1*	ε
107	32.4 m *3*	ε
107m	50.4 s *6*	IT
108	58.0 m *12*	ε
108m	39.6 m *7*	ε
109	4.2 h *1*	ε
109m	1.34 m *7*	IT
109m	0.21 s *1*	IT
110	69.1 m *5*	ε
110	4.9 h *1*	ε
111	2.8049 d *1*	ε
111m	7.7 m *2*	IT
112	14.97 m *10*	ε 56%, β- 44%
112m	20.56 m *6*	IT
113	4.3% *2*	
113m	1.6582 h *6*	IT
114	71.9 s	β- 99.5%, ε 0.5%
114m	49.51 d *1*	IT 95.6%, ε 4.4%
115	4.41×10^{14} y *25*	β- 95.7% *2*
115m	4.486 h *4*	IT 95%, β- 5%
116	14.10 s *3*	β- 99.94%, ε<0.06%
116m	54.41 m *3*	β-
116m	2.18 s *4*	IT
117	43.8 m *7*	β-
117m	116.5 m *7*	β- 52.9%, IT 47.1%
118	5.0 s *5*	β-
118m	4.45 m *5*	β-
118m	8.5 s *3*	IT 98.6%, β- 1.4%
119	2.4 m *1*	β-
119m	18.0 m *3*	β- 97.5%, IT 2.5%
120	3.08 s *8*	β-
120	46.2 s *8*	β-
120	47.3 s *5*	β-
121	23.1 s *6*	β-
121m	3.88 m *10*	β- 98.6%, IT 1.2%
122	1.5 s *3*	β-
122m	10.3 s *6*	β-
122m	10.8 s *4*	β-
123	5.98 s *6*	β-
123m	47.8 s *5*	β-
124	3.17 s *5*	β-
49 In *124m*	3.4 s *5*	β-
125	2.33 s *4*	β-
125m	12.2 s *1*	β-
126	1.63 s *5*	β-
126m	1.5 s *2*	β-
127	1.15 s *5*	β-
127m	3.76 s *3*	β-, β-n
128	0.80 s *1*	β-, β-n
128m	0.7 s *1*	β-, β-n
129	0.63 s *4*	β-, β-n
129m	1.23 s *2*	β-, β-n
130	0.32 s *2*	β-, β-n 0.9%
130m	0.55 s *1*	β-
130m	0.55 s *1*	β-
130m	0.55 s *1*	β-n<1.67%
130m	0.55 s *1*	β-n<1.67%
131	0.27 s *2*	β-, β-n
131m	0.32 s *6*	β-
131m	0.35 s *5*	β-
132	0.203 s *6*	β-, β-n
133	180 ms *20*	β-, β-n
50 Sn 103	7 s *3*	ε, εp
104	21.4 s *9*	ε
105	31 s *6*	ε, εp
106	2.10 m *15*	ε
107	2.90 m *5*	ε
108	10.30 m *8*	ε
109	18.0 m *2*	ε
110	4.11 h *10*	ε
111	35.3 m *6*	ε
112	0.97% *1*	
113	115.09 d *4*	ε
113m	21.4 m *4*	IT 91.1%, ε 8.9%
114	0.65% *1*	
115	0.36% *1*	
116	14.53% *11*	
117	7.68% *7*	
117m	13.60 d *4*	IT
118	24.22% *11*	
119	8.58% *4*	
119m	293.0 d *13*	IT
120	32.59% *10*	
121	27.06 h *4*	β-
121m	55 y *5*	IT 77.6%, β- 22.4%
122	4.63% *3*	
123	129.2 d *4*	β-
123m	40.08 m *7*	β-
124	5.79% *5*	
125	9.64 d *3*	β-
125m	9.52 m *5*	β-
126	$\approx1.0\times10^{5}$ y	β-
127	2.10 h *4*	β-
127m	4.13 m *3*	β-
128	59.1 m *5*	β-
128m	6.5 s *5*	IT
129	2.4 m *1*	β-
129m	6.9 m *1*	β-, IT 0.0002%
130	3.72 m *4*	β-
130m	1.7 m *1*	β-
131	39 s *2*	β-
131m	61 s *2*	β-
132	40 s *1*	β-
133	1.44 s *4*	β-, β-n 0.08%
134	1.04 s *2*	β-, β-n 17%
51 Sb 108	7.0 s *5*	ε
109	17.0 s *7*	ε

TABLE OF NUCLIDES (cont.)

Isotope Z El A	T1/2 or Abundance	Decay Mode
51 Sb 110	24 s *1*	ε
111	75 s *1*	ε
112	51.4 s *10*	ε
113	6.67 m *7*	ε
114	3.49 m *3*	ε
115	32.1 m *3*	ε
116	15.8 m *8*	ε
116m	60.3 m *6*	ε
117	2.80 h *1*	ε
118	3.6 m *1*	ε
118m	5.00 h *2*	ε
119	38.1 h *2*	ε
120	15.89 m *4*	ε
120m	5.76 d *2*	ε
121	57.36% *15*	
122	2.70 d *1*	β- 97.6%, ε 2.4%
122m	4.21 m *2*	IT
123	42.64% *15*	
124	60.20 d *3*	β-
124m	93 s *5*	IT 75%, β- 25%
124m	20.2 m *2*	IT
125	2.73 y *3*	β-
126	12.4 d *1*	β-
126m	19.0 m *3*	β- 86%, IT 14%
126n	≈11 s	IT
127	3.85 d *5*	β-
128	9.01 h *3*	β-
128m	10.4 m *2*	β- 96.4%, IT 3.6%
129	17.7 m	β-
129	4.40 h *1*	β-
130	39.5 m *8*	β-
130m	6.3 m *2*	β-
131	23 m *2*	β-
132	4.2 m *1*	β-
132m	2.8 m *1*	β-
133	2.5 m *1*	β-
134	0.85 s *10*	β-
134	10.43 s *14*	β-, β-n 0.1%
135	1.71 s *2*	β-, β-n 16.4%
136	0.82 s *2*	β-, β-n 24%
52 Te 106	70 μs *20*	α
107	3.6 ms +6-4	α 70%, ε 30%
108	2.1 s *1*	α 68%, ε 32%
109	4.6 s *3*	ε 96%, α 4%, εp
110	18.6 s *8*	ε, α
111	19.3 s *4*	ε, εp
112	2.0 m *2*	ε
113	1.7 m *2*	ε
114	15.2 m *7*	ε
115	5.8 m *2*	ε
115m	6.7 m *4*	ε, IT
116	2.49 h *4*	ε
117	62 m *2*	ε
118	6.00 d *2*	ε
119	16.05 h *5*	ε
119m	4.69 d *4*	ε
120	0.095% *5*	
121	16.78 d *35*	ε
121m	154 d *7*	IT 88.6%, ε 11.4%
122	2.59% *1*	
123	1.3×10^{13} y	ε
	0.905% *5*	
123m	119.7 d *1*	IT
124	4.79% *2*	
125	7.12% *2*	
125m	58 d *1*	IT
126	18.93% *3*	
52 Te *127*	9.35 h *7*	β-
127m	109 d *2*	IT 97.6%, β- 2.4%
128	$>8.\times10^{24}$ y	2β-
	31.70% *2*	
129	69.6 m *2*	β-
129m	33.6 d *1*	IT 64%, β- 36%
130	$\leq1.25\times10^{21}$ y	
	33.87% *7*	
131	25.0 m *1*	β-
131m	30 h *2*	β- 77.8%, IT 22.2%
132	78.2 h *8*	β-
133	12.5 m *3*	β-
133m	55.4 m *4*	β- 82.5%, IT 17.5%
134	41.8 m *8*	β-
135	19.0 s *2*	β-
136	17.5 s *2*	β-, β-n 1.1%
137	2.49 s *5*	β-, β-n 2.7%
138	1.4 s *4*	β-, β-n 6.3%
53 I 109	0.11 ms *2*	p
110	0.65 s *2*	ε 83%, α 17%, εα, εp
111	2.5 s *2*	ε 99.9%, α≈0.1%
112	3.42 s *11*	ε, α≈0.0012%, εα, εp
113	6.6 s *2*	ε, α 3.3×10^{-7}%
114	2.1 s *2*	ε, εp
115	1.3 m *2*	ε
116	2.91 s *15*	ε
117	2.22 m *4*	ε
118	13.7 m *5*	ε
118m	8.5 m *5*	ε
119	19.1 m *4*	ε
120	81.0 m *6*	ε
120m	53 m *4*	ε
121	2.12 h *1*	ε
122	3.63 m *6*	ε
123	13.2 h *1*	ε
124	4.18 d *2*	ε
125	60.14 d *11*	ε
126	13.02 d *7*	ε 56.3%, β- 43.7%
127	100%	
128	24.99 m *2*	β- 93.1%, ε 6.9%
129	1.57×10^{7} y *4*	β-
130	12.36 h *3*	β-
130m	9.0 m *1*	IT 84%, β- 16%
131	8.04 d *1*	β-
132	2.30 h *3*	β-
132m	83.6 m *17*	IT 86%, β- 14%
133	20.8 h *1*	β-
133m	9 s *2*	IT
134	52.6 m *4*	β-
134m	3.69 m *7*	IT 97.7%, β- 2.3%
135	6.57 h *2*	β-
136	83.4 s *10*	β-
136m	46.9 s *10*	β-
137	24.5 s *2*	β-, β-n 7.1%
138	6.49 s *7*	β-n 5.5%, β-
139	2.29 s *2*	β-, β-n 9.9%
140	0.86 s *4*	β-, β-n 9.4%
141	0.43 s *2*	β-, β-n 21.2%
142	≈0.2 s	β-
54 Xe 110	≈0.2 s	α, ε
111	0.74 s *20*	α
112	2.7 s *8*	ε 99.16%, α 0.84%

TABLE OF NUCLIDES (cont.)

Isotope Z El A	T1/2 or Abundance	Decay Mode
54 Xe 113	2.74 s *8*	ε 99.97%, εp 4.2%, α 0.04%, εα
114	10.0 s *4*	ε
115	18 s *4*	εα, ε, εp
116	56 s *2*	ε>0%
117	61 s *2*	ε, εp 0.003%
118	3.8 m *9*	ε
119	5.8 m *3*	ε
120	40 m *1*	ε
121	39.0 m *5*	ε
122	20.1 h *1*	ε
123	2.08 h *2*	ε
124	0.10% *1*	
125	16.9 h *2*	ε
125m	57 s *1*	IT
126	0.09% *1*	
127	36.4 d *1*	ε
127m	69.2 s *9*	IT
128	1.91% *3*	
129	26.4% *6*	
129m	8.89 d *2*	IT
130	4.1% *1*	
131m	11.9 d *1*	IT
133	5.243 d *1*	β-
133m	2.19 d *1*	IT
134	10.4% *2*	
134m	290 ms *17*	IT
135	9.14 h *2*	β-
135m	15.29 m *5*	IT, β- 0.004%
136	$\geq 2.36\times10^{21}$ y 8.9% *1*	2β-
137	3.818 m *13*	β-
138	14.08 m *8*	β-, β-n
139	39.68 s *14*	β-
140	13.60 s *10*	β-
141	1.73 s *1*	β-, β-n 0.04%
142	1.22 s *2*	β-
143	0.30 s *3*	β-
144	1.15 s *20*	β-
145	0.9 s *3*	β-, β-n
146		β-
55 Cs 113	33 μs *7*	p≈100%
114	0.57 s *2*	ε≈100%, εp 7%, εα 0.16%, α 0.02%
115	1.4 s *8*	ε, εp
116	3.84 s *16*	ε, εα>0%, εp>0%
116	0.70 s *4*	ε, εα, εp
117m	6.5 s *4*	ε
117n	8.4 s *6*	ε
118m	14 s *2*	εα, ε, εp
118n	17 s *3*	εα, ε, εp
119	37.7 s *10*	ε
119	28 s *1*	
120	57 s *6*	ε, εp≤1.0×10^{-5}%
120	64 s *3*	ε
121	2.27 m *5*	ε
121m	121 s *3*	ε, IT
122	21.0 s *7*	ε
122m	0.36 s *2*	IT
122n	4.5 m *2*	ε
123	5.87 m *5*	ε
123m	1.60 s *15*	IT
124	30.8 s *5*	ε
124m	6.3 s *2*	IT
125	45 m *1*	ε
126	1.64 m *2*	ε
127	6.25 h *10*	ε

Isotope Z El A	T1/2 or Abundance	Decay Mode
55 Cs 128	3.62 m *2*	ε
129	32.06 h *6*	ε
130	29.21 m *4*	ε 98.4%, β- 1.6%
130m	3.46 m *6*	IT 99.84%, ε 0.16%
131	9.69 d *1*	ε
132	6.475 d *10*	ε 98%, β- 2%
133	100%	
134	2.062 y *5*	β-, ε 0.0003%
134m	2.91 h *1*	IT
135	2.3×10^{6} y *3*	β-
135m	53 m *2*	IT
136	13.16 d *3*	β-
136m	19 s *2*	IT, β-?
137	30.1 y *2*	β-
138	32.2 m *1*	β-
138m	2.91 m *8*	IT 81%, β- 19%
139	9.27 m *5*	β-
140	63.7 s *3*	β-
141	24.94 s *6*	β-, β-n 0.03%
142	1.70 s *2*	β-, β-n 0.28%
143	1.78 s *1*	β-, β-n 1.62%
144	1.01 s *1*	β-, β-n 3.17%
144m	<1 s	β-
145	0.594 s *13*	β-, β-n 13.8%
146	0.343 s *7*	β-, β-n 13.2%
147	0.225 s *5*	β- 57%, β-n 43%
148	158 ms *7*	β-
56 Ba 117	1.8 s *1*	ε, εα, εp
119	5.35 s *30*	ε, εp
120	32 s *5*	ε
121	29.7 s *15*	ε, εp 0.02%
122	1.95 m *15*	ε
123	2.7 m *4*	ε
124	11.9 m *10*	ε
125	3.5 m *4*	ε
125	8 m	ε
126	100 m *2*	ε
127	12.7 m *4*	ε
128	2.43 d *5*	ε
129	2.23 h *11*	ε
129m	2.17 h *4*	ε
130	0.106% *2*	
131	11.8 d *2*	ε
131m	14.6 m *2*	IT
133	10.52 y *13*	ε
133m	38.9 h *1*	IT 99.99%, ε 0.01%
134	2.42% *4*	
135	6.593% *24*	
135m	28.7 h *2*	IT
136	7.85% *5*	
136m	0.3084 s *19*	IT
137	11.23% *5*	
137m	2.552 m *1*	IT
138	71.70% *9*	
139	83.06 m *28*	β-
140	12.752 d *3*	β-
141	18.27 m *7*	β-
142	10.6 m *2*	β-
143	14.33 s *8*	β-
144	11.5 s *2*	β-, β-n 3.8%
145	4.31 s *16*	β-
146	2.22 s *7*	β-
147	0.893 s *1*	β-, β-n 0.02%
148	0.607 s *25*	β-, β-n≤0.02%
149	0.356 s *8*	β-n 0.43%

TABLE OF NUCLIDES (cont.)

Isotope Z El A	T1/2 or Abundance	Decay Mode
57 La 120	2.8 s *2*	ε, εp
122	8.7 s *7*	ε, εp
123	17 s *3*	ε
124	29 s *3*	ε
125	76 s *6*	ε
126	1.0 m *3*	ε
127	3.8 m *5*	ε
127m	5.0 m *5*	
128	5.0 m *3*	ε
129	11.6 m *2*	ε
129m	0.56 s *5*	IT
130	8.7 m *1*	ε
131	59 m *2*	ε
132	4.8 h *2*	ε
132m	24.3 m *5*	IT 76%, ε 24%
133	3.912 h *8*	ε
134	6.45 m *16*	ε
135	19.5 h *2*	ε
136	9.87 m *3*	ε
137	6×10^{4} y *2*	ε
138	1.05×10^{11} y *2*	ε 66.4%,
	0.0902% *2*	β- 33.6%
139	99.9098% *2*	
140	1.6781 d *3*	β-
141	3.92 h *3*	β-
142	91.1 m *5*	β-
143	14.2 m *1*	β-
144	40.8 s *4*	β-
145	24.8 s *20*	β-
146	6.27 s *10*	β-
146m	10.0 s *1*	β-
147	4.015 s *8*	β-, β-n 0.04%
148	1.05 s *1*	β-, β-n 0.11%
149	1.2 s *4*	β-, β-n
58 Ce 123	3.8 s *2*	ε, εp
124	6 s *2*	ε
125	10 s *1*	ε, εp
126	50 s *6*	ε
127	32 s *4*	ε
128	6 m *2*	ε
129	3.5 m *5*	ε
130	25 m *2*	ε
131	10 m *1*	ε
131	5 m *1*	ε
132	3.5 h *1*	ε
133	4.9 h *4*	ε
133m	97 m *4*	ε
134	75.9 h *9*	ε
135	17.7 h *2*	ε
135m	20 s *1*	IT
136	0.19% *1*	
137	9.0 h *3*	ε
137m	34.4 h *3*	IT 99.22%,
		ε 0.78%
138	0.25% *1*	
139	137.640 d *23*	ε
139m	54.8 s *10*	IT
140	88.43% *10*	
141	32.501 d *5*	β-
142	$>5\times10^{16}$ y	
	11.13% *10*	
143	33.10 h *5*	β-
144	284.893 d *8*	β-
145	3.01 m *6*	β-
146	13.52 m *13*	β-
147	56.4 s *10*	β-
148	56 s *1*	β-
58 Ce *149*	5.2 s *3*	β-
150	4.0 s *6*	β-
151	1.02 s *6*	β-
152	3.1 s *3*	β-
59 Pr 124	1.2 s *2*	ε, εp
126	3.2 s *6*	ε, εp
128	3.2 s *5*	ε, εp
129	24 s *5*	ε
130	40.0 s *4*	ε
131	1.7 m *4*	ε
132	1.6 m *3*	ε
133	6.5 m *3*	ε
134	17 m *2*	ε
134m	11 m	ε
135	24 m *2*	ε
136	13.1 m *1*	ε
137	1.28 h *3*	ε
138	1.45 m *5*	ε
138m	2.1 h *1*	ε
139	4.41 h *4*	ε
140	3.39 m *1*	ε
141	100%	
142	19.12 h *4*	β- 99.98%,
		ε 0.02%
142m	14.6 m *5*	IT
143	13.57 d *2*	β-
144	17.28 m *5*	β-
144m	7.2 m *3*	IT 99.93%,
		β- 0.07%
145	5.984 h *10*	β-
146	24.15 m *18*	β-
147	13.6 m *5*	β-
148	2.27 m *4*	β-
148m	2.0 m *1*	β-
149	2.26 m *7*	β-
150	6.19 s *16*	β-
151	18.90 s *7*	β-
152	3.24 s *19*	β-
153	4.3 s *2*	β-
154	2.3 s *1*	β-
60 Nd 127	1.8 s *4*	ε, εp
128	4 s *2*	ε, εp
129	4.9 s *2*	ε, εp
130	28 s *3*	ε
131	24 s *3*	ε, εp
131	25 s	
132	1.8 m *2*	ε
133	70 s *10*	ε
133m	<2 m	ε
134	8.5 m *15*	ε
135	12.4 m *6*	ε
135m	5.5 m *5*	ε
136	50.65 m *33*	ε
137	38.5 m *15*	ε
137m	1.60 s *15*	IT
138	5.04 h *9*	ε
139	29.7 m *5*	ε
139m	5.50 h *20*	ε 88.2%, IT 11.8%
140	3.37 d *2*	ε
141	2.49 h *3*	ε
141m	62.4 s *9*	IT 99.97%,
		ε 0.03%
142	27.13% *10*	
143	12.18% *5*	
144	2.29×10^{15} y *16*	α
	23.80% *10*	
145	8.30% *5*	

TABLE OF NUCLIDES (cont.)

Isotope Z El A	T1/2 or Abundance	Decay Mode
60 Nd *146*	17.19% *8*	
147	10.98 d *1*	β-
148	5.76% *3*	
149	1.72 h *1*	β-
150	>1×10^18 y	2β-
	5.64% *3*	
151	12.44 m *7*	β-
152	11.4 m *2*	β-
153	28.9 s *4*	β-
154	25.9 s *2*	β-
155	8.9 s *2*	β-
156	5.5 s *1*	β-
61 Pm 130	2.2 s *5*	ε, εp
132	5.0 s *7*	ε, εp
133	12 s *3*	ε
134	24 s *2*	ε
135	49 s *7*	ε
136	≈107 s	ε
136	107 s *6*	ε
137	2.4 m *1*	ε
138	10 s *2*	ε
138m	3.24 m *5*	ε
138m	3.24 m	
139	4.15 m *5*	ε
139m	180 ns *20*	IT, ε?
140	9.2 s *2*	ε
140m	5.95 m *5*	ε
141	20.90 m *5*	ε
142	40.5 s *5*	ε
143	265 d *7*	ε
144	363 d *14*	ε
145	17.7 y *4*	ε, α 3×10^-7%
146	5.53 y *5*	ε 66%, β- 34%
147	2.6234 y *2*	β-
148	5.370 d *9*	β-
148m	41.29 d *11*	β- 95%, IT 5%
149	53.08 h *5*	β-
150	2.68 h *2*	β-
151	28.40 h *4*	β-
152	4.1 m *1*	β-
152m	7.52 m *8*	β-
152m	13.8 m *2*	β-, IT
153	5.4 m *2*	β-
154	1.73 m *10*	β-
154m	2.68 m *7*	β-
155	48 s *4*	β-
156	26.7 s *1*	β-
157	10.90 s *20*	β-
158	4.8 s *5*	β-
62 Sm 131	1.2 s *2*	ε, εp,
133	2.9 s *2*	ε, εp
134	11 s *2*	ε
135	10 s *2*	ε, εp
136	43 s *3*	ε
137	45 s *1*	ε
138	3.0 m *3*	ε
139	2.57 m *10*	ε
139m	10.7 s *6*	IT 93.7%, ε 6.3%
140	14.82 m *10*	ε
141	10.2 m *2*	ε
141m	22.6 m *2*	ε 99.69%, IT 0.31%
142	72.49 m *5*	ε
143	8.83 m *1*	ε
143m	66 s *2*	IT 99.66%, ε 0.34%
144	3.1% *1*	

Isotope Z El A	T1/2 or Abundance	Decay Mode
62 Sm 145	340 d *3*	ε
146	10.3×10^7 y *5*	α
147	1.06×10^11 y *2*	α
	15.0% *2*	
148	7×10^15 y *3*	α
	11.3% *1*	
149	>2×10^16 y	
	13.8% *1*	
150	7.4% *1*	
151	90 y *8*	β-
152	26.7% *2*	
153	46.27 h *1*	β-
154	22.7% *2*	
155	22.3 m *2*	β-
156	9.4 h *2*	β-
157	8.07 m *12*	β-
158	5.51 m *9*	β-
159	11.2 s *2*	β-
160	9.6 s *3*	β-
63 Eu 134	0.5 s *2*	ε, εp
135	1.5 s *2*	ε
136	3.9 s *5*	ε, εp
136m	≈3.2 s	
137	11 s *2*	ε
138	12.1 s *6*	ε
139	17.9 s *6*	ε
140	1.54 s *13*	ε
140m	0.125 s *2*	ε
141	40.0 s *7*	ε
141m	2.7 s *3*	IT 93%, ε 7%
142	2.4 s *2*	ε
142m	1.22 m *2*	ε
143	2.63 m *5*	ε
144	10.2 s *1*	ε
145	5.93 d *4*	ε
146	4.59 d *3*	ε
147	24.1 d *6*	ε, α 0.0022%
148	54.5 d *5*	ε, α 9.4×10^-7%
149	93.1 d *4*	ε
150	35.8 y *10*	ε
150m	12.8 h *1*	β- 89%, ε 11%
151	47.8% *5*	
152	13.542 y *10*	ε 72.08%, β- 27.92%
152m	9.274 h *9*	β- 72%, ε 28%
152m	96 m *1*	IT
153	52.2% *5*	
154	8.592 y *5*	β- 99.98%, ε 0.02%
154m	46.0 m *4*	IT
155	4.68 y *5*	β-
156	15.19 d *8*	β-
157	15.18 h *3*	β-
158	45.9 m *2*	β-
159	18.1 m *1*	β-
160	38 s *4*	β-
161	26 s *3*	β-
162	10.6 s *10*	β-
64 Gd 137	7 s *3*	ε, εp
139	4.9 s *10*	ε, εp
140	16 s *1*	ε
141	≈20 s	ε, εp 0.03%
141m	24.5 s *9*	ε 86%, IT 14%
142	70.2 s *6*	ε
143	39 s *2*	ε
143m	112 s *2*	ε
144	4.5 m *1*	ε

TABLE OF NUCLIDES (cont.)

Isotope Z El A	T1/2 or Abundance	Decay Mode
64 Gd 145	23.0 m *4*	ε
145m	85 s *3*	IT 94.3%, ε 5.7%
146	48.27 d *10*	ε
147	38.06 h *12*	ε
148	74.6 y *30*	α
149	9.4 d *3*	ε, α
150	1.79×10^{6} y *8*	α
151	124 d *1*	ε, α 1.0×10^{-6}%
152	1.08×10^{14} y *8*	α
	0.20% *1*	
153	241.6 d *2*	ε
154	2.18% *3*	
155	14.80% *5*	
156	20.47% *4*	
157	15.65% *3*	
158	24.84% *12*	
159	18.56 h *8*	β-
160	21.86% *4*	
161	3.66 m	β-
162	8.4 m *2*	β-
163	68 s *3*	β-
164	45 s *3*	β-
65 Tb 140	2.4 s *4*	ε, εp
141	3.5 s *2*	ε
141m	7.9 s *6*	ε
142	597 ms *17*	ε, εp≈3.0×10^{-7}%
142m	303 ms *7*	ε?, εp?, IT?
143	12 s *1*	ε
143m	<17 s	
144	≈1 s	ε
144m	4.25 s *15*	IT 66%, ε 34%
145m	29.5 s *15*	ε
146	8 s *4*	ε
146m	23 s *2*	ε
147	1.7 h *1*	ε
147m	1.83 m *6*	ε
148	60 m *1*	ε
148m	2.20 m *5*	ε
149	4.13 h *2*	ε 84.2%, α 15.8%
149m	4.16 m *4*	ε, α
150m	5.8 m *2*	ε
150m	3.48 h *16*	ε, α<0.05%
151	17.609 h *1*	ε, α 0.0095%
151m	25 s *3*	IT 93.8%, ε 6.2%
152	17.5 h *1*	ε, α<7.0×10^{-7}%
152m	4.2 m *1*	IT 78.9%, ε 21.1%
153	2.34 d *1*	ε
154	21.5 h *4*	ε, β-<0.1%
154m	9.0 h *5*	ε 78.2%, IT 21.8% β-<0.1%
154m	22.7 h *5*	ε 98.2%, IT 1.8%
155	5.32 d *6*	ε
156	5.35 d *10*	ε, β-?
156m	24.4 h *10*	IT
156m	5.3 h *2*	ε, IT
157	99 y *10*	ε
158	180 y *11*	ε 83.4%, β- 16.6%
158m	10.5 s *2*	IT, β-<0.6%, ε<0.01%
159	100%	
160	72.3 d *2*	β-
161	6.88 d *3*	β-
162	7.76 m *10*	β-
163	19.5 m *3*	β-
164	3.0 m *1*	β-
165	2.11 m *10*	β-

Isotope Z El A	T1/2 or Abundance	Decay Mode
66 Dy 141	0.9 s *2*	ε, εp
142	2.3 s *3*	ε, εp≈8.0×10^{-5}%
143	3.9 s *4*	ε, εp
144	9.1 s *4*	ε, εp
145m	13.6 s *10*	ε
146	29 s *3*	ε
146m	150 ms *20*	IT
147	40 s *10*	ε, εp
147m	55.7 s *5*	ε 67%, IT 33%
148	3.1 m *1*	ε
149	4.23 m *18*	ε
150	7.17 m *5*	ε 64%, α 36%
151	17.9 m *3*	ε 94.4%, α 5.6%
152	2.38 h *2*	ε 99.9%, α 0.1%
153	6.4 h *1*	ε 99.99%, α 9.4×10^{-3}%
154	3.0×10^{6} y *15*	α
155	10.0 h *3*	ε
156	0.06% *1*	
157	8.14 h *4*	ε
158	0.10% *1*	
159	144.4 d *2*	ε
160	2.34% *5*	
161	18.9% *1*	
162	25.5% *2*	
163	24.9% *2*	
164	28.2% *2*	
165	2.334 h *6*	β-
165m	1.257 m *6*	IT 97.76%, β- 2.24%
166	81.6 h *1*	β-
167	6.20 m *8*	β-
168	8.5 m *5*	β-
67 Ho 144	0.7 s *1*	ε, εp
146	3.6 s *3*	ε, εp
147	5.8 s *4*	ε, εp
148	2.2 s *11*	ε
148m	9.59 s *15*	ε, εp 0.08%
149	>30 s	ε
149m	21.4 s *18*	ε
150	26 s *2*	ε
150	72 s *4*	ε
151	35.2 s *1*	ε 78%, α 22%
151m	47.2 s *10*	α>40%
152	161.8 s *3*	ε 88%, α 12%
152m	49.5 s *3*	ε 89.2%, α 10.8%
153	2.0 m *1*	ε 99.95%, α 0.05%
153m	9.3 m *5*	ε 99.82%, α 0.18%
154	11.8 m *5*	ε 99.98%, α 0.02%
154m	3.25 m *10*	ε, α<0.001%
155	48 m *1*	α, ε
156	56 m *1*	ε
157	12.6 m *2*	ε
158	11.3 m *4*	ε
158m	27 m *2*	IT>81%, ε<19%
158m	21.3 m *23*	ε
159	33.05 m *1*	ε
159m	8.30 s	IT
160	25.6 m *3*	ε
160m	5.02 h *5*	IT 65%, ε 35%
160m	3 s	
161	2.48 h *5*	ε
161m	6.76 s *7*	IT
162	15 m *1*	ε
162m	67.0 m *10*	IT 63%, ε 37%
163	4570 y *25*	ε

TABLE OF NUCLIDES (cont.)

Isotope Z El A	T1/2 or Abundance	Decay Mode
67 Ho 163m	1.09 s 3	IT
164	29 m 1	ε 60%, β- 40%
164m	37.5 m +15-5	IT
165	100%	
166	26.80 h 2	β-
166m	1.20×10³ y 18	β-
167	3.1 h 1	β-
168	2.99 m 7	β-
169	4.7 m 1	β-
170	2.76 m 5	β-
170m	43 s 2	β-
68 Er 147	2.5 s 2	ε, εp
147m	≈2.5 s	ε, εp
148	4.6 s 2	ε
149	10.7 s 4	ε, εp
149m	10.8 s 6	ε, εp, IT
150	18.5 s 7	ε
151	23.5 s 13	ε
152	10.3 s 1	α 90%, ε 10%
153	37.1 s 2	α 53%, ε 47%
154	3.68 m 15	ε 99.53%, α 0.47%
155	5.3 m 3	ε 99.98%, α 0.02%
156	19.5 m 10	ε
157	18.65 m 10	ε, α?
158	2.24 h 7	ε
159	36 m 1	ε
160	28.58 h 9	ε
161	3.21 h 3	ε
162	0.14% 1	
163	75.0 m 4	ε
164	1.61% 1	
165	10.36 h 4	ε
166	33.6% 2	
167	22.95% 13	
167m	2.269 s 6	IT
168	26.8% 2	
169	9.40 d 2	β-
170	14.9% 1	
171	7.52 h 3	β-
172	49.3 h 3	β-
173	1.4 m 1	β-
174	3.3 m 2	β-
69 Tm 147	0.56 s 4	ε≈90%, p≈10%
148m	0.7 s 2	ε
149	0.9 s 2	ε
150	2.3 s 4	ε
151m	4.13 s 11	ε
151m	5.2 s 20	ε
152	5.2 s 6	ε
152m	8.0 s 10	ε
153	1.48 s 1	α 91%, ε 9%
153m	2.5 s 2	α 95%, ε 5%
154	3.30 s 7	α 90%, ε 10%
154	8.1 s 3	ε 56%, α 44%
155	32 s 7	ε>94%, α<6%
156	83.8 s 18	ε 99.91%, α 0.09%
156m	19 s 3	α
157	3.5 m 2	ε
158	4.02 m 10	ε
158m	≈20 s	
159	9.15 m 17	ε
160	9.4 m 3	ε
160m	74.5 s 15	ε 15%
161	33 m 3	ε
162	21.7 m 2	ε
162m	24.3 s 17	IT 82%, ε 18%
163	1.810 h 5	ε
69 Tm 164	2.0 m 1	ε
164	5.1 m 1	IT≈80%, ε≈20%
165	30.06 h 3	ε
166	7.70 h 3	ε
167	9.25 d 2	ε
168	93.1 d 2	ε 99.99%, β- 0.01%
169	100%	
170	128.6 d 3	β- 99.85%, ε 0.15%
171	1.92 y 1	β-
172	63.6 h 2	β-
173	8.24 h 8	β-
174	5.4 m 1	β-
175	15.2 m 5	β-
176	1.9 m 1	β-
177	130 s 40	
70 Yb 151	≈1.6 s	ε, εp
151m	≈1.6 s	ε, εp
152	3.1 s 2	ε
153	4.2 s 1	α 50%, ε 50%
154	0.402 s 17	α≈98%, ε≈2%
155	1.72 s 12	α 84%, ε 16%
156	26.1 s 7	ε 90%, α 10%
157	38.6 s 10	ε 99.5%, α 0.5%
158	1.57 m 9	ε, α≈0.003%
159	1.40 m 20	ε
160	4.8 m 2	ε
161	4.2 m 2	ε
162	18.87 m 19	ε
163	11.05 m 25	ε
164	75.8 m 17	ε
165	9.9 m 3	ε
166	56.7 h 1	ε
167	17.5 m 2	ε
168	0.13% 1	
169	32.022 d 8	ε
169m	46 s 2	IT
170	3.05% 5	
171	14.3% 2	
172	21.9% 3	
173	16.12% 18	
174	31.8% 4	
175	4.19 d 1	β-
176	12.7% 1	
176m	11.4 s 3	IT≥90%, β-<10%
177	1.9 h 1	β-
177m	6.41 s 2	IT
178	74 m 3	β-
179	8.1 m 8	β-
180	2.4 m 5	β-
71 Lu 151	85 ms 10	p
152	0.7 s 1	ε
154	0.96 s 10	ε
155	70 ms 6	α 79%, ε 21%
155m	2.60 ms 7	α
156	≈0.5 s	α≈70%, ε
156m	0.18 s 2	α≈95%, ε?, IT?
157	5.4 s 2	ε 94%, α 6%
158	10.4 s 1	ε>98.5%, α<1.5%
159	12.3 s 1	ε, α 0.04%
160	35.5 s 8	ε
161	72 s	ε
162	1.37 m 2	ε
162m	1.5 m	ε
162m	1.9 m	ε
163	238 s 8	ε

TABLE OF NUCLIDES (cont.)

Isotope Z El A	T1/2 or Abundance	Decay Mode
71 Lu 164	3.14 m *3*	ε
165m	10.74 m *10*	ε
165n	12 m	
166	2.65 m *10*	ε
166m	1.41 m *10*	ε 58%, IT 42%
166n	2.12 m *10*	ε>80%, IT<20%
167	51.5 m *10*	ε
168	5.5 m *1*	ε
168m	6.7 m *4*	ε>95%, IT<5%
169	34.06 h *5*	ε
169m	160 s *10*	IT
170	2.00 d *3*	ε
170m	0.67 s *10*	IT
171	8.24 d *3*	ε
171m	79 s *2*	IT
172	6.70 d *3*	ε
172m	3.7 m *5*	IT
173	1.37 y *1*	ε
174	3.31 y *5*	ε
174m	142 d *2*	IT 99.38%, ε 0.62%
175	97.41% *2*	
176	3.78×10^{10} y *2*	β-
	2.59% *2*	
176m	3.635 h *3*	β- 99.91%, ε 0.1%
177	6.71 d *1*	β-
177m	160.9 d *3*	β- 79%, IT 21%
178	28.4 m *2*	β-
178m	23.1 m *3*	β-
179	4.59 h *6*	β-
180	5.7 m *1*	β-
181	3.5 m *3*	β-
182	2.0 m *2*	β-
183	58 s *4*	β-
184	≈20 s	β-
72 Hf 154	2 s *1*	α?, ε
155	0.89 s *12*	α, ε
156	25 ms *4*	α
157	110 ms *6*	α 91%, ε 9%
158	2.9 s *2*	ε 54%, α 46%
159	5.6 s *5*	ε 88%, α 12%
160	≈12 s	ε 97.7%, α 2.3%
161	17 s *2*	α, ε
162	37.6 s *8*	ε 99.99%, α 0.01%
163	40.0 s *6*	ε
164	2.8 m *2*	ε
165	1.7 m *1*	ε
166	6.77 m *30*	ε
167	2.05 m *5*	ε
168	25.95 m *20*	ε
169	3.24 m *4*	ε
170	16.01 h *13*	ε
171	12.1 h *4*	ε
172	1.87 y *3*	ε
173	23.6 h *1*	ε
174	2.0×10^{15} y *4*	α
	0.162% *2*	
175	70 d *2*	ε
176	5.206% *4*	
177	18.606% *3*	
177m	1.08 s *6*	IT
177n	51.4 m *5*	IT
178	27.297% *3*	
178m	4.0 s *2*	IT
178n	31 y *1*	IT
179	13.629% *5*	
179m	18.67 s *3*	IT
72 Hf 179n	25.1 d *3*	IT
180	35.100% *6*	
180m	5.5 h *1*	IT≥98.6%, β-<1.4%
181	42.39 d *6*	β-
182	9×10^{8} y *2*	β-
182m	61.5 m *15*	β- 58%, IT 42%
183	1.067 h *17*	β-
184	4.12 h *5*	β-
73 Ta 157	5.3 ms *18*	α>77%
158	36.8 ms *16*	α 93%, ε 7%
159	0.57 s *18*	α 80%, ε 20%
160	1.4 s *2*	α
161	2.7 s *2*	ε≈95%, α≈5%
162	3.52 s *12*	α, ε
163	11.0 s *8*	ε≈99.8%, α≈0.2%
164	14.2 s *3*	ε 99.98%, α 0.02%
165	31.0 s *15*	ε
166	34.4 s *5*	ε
167	1.4 m *3*	ε
168	2.44 m *35*	ε
169	4.9 m *4*	ε
170	6.76 m *6*	ε
171	23.3 m *3*	ε
172	36.8 m *3*	ε
173	3.14 h *13*	ε
174	1.05 h *3*	ε
175	10.5 h *2*	ε
176	8.09 h *5*	ε
177	56.6 h *1*	ε
178	9.31 m *3*	ε
178	2.36 h *8*	ε
179	1.79 y *8*	ε
180	8.152 h *6*	ε 86%, β- 14%
180m	$>1.2\times10^{15}$ y	
	0.012% *2*	
181	99.988% *2*	
182	114.43 d *3*	β-
182m	283 ms *3*	IT
182n	15.84 m *10*	IT
183	5.1 d *1*	β-
184	8.7 h *1*	β-
185	49 m *2*	β-
186	10.5 m *5*	β-
74 W 158	≈1.4 ms	α
159	7.3 ms *27*	α
160	81 ms *15*	α
161	410 ms *40*	α≈82%, ε≈18%
162	1.39 s *4*	ε 54%, α 46%
163	2.75 s *25*	ε 59%, α 41%
164	6.4 s *8*	ε 97.4%, α 2.6%
165	5.1 s *5*	ε>98.5%, α<1.5%
166	16 s *3*	ε 99.4%, α 0.6%
167	19.9 s *5*	α, ε
168	53 s *2*	ε
169	1.3 m *1*	ε
170	4 m *1*	ε
171	2.4 m *1*	ε, α
172	6.7 m *10*	ε
173m	7.97 m *27*	ε
174	31 m *1*	ε
175	34 m *1*	ε
176	2.5 h *1*	ε
177	135 m *3*	ε
178	21.6 d *3*	ε
179	37.5 m *5*	ε

TABLE OF NUCLIDES (cont.)

Isotope Z	El	A	T1/2 or Abundance	Decay Mode
74	W	179m	6.4 m *1*	IT 99.72%, ε 0.28%
		180	0.12% *3*	
		181	121.2 d *2*	ε
		182	26.3% *2*	
		183	14.28% *5*	
		183m	5.2 s *3*	IT
		184	$>3\times10^{17}$ y 30.7% *2*	
		185	75.1 d *3*	β-
		185m	1.67 m *3*	IT
		186	28.6% *2*	
		187	23.72 h *6*	β-
		188	69.4 d *5*	β-
		189	11.5 m *3*	β-
		190	30.0 m *15*	β-
75	Re	161	10 ms *+15-5*	α
		162	100 ms *30*	α
		163	260 ms *40*	α 64%, ε 36%
		164	0.88 s *24*	α 58%, ε 42%
		165	2.4 s *6*	ε 87%, α 13%
		166	2.2 s *4*	α, ε
		167	6.1 s *2*	ε≈99.3%, α≈0.7%
		168	6.9 s *8*	α, ε
		168m	6.6 s *15*	α, ε
		169m	12.9 s *11*	α
		170	8.0 s *5*	ε
		171	15.2 s	α
		172	15 s *3*	α, ε
		172m	55 s *5*	α, ε, IT
		173	1.98 m *26*	ε
		174	2.40 m *4*	ε
		175	5.8 m	ε
		176	5.3 m *3*	ε
		177	14.0 m *10*	ε
		178	13.2 m *2*	ε
		179	19.5 m *1*	ε
		180	2.44 m *6*	ε
		181	19.9 h *7*	ε
		182	64.0 h *5*	ε
		182m	12.7 h *2*	ε
		183	70.0 h *14*	ε
		184	38.0 d *5*	ε
		184m	169 d *8*	IT 75.4%, ε 24.6%
		185	37.40% *2*	
		186	90.64 h *9*	β- 93.1%, ε 6.9%
		186m	2.0×10^{5} y *5*	IT, β-<10%
		187	4.35×10^{10} y *13*	β-, α<1.0×10^{-4}%
			62.60% *2*	
			62.60% *2*	
		188	16.98 h *2*	β-
		188m	18.6 m *1*	IT
		189	24.3 h	β-
		190	3.1 m *3*	β-
		190m	3.2 h *2*	β- 54.4%, IT 45.6%
		191	9.8 m *5*	β-
		192	16 s *1*	β-
76	Os	163	?	α, ε
		164	41 ms *20*	α, ε
		165	65 ms *+70-30*	α≥60%, ε≤40%
		166	181 ms *38*	α 72%, ε 28%
		167	0.83 s *12*	α 67%, ε 33%
		168	2.2 s *1*	ε 51%, α 49%
		169	3.2 s *2*	ε 84%, α 16%
		170	7.1 s *2*	ε 88%, α 12%
		171	8.0 s *7*	ε 98.3%, α 1.7%
76	Os	172	19 s *2*	ε 99.8%, α 0.2%
		173	16 s *5*	ε 99.98%, α 0.02%
		174	44 s *4*	ε 99.98%, α 0.02%
		175	1.4 m *1*	ε
		176	3.6 m *5*	ε
		177	2.8 m	ε
		178	5.0 m *4*	ε
		179	6.5 m *3*	ε
		180	21.5 m *4*	ε
		181	2.7 m *1*	ε
		181m	105 m *3*	ε
		182	22.10 h *25*	ε
		183	13.0 h *5*	ε
		183m	9.9 h *3*	ε 85%, IT 15%
		184	$>5.6\times10^{13}$ y 0.02% *1*	
		185	93.6 d *5*	ε
		186	2.0×10^{15} y *11* 1.58% *10*	α
		187	1.6% *1*	
		188	13.3% *2*	
		189	16.1% 3	
		189m	5.8 h *1*	IT
		190	26.4% *4*	
		190m	9.9 m *1*	IT
		191	15.4 d *1*	β-
		191m	13.10 h *5*	IT
		192	41.0% 3	
		192m	6.1 s	IT
		193	30.5 h *4*	β-
		194	6.0 y *2*	β-
		195	6.5 m	β-
		196	34.9 m *2*	β-
77	Ir	166	>5 ms	α
		167	>5 ms	α
		168	?	α
		169	0.4 s *1*	α
		170	1.05 s *15*	α 75%, ε 25%
		171	1.5 s *1*	α, ε?
		172	2.1 s *1*	ε≈97%, α≈3%
		173	3.0 s *10*	ε 97.98%, α 2.02%
		174	4 s *1*	ε 99.53%, α 0.47%
		175	4.5 s *10*	α
		176	8 s *1*	ε 97.9%, α 2.1%
		177	21 s *2*	α
		178	12 s *2*	ε
		179	4 m *1*	ε
		180	1.5 m *1*	ε
		181	4.90 m *15*	ε
		182m	15 m *1*	ε
		183	57 m *4*	ε
		184	3.09 h *3*	ε
		185	14.4 h *1*	ε
		186	16.64 h *3*	ε
		186m	2.0 h *1*	ε, IT
		187	10.5 h *3*	ε
		188	41.5 h *5*	ε
		189	13.2 d *1*	ε
		190	11.78 d *10*	ε
		190m	1.2 h	IT
		190m	3.25 h *20*	ε 94.4%, IT 5.6%
		191	37.3% *5*	
		191m	4.94 s *3*	IT
		191m	5.5 s *7*	IT
		192	73.831 d *8*	β- 95.4%, ε 4.6%
		192m	1.45 m *5*	IT 99.98%, β- 0.02%

TABLE OF NUCLIDES (cont.)

Isotope Z El A	T1/2 or Abundance	Decay Mode
77 Ir 192m	241 y *9*	IT
193	62.7% *5*	
193m	10.53 d *4*	IT
194	19.15 h *3*	β-
194m	171 d *11*	β-
195	2.5 h *2*	β-
195m	3.8 h *2*	β- 95%, IT 5%
196	52 s *2*	β-
196m	1.40 h *2*	β-
197	5.8 m *5*	β-
197m	8.9 m *3*	β- 99.75%, IT 0.25%
198	8 s *1*	β-
78 Pt 168	?	α
169	2.5 ms *+25-1*	α
170	6 ms *+5-2*	α
171	25 ms *9*	α
172	0.10 s *1*	α 98%, ε 2%
173	342 ms *18*	α 84%, ε 16%
174	0.90 s *1*	α 83%, ε 17%
175	2.52 s *8*	α 64%, ε
176	6.33 s *15*	ε 62%, α 38%
177	11 s *2*	ε 91%, α 9%
178	21.0 s *6*	ε 92.3%, α 7.7%
179	43 s *10*	ε 99.76%, α 0.24%
180	52 s *3*	ε, α≈0.3%
181	51 s *5*	ε, α≈0.06%
182	2.2 m *1*	ε≈99.98%, α≈0.02%
183	6.5 m *10*	ε, α≈0.0013%
183m	43 s *5*	ε, IT
184	17.3 m *2*	ε, α≈0.001%
185	70.9 m *24*	ε
185m	33.0 m *8*	ε 99%, IT<2%
186	2.0 h *1*	ε, α≈1.4×10^{-4}%
187	2.35 h *3*	ε
188	10.2 d *3*	ε, α 2.6×10^{-5}%
189	10.87 h *12*	ε
190	6.5×10^{11} y *3* 0.01% *1*	α
191	2.9 d *1*	ε
192	0.79% *5*	
193	50 y *9*	ε
193m	4.33 d *3*	IT
194	32.9% *5*	
195	33.8% *5*	
195m	4.02 d *1*	IT
196	25.3% *5*	
197	18.3 h *3*	β-
197m	95.41 m *18*	IT 96.7%, β- 3.3%
198	7.2% *2*	
199	30.8 m *4*	β-
199m	13.6 s *4*	IT
200	12.5 h *3*	β-
201	2.5 m *1*	β-
79 Au 173	59 ms *+45-18*	α
174	120 ms *20*	α>0%
175	0.20 s *2*	α
176	1.25 s *30*	α, ε
177	1.3 s *4*	α
178	2.6 s *5*	ε≤60%, α≥40%
179	7.5 s *4*	ε 78%, α 22%
180	8.1 s *3*	ε≤98.2%, α≥1.8%
181	11.4 s *5*	ε 98.5%, α 1.5%
182	21 s *1*	ε, α 0.038%
183	42.0 s *12*	ε 99.64%, α 0.36%
184	53.0 s *14*	ε, α 0.02%
79 Au 185	4.3 m *1*	ε 99.9%, α 0.1%
185m	6.8 m *3*	ε, IT
186	10.7 m *5*	ε
187	8.4 m *3*	ε, α 3.0×10^{-3}%
187m	2.3 s *1*	IT
188	8.84 m *6*	ε
189	28.7 m *3*	ε, α<3.0×10^{-5}%
189m	4.59 m *11*	ε, IT>0%
190	42.8 m *10*	ε, α<1.0×10^{-6}%
191	3.18 h *8*	ε
191m	0.92 s *11*	IT
192	4.94 h *9*	ε
193	17.65 h *15*	ε
193m	3.9 s *3*	IT 99.97%, ε≈0.03%
194	38.02 h *10*	ε
195	186.09 d *4*	ε
195m	30.5 s *2*	IT
196	6.183 d *10*	ε 92.5%, β- 7.5%
196m	8.1 s *2*	IT
196m	9.7 h *1*	IT
197	100%	
197m	7.73 s *6*	IT
198	2.6935 d *4*	β-
198m	2.30 d *4*	IT
199	3.139 d *7*	β-
200	48.4 m *3*	β-
200m	18.7 h *5*	β- 82%, IT 18%
201	26 m *1*	β-
202	28.8 s *19*	β-
203	53 s *2*	β-
204	39.8 s *9*	β-
80 Hg 175	≈20 ms	α
176	34 ms *+18-9*	α≈100%
177	0.17 s *5*	α≈85%, ε≈15%
178	0.26 s *3*	α≈50%, ε≈50%
179	1.09 s *4*	α≈53%, ε≈47%, εp≈0.15%
180	3.0 s *3*	ε 51%, α 49%
181	3.6 s *3*	ε 64%, α 36%
182	11.3 s *5*	ε 84.8%, α 15.2%
183	8.8 s *5*	ε 74.5%, α 25.5%, εp 0.06%
184	30.6 s *3*	ε 98.89%, α 1.11%
185	49 s *1*	ε 94%, α 6%
185m	21 s *1*	IT 54%, ε 46%, α≈0.03%
186	1.38 m *7*	ε 99.98%, α 0.02%
187	2.4 m *3*	ε, α>1.2×10^{-4}%
187m	1.9 m *3*	ε, α>2.5×10^{-4}%
188	3.25 m *15*	ε, α 3.7×10^{-5}%
189	7.6 m *1*	ε, α<3.0×10^{-5}%
189m	8.6 m *1*	ε, α<3.0×10^{-5}%
190	20.0 m *5*	ε, α<5.0×10^{-5}%
191	49 m *10*	ε
191m	50.8 m *15*	ε
192	4.85 h *20*	ε
193	3.80 h *15*	ε
193m	11.8 h *2*	ε 92.9%, IT 7.1%
194	520 y *32*	ε
195	9.9 h *5*	ε
195m	41.6 h *8*	IT 54.2%, ε 45.8%
196	0.15% *1*	
197	64.14 h *5*	ε
197m	23.8 h *1*	IT 93%, ε 7%
198	9.97% *8*	
199	16.87% *10*	

TABLE OF NUCLIDES (cont.)

Isotope Z El A	T1/2 or Abundance	Decay Mode
80 Hg 199m	42.6 m *2*	IT
200	23.10% *16*	
201	13.10% *8*	
202	29.86% *20*	
203	46.612 d *18*	β-
204	6.87% *4*	
205	5.2 m *1*	β-
206	8.15 m *10*	β-
207	2.9 m *2*	β-
81 Tl 179	0.16 s *+9-4*	α
179m	1.4 ms *5*	α
182		α
183m	60 ms *15*	α
184	11 s *1*	ε 97.9%, α 2.1%
185m	1.8 s *1*	α, IT
186m	27.5 s *10*	ε, α 6.0×10^{-4}%
186m	2.9 s *2*	IT
187	≈51 s	ε<100%, α>0%
187m	15.60 s *12*	ε<100%, IT<100%, α>0%
188m	71 s *2*	ε
188m	71 s *1*	ε
189	2.3 m *2*	ε
189m	1.4 m *1*	ε, IT<4%
190m	2.6 m *3*	ε
190m	3.7 m *3*	ε
191m	5.22 m *16*	ε
192	9.6 m *4*	ε
192	10.8 m *2*	ε
193	21.6 m *8*	ε
193m	2.11 m *15*	IT 75%, ε 25%
194	33.0 m *5*	ε, α<1.0×10^{-7}%
194m	32.8 m *2*	ε
195	1.16 h *5*	ε
195m	3.6 s *4*	IT
196	1.84 h *3*	ε
196m	1.41 h *2*	ε 95.5%, IT 4.5%
197	2.84 h *4*	ε
197m	0.54 s *1*	IT
198	5.3 h *5*	ε
198m	1.87 h *3*	ε 56%, IT 44%
199	7.42 h *8*	ε
200	26.1 h *1*	ε
201	72.912 h *17*	ε
202	12.23 d *2*	ε
203	29.524% *9*	
204	3.78 y *2*	β- 97.43%, ε 2.57%
205	70.476% *9*	
206	4.199 m *15*	β-
206m	3.74 m *3*	IT
207	4.77 m *2*	β-
207m	1.33 s *11*	IT, β-<0.1%
208	3.053 m *4*	β-
209	2.20 m *7*	β-
210	1.30 m *3*	β-, β-n 0.007%
82 Pb 182	55 ms *+40-35*	α
183	300 ms *80*	α
184	0.55 s *6*	α
185	4.1 s *3*	α
186	4.79 s *5*	α
187m	15.2 s *3*	α, ε
187m	18.3 s *3*	ε 98%, α 2%
188	24.2 s *10*	ε 78%, α 22%
189m	51 s 3	ε>99%, α≈0.4%
190	1.2 m *1*	ε 99.1%, α 0.9%
191	1.33 m *8*	ε 99.99%, α 0.01%
82 Pb 191m	2.18 m *8*	ε
192	3.5 m *1*	ε 99.99%, α 0.01%
193	?	ε
193m	5.8 m *2*	ε
194	12.0 m *5*	ε, α 7.3×10^{-6}%
195	≈15 m	ε
195m	15.0 m *12*	ε
196	37 m *3*	ε, α<0.0001%
197	8 m *2*	ε
197m	43 m *1*	ε 81%, IT 19%, α<3.0×10^{-4}%
198	2.40 h *10*	ε
199	90 m *10*	ε
199m	12.2 m *3*	IT 93%, ε 7%
200	21.5 h *4*	ε
201	9.33 h *3*	ε
201m	61 s *2*	IT>99%, ε<1%
202	52.5×10^{3} y *28*	ε, α<1%
202m	3.53 h *1*	IT 90.5%, ε 9.5%
203	51.873 h *9*	ε
203m	6.3 s *2*	IT
203m	0.46 s *2*	IT
204	≥1.4×10^{17} y 1.4% *1*	
204m	67.2 m *3*	IT
205	1.52×10^{7} y *7*	ε
206	24.1% *1*	
207	22.1% *1*	
207m	0.805 s *10*	IT
208	52.4% *1*	
209	3.253 h *14*	β-
210	22.3 y *2*	β-, α 1.9×10^{-6}%
211	36.1 m *2*	β-
212	10.64 h *1*	β-
213	10.2 m *3*	β-
214	26.8 m *9*	β-
83 Bi 187	35 ms *4*	α>50%
187m	8 ms *6*	α
188m	44 ms *3*	α, ε
188m	0.21 s *9*	α, ε
189	680 ms *30*	α>50%, ε<50%
190m	6.2 s *1*	α 68%, ε 32%
190m	6.3 s *1*	α 82%, ε 18%
191	12 s *1*	α 60%, ε 40%
191m	150 ms *15*	α>50%, ε<50%
192	37 s *3*	α 18%, ε
192	39.6 s *4*	α 9.2%, ε
193	67 s *3*	ε 95%, α 5%
193m	3.2 s *7*	α 90%, ε≈10%
194	106 s *3*	ε
194m	92 s *5*	ε 99.93%, α 0.07%
194m	125 s *2*	ε 99.79%, α 0.21%
195	183 s *4*	ε 99.97%, α 0.03%
195m	87 s *1*	ε 67%, α 33%
196m	4.6 m *5*	ε, IT
196m	5 m	ε
197	UNKNOWN	ε, α 1.0×10^{-4}%
197m	5.2 m *6*	α 55%, ε 45%, IT<0.3%
198	11.85 m *18*	ε
198m	7.7 s *5*	IT
199	27 m *1*	ε
199m	24.70 m *15*	ε 99%, IT≤2%, α≈0.01%
200	36.4 m *5*	ε
200m	31 m *2*	ε>90%, IT<10%
200m	0.40 s *5*	IT

TABLE OF NUCLIDES (cont.)

Isotope Z El A	T1/2 or Abundance	Decay Mode
83 Bi 201	108 m *3*	ε, α<1×10⁻⁴%
201m	59.1 m *6*	ε>93%, IT≤6.8%, α≈0.3%
202	1.72 h *5*	ε, α<1×10⁻⁵%
203	11.76 h *5*	ε, α≈1.0×10⁻⁵%
204	11.22 h *10*	ε
205	15.31 d *4*	ε
206	6.243 d *3*	ε
207	32.2 y *9*	ε
208	3.68×10⁵ y *4*	ε
209	100%	
210	5.013 d *5*	α 1.3×10⁻⁴%, β-
210m	3.0×10⁶ y *1*	α
211	2.14 m *2*	α 99.72%, β- 0.28%
212	60.55 m *6*	β- 64.06%, α 35.94%, β-α 0.014%
212m	25 m	α≤93%, β-≥7%
212m	9 m	β-
213	45.59 m *6*	β- 97.84%, α 2.16%
214	19.9 m *4*	β- 99.98%, α 0.02%
215	7.4 m *6*	β-
84 Po 192	0.034 s *3*	α
193m	260 ms *20*	α
193m	360 ms *50*	α
194	0.44 s *6*	α
195	4.5 s *5*	α 75%, ε 25%
195m	2.0 s *2*	α≈90%, ε≈10%, IT<0.01%
196	5.5 s *5*	α, ε
197	56 s *3*	ε 56%, α 44%, α 44%
197m	26 s *2*	α 84%, α 84%, ε 16%, IT 0.01%
198	1.76 m *3*	α 70%, ε 30%
199	5.2 m *1*	ε 88%, α 12%
199m	4.2 m *1*	ε 59%, α 39%, IT 2.1%
200	11.5 m *1*	ε 85%, α 15%
201	15.3 m *2*	ε 98.4%, α 1.6%
201m	8.9 m *2*	ε 57%, IT 40%, α≈2.9%
202	44.7 m *5*	ε 98%, α 2%
203	34.8 m *14*	ε 99.89%, α 0.11%
203m	1.2 m *2*	IT, ε 4.5%, α≈0.04%
204	3.53 h *2*	ε 99.34%, α 0.66%
205	1.66 h *2*	ε 99.96%, α 0.04%
206	8.8 d *1*	ε 94.55%, α 5.45%
207	5.80 h *2*	ε 99.98%, α 0.02%
207m	2.8 s *2*	IT
208	2.898 y *2*	α, ε
209	102 y *5*	α 99.74%, ε 0.26%
210	138.376 d *2*	α
211	0.516 s *3*	α
211m	25.2 s *6*	α
212	0.298 μs *3*	α
212m	45.1 s *6*	α
213	4.2 μs *8*	α
214	164.3 μs *20*	α
215	1.780 ms *4*	α, β- 0.0002%
216	0.145 s *2*	α
217	<10 s	α>95%, β-<5%
218	3.10 m *1*	α 99.98%, β- 0.02%
85 At 194	0.18 s *8*	α
195	?	α>75%, ε<25%
196	0.3 s *1*	α
197	0.35 s *4*	α 96%, ε 4%
197m	3.7 s *25*	α≤100%, ε
198	4.9 s *5*	α, ε
198m	1.5 s *3*	α, ε, IT
199	7.2 s *5*	α 90%, ε 10%
200	43 s *2*	ε 65%, α 35%
200m	4.3 s *3*	IT≈80%, α≈10%, ε≈10%
201	89 s *3*	α 71%, ε 29%
202	181 s *3*	ε 88%, α 12%
202m	≤1.5 s	IT
203	7.4 m *2*	ε 69%, α 31%
204	9.2 m *2*	ε 95.7%, α 4.3%
205	26.2 m *5*	ε 90%, α 10%
206	30.0 m *6*	ε 99.11%, α 0.89%
207	1.80 h *4*	ε 91.3%, α 8.7%
208	1.63 h *3*	ε 99.45%, α 0.55%
209	5.41 h *5*	ε 95.9%, α 4.1%
210	8.1 h *4*	ε 99.82%, α 0.18%
211	7.214 h *7*	ε 58.3%, α 41.7%
212	0.314 s *2*	α
212m	0.119 s *3*	α
213	0.11 μs *2*	α
214	558 ns *10*	α
214m	265 ns *30*	α
214m	760 ns *15*	α
215	0.10 ms *2*	α
216	0.30 ms *3*	α, ε<0.006%, β-<3×10⁻⁷%
217	32.3 ms *4*	α 99.99%, β- 0.01%
218	1.6 s *4*	α 99.9%, β- 0.1%
219	0.9 m *1*	α 97%, β- 3%
221	2.3 m *2*	β-
86 Rn 198		α, ε
198m	50 ms *9*	α, ε, IT
199	0.62 s *3*	α 95%, ε 5%
199m	0.3 s *1*	α, ε
200	1.06 s *2*	α≈98%, ε≈2%
201	7.0 s *4*	α≈80%, ε≈20%
201m	3.8 s *4*	α≈90%, ε≈10%, IT
202	9.85 s *20*	ε<30%, α
203	45 s *3*	α 66%, ε 34%
203m	28 s *2*	α≈80%, ε≈20%, IT<0.1%
204	1.24 m *3*	α 68%, ε 32%
205	170 s *4*	ε 77%, α 23%
206	5.67 m *17*	α 62%, ε 38%
207	9.3 m *2*	ε 77%, α 23%
208	24.35 m *14*	α 62%, ε 38%
209	28.5 m *10*	ε 83%, α 17%
210	2.4 h *1*	α 96%, ε 4%
211	14.6 h *2*	ε 74%, α 26%
212	24 m *2*	α
213	25.0 ms *2*	α
214	0.27 μs *2*	α
214m	0.7 ns *3*	α
214m	6.5 ns *30*	α
215	2.30 μs *10*	α
216	45 μs *5*	α
217	0.54 ms *5*	α
218	35 ms *5*	α
219	3.96 s *1*	α
220	55.6 s *1*	α
221	25 m *2*	β- 78%, α 22%

TABLE OF NUCLIDES (cont.)

Isotope Z El A	T1/2 or Abundance	Decay Mode
86 Rn 222	3.8235 d *3*	α
223	23 m *1*	β-
224	107 m *3*	β-
225	4.5 m *3*	β-
226	6.0 m *5*	β-
227	23 s *1*	β-
228	65 s *2*	β-
87 Fr 201	48 ms *15*	α, ε<1%
202	0.34 s *4*	α≈97%, ε≈3%
203	0.55 s *2*	α≈95%, ε≈5%
204	2.1 s *2*	α≈80%, ε≈20%
205	3.85 s *10*	α, ε<1%
206	15.9 s *2*	α 88%, ε 12%
206m	0.7 s *1*	α
207	14.8 s *1*	α 95%, ε 5%
208	59.1 s *3*	α 90%, ε 10%
209	50.0 s *3*	α 89%, ε 11%
210	3.18 m *6*	α 60%, ε 40%
211	3.10 m *2*	α>70%, ε<30%
212	20.0 m *6*	ε 57%, α 43%
213	34.6 s *3*	α 99.45%, ε 0.55%
214	5.0 ms *2*	α
214m	3.35 ms *5*	α
215	0.12 μs	α
216	0.70 μs *2*	α, ε<2×10^{-7}%
217	22 μs *5*	α
218	1.0 ms *6*	α
219	21 ms *1*	α
220	27.4 s *3*	α 99.65%, β- 0.35%
221	4.9 m *2*	α, β-<0.1%
222	14.2 m *3*	β-
223	21.8 m *4*	β- 99.99%, α 0.01%
224	3.30 m *10*	β-
225	4.0 m *2*	β-
226	48 s *1*	β-
227	2.48 m *3*	β-
228	39 s *1*	β-
229	50 s *20*	β-
230	19.1 s *5*	β-
231	17.5 s *8*	β-
88 Ra 206	0.24 s *2*	α≈100%
207	1.3 s *2*	α≈90%, ε≈10%
208	1.3 s *2*	α 95%, ε 5%
209	4.6 s *2*	α
210	3.7 s *2*	α 96%, ε 4%
211	13 s *2*	α>93%, ε<7%
212	13.0 s *2*	α≈94%, ε≈6%
213	2.74 m *6*	α 80%, ε 20%
213m	2.1 ms *1*	IT 99%, α 1%
214	2.46 s *3*	α 99.94%, ε 0.06%
215	1.59 ms *9*	α
216	182 ns *10*	α, ε
217	1.6 μs *2*	α
218	25.6 μs *11*	α
219	10 ms *3*	α
220	25 ms *5*	α
221	28 s *2*	α
222	38.0 s *5*	α, ^{14}C 3×10^{-6}%
223	11.434 d *2*	α, ^{14}C w
224	3.66 d *4*	α, ^{12}C 4.3×10^{-9}%
225	14.9 d *2*	β-
226	1600 y *7*	α, ^{14}C 3×10^{-9}%
227	42.2 m *5*	β-
228	5.75 y *3*	β-
229	4.0 m *2*	β-
88 Ra 230	93 m *2*	β-
231	1.72 m *5*	β-
232	250 s *50*	β-
89 Ac 209	0.10 s *5*	α
210	0.35 s *5*	α 96%, ε 4%
211	0.25 s *5*	α>99.8%, ε<0.2%
212	0.93 s *5*	α≈98%, ε≈2%
213	0.80 s *5*	α
214	8.2 s *2*	α≥89%, ε≤11%
215	0.17 s *1*	α 99.91%, ε 0.09%
216	≈0.33 ms	α
216m	0.33 ms *2*	α
217	0.07 μs *1*	α
217m	0.74 μs *4*	α
218	1.12 μs *11*	α
219	7 μs *2*	α
220	26.1 ms *5*	α, ε 5×10^{-4}%
221	52 ms *2*	α
222	5.0 s *5*	α 99%, ε≤2%
222m	63 s *4*	α≥88%, IT≤10%, ε≤2%
223	2.2 m *1*	α 99%, ε 1%
224	2.9 h *2*	ε 90.9%, α 9.1%, β-<1.6%
225	10.0 d *1*	α
226	29.4 h *1*	β- 83%, ε 17%, α 0.006%
227	21.773 y *3*	β- 98.62%, α 1.38%
228	6.15 h *2*	β-, α 5×10^{-6}%
229	62.7 m *5*	β-
230	122 s *3*	β-
231	7.5 m *1*	β-
232	119 s *5*	β-
233	145 s *10*	β-
234	44 s *7*	β-
90 Th 212	30 ms *20*	α
213	150 ms *25*	α
214	100 ms *25*	α
215	1.2 s *2*	α
216	0.028 s *2*	α, ε≈0.006%
216	0.18 ms *4*	IT≈97%, α≈3%
217	0.252 ms *7*	α
218	109 ns *13*	α
219	1.05 μs *3*	α
220	9.7 μs *6*	α, ε 2×10^{-7}%
221	1.68 ms *6*	α
222	2.8 ms *3*	α
223	0.66 s *1*	α
224	1.05 s *2*	α
225	8.72 m *4*	α≈90%, ε≈10%
226	30.6 m *1*	α
227	18.718 d *5*	α
228	1.9131 y *9*	α
229	7340 y *160*	α
230	7.538×10^{4} y *30*	α, SF?
231	25.52 h *1*	β-, α w
232	1.405×10^{10} y *6* 100%	α, SF?
233	22.3 m *1*	β-
234	24.10 d *3*	β-
235	7.2 m *2*	β-
236	37.5 m *2*	β-
91 Pa 215	≈14 ms	α
216	0.20 s *4*	α≈80%, ε≈20%
217	4.9 ms *6*	α

TABLE OF NUCLIDES (cont.)

Isotope Z El A	T1/2 or Abundance	Decay Mode
91 Pa 217m	1.6 ms *8*	α
218	0.12 ms *+4-2*	α
221	5.9 μs *17*	α
222	≈4.3 ms	α
223	6.5 ms *10*	α
224	0.95 s *15*	α 99.9%, ε 0.1%
225	1.7 s *2*	α
226	1.8 m *2*	α 74%, ε 26%
227	38.3 m *3*	α≈85%, ε≈15%
228	22 h *1*	ε 98.15%, α 1.85%
229	1.50 d *5*	ε 99.52%, α 0.48%
230	17.4 d *5*	ε 91.6%, β- 8.4%, α w
231	3.276×10^4 y *11*	α, SF?
232	1.31 d *2*	β-, ε≈0.2%
233	26.967 d *2*	β-
234	6.70 h *5*	β-
234m	1.17 m *3*	β- 99.87%, IT 0.13%
235	24.4 m *2*	β-
236	9.1 m *2*	β-, SF w
237	8.7 m *2*	β-
238	2.3 m *1*	β-
92 U 222	1.0 μs *+10-4*	α
225	50 ms *30*	α
226	0.5 s *2*	α
227	1.1 m *3*	α
228	9.1 m *2*	α>95%, ε<5%
229	58 m *3*	ε≈80%, α≈20%
230	20.8 d	α
231	4.2 d *1*	ε, α 0.006%
232	68.9 y *4*	α, SF w
233	1.592×10^5 y *2*	α, SF<6.0×10^{-9}%
234	2.45×10^5 y *2*	α, SF w
	0.0055% *5*	
235	703.8×10^6 y *5*	α, SF w
	0.720% *1*	
235m	≈25 m	IT
236	2.3415×10^7 y *14*	α, SF w
237	6.75 d *1*	β-
238	4.468×10^9 y *3*	α,
	99.2745% *15*	SF 0.0001%
239	23.50 m *5*	β-
240	14.1 h *1*	β-, α
242	16.8 m *5*	β-
93 Np 228	1.00 m *8*	SF?
229	4.0 m *2*	α>50%, ε<50%
230	4.6 m *3*	ε≤97%, α≥3%
231	48.8 m *2*	ε 98%, α 2%
232	14.7 m *3*	ε, α≈0.003%
233	36.2 m *1*	ε, α≤1.0×10^{-3}%
234	4.4 d *1*	ε
235	396.2 d *12*	ε, α 0.0014%
236	115×10^3 y *12*	ε 91%, β- 8.9%, α
236m	22.5 h *4*	ε 52%, β- 48%
237	2.14×10^6 y *1*	α, SF≤2×10^{-1}%
238	2.117 d *2*	β-
239	2.355 d *4*	β-
240	7.22 m *2*	β- 99.89%
240	61.9 m *2*	β-
240m	7.22 m *2*	IT 0.11%
241	13.9 m *2*	β-
242	2.2 m *2*	β-
242	5.5 m *1*	β-
94 Pu 232	34.1 m *7*	ε≈80%, α≈20%
233	20.9 m *4*	ε 99.88%, α 0.12%
234	8.8 h *1*	ε 94%, α 6%
94 Pu 235	25.3 m *10*	ε, α 0.0027%
236	2.87 y *1*	α, SF w
237	45.2 d *1*	ε, α 0.004%
237m	0.18 s *2*	IT
238	87.74 y *4*	α, SF w
239	24119 y *26*	α, SF
240	6563 y *7*	α, SF 5.7×10^{-6}%
241	14.35 y *10*	β-, α
242	3.733×10^5 y *12*	α, SF 5.5×10^{-4}%
243	4.956 h *3*	β-
244	8.08×10^7 y *10*	α 99.88%, SF 0.12%
245	10.5 h *1*	β-
246	10.84 d *2*	β-
247	2.27 d *23*	β-
95 Am 232	55 s *7*	ε≈98%, α≈2%, εSF
234	2.6 m *2*	α?, ε
237	73.0 m *10*	ε 99.98%, α 0.02%
238	98 m *2*	ε>99.99%, α 0.0001%
239	11.9 h *1*	ε 99.99%, α 0.01%
240	50.8 h *3*	ε, α 1.9×10^{-4}%
241	432.7 y *6*	α, SF
242	16.02 h *2*	β- 82.7%, ε 17.3%
242m	141 y *2*	IT 99.54%, α 0.46%, SF
243	7380 y *40*	α, SF w
244	10.1 h *1*	β-
244m	≈26 m	β- 99.96%, ε 0.04%
245	2.05 h *1*	β-
246	39 m *3*	β-
246m	25.0 m *2*	β-, IT<0.01%
247	23.0 m *13*	β-
248	?	β-
96 Cm 238	2.4 h *1*	ε≥90%, α≤10%
239	≈2.9 h	ε, α<0.1%
240	27 d *1*	α>99.5%, ε<0.5%
240	27 d *1*	SF 3.9×10^{-6}%
241	32.8 d *2*	ε 99%, α 1%
242	162.79 d *9*	α, SF 6.2×10^{-6}%
243	29.1 y *1*	α 99.76%, ε 0.24%
244	18.10 y *2*	α, SF 1×10^{-4}%
245	8500 y *100*	α, SF w
246	4730 y *100*	α 99.97%, SF 0.03%
247	1.56×10^7 y *5*	α
248	3.40×10^5 y *4*	α 91.74%, SF 8.26%
249	64.15 m *3*	β-
250	9700 y	SF≈80%, α≈11%, β-≈9%
251	16.8 m *2*	β-
252	<2 d	β-
97 Bk 240	4.8 m *8*	ε≈100%, εSF w
242	7.0 m *13*	ε
243	4.5 h *2*	ε 99.85%, α 0.15%
244	4.35 h *15*	ε 99.99%, α 0.006%
245	4.94 d *3*	ε 99.88%, α 0.12%
246	1.80 d *2*	ε, α<0.2%
247	1380 y *250*	α
248	23.7 h *2*	β- 70%, ε 30%, α<0.001%
248	>9 y	α>70%
249	320 d *6*	β-, α 1.4×10^{-3}%, SF 4.7×10^{-8}%

TABLE OF NUCLIDES (cont.)

Isotope Z	El	A	T1/2 or Abundance	Decay Mode
97	Bk	250	3.217 h *5*	$\beta-$
		251	55.6 m *11*	$\beta-$, $\alpha\approx1.0\times10^{-5}$%
98	Cf	239	42 s	α
		240	1.06 m *15*	$\alpha\approx100$%
		241	3.78 m *70*	$\varepsilon\approx90$%, $\alpha\approx10$%
		242	3.49 m *12*	α, ε?
		243	10.7 m *5*	$\varepsilon\approx86$%, $\alpha\approx14$%
		244	19.4 m *6*	α
		245	43.6 m *8*	$\varepsilon\approx70$%, $\alpha\approx30$%
		246	35.7 h *5*	α, $\varepsilon<5.0\times10^{-4}$%, SF 2.0×10^{-4}%
		247	3.11 h *3*	ε 99.96%, α 0.03%
		248	333.5 d *28*	α, SF 0.0029%
		249	351 y *2*	α, SF 5.2×10^{-7}%
		250	13.08 y *9*	α 99.92%, SF 0.08%
		251	898 y *44*	α
		252	2.645 y *8*	α 96.91%, SF 3.09%
		253	17.81 d *8*	$\beta-$ 99.69%, α 0.31%
		254	60.5 d *2*	SF 99.69%, α 0.31%
		255	85 m *18*	$\beta-$
		256	12.3 m *12*	SF, $\beta-<1$%, $\alpha\approx1.0\times10^{-6}$%
99	Es	243	21 s *2*	$\varepsilon\leq70$%, $\alpha\geq30$%
		244	37 s *4*	ε 96%, α 4%
		245	1.33 m *15*	ε 60%, α 40%
		246	7.7 m *5*	ε 90.1%, α 9.9%
		247	4.7 m *3*	$\varepsilon\approx93$%, $\alpha\approx7$%
		248	27 m *4*	$\varepsilon>99$%, $\alpha\approx0.25$%
		249	102.2 m *6*	ε 99.43%, α 0.57%
		250	2.22 h *5*	$\varepsilon\geq99$%, $\alpha\leq1$%
		250	8.6 h *1*	$\varepsilon>97$%, $\alpha<3$%
		251	33 h *1*	ε 99.51%, α 0.49%
		252	471.7 d *19*	α 76%, ε 24%, $\beta-\approx0.01$%
		253	20.47 d *3*	α, SF 8.7×10^{-6}%
		254	275.7 d *5*	α, $\varepsilon<1.0\times10^{-4}$%, SF $<3.0\times10^{-6}$%, $\beta-$ 1.7×10^{-6}%
		254m	39.3 h *2*	$\beta-$ 98%, IT<3%, α 0.33%, ε 0.08%, SF<0.05%
		255	39.8 d *12*	$\beta-$ 92%, α 8%, SF 4.1×10^{-3}%
		256	25.4 m *24*	$\beta-$
		256	≈7.6 h	$\beta-$
100	Fm	242	0.8 ms *2*	SF
		243	0.18 s *+8-4*	α 40%
		244	3.7 ms *4*	SF
		245	4.2 s *13*	α
		246	1.1 s *2*	α 92%, SF 8%, $\varepsilon\leq1$%
		247	35 s *4*	α 50%, ε 50%
		247	9.2 s *23*	α
		248	36 s *3*	α 99%, $\varepsilon\approx1$%, SF≈0.05%
		249	2.6 m *7*	$\varepsilon\approx85$%, $\alpha\approx15$%
		250	30 m *3*	$\alpha>90$%, $\varepsilon<10$%, SF $\approx6.0\times10^{-4}$%
		250m	1.8 s *1*	IT>80%
		251	5.30 h *8*	ε 98.2%, α 1.8%
		252	25.39 h *5*	α, SF 0.0023%
		253	3.00 d *12*	ε 88%, α 12%
100	Fm	254	3.240 h *2*	α 99.94%, SF 0.06%
		255	20.07 h *7*	α, SF 2.4×10^{-5}%
		256	157.6 m *13*	SF 91.9%, α 8.1%
		257	100.5 d *2*	α 99.79%, SF 0.21%
		258	370 μs *43*	SF
		259	1.5 s *3*	SF
101	Md	247	3 s	α
		248	7 s *3*	ε 80%, α 20%
		249	24 s *4*	$\alpha\approx70$%, $\varepsilon\approx30$%
		250	52 s *6*	ε 93%, α 7%
		251	4.0 m *5*	$\varepsilon\geq90$%, $\alpha\leq10$%
		252	2.3 m *8*	$\alpha<50$%, $\varepsilon>50$%
		253		α, ε
		254	10 m *3*	ε
		254	28 m *8*	ε
		255	27 m *2*	ε 92%, α 8%
		256	76 m *4*	ε 90.7%, α 9.3%, SF<3%
		257	5.3 h *3*	ε 90%, α 10%, SF<4%
		258	60 m *2*	ε
		258	55 d *4*	α
		259	103 m *12*	SF>97%, $\alpha<3$%
		260	31.8 d *5*	SF≈70%, $\alpha\leq25$%, $\varepsilon<15$%, $\beta-<10$%
102	No	250	0.25 ms *5*	SF, $\alpha\approx0.05$%
		251	0.8 s *3*	$\alpha\approx100$%, $\varepsilon\approx1$%
		252	2.30 s *22*	α 73.1%, SF 26.9%
		253	1.7 m *3*	$\alpha\approx80$%, $\varepsilon\approx20$%
		254	55 s *3*	α 90%, ε 10%, SF 0.25%
		254m	0.28 s *4*	IT>80%
		255	3.1 m *2*	α 61.4%, ε 38.6%
		256	3.3 s *2*	α 99.8%, SF≤0.25%
		257	25 s *2*	$\alpha\approx100$%
		258	≈1.2 ms	SF, α 0.001%
		259	58 m *5*	α 75%, ε 25%, SF<10%
		260	106 ms *8*	SF
103	Lr	252	≈1 s	$\alpha\approx90$%, $\varepsilon\approx10$%, SF<1%
		253	1.3 s *+6-3*	α 90%, SF<20%, $\varepsilon\approx1$%
		254	13 s *2*	α 78%, ε 22%, SF<0.1%
		255	22 s *4*	α 85%, $\varepsilon<30$%
		256	28 s *3*	$\alpha>80$%, $\varepsilon<20$%, SF<0.03%
		257	0.646 s *25*	α
		258	4.3 s *5*	$\alpha>95$%, $\varepsilon<5$%
		259	5.4 s *8*	$\alpha>50$%, SF<50%, $\varepsilon<0.5$%
		260	180 s *30*	α 75%, $\varepsilon\approx15$%, SF<10%
		261	39 m *12*	SF
		262	3.6 h *3*	ε
104	Rf	253	≈1.8 s	$\alpha\approx50$%, SF≈50%
		254	0.5 ms *2*	SF, $\alpha\approx0.3$%
		255	1.5 s *2*	SF 52%, α 48%
		256	6.7 ms *2*	SF 98%, α 2.2%
		257	4.7 s *3*	α 79.6%, ε 18%, SF 2.4%

TABLE OF NUCLIDES (cont.)

Isotope Z El A	T1/2 or Abundance	Decay Mode
104 Rf 258	12 ms *2*	SF≈87%, α≈13%
259	3.1 s *7*	α 93%, SF 7%, ε≈0.3%
260	20.1 ms *7*	SF≈98%, α≈2%
261	65 s *10*	α>80%, ε≤10%, SF<10%
262	47 ms *5*	SF
105 Ha 255	1.6 s *+6-4*	α≈80%, SF≈20%
256	2.6 s *+14-8*	α≤90%, SF≤40%, ε≈10%
257	1.3 s *+5-3*	α 82%, SF 17%, ε 1%
258	4.4 s *+9-6*	α 67%, ε 33%, SF<1%
258	20 s *10*	ε
259	? ?	
260	1.52 s *13*	α≥90%, SF≤9.6%, ε<2.5%
105 Ha 261	1.8 s *4*	α>50%, SF<50%
262	34 s *4*	SF 71%, α 26%, ε≈3%
263	26 m *2*	α≤100%
106 259	0.48 s *+28-1*	α 90%, SF<20%
260	3.6 ms *+9-6*	α 50%, SF 50%
261	0.23 s *3*	α 95%, SF<10%
263	0.8 s *2*	SF≈70%, α≈30%
107 260		α
261	11.8 ms *+53-2*	α 95%, SF<10%
262	102 ms *26*	α≥80%, SF≤20%
262m	8.0 ms *21*	α>70%, SF<30%
108 263	?	α
264	0.08 ms *+40-4*	α
265	1.8 ms *+22-7*	α≈100%
109 266	3.4 ms *+16-13*	α

Chapter 3

PROMPT GAMMA RAYS FROM THERMAL NEUTRON CAPTURE

Extracted from the database

A catalogue of γ rays emitted following thermal neutron capture in natural elements is given in two tables. A diskette for these tables is enclosed in the book. In the first table, γ rays are arranged by element and by γ ray energy; the γ ray energy, energy uncertainty and γ ray intensity are given. In the second table, the γ rays are arranged in the order of increasing energy. Each line contains the γ ray energy and intensity, and the element identification. Listed are only prompt γ rays from thermal neutron capture in all elements with Z = 1 through Z = 83 (except ^{61}Pm) and in ^{232}Th; γ rays with intensities higher than 2% are included. The intensities are given in terms of γ rays emitted per 100 neutron radiative captures. Gamma rays from decays of the residual nuclei are not included. Gamma ray energy uncertainties in the first table are given in keV. The complete database was published in Ref. [1].

REFERENCE

[1] LONE, M.A., LEAVITT, R.A., HARRISON, D.A., Prompt gamma rays from thermal-neutron capture, At. Data Nucl. Data Tables **26** (1981) 511.

Chapter 4

NUCLEAR DECAY GAMMA RAYS WITH INTENSITIES HIGHER THAN 5%

An extract from the ENSDF radioactivity database

The table (for which a diskette is enclosed in the book) contains data on γ rays with intensities higher than 5%, extracted from the computer based catalogue developed by Ekstroem and Spanier [1]. The γ rays are ordered by energy, which makes the table very useful for identifying the decaying nuclides. Gamma rays with energies higher than 120 keV are listed. These limitations had to be introduced to cut down the volume of the table to the acceptable limit. It should be understood that there may be decays in which the most intense γ line has an intensity of less than 5%. Such decays will not be listed in the table. Usually, such nuclides are not important for practical geophysics applications. Data for all known isotopic species are included in the Table of Nuclides (Chapter 2) in this Handbook.

EXPLANATION OF THE TABLE

Column 1

Energy of the γ rays in keV.

Column 2

Uncertainty of the γ ray energy; the values corrspond to the last digits in column 1, e.g. 120.17 $\pm$ 10 keV or 120.34 $\pm$ 5 keV.

Column 3

Intensity of the γ rays and its uncertainty. If a % sign is given at the right of the intensity field, the intensity is given in normalized units: γ ray intensity per 100 decays. For internally converted transitions, only the fraction of the intensity that decays by γ rays is listed (no % sign). The uncertainty is given in the same way as in column 2.

Column 4

Parent nucleus and decay mode. B+ is positron decay, B− is electron decay, EC is electron capture and IT means isomeric transition.

Column 5

Half-lives of the nuclides in the following units:

AS	attoseconds	(10^{-18} s)	S	seconds
FS	femtoseconds	(10^{-15} s)	M	minutes
PS	picoseconds	(10^{-12} s)	H	hours
NS	nanoseconds	(10^{-9} s)	D	days (24 H)
US	microseconds	(10^{-6} s)	Y	years (365.256 D)
MS	milliseconds	(10^{-3} s)		

Column 6

Uncertainty of the half-life values.

Column 7

The two most intensive γ rays in the decay. This column is useful for identifying the unknown γ ray.

REFERENCE

[1] EKSTROEM, P., SPANIER, L., The ENSDF Radioactivity Data Base for IBM-PC and Computer Network Access, Rep. LUNFDG/(NFFR-3059)/1-11, Lund University, Lund (1989).

Chapter 5

SPECTRA OF NEUTRON SOURCES

This chapter contains data for the following most widely used sources:

Am–Be source
Pu–Be source
^{252}Cf fission neutron source
14 MeV neutron generator using the D–T reaction

5.1. ISOTOPIC (α,n) SOURCES

Isotopic (α,n) sources consist of a mixture of α emitting radioactive isotopes with light nuclei. The α particles interact with light nuclei, and neutrons are emitted as a result of (α,n) and (α,α') reactions. A number of different light elements produce neutrons when they are bombarded by α particles from the decay of heavy elements. As an example, yields of neutrons for different light elements bombarded with α particles from the decay of ^{210}Po are shown in Table 5.1 [1].

TABLE 5.1. (α,n) REACTIONS ON LIGHT NUCLEI

Target	Q-values	Neutron yield per 10^6 alphas
^{7}Li	−2.79	2.6
^{9}Be	5.70	80
^{10}B	1.60	13
^{11}B	0.16	26
^{13}C	2.22	10
^{18}O	−0.70	29
^{19}F	−1.95	12

As can be seen from the table, beryllium gives the highest neutron yield. Some of the elements listed cannot be incorporated directly into a source and only their chemical compounds can be used. This reduces the neutron yield. The most convenient light element to be used in a source is beryllium, and practically all commercially manufactured isotopic neutron sources actually use this element.

A similar situation exists in the case of α radioactive heavy isotopes. The main requirements for them to be used in neutron sources are a sufficiently long half-life and a low γ ray emission. A reasonable compromise for these two quantities is found in the case of ^{239}Pu and ^{241}Am. This explains why the most widely used isotopic sources are made on the basis of ^{239}Pu–^{9}Be or ^{241}Am–^{9}Be mixtures.

When using isotopic neutron sources it is necessary to take into account variations of the neutron emission with time and modifications in the spectrum caused by interactions of neutrons inside the source.

Corrections of the half-life can easily be dealt with, but, in the case of ^{239}Pu, one should know the quantities of ^{240}Pu and ^{241}Pu that are usually present in commercial materials as impurities. The appropriate corrections of the decay and growth should be inserted.

The physical composition and mass of a neutron source can affect its spectrum to some extent. The causes for spectrum deformation are the following [1]:

— Elastic and inelastic neutron collisions within the source;
— Neutron induced fission within the α emitter;
— The ^{9}Be(n,2n) reaction;
— The ^{9}Be(γ,n) reaction (occurs only with ^{226}Ra);
— Reduction of the effective α energy by slowing down of the α particle within the α emitting cluster.

For sources not exceeding 2 cm in capsule dimensions, the first three causes do not deform the spectrum by more than the existing uncertainties. For larger source dimensions, some softening of the neutron spectrum should be expected.

There is also another reason why small sources should be preferred: the neutron emission from such sources is very close to isotropic, and no corrections for neutron emission angles are needed. For larger sources, which usually have a cylindrical shape, the angular anisotropy of the neutron emission should be measured and corrected for. In general, for cylindrical sources, the neutron emission is peaked sideways and is minimal in the direction of the cylinder axis.

Spectral distortion by the last of the five causes listed above is a function of the size of the clusters of α emitting material. The latter should be made as small as possible and should be much smaller than the range of emitted α particles. The proper fabrication process usually produces homogeneous sources in the form of alloys or very fine powder mixtures (5–10 μm particles). For such sources the neutron spectrum is reproducible enough; it was calculated and compared with experimental measurements in Refs [2, 3]. We have digitized these data and put them into ENDF/B-like format for ^{241}Am–^{9}Be and ^{239}Pu–^{9}Be neutron isotopic sources. The data are presented in Fig. 5.1.

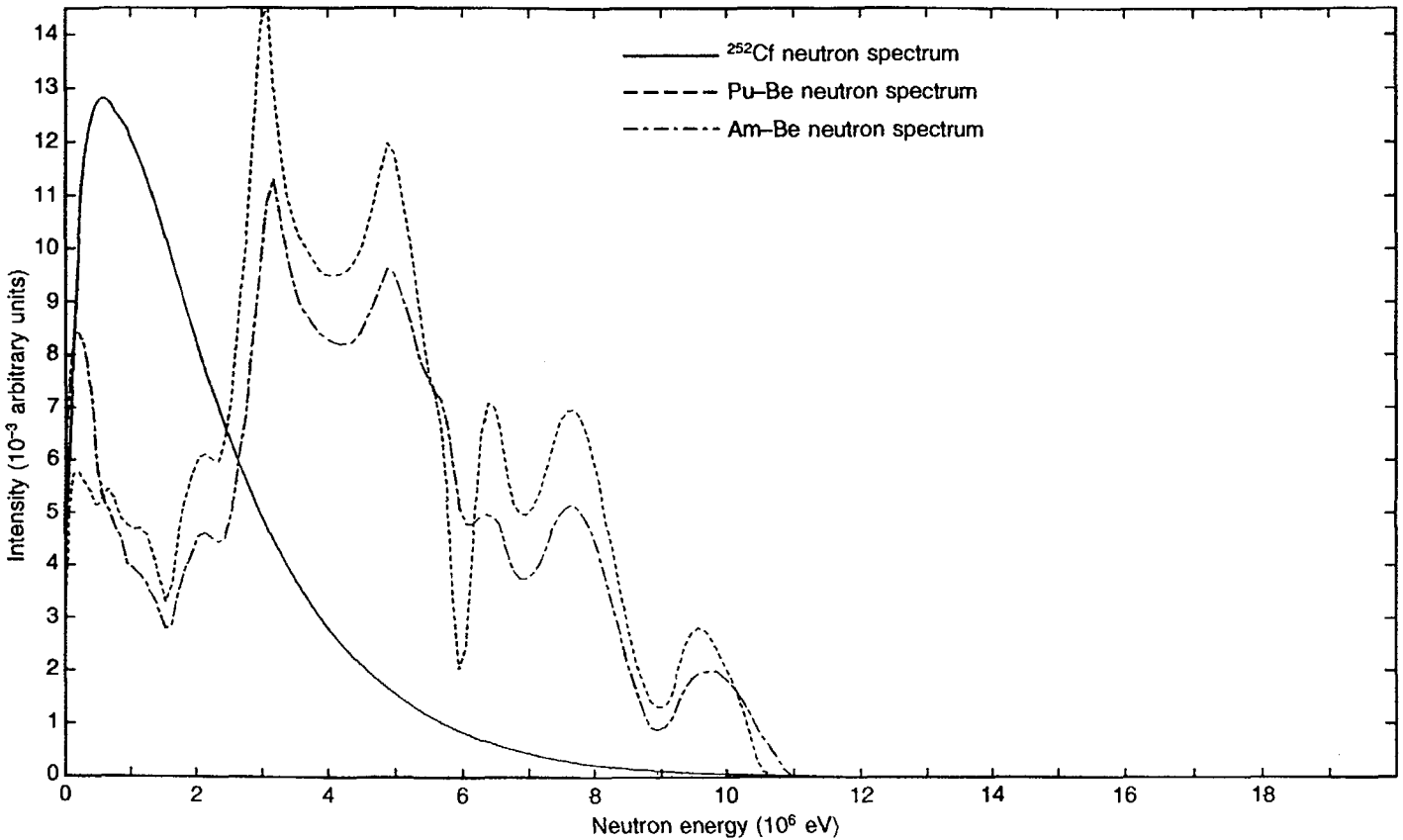

FIG. 5.1. Neutron spectra from isotopic sources.

TABLE 5.2. EVALUATED SPECTRAL DISTRIBUTION OF THE ^{252}Cf FISSION NEUTRON SOURCE

E_L (MeV)	E_U (MeV)	Average value	Relative standard deviation[a] (%)
0.0	0.5	1.253×10^{-1}	3.79
0.5	1.0	1.691×10^{-1}	1.01
1.0	1.5	1.544×10^{-1}	1.63
1.5	2.0	1.294×10^{-1}	1.16
2.0	2.5	1.034×10^{-1}	0.95
2.5	3.0	8.056×10^{-2}	1.75
3.0	3.5	6.160×10^{-2}	1.76
3.5	4.0	4.650×10^{-2}	1.25
4.0	4.5	3.480×10^{-2}	1.95
4.5	5.0	2.587×10^{-2}	1.96
5.0	5.5	1.913×10^{-2}	1.96
5.5	6.0	1.408×10^{-2}	1.97
6.0	6.5	1.025×10^{-2}	2.15
6.5	7.0	7.376×10^{-3}	2.15
7.0	8.0	3.793×10^{-3}	2.15
8.0	8.5	2.675×10^{-3}	5.32
8.5	9.0	1.912×10^{-3}	5.37
9.0	9.5	1.363×10^{-3}	5.46
9.5	10.0	9.695×10^{-4}	5.53
10.0	11.0	1.177×10^{-3}	5.39
11.0	12.0	5.863×10^{-4}	5.60
12.0	13.0	2.839×10^{-4}	7.40
13.0	14.0	1.502×10^{-4}	6.39
14.0	15.0	7.663×10^{-5}	6.48
15.0	16.0	3.790×10^{-5}	7.07
16.0	17.0	1.860×10^{-5}	7.64
17.0	18.0	9.150×10^{-6}	7.97
18.0	19.0	4.503×10^{-6}	8.15
19.0	20.0	2.215×10^{-6}	8.24

[a] Correlation matrix given in Table 5.3.

TABLE 5.3. CORRELATION MATRIX OF THE EVALUATED ^{252}Cf FISSION NEUTRON SOURCE

Energy range (MeV)	Correlation matrix (×100)																												
0.0 – 0.5	100																												
0.5 – 1.0	-57	100																											
1.0 – 1.5	-48	44	100																										
1.5 – 2.0	-44	19	-3	100																									
2.0 – 2.5	-53	6	-15	57	100																								
2.5 – 3.0	-29	-17	-20	-11	40	100																							
3.0 – 3.5	-29	-16	-19	-10	41	68	100																						
3.5 – 4.0	-36	-10	-19	-4	18	27	27	100																					
4.0 – 4.5	-20	-3	-9	1	-11	-19	-18	53	100																				
4.5 – 5.0	-20	-2	-9	1	-10	-18	-18	54	72	100																			
5.0 – 5.5	-20	-2	-9	2	-9	-18	-17	54	72	72	100																		
5.5 – 6.0	-20	-2	-9	2	-9	-17	-17	54	72	72	72	100																	
6.0 – 6.5	-18	13	1	15	10	-4	-4	-2	-1	-0	-0	-0	100																
6.5 – 7.0	-18	13	1	16	10	-4	-3	-2	-0	-0	-0	-0	76	100															
7.0 – 7.5	-18	13	1	16	11	-4	-3	-1	-0	-0	0	0	76	76	100														
7.5 – 8.0	-18	13	1	16	11	-4	-3	-1	-0	0	0	0	76	76	76	100													
8.0 – 8.5	7	-6	-3	-6	-6	-2	-2	-4	-3	-3	-4	-4	-20	-20	-21	-21	100												
8.5 – 9.0	6	-6	-3	-6	-6	-2	-2	-4	-3	-3	-3	-3	-19	-20	-20	-20	36	100											
9.0 – 9.5	6	-5	-3	-5	-5	-1	-1	-4	-3	-3	-3	-3	-18	-19	-19	-19	37	37	100										
9.5 – 10	6	-5	-3	-5	-5	-1	-1	-3	-3	-3	-3	-3	-18	-18	-19	-19	38	38	39	100									
10 – 11	6	-5	-3	-5	-5	-1	-1	-3	-3	-3	-3	-3	-19	-19	-19	-20	36	37	38	39	100								
11 – 12	6	-5	-3	-5	-5	-1	-1	-3	-3	-3	-3	-3	-17	-18	-18	-18	38	39	40	41	39	100							
12 – 13	1	-1	-1	-0	-1	-0	-0	0	1	1	1	1	1	1	1	1	-5	-5	-5	-5	-5	-8	100						
13 – 14	1	-1	-1	-0	-1	-1	-1	0	1	1	1	1	1	1	1	1	2	2	2	2	2	-0	-17	100					
14 – 15	1	-1	-1	-0	-1	-1	-0	0	1	1	1	1	1	1	1	1	4	4	4	3	4	3	-6	-26	100				
15 – 16	0	-1	-1	-0	-0	-0	-0	0	1	1	1	1	1	1	1	1	3	3	3	3	3	2	3	-15	-14	100			
16 – 17	0	-0	-1	-0	-0	-0	-0	0	1	1	1	1	1	1	1	1	2	2	2	2	2	1	7	-6	-5	2	100		
17 – 18	0	-0	-1	0	-0	-0	-0	0	1	1	1	1	1	1	1	1	2	2	2	2	2	1	10	-2	-0	6	12	100	
18 – 19	0	-0	-1	0	-0	-0	-0	0	1	1	1	1	1	1	1	1	2	1	1	1	1	0	12	0	2	9	14	17	100
19 – 20	0	-0	-1	0	-0	-0	-0	0	1	1	1	1	1	1	1	1	1	1	1	1	1	0	12	2	4	10	15	17	19	100

Taken from Technical Reports Series No. 273, p. 176.

5.2. NEUTRON SPECTRUM OF SPONTANEOUS FISSION OF ^{252}Cf

At present, the ^{252}Cf spontaneous fission neutron field is the only one which is technically easy to realize and reproduce with the highest degree of reliability. This is the reason why the ^{252}Cf neutron field was chosen as an international standard in 1976 [4]. Since then, considerable effort was devoted to measurements and theoretical calculations of this spectrum. The most recent evaluation and the most complete one is by Mannhart [5]. We give the results of his evaluation. This is based on the available integral measurement results and implicitly takes into account some recent direct spectrum measurements. The covariance information for this evaluation is most complete and up to date. The spectral distribution (normalized to 1) and its standard deviations in per cent are given in Table 5.2. The correlation matrix for the same energy grid structure is given in Table 5.3.

For a quick reference, it may be convenient to use the older evaluation by Heaton et al. [6] from the former United States National Bureau of Standards; this evaluation is given analytically.

The following analytical expression for the neutron spectrum of ^{252}Cf is given in Ref. [6]:

$$X_{\mathrm{Cf}}(E) = [0.6672\sqrt{E}\exp(-E/1.42)]\,\mu(E) \quad (E \text{ in MeV})$$

The values of $\mu(E)$ should be taken from the following list:

Energy interval (MeV)	$\mu(E)$
0 – 0.25	$0.763 + 1.20\,E$
0.25 – 0.8	$1.098 - 0.14\,E$
0.8 – 1.5	$0.9668 + 0.024\,E$
1.5 – 6.0	$1.0037 - 0.00062\,E$
6.0 – 20	$\exp[-0.03(E-6.0)]$

The deviations from Mannhart's evaluation will be within the standard deviations shown in Table 5.2 for neutron energies below 12 MeV and somewhat higher in the 12–20 MeV range.

5.3. 14 MeV D–T NEUTRON GENERATORS

Fast monoenergetic neutrons can be produced by nuclear reactions induced by projectiles from an accelerator. The D–T reaction is the one most widely used for this purpose. The deuterons are accelerated in electrostatic generators up to energies above the threshold of the T(d,n)^{4}He reaction which produces neutrons with energies of around 14 MeV. The D–T interaction can proceed through several different channels, and the yields of different channels depend on the kinetic energy of the accelerated incident deuterons and on the angle at which the neutrons are emitted. Table 5.4 [7] summarizes the Q-values, the energy thresholds and the neutron energies for the D–T reaction at 0° neutron emission angle in the laboratory system.

TABLE 5.4. Q-VALUES, THRESHOLDS AND NEUTRON ENERGIES AT 0°_{lab} FOR THE D–T REACTION

Exit channel	n + ^{4}He	n + p + t	2n + ^{3}He	n + d + d	2n + p + d	3n + 2p
E_{in}	$E_n(0^\circ_{lab})$	$E_{n\,max1}$	$E_{n\,max2}$	$E_{n\,max3}$	$E_{n\,max4}$	$E_{n\,max5}$
0.000	14.028					
3.711	20.461	0.298				
4.985	21.964	2.000	0.400			
10.443	27.891	7.356	6.416	0.838		
14.159	31.717	10.006	5.763	1.136		
17.876	35.465	14.472	13.573	9.521	6.414	1.435
Q-values	17.589	-2.225	-2.988	-6.257	-8.482	-10.707

The D–T interaction at low energies of incident deuterons mainly proceeds through the T(d,n)^{4}He channel. This reaction has a resonance with a large cross-section at 107 keV. The Q-value of the reaction (+17.59 MeV) is very high and, therefore, 14 MeV neutrons can be produced with low energy accelerators. Reviews of such 14 MeV neutron generators can be found in Refs [7, 8].

The energy of the neutrons depends on the angle of emission relative to the beam direction; it is maximal at 0°_{lab} and decreases with the increase of the emission angle. This feature is used in experiments; targets can be irradiated with neutrons of different energies, depending on the position of the irradiated samples relative to the neutron producing target. The intensity of the neutron beam also depends on the emission angle. These dependences are shown in Figs 5.2 to 5.4.

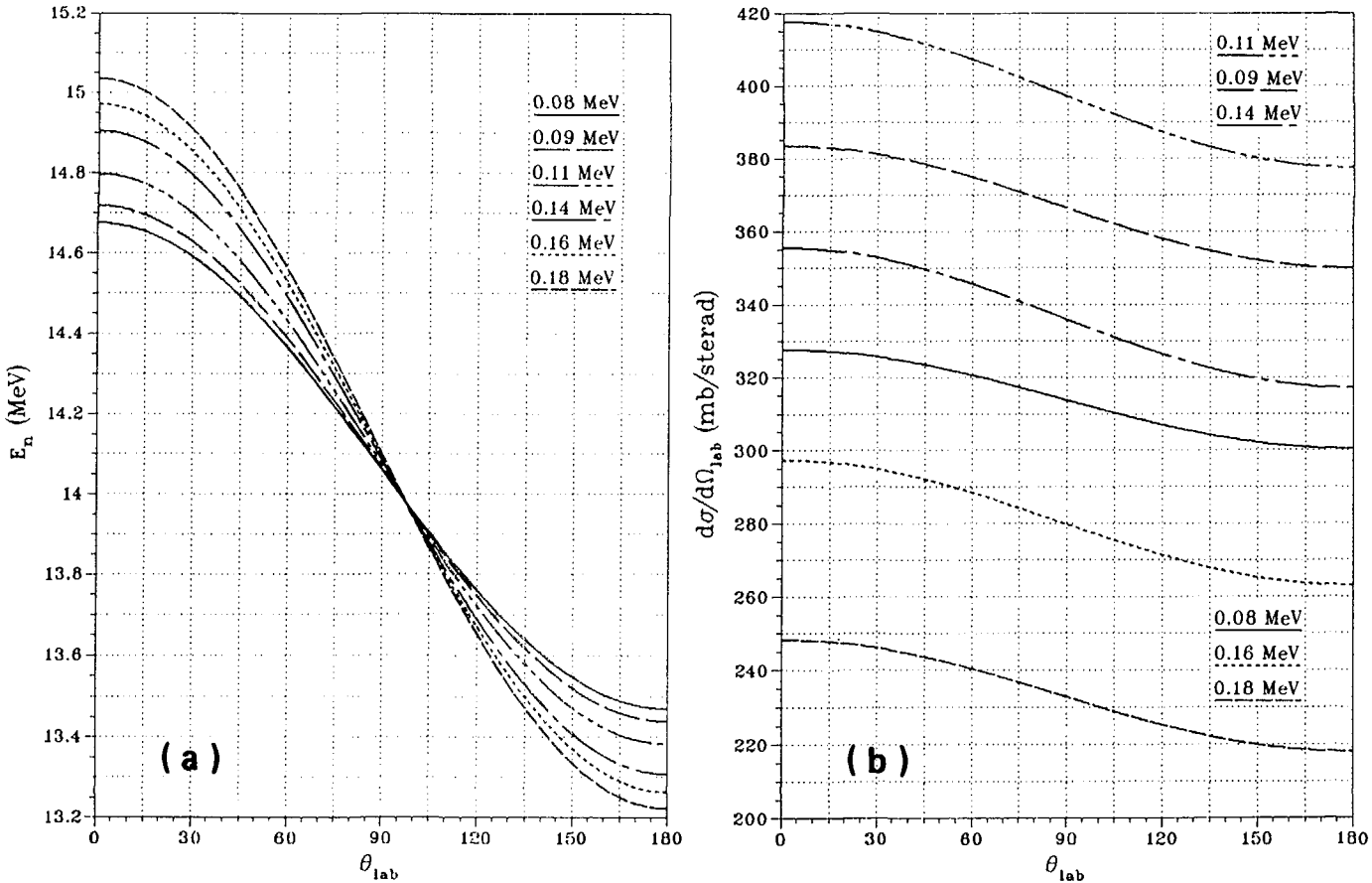

FIG. 5.2. Angular dependence of the neutron beam energies and differential (D–T)^{4}He,n cross-sections for different energies of incident deuterons. (Taken from Technical Reports Series No. 273, p. 131.)

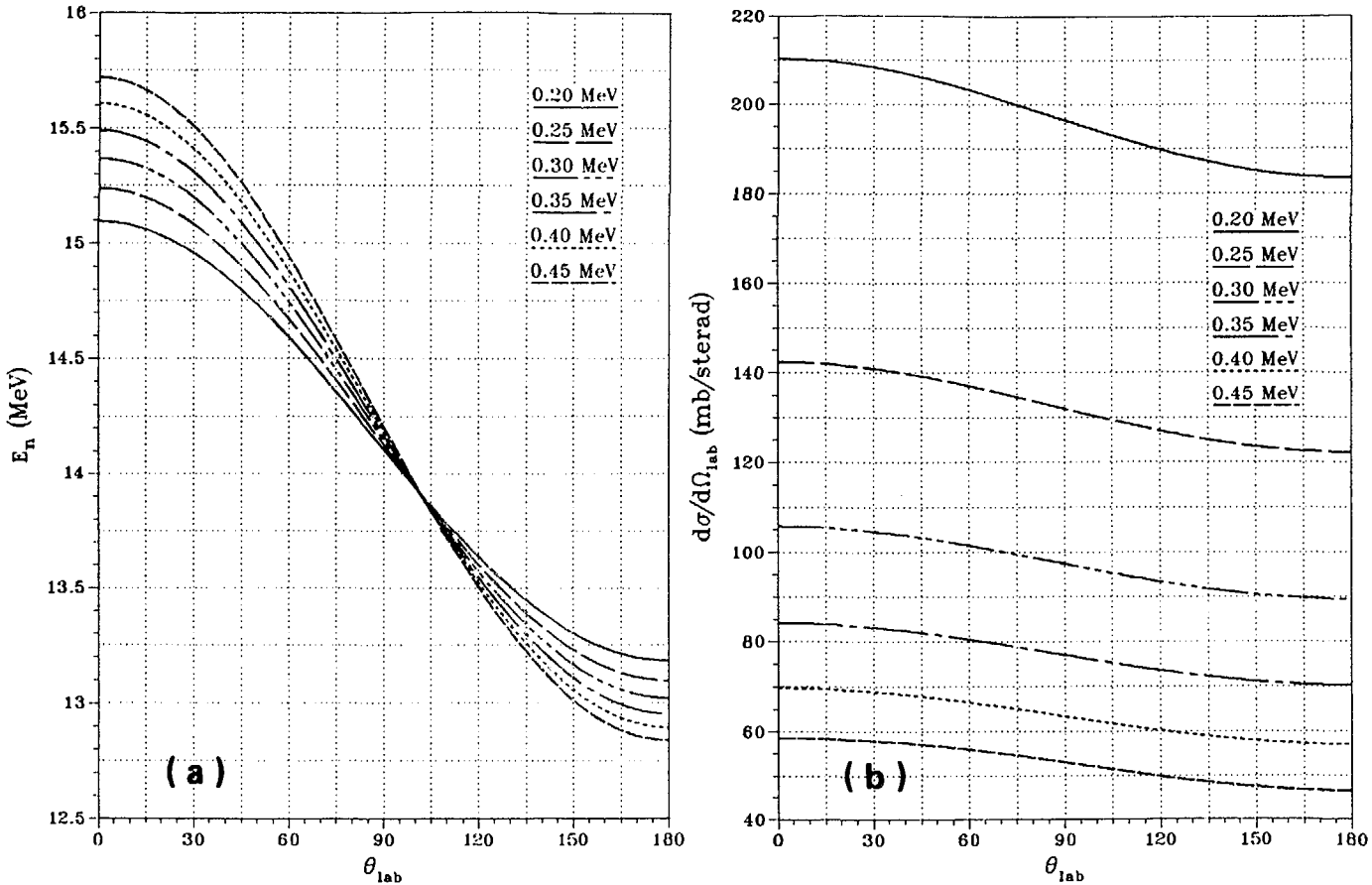

FIG. 5.3. Angular dependence of the neutron beam energies and differential (D–T)^{4}He,n cross-sections for different energies of incident deuterons. (Taken from Technical Reports Series No. 273, p. 132.)

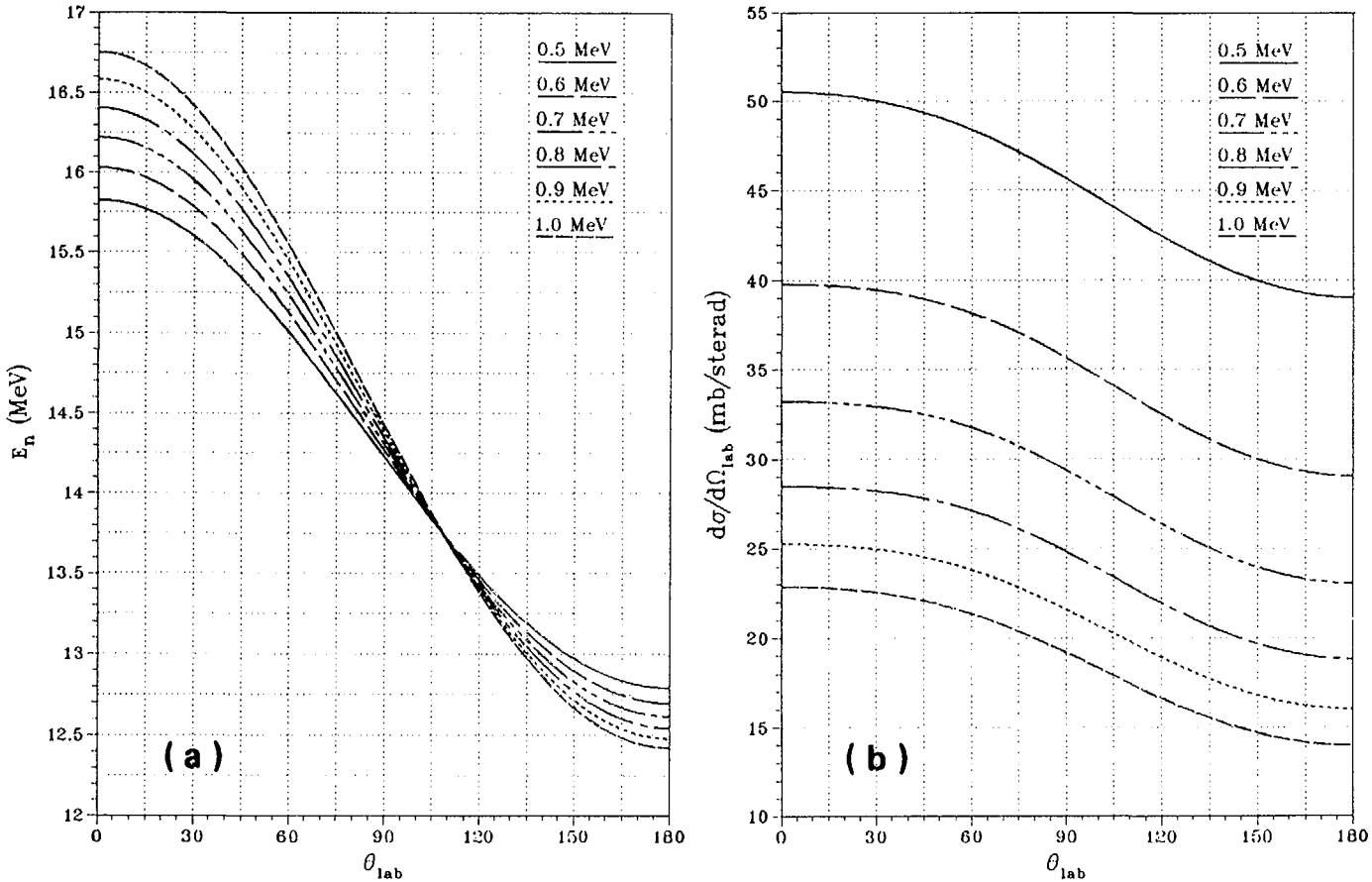

FIG. 5.4. Angular dependence of the neutron beam energies and differential (D–T)^{4}He,n cross-sections for different energies of incident deuterons. (Taken from Technical Reports Series No. 273, p. 133.)

REFERENCES

[1] GEIGER, K.W., "Radioactive Be(α,n) and Be(γ,n) sources", Neutron Source Properties (Proc. IAEA Consultants Meeting Debrecen, 1980), INDC(NDS)-114, International Nuclear Data Committee, IAEA, Vienna (1980) 43.

[2] GEIGER, K.W., VAN DER ZWAN, L., Radioactive neutron source spectra from ^{9}Be(α,n) cross-section data, Nucl. Instrum. Methods **131** (1975) 315.

[3] GEIGER, K.W., VAN DER ZWAN, L., The neutron spectrum of a ^{241}Am–Be(α,n) source as simulated by accelerator produced α-particles, Int. J. Appl. Radiat. Isot. **21** (1970) 193.

[4] INTERNATIONAL ATOMIC ENERGY AGENCY, Neutron Cross-Sections for Reactor Dosimetry (Proc. Consultants Meeting Vienna, 1976), IAEA-TECDOC-208, IAEA, Vienna (1976).

[5] MANNHART, W., "The neutron spectrum of spontaneous fission of californium-252", Handbook on Nuclear Activation Data, Technical Reports Series No. 273, IAEA, Vienna (1987) 163.

[6] HEATON, H.T., et al., in Proc. NEANDC/NEACRP Specialists Meeting Argonne, IL, 1976, Rep. ANL-76-90, Argonne National Laboratory, Argonne, IL (1976).

[7] CSIKAI, J., Production of 14 MeV Neutrons by Low Voltage Accelerators, Rep. INDC(NDS)-114, International Nuclear Data Committee, IAEA, Vienna (1980) 265.

[8] BARSCHALL, H.H., 14 MeV D–T Sources, Neutron Sources for Basic Physics and Applications, Pergamon Press, Oxford (1983) 57.

[9] DROSG, M., SCHWERER, O., "Production of monoenergetic neutrons between 0.1 and 23 MeV: Neutron energies and cross-sections", Handbook on Nuclear Activation Data, Technical Reports Series No. 273, IAEA, Vienna (1987) 83.

Chapter 6

NEUTRON INDUCED REACTION CROSS-SECTION DATA FOR NUCLIDES REQUIRED FOR BOREHOLE LOGGING AND MINERAL ANALYSIS

6.1. DATA TYPES AND FORMATS

This chapter contains numerical and graphical data for the elements that are of primary importance for borehole logging and mineral analysis applications. These data for the individual elements are presented in subsections. Each of these subsections contains data both for a natural element and for separate isotopes of this element. Nuclear reaction cross-sections of thermal neutron capture are given for natural elements, and cross-sections of specific reactions, leading to the emission of γ radiation through inelastic scattering processes or to the formation of delayed radioactivities, are given for separate isotopes. For the convenience of the user, some non-nuclear data for elements are also given in the beginning of each subsection. These numerical data are presented in units of the International System of Units (SI units).

The following quantities are given:

The *relative atomic mass* of an element N, $A_r(N)$, is defined as the ratio of the average mass per atom of the natural isotopic composition of an element ($m(N)$) to 1/12 of the mass of an atom of the ^{12}C nuclide (carbon mass unit). This is usually written as

$$A_r(N) = \frac{m(N)}{(1/12)\cdot m(^{12}C)} = \frac{m(N)}{m_u}$$

The *molar mass* of an element N, $M(N)$, is numerically equal to the relative atomic mass and is expressed as

$$M(N)\ [\mathrm{kg\cdot mol^{-1}}] = A_r(N)\cdot N_A\cdot m_u$$

where N_A is the Avogadro constant in $\mathrm{kmol^{-1}}$ and m_u is the atomic mass in kg. The *number of atoms per unit mass* is given by

$$N_m\ [\mathrm{kg^{-1}}] = \frac{N_A}{M(N)} = \frac{N_A}{A_r(N)\cdot N_A\cdot m_u} = \frac{1}{m(N)}$$

The *isotope mole fraction* of an isotope i can be expressed as

$$x(i) = n_i \Big/ \sum_j n_j$$

where n_i is the number of atoms of isotope i and the summation is extended over all naturally occurring isotopes.

The relative atomic masses and isotope mole fractions are quoted from the most recent Element by Element Review of Atomic Weights by Peiser et al. [1], and the mass densities are taken from the last edition of the Handbook of Chemistry and Physics [2].

The lowest excited energy levels are given for the important isotopes. The energies of γ rays emitted in the process of inelastic scattering are given for the most intensive γ transitions of practical importance. These data are taken from the Atlas of Gamma Ray Spectra from the Inelastic Scattering of Reactor Fast Neutrons by Ahmed et al. [3].

The elemental analysis is carried out in most cases by a measurement of the γ ray spectra from the samples or the bulk media during the neutron irradiation or after the irradiation. The γ ray spectra are measured, and the energies and intensities of the γ ray peaks are determined. In many cases it is necessary also to determine the decay rate (or the half-lives) of separate γ ray peaks.

The γ rays are emitted either during the irradiation (prompt γ rays) or after the nuclear reaction has taken place (decay of induced radioactivity).

Prompt γ rays are emitted as a result of the following nuclear reactions:

(1) The neutron capture reaction, $A(Z,N) + n \rightarrow A(Z,N+1)$, which leads to the production of an isotope containing one neutron more than the parent nuclide. The cross-section of this reaction is usually much higher at low neutron energies than at 14 MeV.

(2) The inelastic neutron scattering reaction, $A(Z,N) + n \rightarrow A^*(Z,N) \rightarrow A(Z,N) + \gamma$, leads to the production of the same nuclide in excited states. The de-excitation proceeds by γ ray emission. Excitation can take place either to discrete or to continuum excitation levels. In the latter case the emitted γ rays contribute to the continuum part of the γ ray spectrum.

(3) Non-elastic neutron scattering reactions of all types, $A(Z,N) + n \rightarrow A^*(Z \pm X; N \pm Y) \rightarrow A(Z \pm X; N \pm Y) + \gamma$, excluding inelastic scattering (n, n′), can also lead to the formation of product nuclides in excited states which decay promptly by emitting γ rays. These nuclides can differ from the parent in the number of both protons and/or neutrons. Data on cross-section values for the formation of these nuclides versus neutron energy are also given.

The dependence of the thermal neutron capture reaction cross-sections on energy (which is often called excitation function) is given for those cases where this reaction can be used for analysis or where it creates interferences in the analysis of other elements.

Inelastic scattering processes lead to the emission of prompt γ rays by the target nucleus A. Therefore, in this case the excitation energy levels of the target nucleus should be known.

The inelastic scattering γ ray energies and their intensities are given for fast reactor spectrum neutrons because there exists only one compilation of γ ray spectra from inelastic scattering [3]. The evaluated data libraries usually give total inelastic cross-sections, as well as cross-sections for the excitation of discrete levels and for the excitation of continuum levels. The continuum levels cannot be used for analysis, and no data for them are given.

In the case of continuous fast neutron spectra, the population of a given nuclear level takes place either directly during the inelastic scattering process or as a result of cascade γ transitions. The total population P of the nuclear level is defined as the sum of the intensities of the γ transitions from this level. The cascade population P_c is the sum of the intensities of the γ transitions to this level. The difference, $P_s = P - P_c$, is the population of a level taking place directly in the process of inelastic scattering. It is this quantity which is given in evaluated data libraries as the cross-section of the n-th excited level. The difference between P_s and P in general increases with the energy of incident neutrons. In the experiment, the yield of one or more γ lines is measured and then P_s is calculated using the probability of emission of this γ ray and corrections for the experimental measurement conditions. In the case of the ^{252}Cf neutron spectrum and for target nuclei with $A \leq 40$, P_s will be approximately equal to P, and no significant errors should be expected.

At higher energies, for example at 14 MeV, the intensities of the γ lines for medium and heavy elements can differ from the ones quoted in this Handbook by a somewhat larger value than that of the intensity uncertainties given here.

The evaluated data are taken from three libraries: ENDF/B-6 (USA) [4], JENDL-3 (Japan) [5] and ADL-90 (Russia) [6]. All important cross-sections leading to activation of the elements of interest are also given for the energy range from threshold to 20 MeV.

Possible interferences are considered. Excitation functions for each reaction are given in graphical form as well as in the form of tables after the figures.

In order to save space, all tables are given in a rather coarse structure, namely in 30 energy points. The cross-section values in the figures are the 640 group average values, which show the structure of the excitation functions in greater detail. These values do not necessarily coincide with the average values given in the tables, especially in the regions of sharp resonance structures in the excitation functions.

For a quick overview of the relative values of different neutron reaction cross-sections for a given element, pie charts showing the ratio of partial reaction cross-

sections to the total cross-section are presented. They give an immediate indication of which reactions are dominant for an element of interest and permit a preliminary choice of the method of detection of this element. The pie charts were taken from the compilation of Fisher [7].[1]

The Nuclear Data Section of the IAEA is also maintaining a computer library with the numerical data for all the cross-sections given in this Handbook. The data are in the 640 group structure. This library contains also utility codes with which it is possible to obtain data for any other desired group structure. The data are given in the international standard ENDF-6 format [8]. This computer file is available on request from the Nuclear Data Section of the IAEA on magnetic tape or on PC diskettes.

6.2. DETAILED DATA FOR ELEMENTS

6.2.1. **Hydrogen** (Figures on pp. 86 and 87)

Material constants

Relative atomic mass:	$A_r = 1.00794(7)$
Mass density (20°C):	$\rho = 89.88$ g/m^3
Number of atoms per unit mass:	5.975×10^{26} kg^{-1}
Isotope mole fraction (%):	^{1}H 99.985(1) ^{2}H 0.015(1)

The dominant neutron induced reaction cross-sections for hydrogen are shown in Fig. 6.1.

Hydrogen can only be detected through the neutron capture reaction at low neutron energies by counting the 2.223 MeV γ line. There are no significant interfering reactions under normal geophysical conditions. The excitation function for the ^{1}H (n, γ) reaction is shown in Fig. 6.2.

6.2.2. **Boron** (Figures on pp. 88 and 89)

Material constants

Relative atomic mass:	$A_r = 10.811(5)$
Mass density (20°C):	crystal modification: $\rho = 2.34$ Mg/m^3 amorphous modification: $\rho = 2.37$ Mg/m^3

[1] We express our gratitude to Dr. H.M. Fisher for his kind permission to reproduce the pie charts and also for sending us the master copies.

Material constants

Number of atoms per unit mass:	55.7×10^{24} kg^{-1}
Isotope mole fraction (%):	^{10}B 19.9(2)
	^{11}B 80.1(2)

The dominant neutron induced reaction cross-sections for boron are shown in Fig. 6.3.

Boron has an extremely large neutron absorption cross-section at low energies, and its compounds are often used as thermal neutron absorbers. In geophysical conditions, boron can be detected through the ^{10}B$(n,\alpha\gamma)^7$Li reaction to the first excited state with the emission of a prompt 0.478 MeV γ ray. The main difficulty for the quantitative analysis of boron is the large background in this energy region of γ rays from other elements. Besides that, some germanium crystal assemblies contain boron, which provides a constant background rate that has to be corrected for. The excitation function for the ^{10}B$(n,\alpha\gamma)^7$Li reaction is shown in Fig. 6.4.

6.2.3. **Carbon** (Figures and tables on pp. 90–96)

Material constants

Relative atomic mass:	$A_r = 12.011$	
Mass density[2] (20°C):	$\rho = 1.9$ (graphite) Mg/m^3	
Number of atoms per unit mass:	50.14×10^{24} kg^{-1}	
Isotope mole fraction (%):	^{12}C 98.9(3)	
	^{13}C 1.1	
Energies of lowest excitation levels (MeV):	4.439; 7.654; 9.64	
Inelastic γ rays:	*Energy* (MeV)	*Intensity* (%)
	4.438	100

The dominant neutron induced reaction cross-sections for carbon are shown in Fig. 6.5.

As can be readily seen from these pie charts at low incident neutron energies, elastic scattering is the dominating process. Therefore, thermal neutrons can be used for carbon detection with the help of the neutron capture reaction only in the case of high carbon concentrations. One of the cases where this is useful is the analysis performed for coal evaluation.

---

[2] The mass density depends on the allotropic form of the material: amorphous carbon: 1.8–2.1 Mg/m^3, graphite: 1.9–2.3 Mg/m^3, diamond: 3.15–3.53 Mg/m^3.

A more sensitive method of carbon detection uses the inelastic neutron scattering to the 4.438 MeV excited level of ^{12}C. Up to 4.8 MeV incident neutron energy, only weak capture γ rays are detected; above 4.8 MeV, the γ spectra are dominated by the decay of the 4.438 MeV level. In this case, special care should be taken because of direct interference from the $^{16}O\,(n,n'\alpha)\,^{12}C$ reaction populating the same excited state in the residual ^{12}C nucleus. This is often a matter of very serious concern because of the almost uniformly large oxygen concentrations in sediments. To evaluate the contribution of this reaction, the amount of oxygen should be determined. This is usually done using the inelastic scattering reaction for ^{16}O in the same measurement. The ratio of γ ray intensities from ^{12}C and ^{16}O determines the relative concentrations of carbon and oxygen.

Some interference from inelastic scattering on carbon and thermal capture on silicon could be expected. The data for the interfering reactions can be found in the sections giving the data for the corresponding elements.

Excitation functions for neutron capture and inelastic scattering of carbon are given in Figs 6.6 to 6.8, and numerical data are given in the tables after these figures.

It was also recommended to evaluate the possible interference in carbon detection from the capture of fast neutrons in silicon and carbon. The interference (or contribution to the counts at a given peak energy) can be calculated as follows:

$$\Delta\,[\%] = \frac{I_{\text{int}}(n,\gamma)}{I(n,\gamma)} = \frac{\sigma_{\text{int}}(n,\gamma)\cdot I\,\gamma}{\sigma_{\text{meas}}(n,\gamma)\cdot I_{\text{meas}}\,\gamma}\cdot 100$$

for equal numbers of atoms of ^{12}C and of the interfering isotope.

Isotope	Reaction	Product	E_γ (keV)	I_γ (%)	σ (b)	Δ (%)
$^{14}Si^{28}$	n,γ	$^{14}Si^{29}$	4407.6	0.2	0.45×10^{-3}	5×10^{-4}
$^{20}Ca^{40}$	n,γ	$^{20}Ca^{41}$	4418.9	4.9	0.5×10^{-3}	4.2×10^{-2}

6.2.4. **Oxygen** (Figures and tables on pp. 97–104)

Material constants

Relative atomic mass: $A_r = 15.9994(3)$ [3]

Mass density (0°C): 1.429 kg/m^3

[3] The quoted uncertainty includes possible natural variations.

Material constants

Number of atoms per unit mass:	3.764×10^{25} kg^{-1}	
Isotope mole fraction (%):	^{16}O 99.762(15)	
	^{17}O 0.038(3)	
	^{18}O 0.200(12)	
Energies of lowest excitation levels (MeV):	6.05; 6.13; 6.92; 7.12	
Inelastic γ rays:	*Energy* (MeV)	*Intensity* (%)
	1.9830(4)	100
	6.1293(10)	505(120)

The dominant neutron induced reaction cross-sections for oxygen are shown in Fig. 6.9.

As can be seen from the pie charts, at low incident neutron energies the elastic scattering is totally dominating. Oxygen can be detected through the ^{16}O(n,p)^{16}N activation reaction, which has a threshold of about 11 MeV, or through inelastic scattering to the first excited level in ^{16}O (6.13 MeV), with incident neutrons having energies higher than 6.5 MeV. The inelastic scattering is often preferable owing to the general interest in determining the concentration of other elements in addition to oxygen, which could be detected only through inelastic scattering. The signal of the delayed activity of ^{16}N (product of ^{16}O(n,p)) will be present in many cases in measurements of delayed activity since it has a half-life of 7.13 s.

The excitation functions for inelastic scattering of ^{16}O to the first, second and third excited states are shown in Fig. 6.10, and numerical data are given in the tables after this figure.

The excitation function for the ^{16}O(n,p)^{16}N reaction is given in Fig. 6.11, and numerical data are given in the table after this figure.

The ^{16}O(n,n'α) reaction is of interest because it creates interference in the ^{12}C determination through inelastic scattering. The excitation function for this reaction is given in Fig. 6.12, and numerical data are given in the table after this figure.

6.2.5. **Sodium** (Figures and tables on pp. 105–109)

Material constants

Relative atomic mass:	A_r = 22.98977(1)
Mass density (20°C):	0.971 Mg/m^3
Number of atoms per unit mass:	26.19×10^{24} kg^{-1}
Isotope mole fraction (%):	^{23}Na 100

Material constants

Energies of lowest excitation levels (MeV):	0.440(2); 2.0760(4); 2.3909(4); 2.6403(5)	
Inelastic γ rays:	*Energy* (MeV)	*Intensity* (%)
	0.44	100
	1.6358	8.6
	2.6401	2.0

The dominant neutron induced reaction cross-sections for ^{23}Na are given in Fig. 6.13.

Sodium concentrations are typically not very high and detection can be achieved either through neutron capture spectroscopy or through delayed activation measurements. Inelastic scattering measurements were reported as being ineffective for sodium detection. Therefore, data for inelastic cross-sections are not given here.

Activities induced in sodium are due to the following two nuclear reactions:

^{23}Na (n,γ)^{24}Na $\quad T_{1/2} = 14.96$ h
^{23}Na(n,2n)^{22}Na $\quad T_{1/2} = 2.60$ a

The excitation function for the ^{23}Na(n,γ)^{24}Na reaction is shown in Fig. 6.14, and numerical data are given in the table after this figure.

The excitation function for the ^{23}Na(n,2n)^{22}Na reaction is shown in Fig. 6.15, and numerical data are given in the table after this figure.

The capture reaction for ^{23}Na is subject to interferences from the ^{24}Mg(n,p) and ^{27}Al(n,α) reactions, which produce the same radioactive product, ^{24}Na. The corrections are not needed at thermal energies and are very minor for ^{252}Cf fission neutron sources; at higher energies, however, the corrections are much more substantial. Data for these interfering reactions are given in the sections for the corresponding elements.

6.2.6. **Magnesium** (Figures and tables on pp. 110–114)

Material constants

Relative atomic mass:	$A_r = 24.305(1)$
Mass density (20°C):	$\rho = 1.738$ Mg/m^3
Number of atoms per unit mass:	24.78×10^{24} kg^{-1}
Isotope mole fraction (%):	^{24}Mg 78.99(3)
	^{25}Mg 10.00(1)
	^{26}Mg 11.01(2)

Material constants

Energies of lowest excitation levels (MeV):	^{24}Mg	1.36857(10)
		4.1230(6)
		4.2387(6)
	^{25}Mg	0.58491(15)
		0.9746(3)
		1.61171(3)
	^{26}Mg	11.01(2)

Inelastic γ rays:		*Energy* (MeV)	*Intensity* (%)
	^{24}Mg	1.36853(10)	100
		2.754	4.3
		4.239	4.0
	^{25}Mg	0.389	5.6
		0.585	15
		0.9746	5.4
		1.612	6
	^{26}Mg	1.120	3.2
		1.809	11

Magnesium generally occurs at relatively small concentrations, except in dolomitic rocks. Therefore, inelastic scattering is generally not useful for determining magnesium. The dominant neutron induced reaction cross-sections for magnesium are shown in Fig. 6.16.

The thermal neutron capture cross-section is also low; this makes it difficult to use this reaction for magnesium detection. The most sensitive method of magnesium detection is through the delayed ^{27}Mg activity from the ^{26}Mg(n,γ)^{27}Mg reaction. The half-life of ^{27}Mg is 9.5 min; the main γ rays have energies of 0.844 and 1.014 MeV. This delayed activity is subject to potential interferences from the production of ^{27}Mg in the ^{27}Al(n,p)^{27}Mg and ^{30}Si(n,α)^{27}Mg reactions. The data for interference reactions can be found in the sections for these elements.

The excitation functions for the ^{26}Mg(n,γ) and ^{24}Mg(n,p) reactions are shown in Figs 6.17 and 6.18, respectively, and numerical data are given in the tables after these figures.

6.2.7. **Aluminium** (Figures and tables on pp. 115–121)

Material constants

Relative atomic mass: $A_r = 26.98154(1)$

Mass density (20°C): $\rho = 2.6989$ Mg/m^3

Material constants

Number of atoms per unit mass: 22.32×10^{24} kg^{-1}

Isotope mole fraction (%): ^{27}Al 100

Energies of lowest excitation levels (MeV): 0.84376; 1.01442(15); 2.2118(2)

Inelastic γ rays:

Energy (MeV)	*Intensity* (%)
0.8437	60
1.01440(15)	100
1.7208(3)	14(2)
2.2118(2)	52(5)

The dominant neutron induced reaction cross-sections for aluminium are shown in Fig. 6.19.

It is in general possible to detect aluminium through the thermal neutron capture reaction, although, usually, long accumulation times are required. A more sensitive detection method of aluminium involves the registration of the delayed activity of ^{28}Al, which is a product of the neutron capture reaction. As can be seen from the pie charts, the most effective way is to use thermal neutrons. The excitation function for the ^{27}Al (n, γ) reaction is shown in Fig. 6.20, and numerical data are given in the table after this figure.

As the energy of the incident neutrons increases, an increasing contribution to the ^{28}Al activity is generated by the ^{28}Si (n, p) reaction (for the cross-section see Section 6.2.8). The detection of aluminium by inelastic scattering is severely complicated by the decay of the delayed activity of ^{27}Mg.

The ^{27}Al (n, p) reaction creates an interference in the analysis of the magnesium concentration. The excitation function for this reaction is shown in Fig. 6.21, and numerical data are given in the table after this figure.

The ^{27}Al (n, α)^{24}Na reaction creates significant interference in the detection of sodium. The excitation function for this reaction is shown in Fig. 6.22, and numerical data are given in the table after this figure.

The interference appearing during the analysis of the ^{28}Al activity due to the contribution from the ^{28}Si (n, p) reaction can be estimated as

$$\Delta = \frac{I_{^{28}\mathrm{Al}} \text{ from Si}}{I_{^{28}\mathrm{Al}} \text{ from Al}}$$

(the mole fraction of ^{28}Si should be taken into account).

6.2.8. Silicon (Figures and tables on pp. 122–132)

Material constants

Relative atomic mass:	$A_r = 28.0855(3)$	
Mass density (25°C):	$\rho = 2.33$ Mg/m^3	
Number of atoms per unit mass:	21.44×10^{24} kg^{-1}	
Isotope mole fraction (%):	^{28}Si	92.23(1)
	^{29}Si	4.67(1)
	^{30}Si	3.10(1)
Energies of lowest excitation levels (MeV):	^{28}Si	1.7789(3)
		4.6169(12)
		4.9790(17)
	^{29}Si	1.2729(4)
		2.0280(5)
		2.4253(5)
	^{30}Si	2.2350(5)
		3.4979(8)

	Energy (MeV)	*Intensity* (%)
Inelastic γ rays:	1.2728(4)	4.2(10)
	1.7788(3)	100
	2.8379(10)	2.7

The dominant neutron induced reaction cross-sections for silicon are shown in Fig. 6.23.

The silicon concentration is most commonly analysed with the help of the thermal neutron capture reaction. It can also be detected by inelastic scattering, especially through the excitation of the first excited state in the most abundant isotope ^{28}Si with an emission of 1.779 MeV γ rays.

The excitation function for the Si^{nat}(n,γ) reaction is shown in Fig. 6.24, and numerical data are given in the table after this figure.

Figure 6.25 shows the excitation function for the 1.779 MeV level of silicon. It is classified as the second excited level in the natural mixture of silicon isotopes (the first being the lower, 1.2729 MeV, level of ^{29}Si). In using this reaction, some caution must be exercised, since there may be a significant yield of this γ ray from the decay of ^{28}Al from the ^{27}Al(n,γ) and the ^{28}Si(n,p) reactions.

The reaction ^{29}Si(n,p) produces ^{29}Al, which has a half-life of 6.5 min and emits 1.273 MeV γ rays. This activity is sometimes used for inserting corrections into the values of ^{28}Al activity when the latter is produced by both the ^{27}Al(n,γ)

and the $^{28}Si(n,p)$ reactions. The excitation function for the $^{28}Si(n,p)$ reaction is shown in Fig. 6.26, and numerical data are given in the table after this figure.

The excitation function for the $^{29}Si(n,p)^{29}Al$ reaction is shown in Fig. 6.27, and numerical data are given in the table after this figure.

The $^{30}Si(n,\alpha)$ reaction is important because it creates interferences in the analysis of magnesium through measurements of delayed ^{27}Mg activity. The excitation function for the $^{30}Si(n,\alpha)^{27}Mg$ reaction is shown in Fig. 6.28, and numerical data are given in the table after this figure.

6.2.9. **Sulphur** (Figures and tables on pp. 133–137)

Material constants

Relative atomic mass:	$A_r = 32.066(6)$	
Mass density (20°C):	rhombic modification:	$\rho = 2.33$ Mg/m^3
	monoclinic modification:	$\rho = 1.957$ Mg/m^3
Number of atoms per unit mass:	rhombic modification:	18.78×10^{24} kg^{-1}
	monoclinic modification:	18.78×10^{24} kg^{-1}
Isotope mole fraction (%):	^{32}S	95.02(9)
	^{33}S	0.75(1)
	^{34}S	4.21(8)
Energies of lowest excitation levels (MeV):	^{32}S	2.23028(10)
		3.7785(4)
		4.2819(8)
	^{33}S	0.84092(5)
		1.9663(1)
		2.3125(1)
	^{34}S	2.1276(2)
		3.3032(2)
	^{36}S	3.2910(6)
		3.3460(4)
		4.1925(7)

Inelastic γ rays:	*Energy* (MeV)	*Intensity* (%)
	1.5481(3)	3.2(3)
	2.0520(8)	0.5(10)
	2.1275(8)	5.6(5)
	2.2302(10)	100
	2.7761(3)	4.0(4)
	4.2813(15)	4.0(6)

The dominant neutron induced reaction cross-sections for sulphur are shown in Fig. 6.29.

The analysis of sulphur is most efficiently performed with the thermal neutron capture reaction. The delayed activity of ^{37}S can also be observed at low neutron energies ($^{36}S(n,\gamma)^{37}S$). The excitation function for the $^{36}S(n,\gamma)$ reaction is shown in Fig. 6.30, and numerical data are given in the table after this figure.

As the neutron energy increases, the interference from the $^{37}Cl(n,p)^{37}S$ reaction becomes large, which generally precludes the use of the delayed ^{37}S activity in borehole applications.

In fast neutron fields, sulphur can be detected by the $^{34}S(n,p)^{34}P$ reaction, but, again, some interference can be expected from the $^{37}Cl(n,\alpha)^{34}P$ reaction.

The excitation function for the $^{34}S(n,p)^{34}P$ reaction is shown in Fig. 6.31, and numerical data are given in the table after this figure.

The excitation functions for the interfering reactions are given in Section 6.2.10.

6.2.10. Chlorine (Figures and tables on pp. 138–146)

Material constants

Relative atomic mass:	A_r = 35.453(1)	
Mass density (20°C):	3.214 Mg/m^3	
Number of atoms per unit mass:	1.699×10^{25} kg^{-1}	
Isotope mole fraction (%):	^{35}Cl	75.77(5)
	^{37}Cl	24.23(5)
Energies of lowest excitation levels (MeV):	^{35}Cl	1.21954(10)
		1.76330(10)
		2.64575(20)
	^{37}Cl	1.72654(10)
		3.0864(3)
		3.10343(15)

Inelastic γ rays:		*Energy* (MeV)	*Intensity* (%)
	^{35}Cl	0.88235(15)	3.8(4)
		0.9305(5)	3.0(10)
		1.21952(10)	100
		1.76327(10)	129
		2.6457(2)	25.7(15)
		2.6940(2)	19.1(15)
		3.0022(2)	15.5(15)

Material constants

Inelastic γ rays:

	Energy (MeV)	*Intensity* (%)
^{35}Cl	3.16252(15)	16.3(15)
^{37}Cl	0.90664(15)	2.9(4)
	1.90664(15)	25(2)
	3.0863(3)	11.2(10)
	3.10329(15)	14.6(15)

The dominant neutron induced reaction cross-sections for chlorine are shown in Fig. 6.32.

Chlorine can most efficiently be observed through the thermal neutron capture reaction because of its large cross-section compared with that of most sedimentary elements. It is also possible to use the delayed activation induced through the $^{37}Cl(n,\gamma)^{38}Cl$ reaction, which is a useful method when a comparison with the sodium concentration is needed.

The excitation function for the $^{37}Cl(n,\gamma)^{38}Cl$ reaction is shown in Fig. 6.33, and numerical data are given in the table after this figure.

If delayed activity is used, some care must be exercised when the K/Cl concentration ratio is large because of interference from the $^{41}K(n,\alpha)$ reaction.

Chlorine can also be measured by activation in fast neutron fields through the $^{35}Cl(n,2n)^{34}Cl^m$, $^{37}Cl(n,p)^{37}S$ and $^{37}Cl(n,\alpha)^{34}P$ reactions. The excitation functions for these reactions are shown in Figs 6.34 to 6.36, and numerical data are given in the tables after these figures.

Usually, only the 32.2m isomer is measured in activation work. The cross-section leading to the formation of the isomer is much higher than that for the transition to the ground state of the ^{34}Cl nucleus. The results of experiments trying to evaluate the contribution of the ground state transition are very uncertain.

In this situation, the sum of the two channels (given in Fig. 6.34) can be used as a value for the $^{34}Cl^m$ production cross-section, with only a few per cent being contributed by the $^{34}Cl^g$ production. No separate evaluated data for the $^{34}Cl^g$ transition exist at present.

6.2.11. Potassium (Figures and tables on pp. 147–149)

Material constants

Relative atomic mass: $A_r = 39.0983(1)$

Mass density (20°C): 0.862 Mg/m^3

Number of atoms per unit mass: 15.403×10^{24} kg^{-1}

Isotope mole fraction (%):

^{39}K	93.2581(30)
^{40}K	0.0117(1)
^{41}K	6.7302(30)

Material constants

Energies of lowest excitation levels (MeV):	^{39}K	2.5229(3)
		2.8139(4)
		3.0187(8)
		3.5972(8)
	^{40}K	0.0296(10)
		0.7999(2)
		0.8916(4)
		1.6464(10)
	^{41}K	0.9806(2)
		1.2933(8)
		1.5601(4)
		1.6767(4)

Inelastic γ rays:		*Energy* (MeV)	*Intensity* (%)
	^{39}K	0.3469(3)	8.0(10)
		0.7837(5)	16(3)
		1.1929(5)	9(2)
		1.3133(4)	12(2)
	^{40}K	0.9806(2)	31(5)
		1.2933(8)	24(6)

The dominant neutron induced reaction cross-sections for potassium are shown in Fig. 6.37.

The determination of potassium is almost always performed through the detection of the naturally radioactive ^{40}K, which has a half-life of 1.28×10^9 years and emits γ rays with an energy of 1.4608 MeV.

The ^{41}K (n, α) reaction creates interferences in the determination of chlorine through measurements of the delayed activity of ^{38}Cl.

The excitation function for the ^{41}K (n, α) reaction is shown in Fig. 6.38, and numerical data are given in the table after this figure.

6.2.12. Calcium (Figures and tables on pp. 150–156)

Material constants

Relative atomic mass:	$A_r = 40.078(4)$
Mass density (20°C):	1.55 Mg/m^3
Number of atoms per unit mass:	15.026×10^{24} kg^{-1}

Material constants

Isotope mole fraction (%):	^{40}Ca	96.941(13)
	^{42}Ca	0.647(3)
	^{43}Ca	0.135(3)
	^{44}Ca	2.086(5)
	^{46}Ca	0.004(3)
	^{48}Ca	0.187(3)
Energies of lowest excitation levels (MeV):	^{40}Ca	3.7371(8)
		3.9044
		4.4021(9)
		5.2500(8)
		5.2801(11)
	^{44}Ca	1.1569(5)
		1.8832(11)
		2.2824(11)
		2.6575(10)

Inelastic γ rays:		*Energy* (MeV)	*Intensity* (%)
	^{40}Ca	0.7550(4)	15(3)
		1.3456(8)	5.5(15)
		1.3757(10)	10(2)
		3.7369(8)	123(9)
		3.9042	100
		5.250(2)	27(5)
		5.628(2)	21(5)
		5.902(4)	16(5)
	^{44}Ca	0.7263(10)	12(3)
		1.1255(10)	8(2)
		1.1569(5)	87(6)
		1.5006(8)	4.6(12)

The dominant neutron induced reaction cross-sections for calcium are shown in Fig. 6.39.

Calcium is usually detected through the thermal capture reaction. However, calcium is one of the few elements whose capture γ rays are subject to significant interferences from the capture γ rays of other common sedimentary elements. The most intense capture line of calcium is at 1.943 MeV, and it is close to the chlorine capture lines at 1.951 and 1.958 MeV. The second most intense line at 6.420 MeV is very close to the capture line of titanium at 6.418 MeV. Calcium can also be determined from the delayed activity produced in the ^{48}Ca (n, γ) reaction. The excitation

functions for the $Ca^{nat}(n,\gamma)$ and $^{48}Ca(n,\gamma)$ reactions are shown in Figs 6.40 and 6.41, respectively, and numerical data are given in the tables after these figures.

The abundance of the ^{48}Ca isotope, however, is very low, and rather high neutron fluxes are needed to obtain good sensitivity.

In the high energy neutron fields, delayed activity from the $^{44}Ca(n,p)^{44}K$ reaction, which is free of contributions from other neutron induced reactions, can be used to improve the precision of the analysis of the calcium concentration. The excitation function for this reaction is shown in Fig. 6.42, and numerical data are given in the table after this figure.

6.2.13. Titanium (Figures and tables on pp. 157–161)

Material constants

Relative atomic mass:	A_r = 47.88(3)	
Mass density (20°C):	4.54 Mg/m^3	
Number of atoms per unit mass:	12.58×10^{24} kg^{-1}	
Isotope mole fraction (%):	^{46}Ti	8.0(1)
	^{47}Ti	7.3(1)
	^{48}Ti	73.8(1)
	^{49}Ti	5.5(1)
	^{50}Ti	5.4(1)
Energies of lowest excitation levels (MeV):	^{46}Ti	0.88925(15)
		2.0097(7)
		2.6116(12)
		2.9618(10)
		3.0585(10)
	^{47}Ti	0.1594(2)
		1.2522(5)
		1.4443(9)
		1.5498(6)
		1.7933(10)
	^{48}Ti	0.9835(10)
		2.2957(3)
		2.4210(3)
		2.9977(6)
		3.2240(4)
	^{49}Ti	1.3819(3)
		1.5423(3)

Material constants

Energies of lowest excitation levels (MeV):	^{49}Ti	1.5864(3)
	^{50}Ti	1.55380(1)
		2.67493(1)
		3.19873(2)

Inelastic γ rays:		*Energy* (MeV)	*Intensity* (%)
	^{46}Ti	0.88924(15)	9.7(8)
		1.0488(7)	0.40(15)
		1.1205(6)	1.9(6)
	^{47}Ti	0.1594(2)	17(2)
		1.0928(4)	2.1(4)
	^{48}Ti	0.9442(6)	1.8(3)
		0.98349(10)	100
		1.3122(2)	8.1(10)
		1.4375(2)	7.7(10)
	^{49}Ti	1.3819(3)	1.7(4)
		1.5423(3)	1.6(4)
		1.6231(4)	1.9(3)
	^{50}Ti	1.5550(3)	3.8(8)

The dominant neutron induced reaction cross-sections for titanium are shown in Fig. 6.43.

Because of the large cross-section of thermal neutron capture in titanium, this reaction can be used efficiently for titanium detection. Some care must be exercised because of the interferences between the capture lines of titanium and those of other common sedimentary elements. Titanium can also be detected through the delayed activity from the ^{50}Ti (n,γ)^{51}Ti reaction. The excitation functions for the Ti^{nat} (n,γ) and ^{50}Ti (n,γ)^{51}Ti reactions are given in Figs 6.44 and 6.45, respectively, and numerical data are given in the tables after these figures.

For the reaction ^{50}Ti (n,γ)^{51}Ti, there is a potential interference from the delayed activity produced by the ^{51}V (p,n)^{51}Ti and ^{54}Cr (n,α)^{51}Ti reactions. However, the contribution from these reactions is usually negligible because of the relatively small concentrations of vanadium and chromium as compared to that of titanium under most circumstances. Data for these two interfering reactions can be found in the sections for these elements.

6.2.14. **Vanadium** (Figures and tables on pp. 162–166)

Material constants

Relative atomic mass:	A_r = 50.9415(1)	
Mass density (18.7°C):	6.11 Mg/m^3	
Number of atoms per unit mass:	11.822×10^{24} kg^{-1}	
Isotope mole fraction (%):	^{50}V	0.250(2)
	^{51}V	99.750(2)
Energies of lowest excitation levels (MeV):	^{50}V	0.2265(3)
		0.32010(10)
		0.3555(3)
	^{51}V	0.32020(10)
		0.92851(15)
		1.6093(2)
		1.8135(2)

Inelastic γ rays:		*Energy* (MeV)	*Intensity* (%)
	^{50}V	0.2265(3)	0.45(10)
	^{51}V	0.32020(10)	100
		0.6085(2)	3.4(10)
		0.92850(15)	16.0(10)
		1.4932(5)	3.1(5)
		1.6093(2)	22(2)
		1.8135(2)	14(2)

The dominant neutron induced reaction cross-sections for natural vanadium are shown in Fig. 6.46.

The most practical way of determining the concentration of vanadium is through the delayed activity from the thermal neutron capture reaction for ^{51}V. The excitation function for the ^{51}V (n,γ) reaction is shown in Fig. 6.47, and numerical data are given in the table after this figure.

This method is, however, not free from interferences. The delayed ^{52}V activity can also be produced in the ^{52}Cr (n,p)^{52}V and ^{55}Mn (n,α)^{52}V reactions. Manganese is often present in greater quantities than vanadium. All of these elements are likely to be contained in steels, so that when logging is performed in cased boreholes or when a portion of the logging instrument is exposed to the neutron flux, interference could become a problem.

Vanadium can also be measured with fast neutrons using the ^{51}V (n,p)^{51}Ti reaction. In this case, interferences could be expected from the ^{54}Cr (n,α)^{51}Ti and ^{50}Ti (n,γ)^{51}Ti reactions.

The $^{51}V(n,p)^{51}Ti$ reaction can also create interference in the determination of titanium via the $^{50}Ti(n,\gamma)^{51}Ti$ reaction. The excitation function for the $^{51}V(n,p)^{51}Ti$ reaction is shown in Fig. 6.48, and numerical data are given in the table after this figure.

6.2.15. Chromium (Figures and tables on pp. 167–178)

Material constants

Relative atomic mass:	A_r = 51.9961(6)	
Mass density (20°C):	7.2 Mg/m^3	
Number of atoms per unit mass:	11.58×10^{24} kg^{-1}	
Isotope mole fraction (%):	^{50}Cr	4.345(9)
	^{52}Cr	83.789(12)
	^{53}Cr	9.501(11)
	^{54}Cr	2.365(5)
Energies of lowest excitation levels (MeV):	^{50}Cr	0.78331(10)
		1.8811(4)
		2.9239(6)
		3.1602(10)
	^{52}Cr	1.43422(10)
		2.3698(2)
		2.6489(3)
		2.7679(2)
		2.9652(3)
		3.1140(5)
	^{53}Cr	0.56434(10)
		1.00650(10)
		1.2897(2)
		1.5367(3)
		1.9742(3)
	^{54}Cr	0.8350(2)
		1.8237(5)
		2.6198(9)

Inelastic γ rays:		*Energy* (MeV)	*Intensity* (%)
	^{50}Cr	0.7833(1)	8.3(6)
		1.0978(3)	0.4(1)
	^{52}Cr	0.6473(2)	2.2(2)
		0.7042(2)	3.3(8)

Material constants

Inelastic γ rays:

	Energy (MeV)	*Intensity* (%)
^{52}Cr	0.7442(3)	1.2(3)
	0.93555(10)	8.4(4)
	1.2147(2)	1.8(3)
	1.2897(2)	5.6(3)
	1.4342(1)	100
	1.53094(15)	8.8(5)
^{53}Cr	0.5302(2)	2.2(2)
	0.56434(10)	8.8(6)
	1.00649(10)	9.1(5)
	1.3337(10)	9.2(5)
^{54}Cr	0.8350(2)	4.1(5)
	0.9887(3)	0.55(15)

The dominant neutron induced reaction cross-sections for natural chromium are shown in Fig. 6.49.

The most practical method to measure chromium is by thermal capture γ rays. The method is free from any noticeable interferences.

The excitation function for the $Cr^{nat}(n,\gamma)$ reaction is shown in Fig. 6.50, and numerical data are given in the table after this figure.

Delayed γ rays from the reaction $^{50}Cr(n,\gamma)^{51}Cr$ may also be used for analysis, but interferences from the reactions $^{54}Fe(n,\alpha)^{51}Cr$ and $^{50}Ti(n,\gamma)^{51}Ti$ can be expected. Both the ^{51}Cr and ^{51}Ti nuclei emit γ rays with an energy of 0.3201 MeV, but their half-lives are different: 27.7 d for ^{51}Cr and only 5.76 min for ^{51}Ti. This difference can be used to eliminate the contribution from ^{51}Ti.

The cross-section for the $^{50}Cr(n,\gamma)^{51}Cr$ reaction is shown in Fig. 6.51, and numerical data are given in the table after this figure.

In fast neutron fields, the $^{52}Cr(n,p)^{52}V$ reaction is the most important one, but potential interferences from the $^{51}V(n,\gamma)^{52}V$ and $^{55}Mn(n,\alpha)^{52}V$ reactions should be expected.

The excitation function for the $^{52}Cr(n,p)^{52}V$ reaction is shown in Fig. 6.52, and numerical data are given in the table after this figure.

In fast neutron fields the inelastic scattering of ^{52}Cr produces an intensive γ ray peak at 1.434 MeV, but this peak may be contaminated by the delayed activity. The excitation function for the $^{52}Cr(n,n')$ reaction is shown in Fig. 6.53, and numerical data are given in the tables after this figure.

The $^{54}Cr(n,\alpha)^{51}Ti$ reaction can create interference in analyses of titanium and vanadium. The excitation function for this reaction is shown in Fig. 6.54, and numerical data are given in the table after this figure.

6.2.16. Manganese (Figures and tables on pp. 179–185)

Material constants

Relative atomic mass:	$A_r = 54.9380(1)$
Mass density:	7.2 Mg/m^3
Number of atoms per unit mass:	10.96×10^{24} kg^{-1}
Isotope mole fraction (%):	^{55}Mn 100
Energies of lowest excitation levels (MeV):	0.1259(2) 0.9844(2) 1.2923(2) 1.52872(15) 1.88445(10) 2.1984(2) 2.2523(2) 2.2688(5)

Inelastic γ rays:

Energy (MeV)	*Intensity* (%)
0.30806(10)	12(2)
0.7387(4)	2.0(4)
0.85845(10)	100
0.8983(2)	3.4(12)
0.9844(2)	6.3(6)
1.0192(4)	4.9(10)
1.16630(10)	27(4)
1.2141(2)	6.5(5)
1.4147(6)	2.2(6)
1.4365(4)	3.5(6)
1.52870(15)	40(4)

The dominant neutron induced reaction cross-sections for ^{55}Mn are shown in Fig. 6.55.

Manganese can be measured through the thermal neutron capture reaction, but the sensitivity of this method is not very high because of the relatively low yield of γ rays. The excitation function for the ^{55}Mn (n,γ) reaction is shown in Fig. 6.56, and numerical data are given in the table after this figure.

A more sensitive way to determine the manganese concentration is by measurement of delayed activity from the capture reaction ^{55}Mn (n,γ)^{56}Mn. In a thermal neutron field, the only spectral interference can come from the delayed activity of ^{27}Mg, which has a γ ray peak at 0.844 MeV (it coincides with the main peak of

^{56}Mn at 0.847 MeV). A half-life analysis is very useful in this case, or, alternatively, other γ lines of ^{56}Mn can be used for analysis.

At higher neutron energies, a significant interference can be produced from the ^{56}Fe (n, p)^{56}Mn reaction, and the resolution of the relative contributions from manganese and iron is needed. The iron concentration can be determined through neutron capture reactions or by analysis of the delayed activities produced from reactions with iron isotopes. The reaction ^{55}Mn (n, 2n)^{54}Mn could be used in this analysis because the rate of production of ^{54}Mn from iron and manganese isotopes is essentially different. The excitation function for this reaction is shown in Fig. 6.57, and numerical data are given in the table after this figure.

In fast neutron fields, the ^{55}Mn (n, α)^{52}V reaction also produces delayed activity, but interferences from the ^{51}V (n, γ)^{52}V and ^{52}Cr (n, p)^{52}V reactions should be taken into account.

The excitation function for the ^{55}Mn (n, α)^{52}V reaction is shown in Fig. 6.58, and numerical data are given in the table after this figure.

The excitation functions for the interfering reactions can be found in the sections for the respective elements.

6.2.17. Iron (Figures and tables on pp. 186–190)

Material constants

Relative atomic mass:	A_r = 55.847(3)	
Mass density:	7.874 Mg/m^3	
Number of atoms per unit mass:	10.78×10^{24} kg^{-1}	
Isotope mole fraction (%):	^{54}Fe	5.8(1)
	^{56}Fe	91.72(30)
	^{57}Fe	2.2(1)
	^{58}Fe	0.28(1)
Energies of lowest excitation levels (MeV):	^{54}Fe	1.40819(19)
		2.5381(3)
		2.5613(4)
		2.9491(6)
	^{56}Fe	0.846753(5)
		2.085054(7)
		2.657541(16)
		2.9417(3)
	^{57}Fe	0.014413(15)
		0.1364745(12)

Material constants

Energies of lowest excitation levels (MeV):	^{57}Fe	0.366761(7)
		0.706428(16)
		1.00715(4)
	^{58}Fe	0.810764(15)
		2.07652(5)
		2.60039(5)

Inelastic γ rays:		*Energy* (MeV)	*Intensity* (%)
	^{54}Fe	1.1300(3)	0.39(4)
		1.1528(4)	0.14(3)
	^{56}Fe	0.84675(2)	100
		1.03745(2)	2.15(10)
	^{57}Fe	0.3525(2)	1.6(2)
		0.3671(2)	0.54(5)
	^{58}Fe	0.8103(2)	0.43(3)
		1.2383(2)	10.5(5)

The dominant neutron induced reaction cross-sections for natural iron are shown in Fig. 6.59.

The neutron thermal capture of iron provides the most direct and efficient means for the analysis of iron concentrations in most cases. The excitation function for the $Fe^{nat}(n,\gamma)$ reaction is shown in Fig. 6.60. The most significant γ ray lines are free from interferences. Numerical data are given in the table after this figure.

The inelastic scattering reaction is not practical because the only intensive inelastic γ ray peak at 0.846 MeV is subject to interferences from several elements.

In the fast neutron fields, iron can be detected through the delayed activity from the $^{56}Fe(n,p)^{56}Mn$ reaction. The excitation function for this reaction is shown in Fig. 6.61, and numerical data are given in the table after this figure.

This method might have interferences from the $^{55}Mn(n,\gamma)^{56}Mn$ and $^{59}Co(n,\alpha)^{56}Mn$ reactions. Possible contributions from these reactions should be evaluated.

6.2.18. Nickel (Figures and tables on pp. 191–195)

Material constants

Relative atomic mass:	$A_r = 58.69(1)$
Mass density (25°C):	8.902 Mg/m^3
Number of atoms per unit mass:	10.26×10^{24} kg^{-1}

Material constants

Isotope mole fraction (%):	^{58}Ni	68.27(1)
	^{60}Ni	26.10(1)
	^{61}Ni	1.13(1)
	^{62}Ni	3.59(1)
	^{64}Ni	0.91(1)
Energies of lowest excitation levels (MeV):	^{58}Ni	1.45430(10)
		2.4591(2)
		2.7757(3)
		2.9035(11)
	^{60}Ni	1.33252(5)
		2.1587(2)
		2.2849(3)
		2.6260(2)
	^{61}Ni	0.067412(3)
		0.282957(2)
		0.656012(3)
		0.90862(1)
		1.01517(11)
	^{62}Ni	1.17291(9)
		2.30180(11)
		2.33635(13)
		3.15798(25)
	^{64}Ni	1.34579(6)
		2.22772(5)

Inelastic γ rays:		*Energy* (MeV)	*Intensity* (%)
	^{58}Ni	0.9613(2)	3.7(5)
		1.00480(15)	12.3(10)
		1.1617(3)	3.3(8)
		1.3169(4)	2.3(10)
		1.3214(2)	8.7(12)
		1.4486(10)	9.9(20)
		1.45428(10)	100
		1.5837(3)	2.6(3)
	^{60}Ni	0.4671(2)	3.2(4)
		0.82608(15)	10.7(8)
		0.9524(3)	2.8(6)
		1.17310(15)	13.3(10)
		1.2935(2)	2.0(5)

Material constants

Inelastic γ rays:		*Energy* (MeV)	*Intensity* (%)
	^{60}Ni	1.3325(2)	60(5)
		2.1589(3)	2.0(4)
	^{61}Ni	0.2830(2)	1.8(3)
		0.6559(5)	0.40(10)
	^{62}Ni	2.3010(6)	0.95(20)
	^{64}Ni	1.3457	1.8(4)

The dominant neutron induced reaction cross-sections for natural nickel are shown in Fig. 6.62.

Analysis of capture γ rays is the most suitable technique for the measurement of nickel concentrations. The highest capture γ line is free from interference. The excitation function for the $Ni^{nat}(n,\gamma)$ reaction is shown in Fig. 6.63, and numerical data are given in the table after this figure.

In fast neutron fields, the inelastic scattering to the first excited level of ^{58}Ni can also be used for nickel detection. The excitation function for the $^{58}Ni(n,n')$ reaction is shown in Fig. 6.64, and numerical data are given in the table after this figure.

Activation with fast neutrons is in most cases not sensitive enough for practical applications.

6.2.19. Copper (Figures and tables on pp. 196–203)

Material constants

Relative atomic mass:	A_r = 63.546(3)	
Mass density (20°C):	8.98 Mg/m^3	
Number of atoms per unit mass:	9.477×10^{24} kg^{-1}	
Isotope mole fraction (%):	^{63}Cu	69.17(2)
	^{65}Cu	30.83(2)
Energies of lowest excitation levels (MeV):	^{63}Cu	0.6698(10)
		0.96204(10)
		1.32701(10)
		1.41212(10)
		1.54704(10)
		1.8613(2)
		2.0118(3)
	^{65}Cu	0.7706(2)

Material constants

Energies of lowest excitation levels (MeV):	^{65}Cu	1.111555(10)
		1.48181(10)
		1.6233(3)
		1.7249(2)
		2.0943(5)

Inelastic γ rays:		*Energy* (MeV)	*Intensity* (%)
	^{63}Cu	0.4502(2)	5.6(8)
		0.5850(2)	2.8(3)
		0.66968(10)	46(2)
		0.8811(15)	3.3(10)
		0.8992(2)	7.8(8)
		0.96203(10)	100
		1.32700(10)	32(3)
		1.41211(10)	15(2)
		1.54703(10)	12(2)
	^{65}Cu	0.3655(2)	14(2)
		1.11554(10)	37(3)
		1.1635(3)	3.8(6)
		1.4429(8)	2.1(5)
		1.48180(10)	12(2)
		1.6233(3)	4.8(10)

The dominant neutron induced reaction cross-sections for natural copper are shown in Fig. 6.65.

The most sensitive method to determine copper is through the decay of activity produced from ^{65}Cu (n, γ)^{66}Cu. The excitation function for this reaction is shown in Fig. 6.66, and numerical data are given in the table after this figure.

Decay γ rays from ^{66}Cu have an intensive peak at 1.0393 MeV, which can overlap with the 1.0144 MeV γ ray peak from the decay of ^{27}Mg produced from ^{27}Al or ^{26}Mg. The magnitude of possible interference should be estimated.

Another possible method to measure copper is through the thermal neutron capture reaction. The excitation function for the Cu^{nat} (n, γ) reaction is shown in Fig. 6.67, and numerical data are given in the table after this figure.

In fast neutron fields, the inelastic scattering reaction yielding a γ ray of 0.962 MeV can be used for copper analysis. The sensitivity will be somewhat less than that in measurements of the delayed activity of ^{66}Cu. The excitation functions for inelastic scattering of ^{63}Cu are shown in Fig. 6.68, and numerical data are given in the tables after this figure.

6.2.20. Tungsten (Figures and table on pp. 204–206)

Material constants

Relative atomic mass:	A_r = 183.85(3)	
Mass density (20°C):	19.35 Mg/m^3	
Number of atoms per unit mass:	3.276×10^{24} kg^{-1}	
Isotope mole fraction (%):	^{180}W	0.13(3)
	^{182}W	26.3(2)
	^{183}W	14.3(1)
	^{184}W	30.67(15)
	^{186}W	28.6(2)
Energies of lowest excitation levels (MeV):	^{180}W	0.103557(7)
		0.337544(11)
		0.688443(11)
		1.006354(10)
		1.117301(10)
	^{182}W	0.1000(3)
		0.32931(15)
		0.68046(10)
		1.13571(12)
		1.1444(4)
		1.22144(10)
		1.25749(15)
	^{183}W	0.046483(4)
		0.0990793(5)
		0.2070115(5)
		0.2088058(6)
		0.2917240(5)
	^{184}W	0.11121(10)
		0.1460
		0.364056(6)
		0.748310(11)
		0.903281(7)
		1.00248(4)
		1.00598(10)
		1.121437(16)
	^{186}W	0.12258(6)
		0.39655(9)

Material constants

Energies of lowest excitation levels (MeV):

^{186}W	0.73786(9)
	0.808611(9)
	0.869081(3)
	0.95274(11)
	1.00667(10)

Inelastic γ rays:

	Energy (MeV)	*Intensity* (%)
^{180}W	No evaluated data	
^{182}W	0.0678(5)	—
	0.1000(3)	1857(360)
	0.1524(2)	41(9)
	0.1565(4)	17(5)
	0.1782(5)	11(4)
	0.22920(15)	296(30)
	0.9279(2)	16(2)
	1.00016(2)	12.7(13)
	1.03560(12)	28(3)
	1.12132(2)	100
^{183}W	0.1616(2)	34(8)
	0.2092(5)	14(3)
	0.2458(3)	13(4)
	0.2932(2)	18(3)
	0.3132(3)	27(5)
	0.3545(6)	2.2(6)
^{184}W	0.11121(10)	859(150)
	0.21521(10)	35(9)
	0.22674(10)	104(15)
	0.252850(10)	280(50)
	0.31804(10)	57(9)
	0.38427(10)	35(4)
	0.79208(10)	118(2)
	0.89477(10)	102(20)
	0.90328(2)	100
	1.0104(3)	23(5)
^{186}W	0.12230(10)	168(45)
	0.2146(3)	54(15)
	0.27394(10)	76(15)
	0.3080(3)	31(3)
	0.61530(10)	59(7)
	0.73840(10)	100

The dominant neutron induced reaction cross-sections for natural tungsten are shown in Fig. 6.69.

The best method to determine tungsten concentrations is to use the measurement of the delayed radioactivity from the $^{186}W(n,\gamma)^{187}W$ reaction. The excitation function for this reaction is shown in Fig. 6.70, and numerical data are given in the table after this figure.

The inelastic scattering in tungsten produces copious γ lines with low intensities. The spectrum is too complicated for analysis, and the comparison with evaluated data is very obscure. The inelastic scattering reaction is not recommended for use in the analysis of tungsten concentrations.

6.2.21. Gold (Figures and tables on pp. 207–211)

Material constants

Relative atomic mass:	A_r = 196.9665(1)
Mass density (20°C):	19.31 Mg/m^3
Number of atoms per unit mass:	3.057×10^{24} kg^{-1}
Isotope mole fraction (%):	^{197}Au 100
Energies of lowest excitation levels (MeV):	0.07735(2) 0.26866(15) 0.27895(2) 0.4092(4) 0.5027(4) 0.54762(10) 0.73689(10)

Inelastic γ rays:

Energy (MeV)	*Intensity* (%)
0.1302(4)	2.1(6)
0.144	2
0.17472(15)	27(4)
0.2020(4)	2.2(5)
0.2687(2)	2.1(3)
0.27895(2)	100
0.5027(4)	17(5)
0.54762(10)	17.2(9)

The dominant neutron induced reaction cross-sections for natural gold are shown in Fig. 6.71.

The best method for gold analysis is to use the $^{197}Au\,(n, n'\gamma)\,^{197}Au$ reaction, yielding 0.279 MeV γ rays. The cross-section of this reaction is shown in Fig. 6.72, and numerical data are given in the table after this figure.

If long activation times are permissible, the delayed γ rays from the reaction $^{197}Au\,(n,\gamma)\,^{198}Au$ are substantially more sensitive. Other fast neutron activations are less sensitive and are not recommended for practical use.

The excitation function for the $^{197}Au\,(n,\gamma)\,^{198}Au$ reaction is shown in Fig. 6.73, and numerical data are given in the table after this figure.

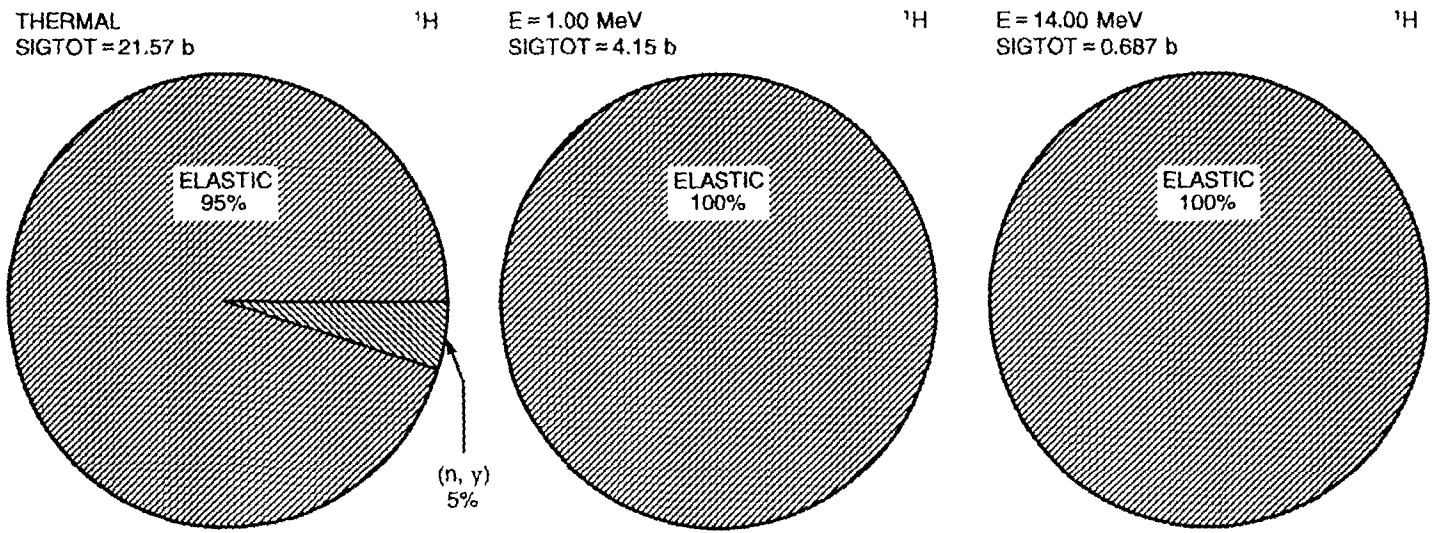

FIG. 6.1. Pie charts of the dominant neutron induced reaction cross-sections for hydrogen [4].

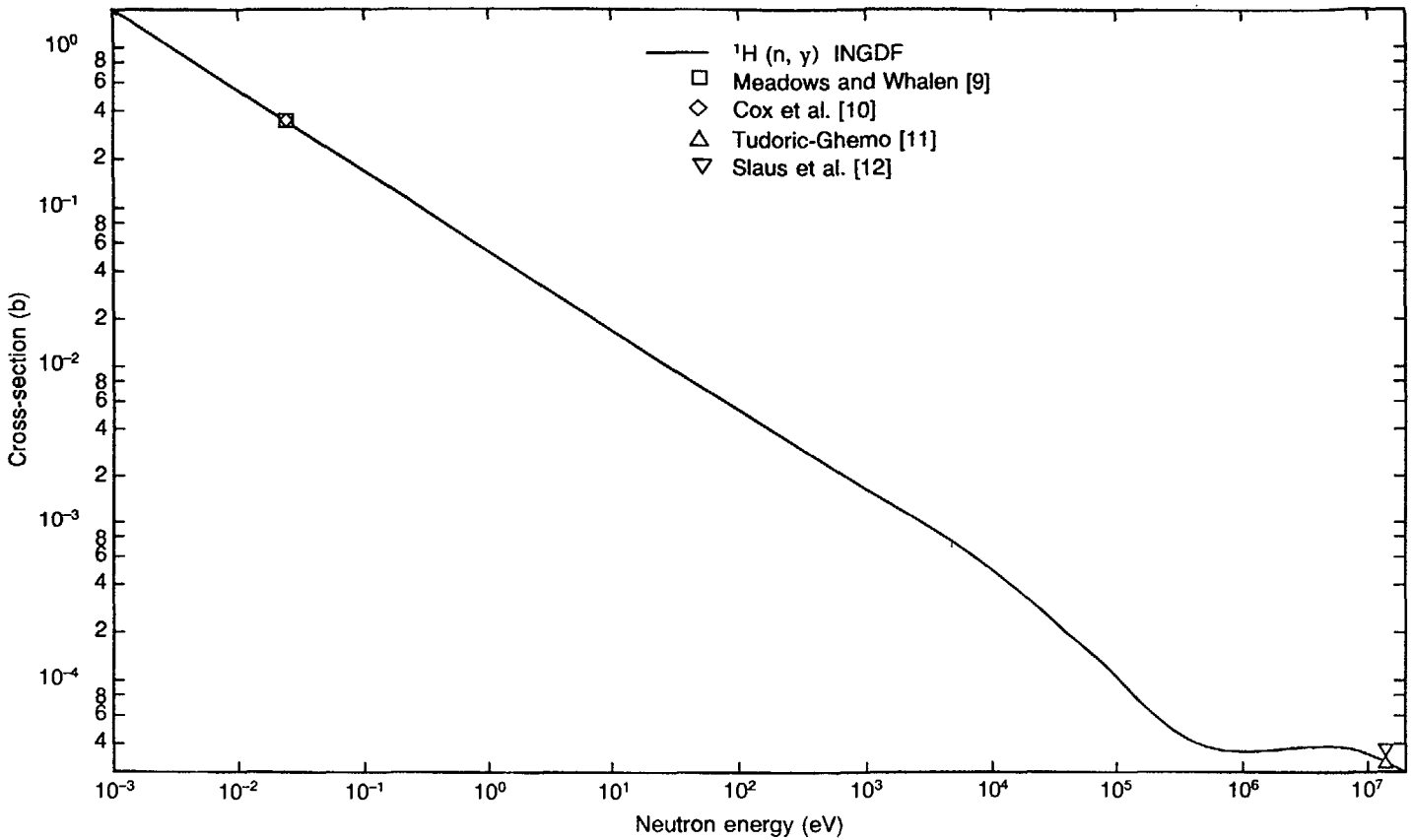

FIG. 6.2. Excitation function for the $^1H(n,\gamma)$ reaction. Evaluated data from Ref. [4].

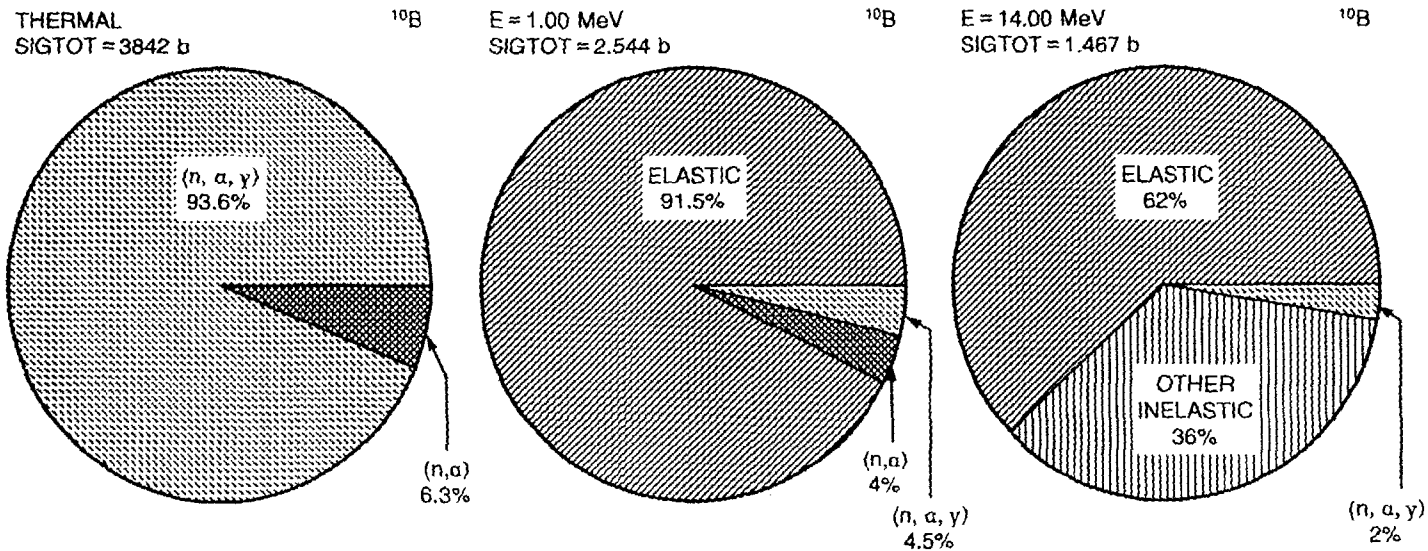

FIG. 6.3. Pie charts of the dominant neutron induced reaction cross-sections for boron.

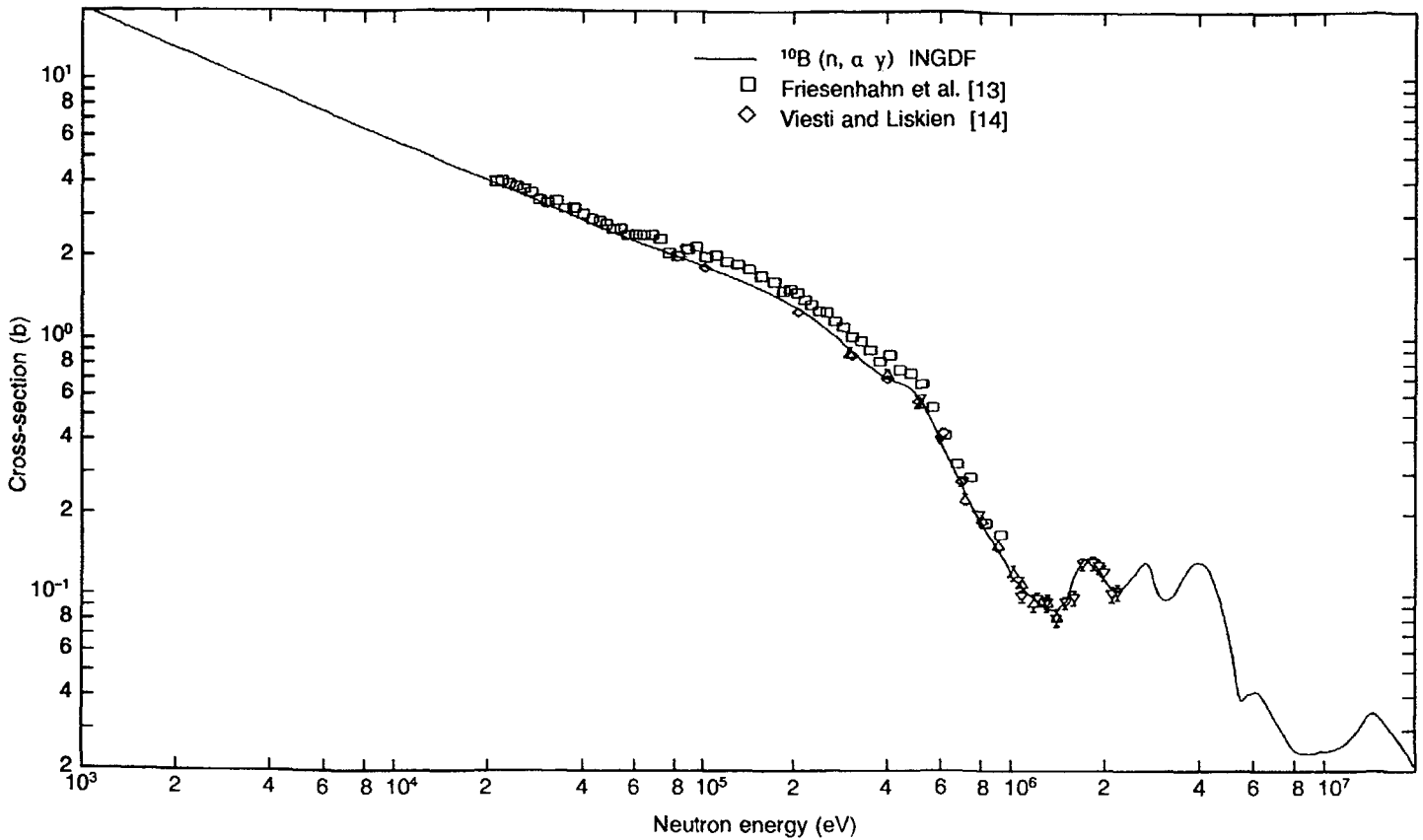

FIG. 6.4. Excitation function for the $^{10}B(n,\alpha\gamma)^{7}Li$ reaction. Evaluated data from Ref. [4].

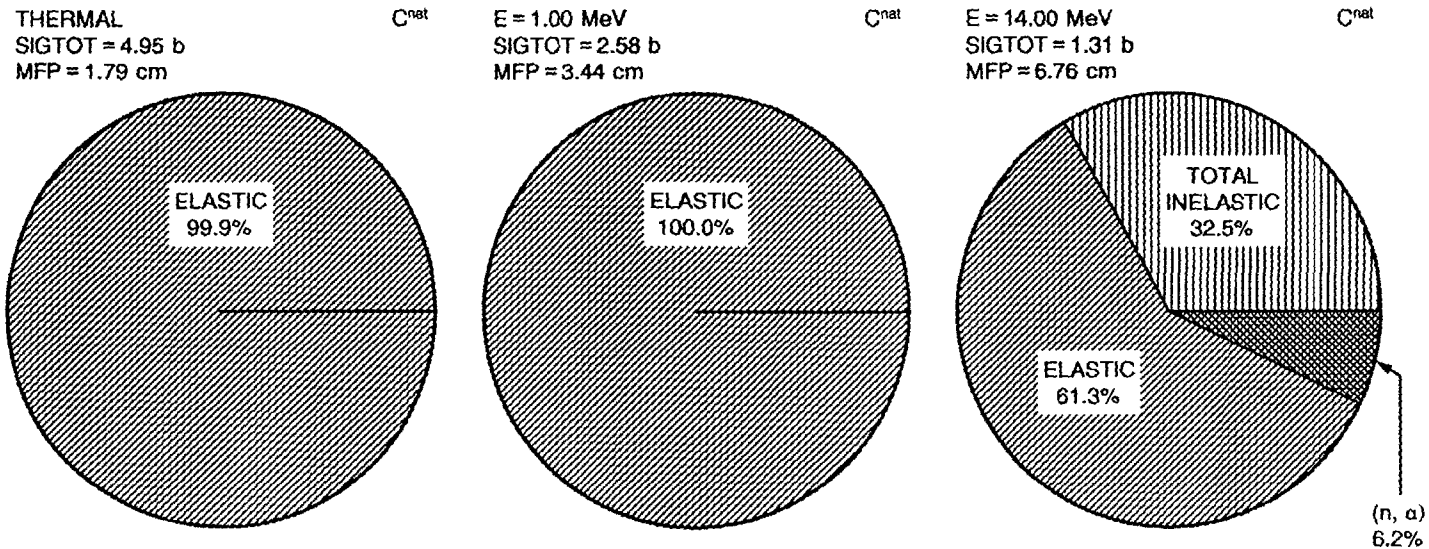

FIG. 6.5. Pie charts of the dominant neutron induced reaction cross-sections for C^{nat} at thermal, 1 MeV and 14 MeV incident energies.

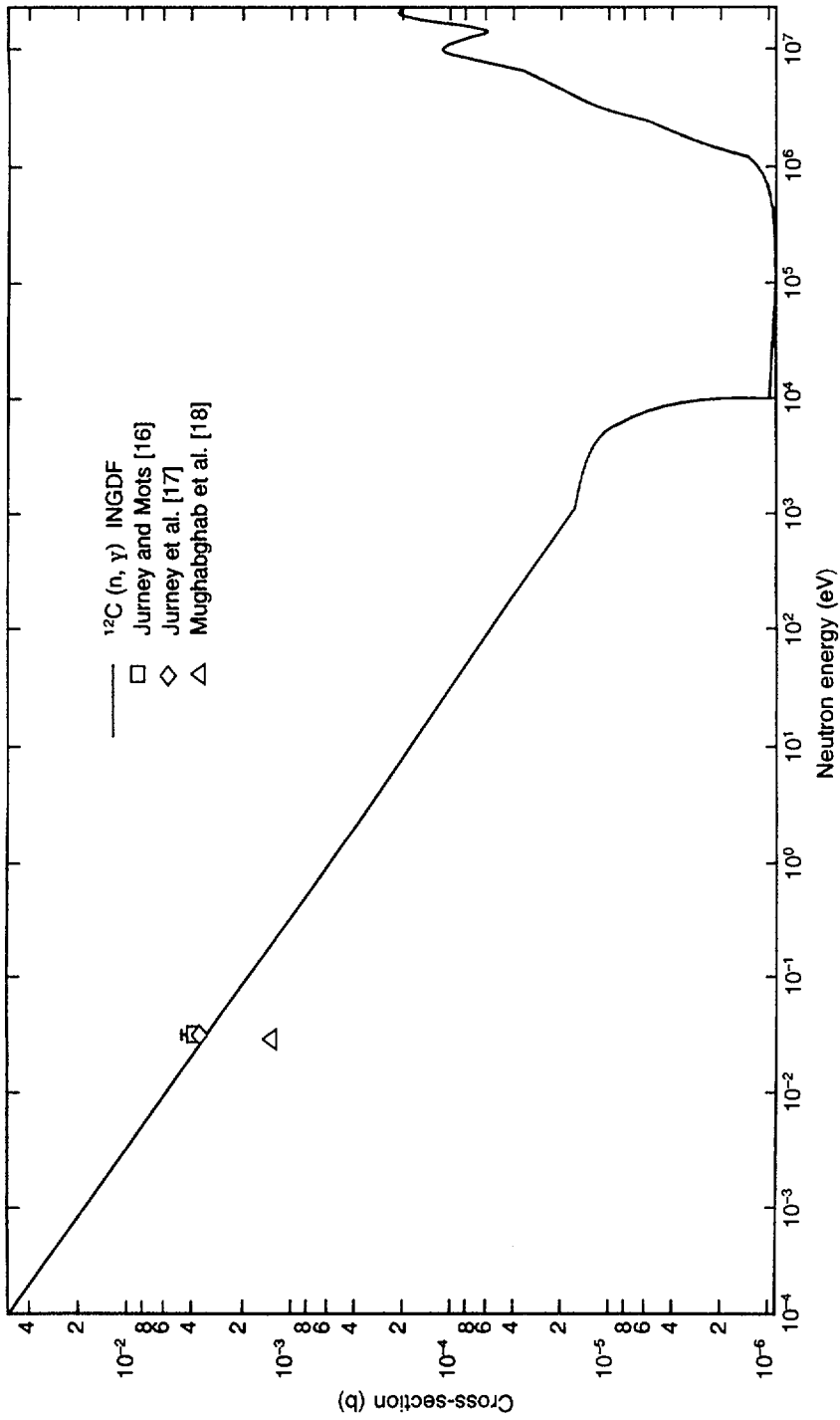

FIG. 6.6. Excitation function for the $^{12}C(n,\gamma)$ reaction. Evaluated data from Ref. [15].

^{12}C (n, γ)

E_n (eV)	σ (b)	E_n (eV)	σ (b)	E_n (eV)	σ (b)
1.00000×10^{-3}	3.09176×10^{-3}	1.00000×10^{-1}	8.22181×10^{-4}	1.00000	2.60004×10^{-4}
1.00000×10^{1}	8.22168×10^{-5}	1.00000×10^{2}	2.60002×10^{-5}	1.00000×10^{3}	9.05098×10^{-6}
1.00000×10^{4}	9.77775×10^{-7}	5.00000×10^{4}	9.27777×10^{-7}	1.00000×10^{5}	9.50003×10^{-7}
5.00000×10^{5}	1.14060×10^{-6}	1.00000×10^{6}	2.19898×10^{-6}	1.50000×10^{6}	4.40087×10^{-6}
2.00000×10^{6}	7.68342×10^{-6}	2.50000×10^{6}	1.21559×10^{-5}	3.00000×10^{6}	1.57083×10^{-5}
3.50000×10^{6}	1.92334×10^{-5}	4.00000×10^{6}	2.29955×10^{-5}	4.50000×10^{6}	2.66376×10^{-5}
5.00000×10^{6}	3.16646×10^{-5}	5.50000×10^{6}	3.96582×10^{-5}	6.00000×10^{6}	5.17319×10^{-5}
6.50000×10^{6}	6.73219×10^{-5}	7.00000×10^{6}	8.72612×10^{-5}	7.50000×10^{6}	1.05329×10^{-4}
8.00000×10^{6}	1.13577×10^{-4}	8.50000×10^{6}	1.14375×10^{-4}	9.00000×10^{6}	1.05700×10^{-4}
9.50000×10^{6}	9.33138×10^{-5}	1.00000×10^{7}	7.91428×10^{-5}	1.10000×10^{7}	6.47552×10^{-5}
1.20000×10^{7}	6.61593×10^{-5}	1.30000×10^{7}	9.33167×10^{-5}	1.40000×10^{7}	1.37671×10^{-4}
1.50000×10^{7}	1.79092×10^{-4}	1.60000×10^{7}	2.04352×10^{-4}	1.70000×10^{7}	2.04006×10^{-4}
1.80000×10^{7}	1.95824×10^{-4}	1.90000×10^{7}	2.04522×10^{-4}		

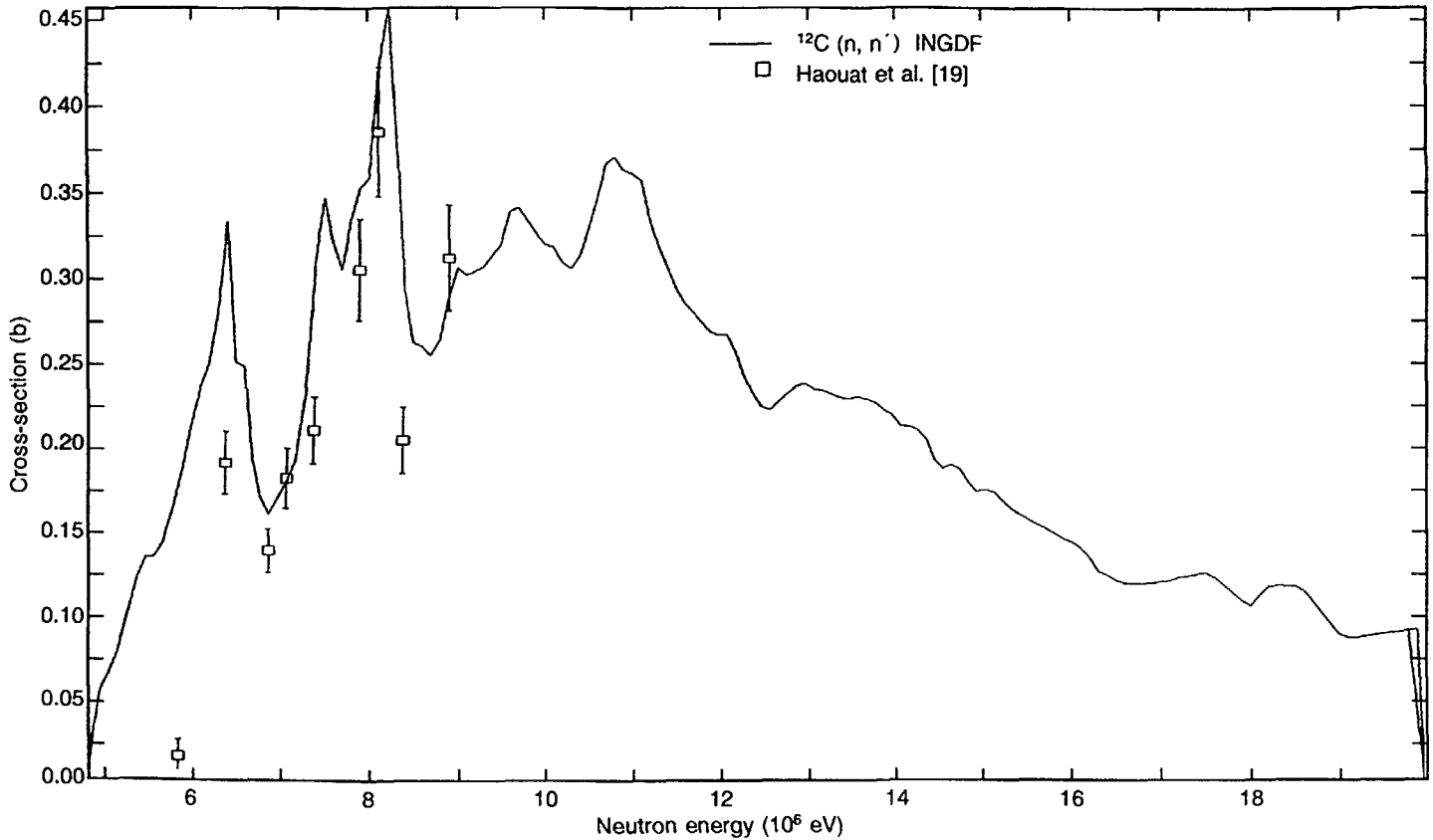

FIG. 6.7. Excitation functions for inelastic scattering of ^{12}C to the first excited level. Evaluated data from Ref. [15].

^{12}C (n, n′)

E_n (eV)	σ (b)	E_n (eV)	σ (b)	E_n (eV)	σ (b)
4.50000×10^{6}	1.20599×10^{-2}	5.00000×10^{6}	9.44265×10^{-2}	5.50000×10^{6}	1.63065×10^{-1}
6.00000×10^{6}	2.66301×10^{-1}	6.50000×10^{6}	1.84202×10^{-1}	7.00000×10^{6}	2.48731×10^{-1}
7.50000×10^{6}	3.31301×10^{-1}	8.00000×10^{6}	3.62125×10^{-1}	8.50000×10^{6}	2.71220×10^{-1}
9.00000×10^{6}	3.06716×10^{-1}	9.50000×10^{6}	3.30164×10^{-1}	1.00000×10^{7}	3.36559×10^{-1}
1.10000×10^{7}	2.96588×10^{-1}	1.20000×10^{7}	2.35171×10^{-1}	1.30000×10^{7}	2.26184×10^{-1}
1.40000×10^{7}	1.92497×10^{-1}	1.50000×10^{7}	1.57002×10^{-1}	1.60000×10^{7}	1.23628×10^{-1}
1.70000×10^{7}	1.17408×10^{-1}	1.80000×10^{7}	1.08082×10^{-1}	1.90000×10^{7}	8.69594×10^{-2}

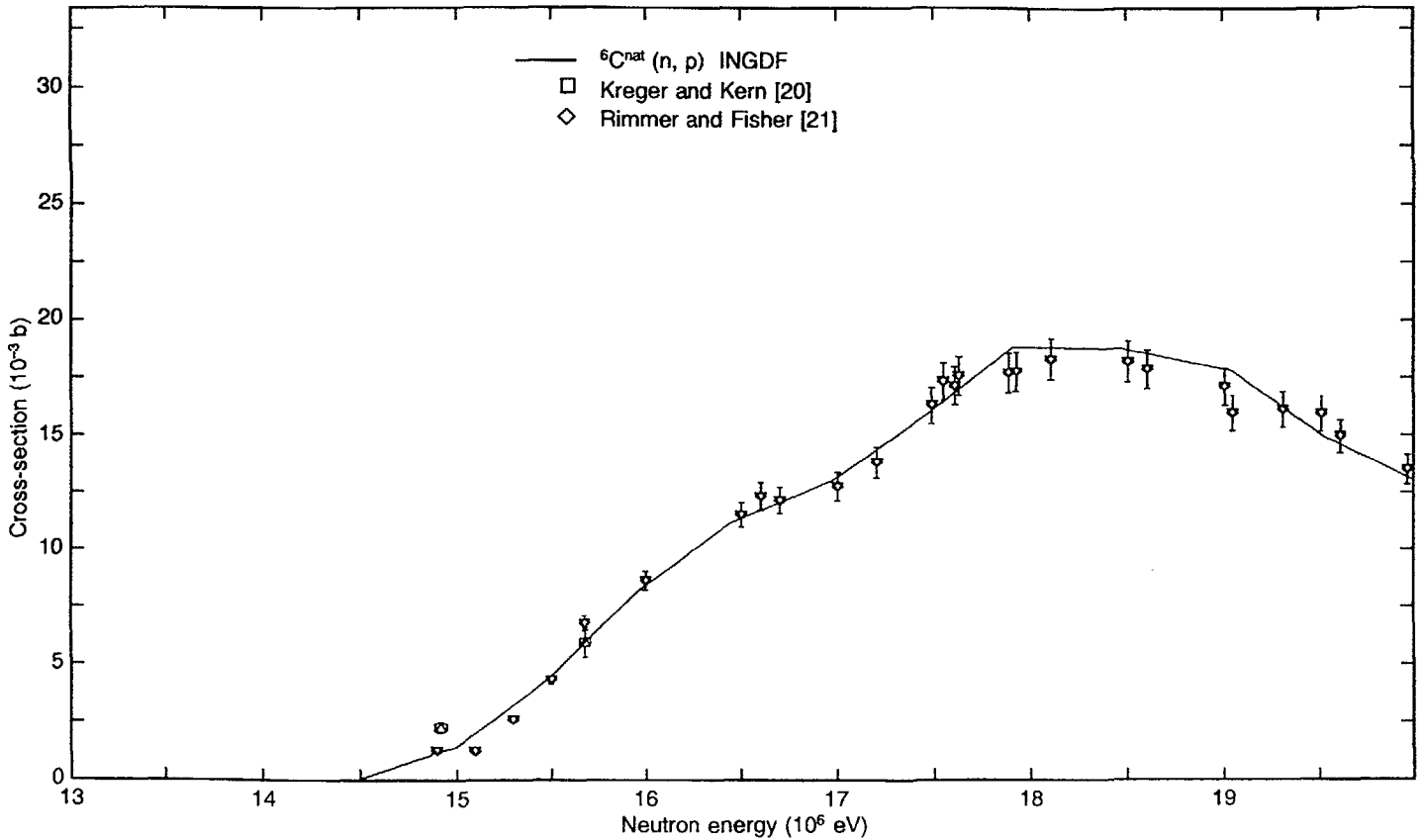

FIG. 6.8. Excitation function for the C(n,p) reaction. Evaluated data from Ref. [15].

C (n, p)

E_n (eV)	σ (b)	E_n (eV)	σ (b)	E_n (eV)	σ (b)
1.40000×10^7	2.51708×10^{-4}	1.50000×10^7	4.41310×10^{-3}	1.60000×10^7	1.10047×10^{-2}
1.70000×10^7	1.63382×10^{-2}	1.80000×10^7	1.87648×10^{-2}	1.90000×10^7	1.53295×10^{-2}

The C(n, p) reaction is the most important activation reaction on carbon. It is not convenient to use it for carbon detection because of the short half-life of the reaction product, ^{12}B (0.02 s), and the rather low cross-section. In some cases, one might consider its contribution to the $E_\gamma = 4.438$ MeV γ line from inelastic scattering on carbon.

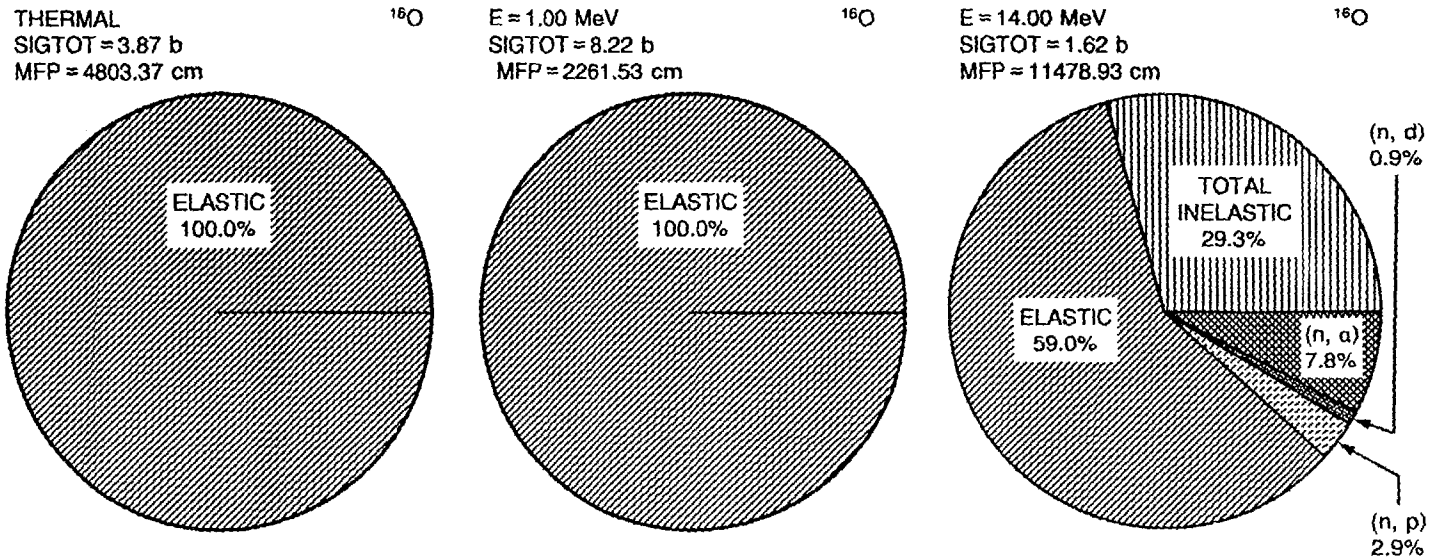

FIG. 6.9. Pie charts of the dominant neutron induced reaction cross-sections for ^{16}O.

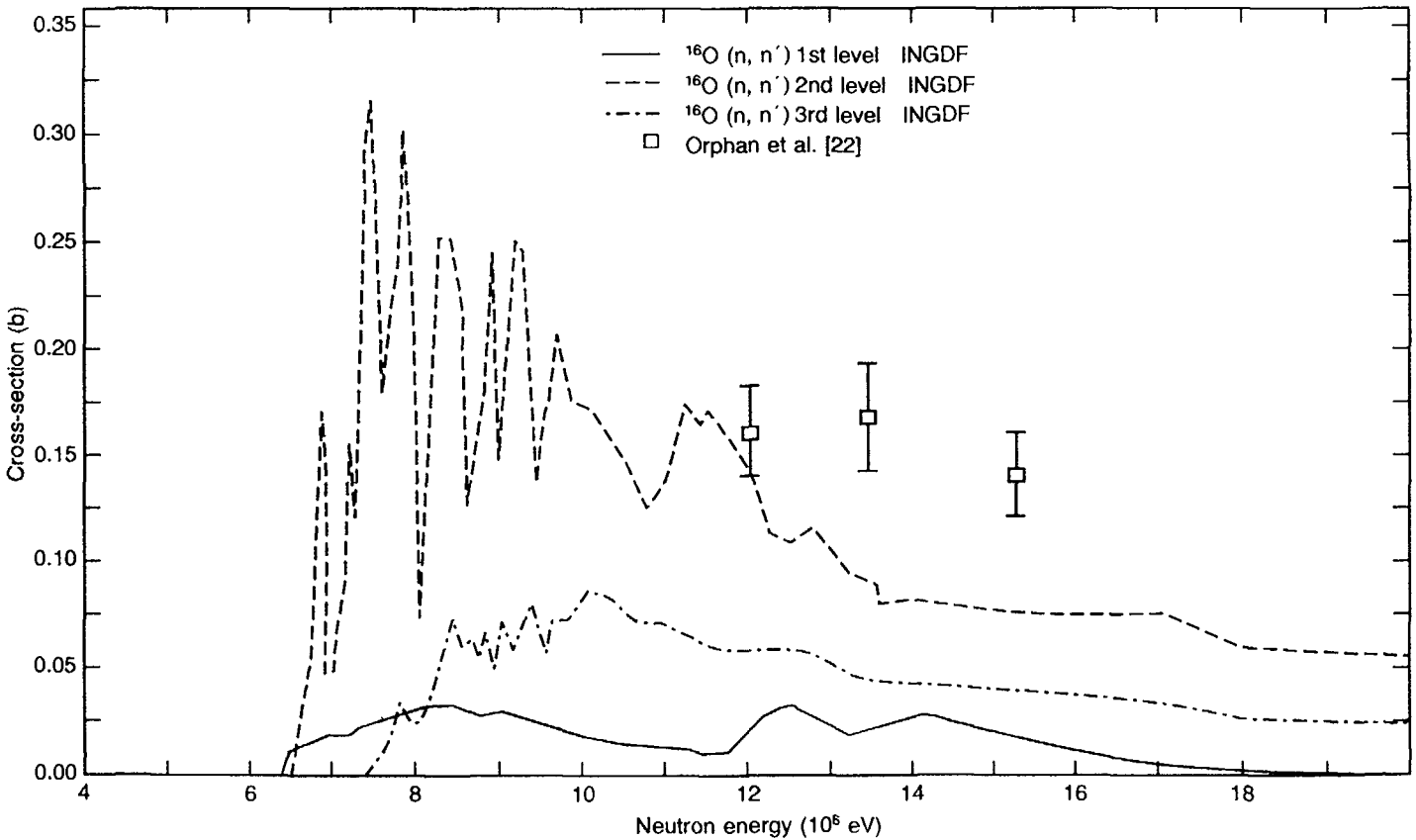

FIG. 6.10. Excitation functions for inelastic scattering of ^{16}O to the first, second and third excited states. Evaluated data from Ref. [23].

Inelastic scattering to the first excited level of ^{16}O

E_n (eV)	σ (b)	E_n (eV)	σ (b)	E_n (eV)	σ (b)
6.00000×10^{6}	7.08006×10^{-4}	6.50000×10^{6}	1.42519×10^{-2}	7.00000×10^{6}	2.03429×10^{-2}
7.50000×10^{6}	2.73483×10^{-2}	8.00000×10^{6}	3.26181×10^{-2}	8.50000×10^{6}	3.02061×10^{-2}
9.00000×10^{6}	2.75498×10^{-2}	9.50000×10^{6}	2.14920×10^{-2}	1.00000×10^{7}	1.52942×10^{-2}
1.10000×10^{7}	1.27436×10^{-2}	1.20000×10^{7}	2.83387×10^{-2}	1.30000×10^{7}	2.31339×10^{-2}
1.40000×10^{7}	2.46869×10^{-2}	1.50000×10^{7}	1.59306×10^{-2}	1.60000×10^{7}	8.38052×10^{-3}
1.70000×10^{7}	3.62767×10^{-3}	1.80000×10^{7}	1.34938×10^{-3}	1.90000×10^{7}	5.55252×10^{-4}

Inelastic scattering to the second excited level of ^{16}O

E_n (eV)	σ (b)	E_n (eV)	σ (b)	E_n (eV)	σ (b)
6.50000×10^{6}	6.61950×10^{-2}	7.00000×10^{6}	1.72891×10^{-1}	7.50000×10^{6}	2.21565×10^{-1}
8.00000×10^{6}	1.88672×10^{-1}	8.50000×10^{6}	1.79539×10^{-1}	9.00000×10^{6}	1.98446×10^{-1}
9.50000×10^{6}	1.84509×10^{-1}	1.00000×10^{7}	1.48455×10^{-1}	1.10000×10^{7}	1.61179×10^{-1}
1.20000×10^{7}	1.14813×10^{-1}	1.30000×10^{7}	8.90257×10^{-2}	1.40000×10^{7}	7.92344×10^{-2}
1.50000×10^{7}	7.55450×10^{-2}	1.60000×10^{7}	7.51548×10^{-2}	1.70000×10^{7}	6.78941×10^{-2}
1.80000×10^{7}	5.86879×10^{-2}	1.90000×10^{7}	5.64247×10^{-2}		

Inelastic scattering to the third excited level of ^{16}O

E_n (eV)	σ (b)	E_n (eV)	σ (b)	E_n (eV)	σ (b)
7.00000×10^{6}	8.62214×10^{-4}	7.50000×10^{6}	2.13854×10^{-2}	8.00000×10^{6}	4.76516×10^{-2}
8.50000×10^{6}	6.06596×10^{-2}	9.00000×10^{6}	7.00955×10^{-2}	9.50000×10^{6}	7.27975×10^{-2}
1.00000×10^{7}	7.77286×10^{-2}	1.10000×10^{7}	6.25816×10^{-2}	1.20000×10^{7}	5.74575×10^{-2}
1.30000×10^{7}	4.53542×10^{-2}	1.40000×10^{7}	4.18428×10^{-2}	1.50000×10^{7}	3.89945×10^{-2}
1.60000×10^{7}	3.56836×10^{-2}	1.70000×10^{7}	3.07394×10^{-2}	1.80000×10^{7}	2.67894×10^{-2}
1.90000×10^{7}	2.50778×10^{-2}				

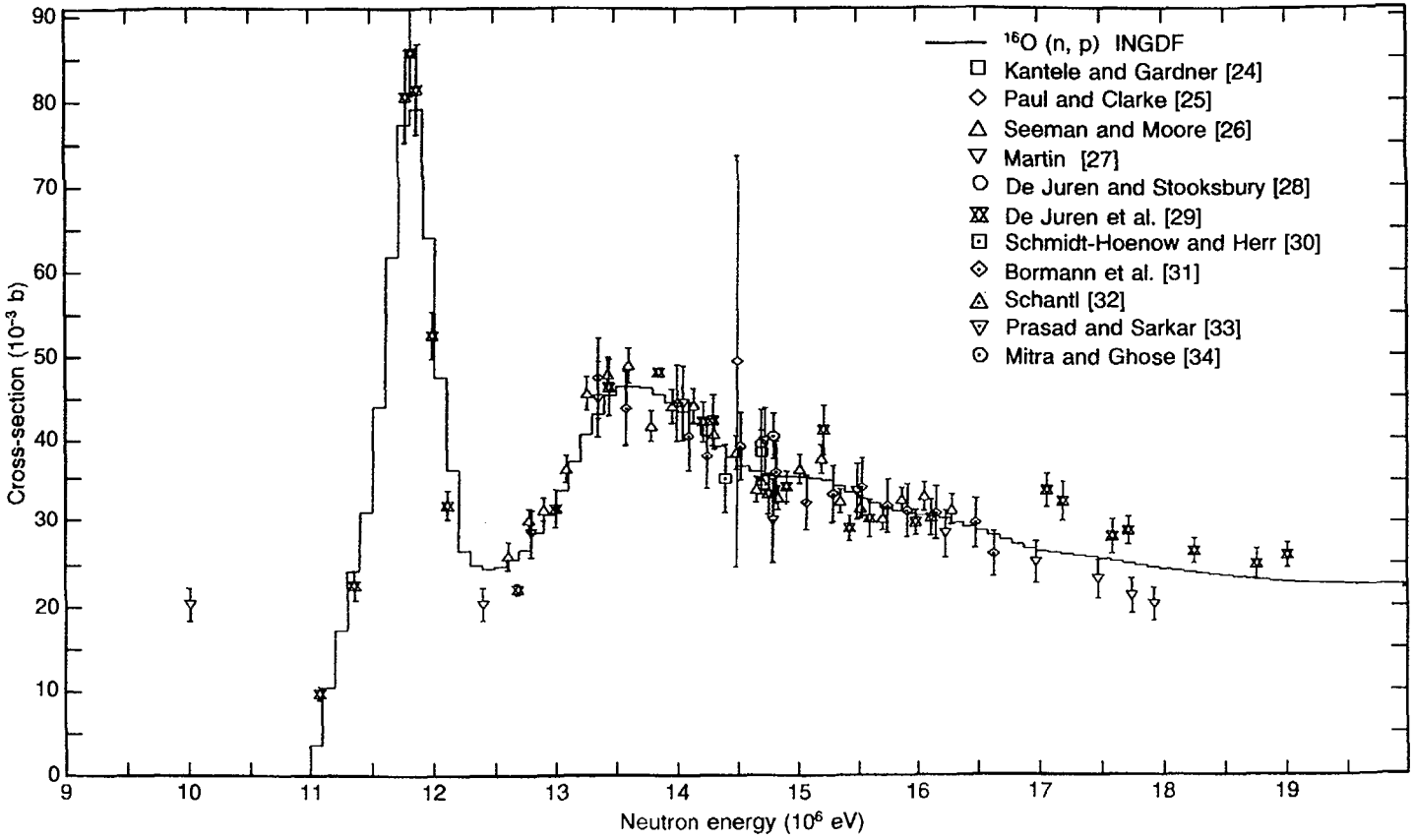

FIG. 6.11. Excitation function for the $^{16}O(n,p)^{16}N$ reaction. Evaluated data from Ref. [23].

$^{16}O\,(n,p)\,^{16}N$

E_n (eV)	σ (b)	E_n (eV)	σ (b)	E_n (eV)	σ (b)
1.10000×10^7	4.10730×10^{-2}	1.20000×10^7	2.94500×10^{-2}	1.30000×10^7	4.25750×10^{-2}
1.40000×10^7	3.79750×10^{-2}	1.50000×10^7	3.31625×10^{-2}	1.60000×10^7	2.89000×10^{-2}
1.70000×10^7	2.54750×10^{-2}	1.80000×10^7	2.35000×10^{-2}	1.90000×10^7	2.25000×10^{-2}

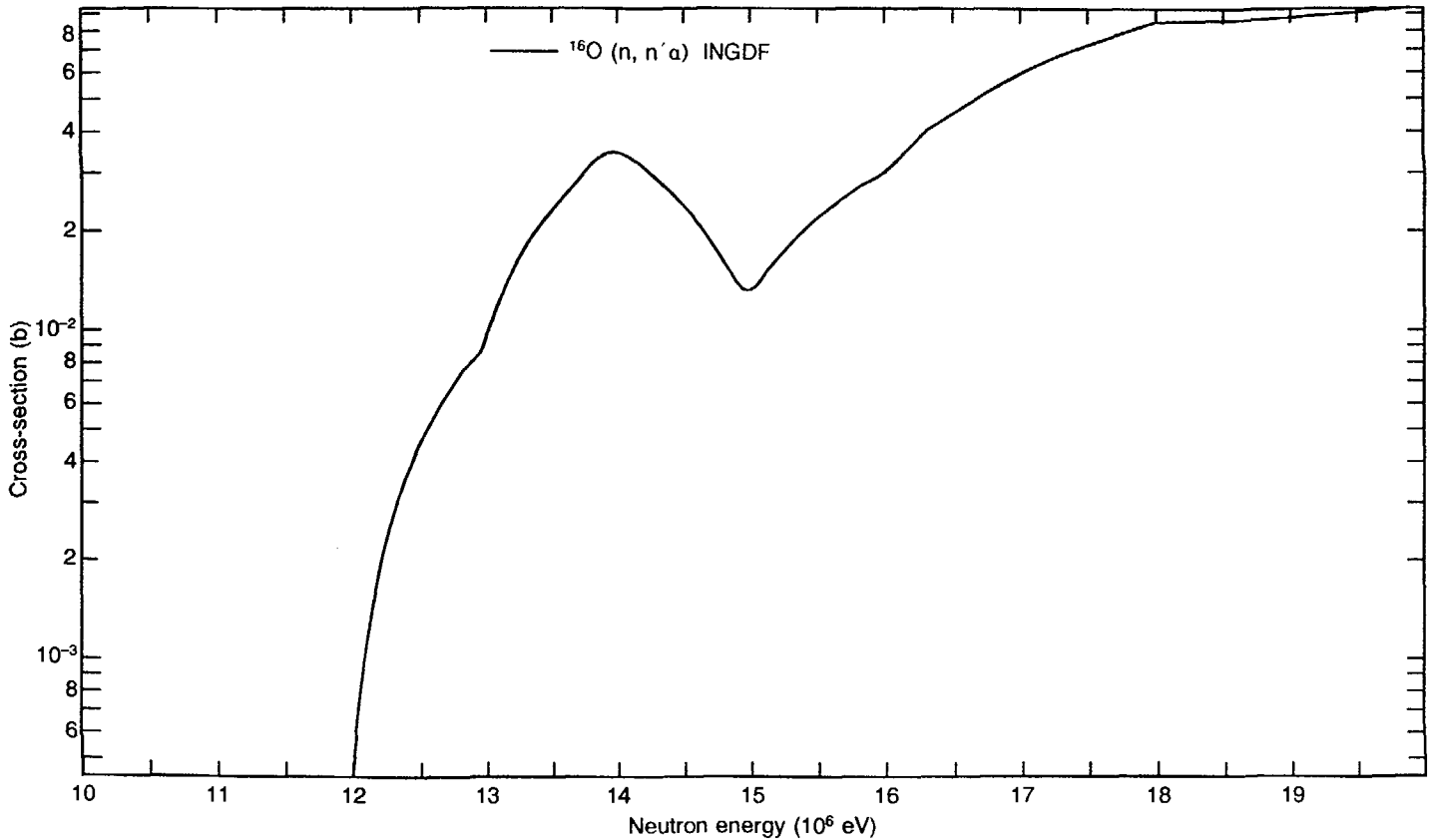

FIG. 6.12. Excitation function for the $^{16}O(n,n'\alpha)$ reaction. Evaluated data from Ref. [23].

^{16}O (n, n′ α)

E_n (eV)	σ (b)	E_n (eV)	σ (b)	E_n (eV)	σ (b)
1.20000×10^7	4.42839×10^{-3}	1.30000×10^7	2.27325×10^{-2}	1.40000×10^7	2.45119×10^{-2}
1.50000×10^7	2.15339×10^{-2}	1.60000×10^7	4.51620×10^{-2}	1.70000×10^7	7.26035×10^{-2}
1.80000×10^7	8.62959×10^{-2}	1.90000×10^7	9.03840×10^{-2}		

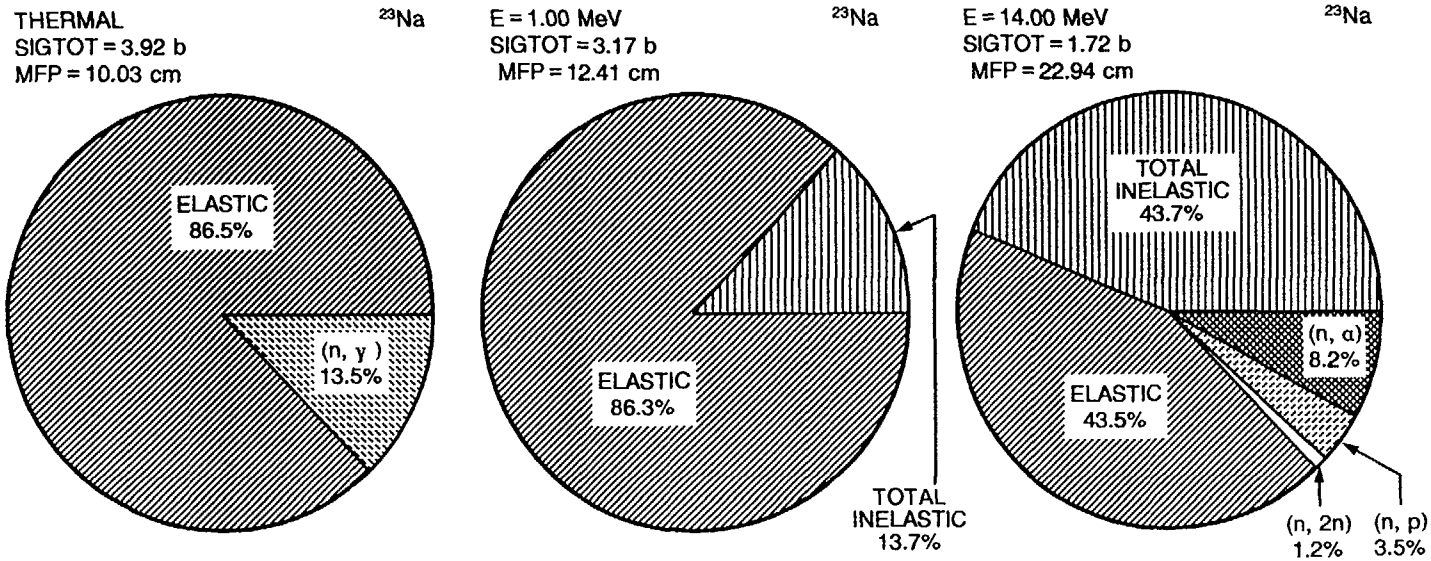

FIG. 6.13. Pie charts of the dominant neutron induced reaction cross-sections for ^{23}Na.

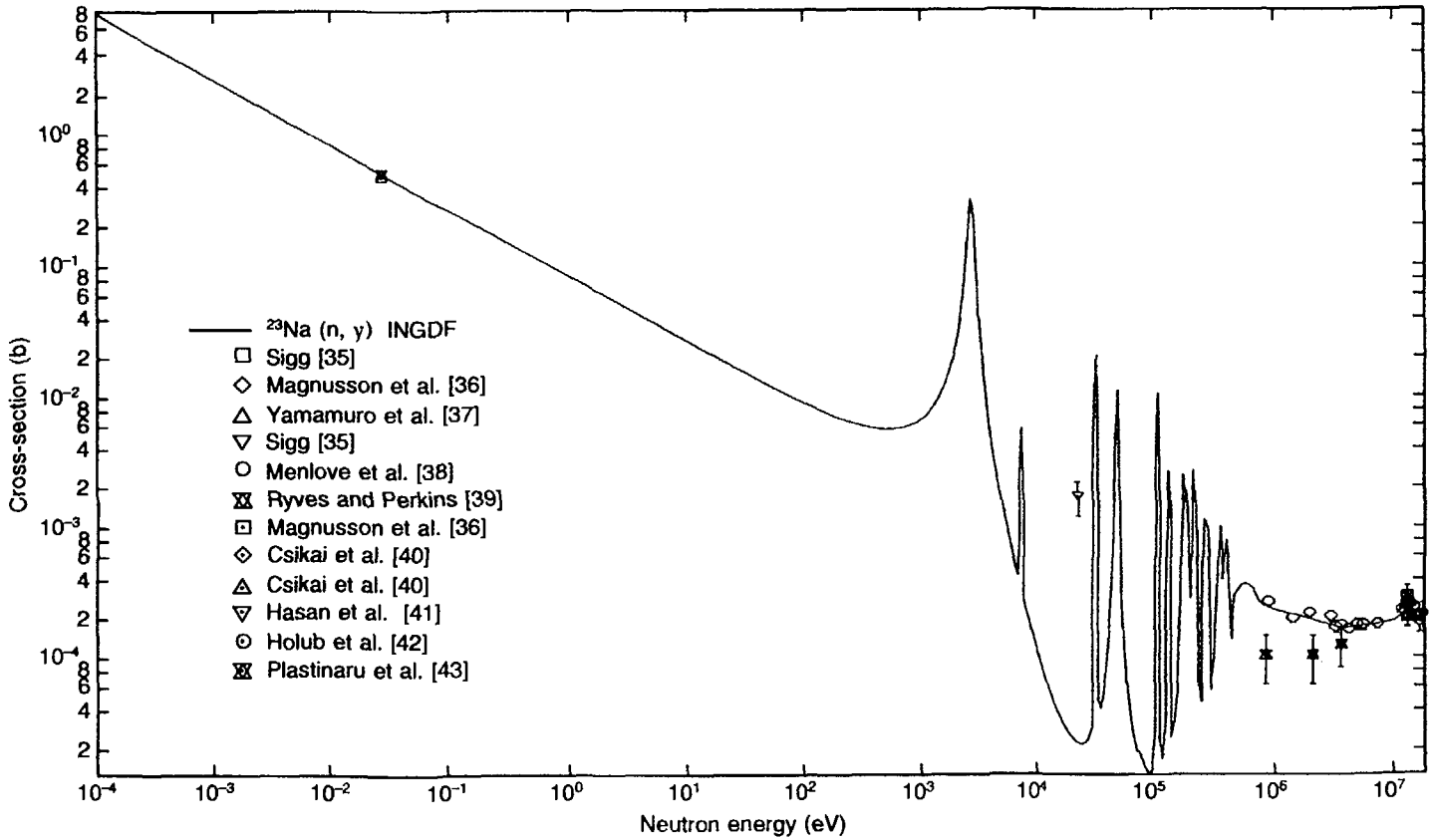

FIG. 6.14. Excitation function for the $^{23}Na(n,\gamma)^{24}Na$ reaction. Evaluated data from Ref. [44].

$^{23}Na\,(n,\gamma)\,^{24}Na$

E_n (eV)	σ (b)	E_n (eV)	σ (b)	E_n (eV)	σ (b)
1.00000×10^{-3}	4.83117×10^{-1}	1.00000×10^{-1}	1.27700×10^{-1}	1.00000	4.05518×10^{-2}
1.00000×10^{1}	1.32460×10^{-2}	1.00000×10^{2}	6.09455×10^{-3}	1.00000×10^{3}	2.26833×10^{-2}
1.00000×10^{4}	1.09054×10^{-3}	5.00000×10^{4}	7.50310×10^{-4}	1.00000×10^{5}	6.88818×10^{-4}
5.00000×10^{5}	2.91547×10^{-4}	1.00000×10^{6}	2.17534×10^{-4}	1.50000×10^{6}	1.98999×10^{-4}
2.00000×10^{6}	1.86209×10^{-4}	2.50000×10^{6}	1.76648×10^{-4}	3.00000×10^{6}	1.69096×10^{-4}
3.50000×10^{6}	1.62818×10^{-4}	4.00000×10^{6}	1.60000×10^{-4}	4.50000×10^{6}	1.60821×10^{-4}
5.00000×10^{6}	1.62462×10^{-4}	5.50000×10^{6}	1.64104×10^{-4}	6.00000×10^{6}	1.65559×10^{-4}
6.50000×10^{6}	1.66828×10^{-4}	7.00000×10^{6}	1.68097×10^{-4}	7.50000×10^{6}	1.69366×10^{-4}
8.00000×10^{6}	1.70774×10^{-4}	8.50000×10^{6}	1.72322×10^{-4}	9.00000×10^{6}	1.73870×10^{-4}
9.50000×10^{6}	1.75345×10^{-4}	1.00000×10^{7}	1.77342×10^{-4}	1.10000×10^{7}	1.81057×10^{-4}
1.20000×10^{7}	1.91111×10^{-4}	1.30000×10^{7}	2.03824×10^{-4}	1.40000×10^{7}	2.21177×10^{-4}
1.50000×10^{7}	2.31541×10^{-4}	1.60000×10^{7}	2.34623×10^{-4}	1.70000×10^{7}	2.37705×10^{-4}
1.80000×10^{7}	2.40787×10^{-4}	1.90000×10^{7}	2.43869×10^{-4}		

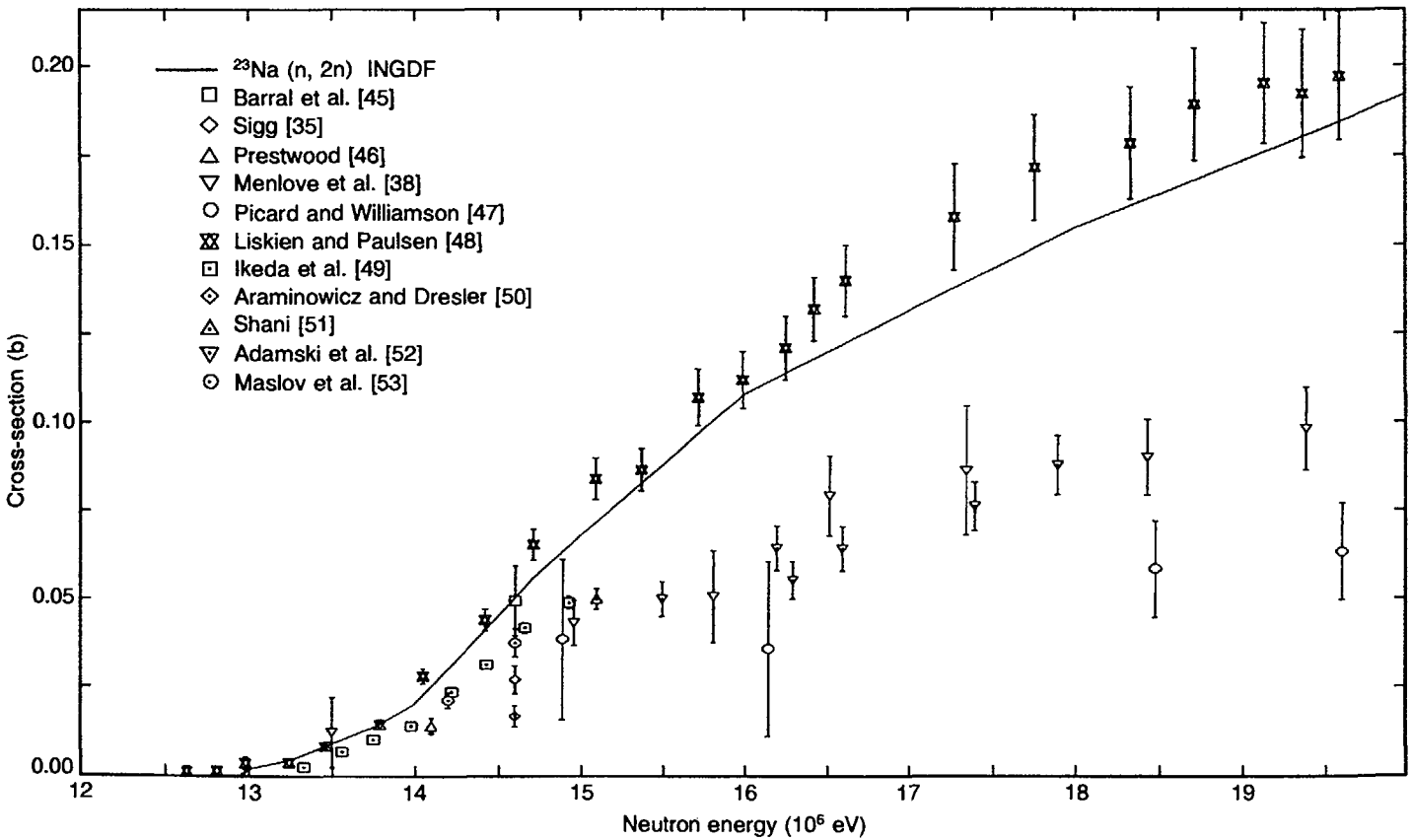

FIG. 6.15. Excitation function for the $^{23}Na(n,2n)^{22}Na$ reaction. Evaluated data from Ref. [44].

$^{23}Na\,(n,2n)\,^{22}Na$

E_n (eV)	σ (b)	E_n (eV)	σ (b)	E_n (eV)	σ (b)
1.20000×10^{7}	4.00000×10^{-5}	1.30000×10^{7}	9.24600×10^{-3}	1.40000×10^{7}	4.49180×10^{-2}
1.50000×10^{7}	8.87000×10^{-2}	1.60000×10^{7}	1.20750×10^{-1}	1.70000×10^{7}	1.44250×10^{-1}
1.80000×10^{7}	1.65500×10^{-1}	1.90000×10^{7}	1.84500×10^{-1}		

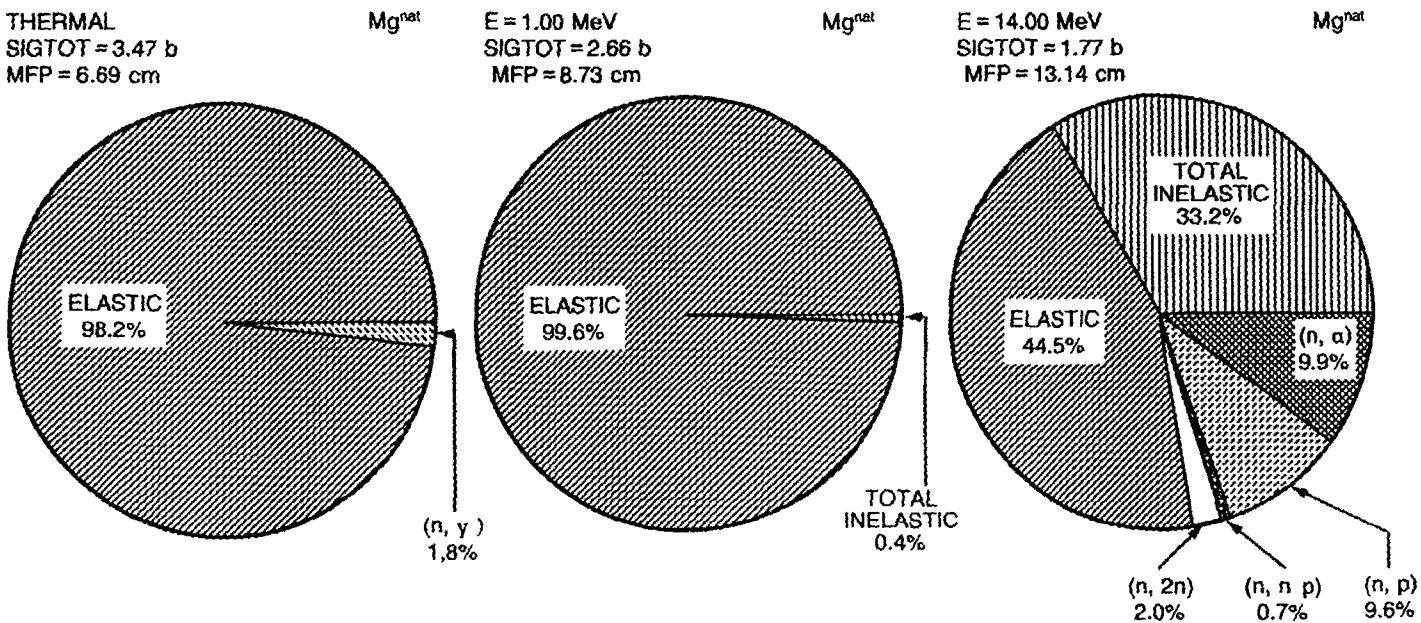

FIG. 6.16. Pie charts of the dominant neutron induced reaction cross-sections for magnesium.

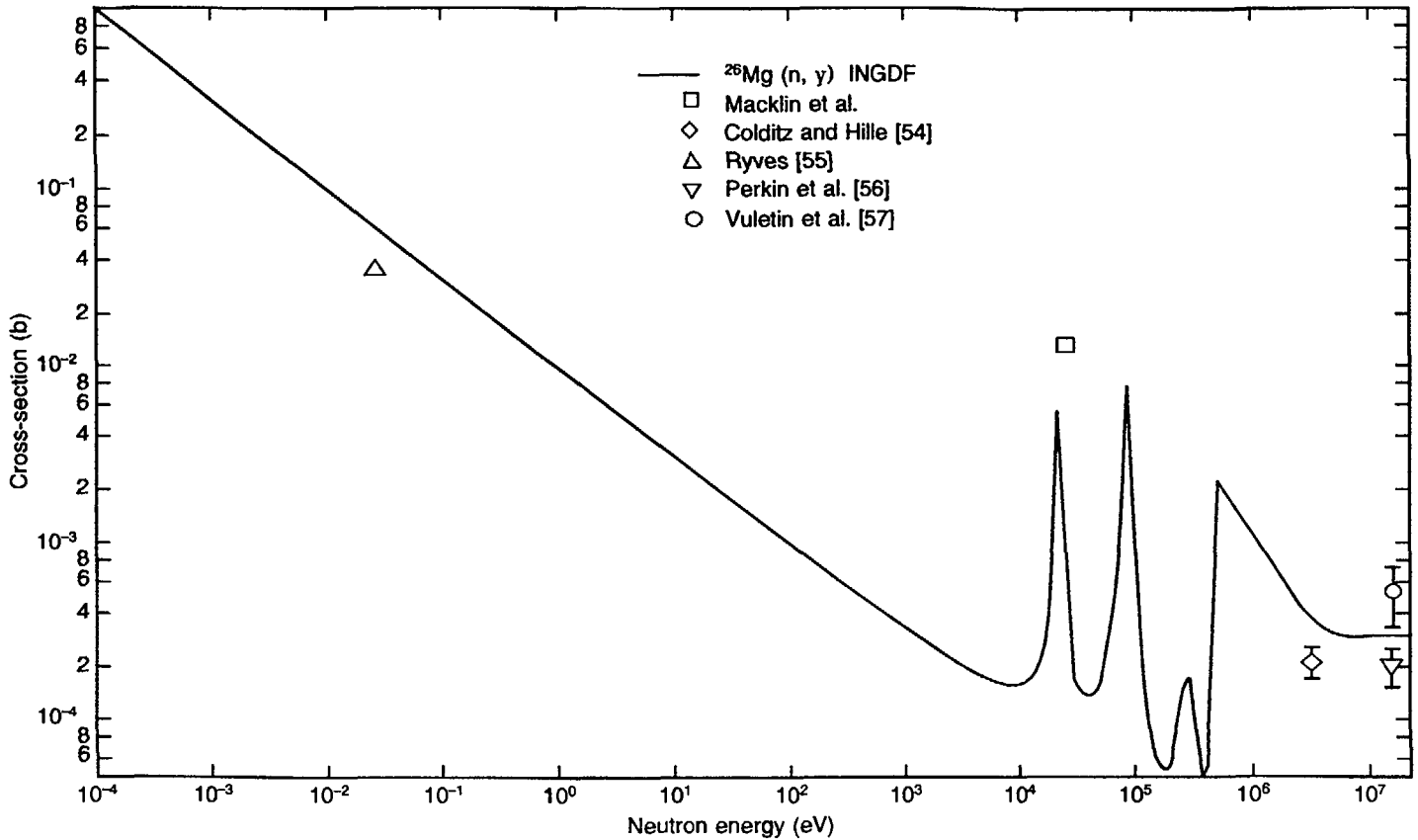

FIG. 6.17. Excitation function for the $^{26}Mg\,(n,\gamma)$ reaction. Evaluated data from Ref. [58].

$^{26}Mg\,(n,\gamma)$

E_n (eV)	σ (b)	E_n (eV)	σ (b)	E_n (eV)	σ (b)
1.00000×10^{5}	5.00430×10^{-5}	5.00000×10^{5}	3.50632×10^{-4}	1.00000×10^{6}	3.76455×10^{-4}
1.50000×10^{6}	3.81977×10^{-4}	2.00000×10^{6}	1.99418×10^{-4}	2.50000×10^{6}	1.75585×10^{-4}
3.00000×10^{6}	1.65179×10^{-4}	3.50000×10^{6}	1.50903×10^{-4}	4.00000×10^{6}	1.50110×10^{-4}
4.50000×10^{6}	1.31096×10^{-4}	5.00000×10^{6}	1.15459×10^{-4}	5.50000×10^{6}	1.08222×10^{-4}
6.00000×10^{6}	1.06471×10^{-4}	6.50000×10^{6}	1.10516×10^{-4}	7.00000×10^{6}	1.19021×10^{-4}
7.50000×10^{6}	1.30580×10^{-4}	8.00000×10^{6}	1.42904×10^{-4}	8.50000×10^{6}	1.42795×10^{-4}
9.00000×10^{6}	1.30361×10^{-4}	9.50000×10^{6}	1.11674×10^{-4}	1.00000×10^{7}	8.79174×10^{-5}
1.10000×10^{7}	6.38471×10^{-5}	1.20000×10^{7}	4.40654×10^{-5}	1.30000×10^{7}	2.75463×10^{-5}
1.40000×10^{7}	1.64732×10^{-5}	1.50000×10^{7}	1.00820×10^{-5}	1.60000×10^{7}	6.61427×10^{-6}
1.70000×10^{7}	4.64357×10^{-6}	1.80000×10^{7}	3.50596×10^{-6}	1.90000×10^{7}	2.82213×10^{-6}

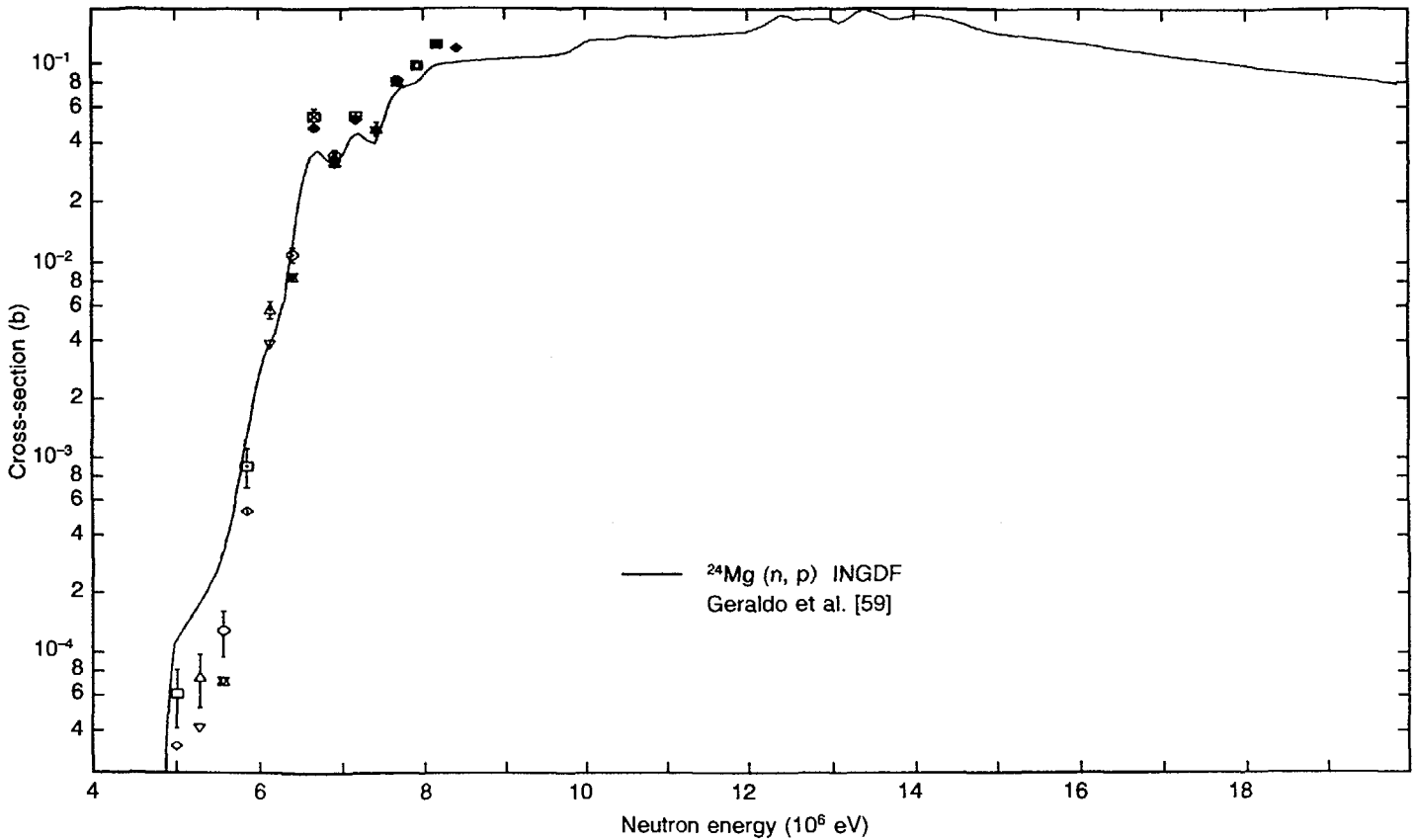

FIG. 6.18. Excitation function for the $^{24}Mg(n,p)$ reaction. Evaluated data from Ref. [58].

^{24}Mg (n, p)

E_n (eV)	σ (b)	E_n (eV)	σ (b)	E_n (eV)	σ (b)
4.50000×10^{6}	1.44627×10^{-6}	5.00000×10^{6}	7.84750×10^{-5}	5.50000×10^{6}	1.53993×10^{-3}
6.00000×10^{6}	1.25000×10^{-2}	6.50000×10^{6}	3.99250×10^{-2}	7.00000×10^{6}	5.40768×10^{-2}
7.50000×10^{6}	9.63284×10^{-2}	8.00000×10^{6}	1.18784×10^{-1}	8.50000×10^{6}	1.20250×10^{-1}
9.00000×10^{6}	1.22350×10^{-1}	9.50000×10^{6}	1.35754×10^{-1}	1.00000×10^{7}	1.58452×10^{-1}
1.10000×10^{7}	1.80828×10^{-1}	1.20000×10^{7}	1.99391×10^{-1}	1.30000×10^{7}	2.03980×10^{-1}
1.40000×10^{7}	1.85750×10^{-1}	1.50000×10^{7}	1.57950×10^{-1}	1.60000×10^{7}	1.31000×10^{-1}
1.70000×10^{7}	1.17850×10^{-1}	1.80000×10^{7}	1.05300×10^{-1}	1.90000×10^{7}	8.90000×10^{-2}

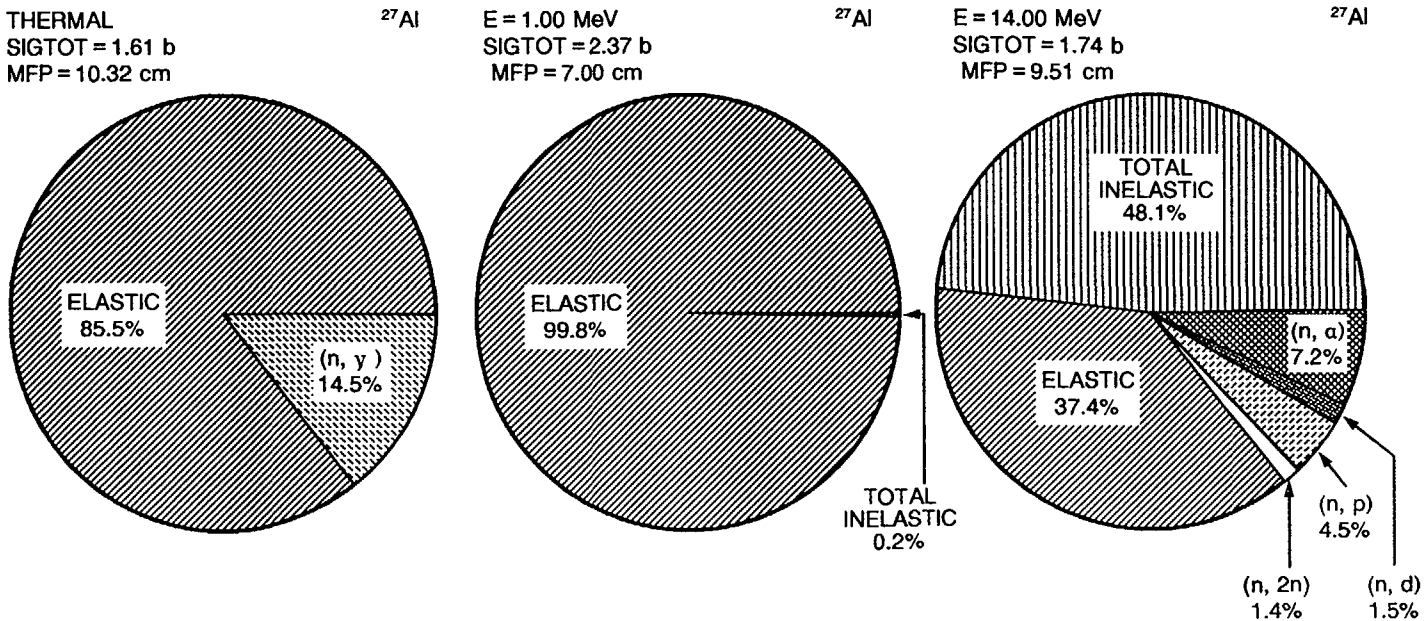

FIG. 6.19. Pie charts of the dominant neutron induced reaction cross-sections for aluminium.

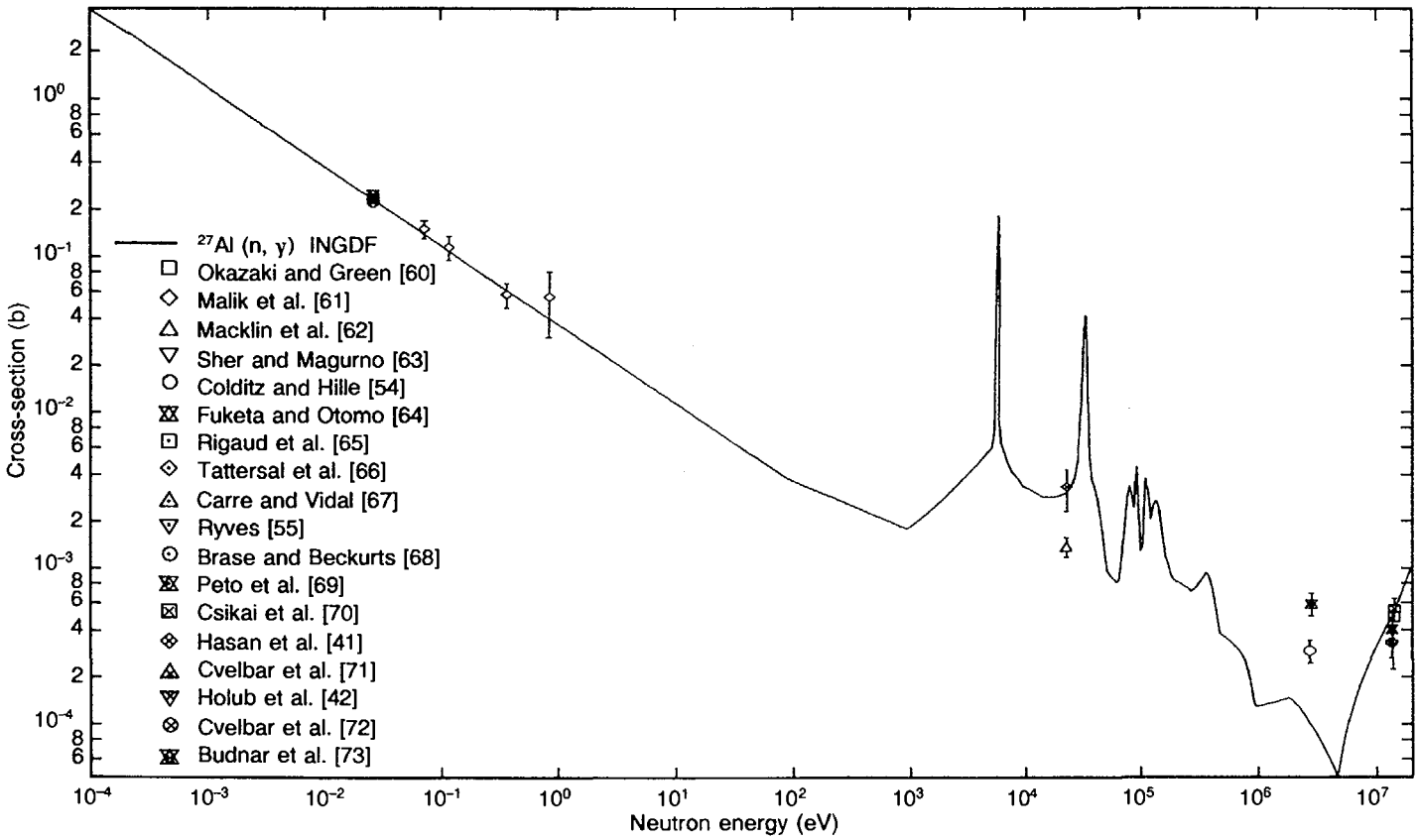

FIG. 6.20. Excitation function for the $^{27}Al(n,\gamma)$ reaction. Evaluated data from Ref. [74].

$^{27}Al(n,\gamma)$

E_n (eV)	σ (b)	E_n (eV)	σ (b)	E_n (eV)	σ (b)
1.00000×10^{-3}	2.12450×10^{-1}	1.00000×10^{-1}	5.61593×10^{-2}	1.00000	1.77682×10^{-2}
1.00000×10^{1}	5.61593×10^{-3}	1.00000×10^{2}	2.31146×10^{-3}	1.00000×10^{3}	9.50734×10^{-3}
1.00000×10^{4}	6.21625×10^{-3}	5.00000×10^{4}	1.98000×10^{-3}	1.00000×10^{5}	1.07850×10^{-3}
5.00000×10^{5}	2.83000×10^{-4}	1.00000×10^{6}	1.35000×10^{-4}	1.50000×10^{6}	1.45000×10^{-4}
2.00000×10^{6}	1.37500×10^{-4}	2.50000×10^{6}	1.12500×10^{-4}	3.00000×10^{6}	9.20002×10^{-5}
3.50000×10^{6}	7.60001×10^{-5}	4.00000×10^{6}	6.25001×10^{-5}	4.50000×10^{6}	5.15001×10^{-5}
5.00000×10^{6}	5.86001×10^{-5}	5.50000×10^{6}	8.38002×10^{-5}	6.00000×10^{6}	1.09000×10^{-4}
6.50000×10^{6}	1.34200×10^{-4}	7.00000×10^{6}	1.59400×10^{-4}	7.50000×10^{6}	1.84600×10^{-4}
8.00000×10^{6}	2.09800×10^{-4}	8.50000×10^{6}	2.35000×10^{-4}	9.00000×10^{6}	2.60200×10^{-4}
9.50000×10^{6}	2.85399×10^{-4}	1.00000×10^{7}	3.23198×10^{-4}	1.10000×10^{7}	3.73598×10^{-4}
1.20000×10^{7}	4.23999×10^{-4}	1.30000×10^{7}	4.74400×10^{-4}	1.40000×10^{7}	5.24800×10^{-4}
1.50000×10^{7}	5.95000×10^{-4}	1.60000×10^{7}	6.84999×10^{-4}	1.70000×10^{7}	7.75000×10^{-4}
1.80000×10^{7}	8.65001×10^{-4}	1.90000×10^{7}	9.55001×10^{-4}		

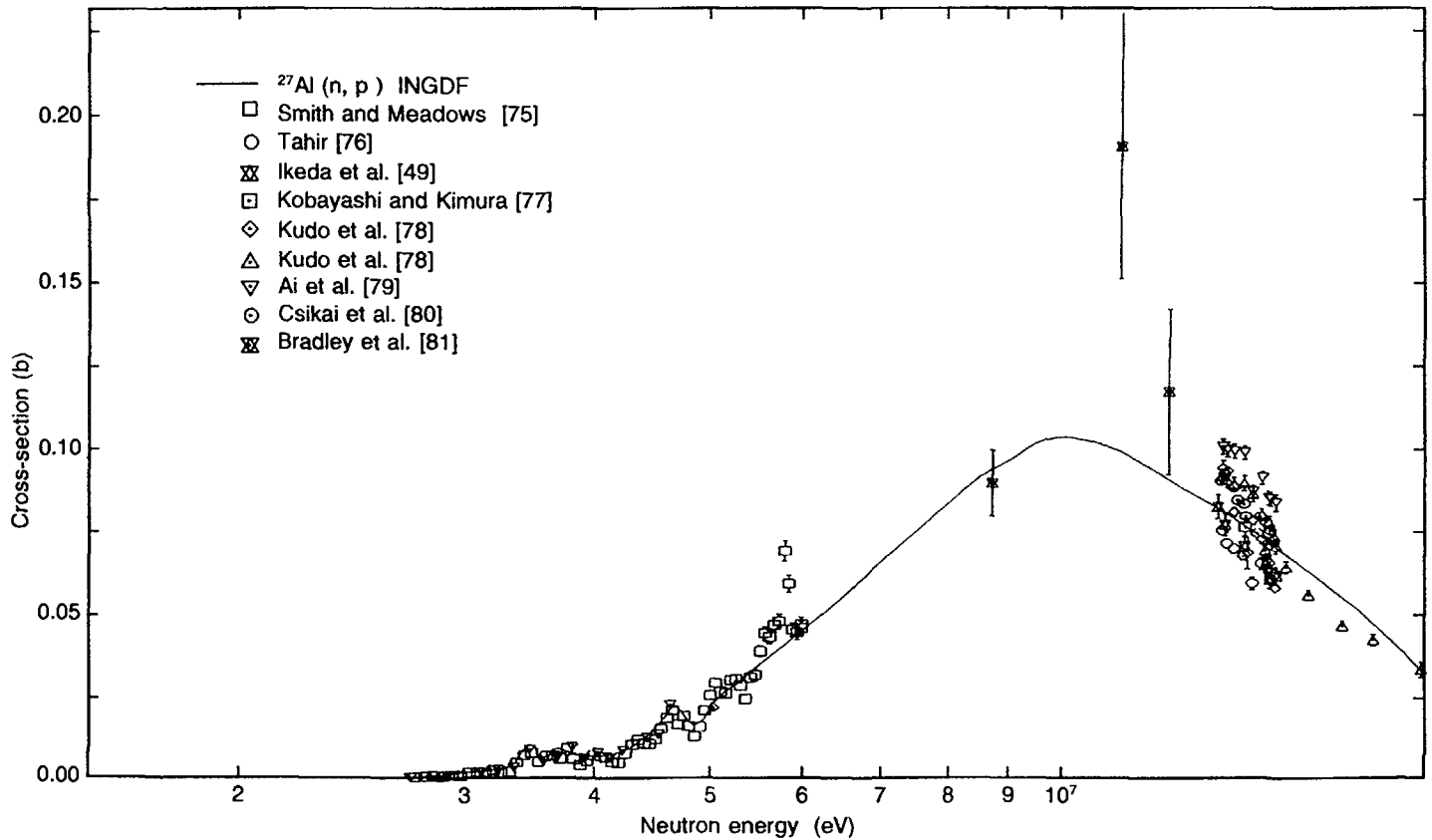

FIG. 6.21. Excitation function for the $^{27}Al(n,p)$ reaction. Evaluated data from Ref. [74].

^{27}Al (n, p)

E_n (eV)	σ (b)	E_n (eV)	σ (b)	E_n (eV)	σ (b)
1.50000×10^{6}	9.44459×10^{-16}	2.00000×10^{6}	4.43160×10^{-6}	2.50000×10^{6}	4.46859×10^{-4}
3.00000×10^{6}	3.71147×10^{-3}	3.50000×10^{6}	7.59469×10^{-3}	4.00000×10^{6}	1.04363×10^{-2}
4.50000×10^{6}	1.91873×10^{-2}	5.00000×10^{6}	2.95914×10^{-2}	5.50000×10^{6}	4.09554×10^{-2}
6.00000×10^{6}	5.16986×10^{-2}	6.50000×10^{6}	6.25158×10^{-2}	7.00000×10^{6}	7.24216×10^{-2}
7.50000×10^{6}	8.13585×10^{-2}	8.00000×10^{6}	8.95897×10^{-2}	8.50000×10^{6}	9.55744×10^{-2}
9.00000×10^{6}	1.00774×10^{-1}	9.50000×10^{6}	1.03666×10^{-1}	1.00000×10^{7}	1.02260×10^{-1}
1.10000×10^{7}	9.60790×10^{-2}	1.20000×10^{7}	8.84080×10^{-2}	1.30000×10^{7}	8.14805×10^{-2}
1.40000×10^{7}	7.39305×10^{-2}	1.50000×10^{7}	6.63499×10^{-2}	1.60000×10^{7}	5.88895×10^{-2}
1.70000×10^{7}	5.16117×10^{-2}	1.80000×10^{7}	4.40083×10^{-2}	1.90000×10^{7}	3.62907×10^{-2}

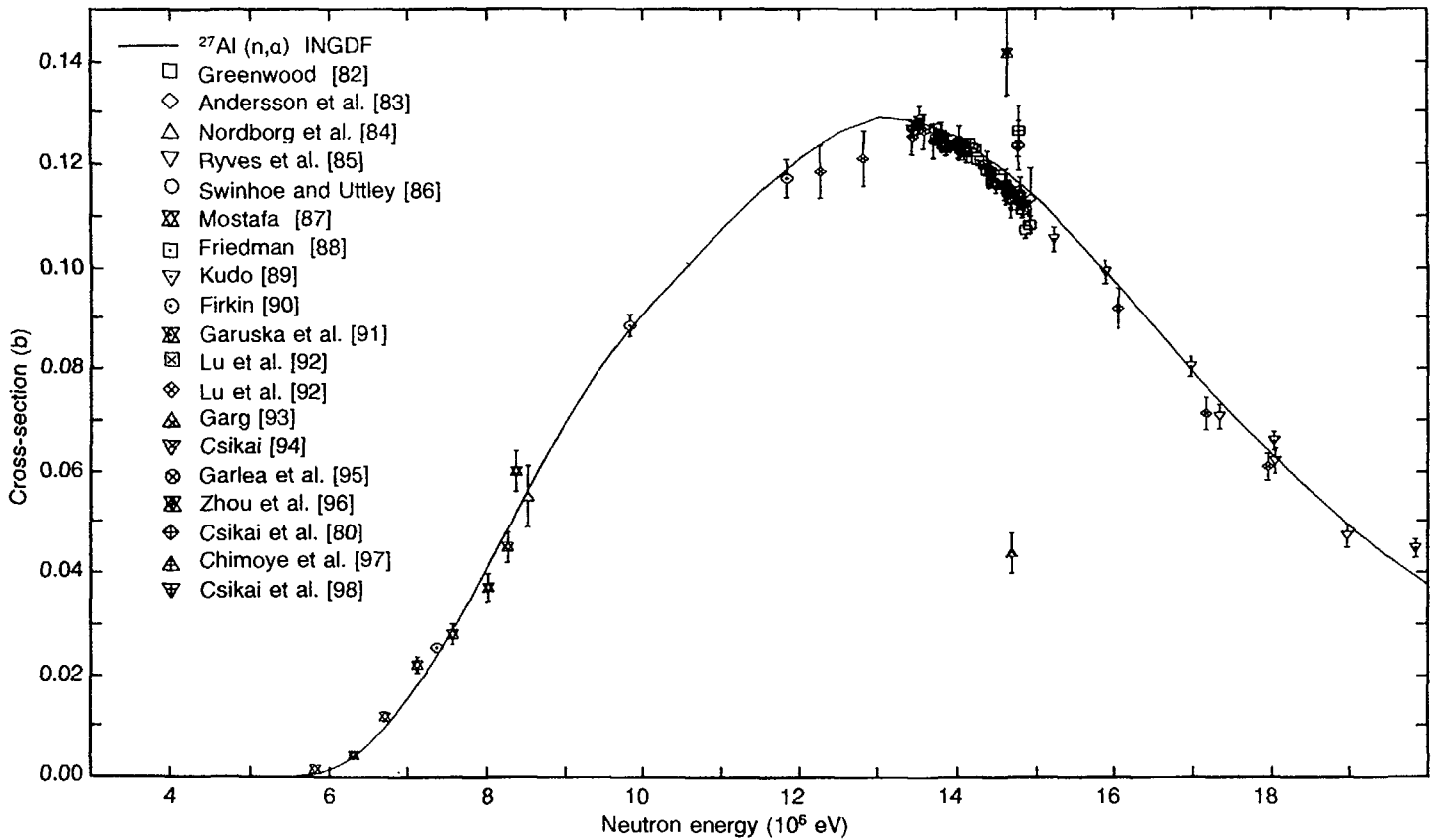

FIG. 6.22. Excitation function for the $^{27}Al(n,\alpha)^{24}Na$ reaction. Evaluated data from Ref. [74].

$^{27}Al\,(n,\alpha)^{24}Na$

E_n (eV)	σ (b)	E_n (eV)	σ (b)	E_n (eV)	σ (b)
3.00000×10^{6}	5.68067×10^{-23}	3.50000×10^{6}	5.20626×10^{-14}	4.00000×10^{6}	3.49178×10^{-9}
4.50000×10^{6}	1.24745×10^{-6}	5.00000×10^{6}	5.03363×10^{-5}	5.50000×10^{6}	6.29435×10^{-4}
6.00000×10^{6}	3.65700×10^{-3}	6.50000×10^{6}	1.09590×10^{-2}	7.00000×10^{6}	2.14700×10^{-2}
7.50000×10^{6}	3.42500×10^{-2}	8.00000×10^{6}	4.87150×10^{-2}	8.50000×10^{6}	6.33850×10^{-2}
9.00000×10^{6}	7.61651×10^{-2}	9.50000×10^{6}	8.66351×10^{-2}	1.00000×10^{7}	9.94810×10^{-2}
1.10000×10^{7}	1.14640×10^{-1}	1.20000×10^{7}	1.25520×10^{-1}	1.30000×10^{7}	1.27345×10^{-1}
1.40000×10^{7}	1.19080×10^{-1}	1.50000×10^{7}	1.05080×10^{-1}	1.60000×10^{7}	8.83030×10^{-2}
1.70000×10^{7}	7.13686×10^{-2}	1.80000×10^{7}	5.66435×10^{-2}	1.90000×10^{7}	4.36685×10^{-2}

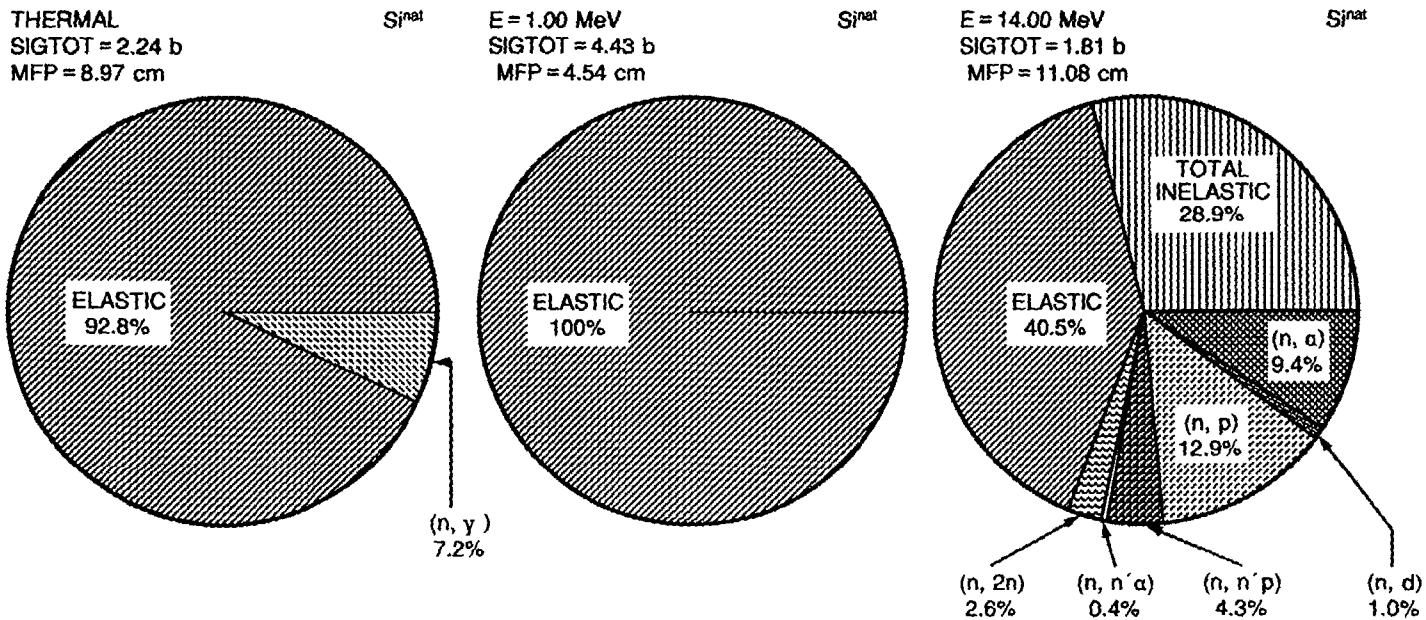

FIG. 6.23. Pie charts of the dominant neutron induced reaction cross-sections for natural silicon.

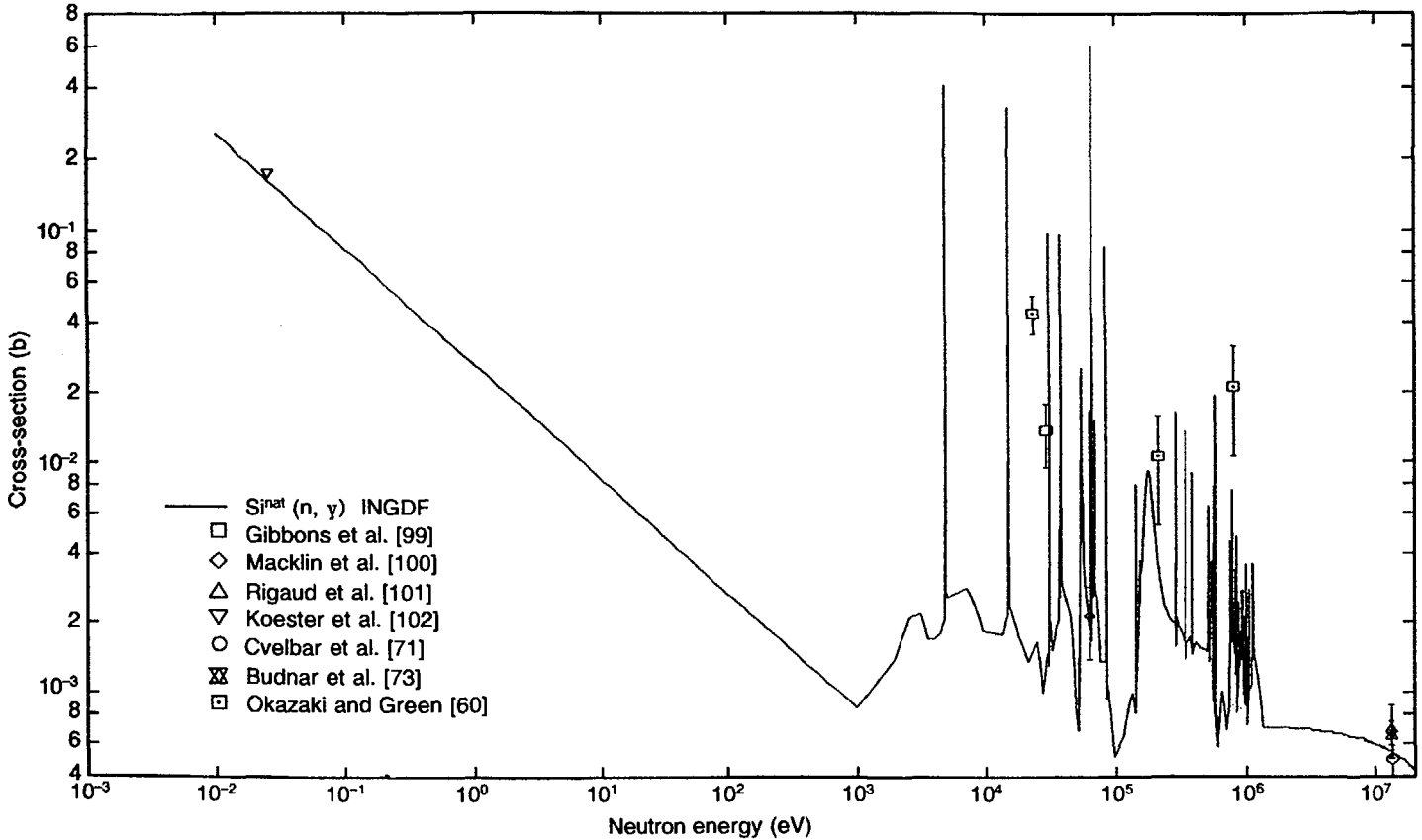

FIG. 6.24. Excitation function for the $Si^{nat}(n,\gamma)$ reaction. Evaluated data from Ref. [103].

$Si^{nat}(n,\gamma)$

E_n (eV)	σ (b)	E_n (eV)	σ (b)	E_n (eV)	σ (b)
1.00000×10^{-3}	1.46851×10^{-1}	1.00000×10^{-1}	3.89160×10^{-2}	1.00000	1.22728×10^{-2}
1.00000×10^{1}	3.89160×10^{-3}	1.00000×10^{2}	1.22872×10^{-3}	1.00000×10^{3}	2.58849×10^{-3}
1.00000×10^{4}	2.61195×10^{-3}	5.00000×10^{4}	4.56156×10^{-3}	1.00000×10^{5}	2.32333×10^{-3}
5.00000×10^{5}	1.46115×10^{-3}	1.00000×10^{6}	1.01852×10^{-3}	1.50000×10^{6}	6.50000×10^{-4}
2.00000×10^{6}	6.45200×10^{-4}	2.50000×10^{6}	6.40000×10^{-4}	3.00000×10^{6}	6.36000×10^{-4}
3.50000×10^{6}	6.27940×10^{-4}	4.00000×10^{6}	6.20000×10^{-4}	4.50000×10^{6}	6.16400×10^{-4}
5.00000×10^{6}	6.10100×10^{-4}	5.50000×10^{6}	6.05200×10^{-4}	6.00000×10^{6}	5.98000×10^{-4}
6.50000×10^{6}	5.90000×10^{-4}	7.00000×10^{6}	5.86000×10^{-4}	7.50000×10^{6}	5.80000×10^{-4}
8.00000×10^{6}	5.80000×10^{-4}	8.50000×10^{6}	5.70700×10^{-4}	9.00000×10^{6}	5.60100×10^{-4}
9.50000×10^{6}	5.56000×10^{-4}	1.00000×10^{7}	5.46000×10^{-4}	1.10000×10^{7}	5.35000×10^{-4}
1.20000×10^{7}	5.24000×10^{-4}	1.30000×10^{7}	5.10000×10^{-4}	1.40000×10^{7}	4.96250×10^{-4}
1.50000×10^{7}	4.86250×10^{-4}	1.60000×10^{7}	4.73750×10^{-4}	1.70000×10^{7}	4.66170×10^{-4}
1.80000×10^{7}	4.50521×10^{-4}	1.90000×10^{7}	4.40000×10^{-4}		

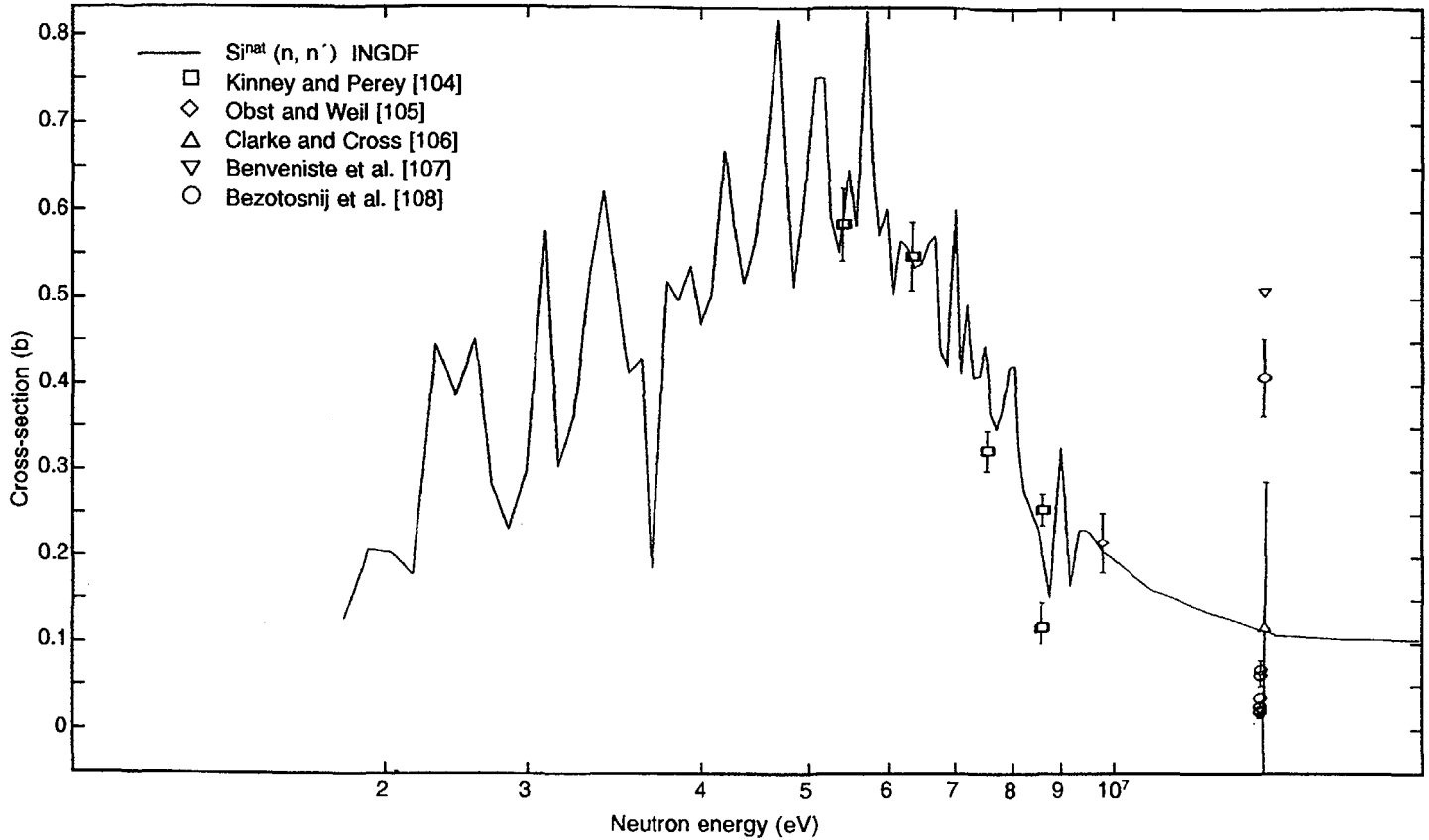

FIG. 6.25. Excitation function for inelastic scattering of Si^{nat} to the 1.779 MeV level. Evaluated data from Ref. [103].

$Si^{nat}(n, n')$

E_n (eV)	σ (b)	E_n (eV)	σ (b)	E_n (eV)	σ (b)
1.50000×10^{6}	6.49175×10^{-2}	2.00000×10^{6}	3.29639×10^{-1}	2.50000×10^{6}	3.36118×10^{-1}
3.00000×10^{6}	4.86195×10^{-1}	3.50000×10^{6}	4.31738×10^{-1}	4.00000×10^{6}	5.48176×10^{-1}
4.50000×10^{6}	6.44494×10^{-1}	5.00000×10^{6}	6.54360×10^{-1}	5.50000×10^{6}	6.56869×10^{-1}
6.00000×10^{6}	5.53760×10^{-1}	6.50000×10^{6}	5.07012×10^{-1}	7.00000×10^{6}	4.65207×10^{-1}
7.50000×10^{6}	3.89694×10^{-1}	8.00000×10^{6}	3.05350×10^{-1}	8.50000×10^{6}	2.24553×10^{-1}
9.00000×10^{6}	2.16632×10^{-1}	9.50000×10^{6}	2.13354×10^{-1}	1.00000×10^{7}	1.78735×10^{-1}
1.10000×10^{7}	1.50814×10^{-1}	1.20000×10^{7}	1.34129×10^{-1}	1.30000×10^{7}	1.21070×10^{-1}
1.40000×10^{7}	1.09734×10^{-1}	1.50000×10^{7}	1.06230×10^{-1}	1.60000×10^{7}	1.04656×10^{-1}
1.70000×10^{7}	1.03997×10^{-1}	1.80000×10^{7}	1.03587×10^{-1}	1.90000×10^{7}	1.03580×10^{-1}

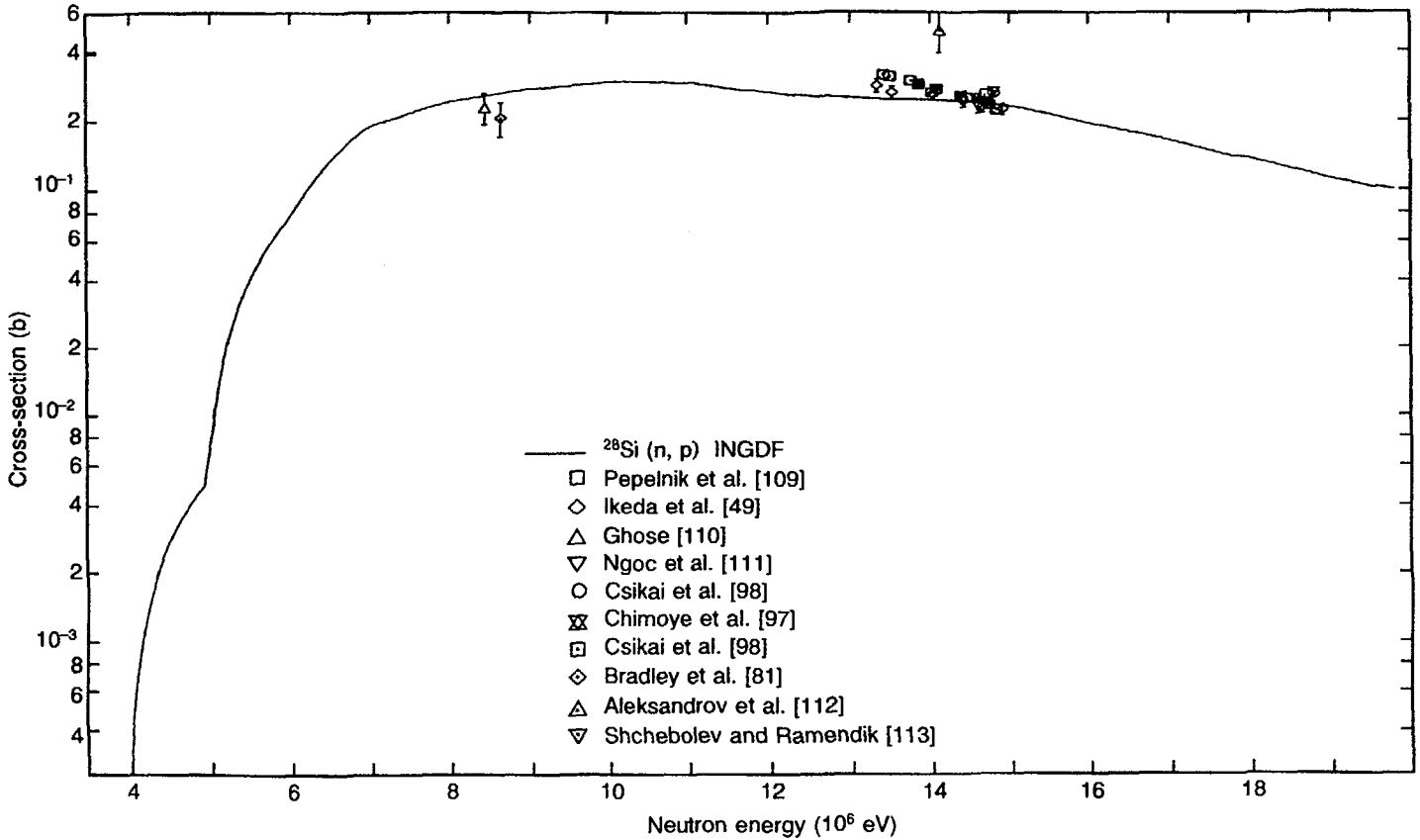

FIG. 6.26. Excitation function for the ^{28}Si(n,p) reaction. Evaluated data from Ref. [114].

^{28}Si (n, p)

E_n (eV)	σ (b)	E_n (eV)	σ (b)	E_n (eV)	σ (b)
4.00000×10^{6}	1.30621×10^{-3}	4.50000×10^{6}	3.91863×10^{-3}	5.00000×10^{6}	2.31873×10^{-2}
5.50000×10^{6}	5.91121×10^{-2}	6.00000×10^{6}	1.05627×10^{-1}	6.50000×10^{6}	1.62732×10^{-1}
7.00000×10^{6}	2.04114×10^{-1}	7.50000×10^{6}	2.29773×10^{-1}	8.00000×10^{6}	2.51659×10^{-1}
8.50000×10^{6}	2.68733×10^{-1}	9.00000×10^{6}	2.81058×10^{-1}	9.50000×10^{6}	2.90718×10^{-1}
1.00000×10^{7}	2.97650×10^{-1}	1.10000×10^{7}	2.83118×10^{-1}	1.20000×10^{7}	2.61952×10^{-1}
1.30000×10^{7}	2.52132×10^{-1}	1.40000×10^{7}	2.45756×10^{-1}	1.50000×10^{7}	2.19883×10^{-1}
1.60000×10^{7}	1.86036×10^{-1}	1.70000×10^{7}	1.55144×10^{-1}	1.80000×10^{7}	1.29560×10^{-1}
1.90000×10^{7}	1.07530×10^{-1}				

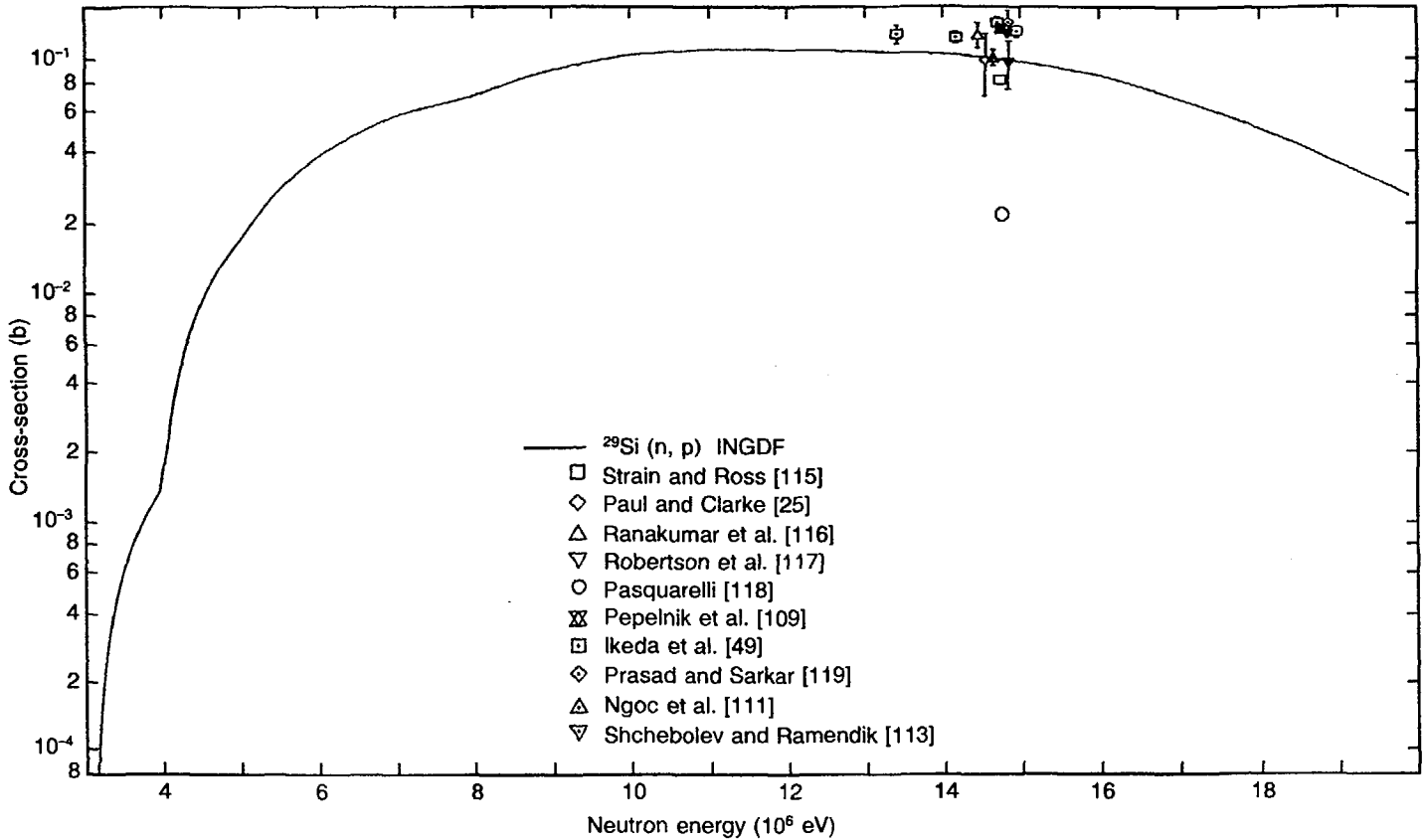

FIG. 6.27. Excitation function for the $^{29}Si(n,p)^{29}Al$ reaction. Evaluated data from Ref. [114].

$^{29}Si\,(n,p)\,^{29}Al$

E_n (eV)	σ (b)	E_n (eV)	σ (b)	E_n (eV)	σ (b)
3.00000×10^{6}	2.55330×10^{-4}	3.50000×10^{6}	1.03728×10^{-3}	4.00000×10^{6}	5.44040×10^{-3}
4.50000×10^{6}	1.34487×10^{-2}	5.00000×10^{6}	2.28838×10^{-2}	5.50000×10^{6}	3.37456×10^{-2}
6.00000×10^{6}	4.39096×10^{-2}	6.50000×10^{6}	5.33760×10^{-2}	7.00000×10^{6}	6.11956×10^{-2}
7.50000×10^{6}	6.73687×10^{-2}	8.00000×10^{6}	7.58448×10^{-2}	8.50000×10^{6}	8.65445×10^{-2}
9.00000×10^{6}	9.53002×10^{-2}	9.50000×10^{6}	1.02667×10^{-1}	1.00000×10^{7}	1.09212×10^{-1}
1.10000×10^{7}	1.12019×10^{-1}	1.20000×10^{7}	1.10508×10^{-1}	1.30000×10^{7}	1.08590×10^{-1}
1.40000×10^{7}	1.03883×10^{-1}	1.50000×10^{7}	9.34996×10^{-2}	1.60000×10^{7}	7.84486×10^{-2}
1.70000×10^{7}	6.05067×10^{-2}	1.80000×10^{7}	4.41648×10^{-2}	1.90000×10^{7}	3.12090×10^{-2}

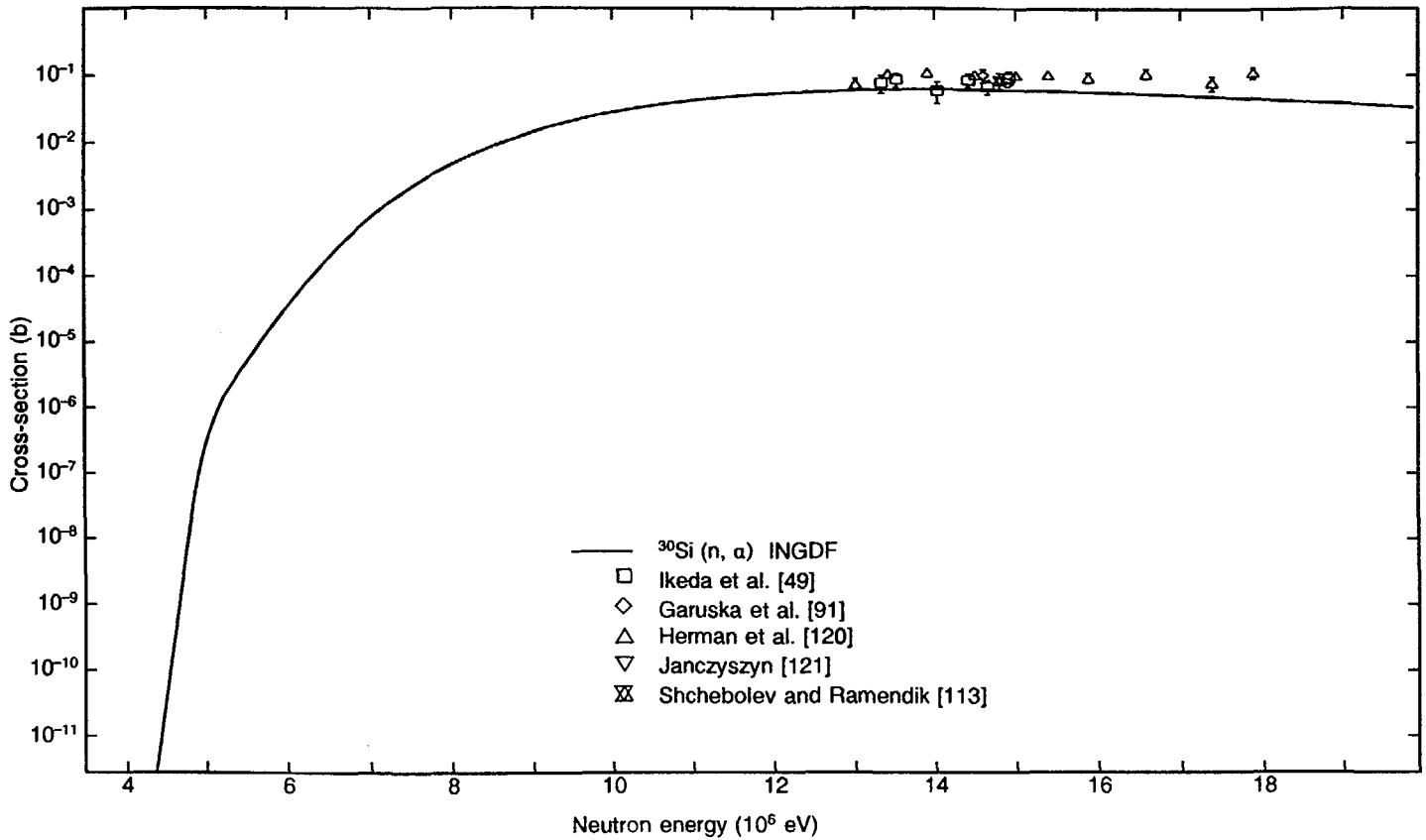

FIG. 6.28. Excitation function for the $^{30}Si(n,\alpha)^{27}Mg$ reaction. Evaluated data from Ref. [114].

$^{30}Si\,(n,\alpha)^{27}Mg$

E_n (eV)	σ (b)	E_n (eV)	σ (b)	E_n (eV)	σ (b)
4.00000×10^{6}	5.89202×10^{-13}	4.50000×10^{6}	2.06220×10^{-11}	5.00000×10^{6}	1.64306×10^{-6}
5.50000×10^{6}	4.92911×10^{-6}	6.00000×10^{6}	9.71699×10^{-5}	6.50000×10^{6}	2.78366×10^{-4}
7.00000×10^{6}	1.25045×10^{-3}	7.50000×10^{6}	3.01342×10^{-3}	8.00000×10^{6}	5.96421×10^{-3}
8.50000×10^{6}	1.11055×10^{-2}	9.00000×10^{6}	1.75366×10^{-2}	9.50000×10^{6}	2.49843×10^{-2}
1.00000×10^{7}	3.77407×10^{-2}	1.10000×10^{7}	5.18279×10^{-2}	1.20000×10^{7}	6.12018×10^{-2}
1.30000×10^{7}	6.66474×10^{-2}	1.40000×10^{7}	6.64056×10^{-2}	1.50000×10^{7}	6.35136×10^{-2}
1.60000×10^{7}	5.87715×10^{-2}	1.70000×10^{7}	5.31867×10^{-2}	1.80000×10^{7}	4.60126×10^{-2}
1.90000×10^{7}	3.86153×10^{-2}				

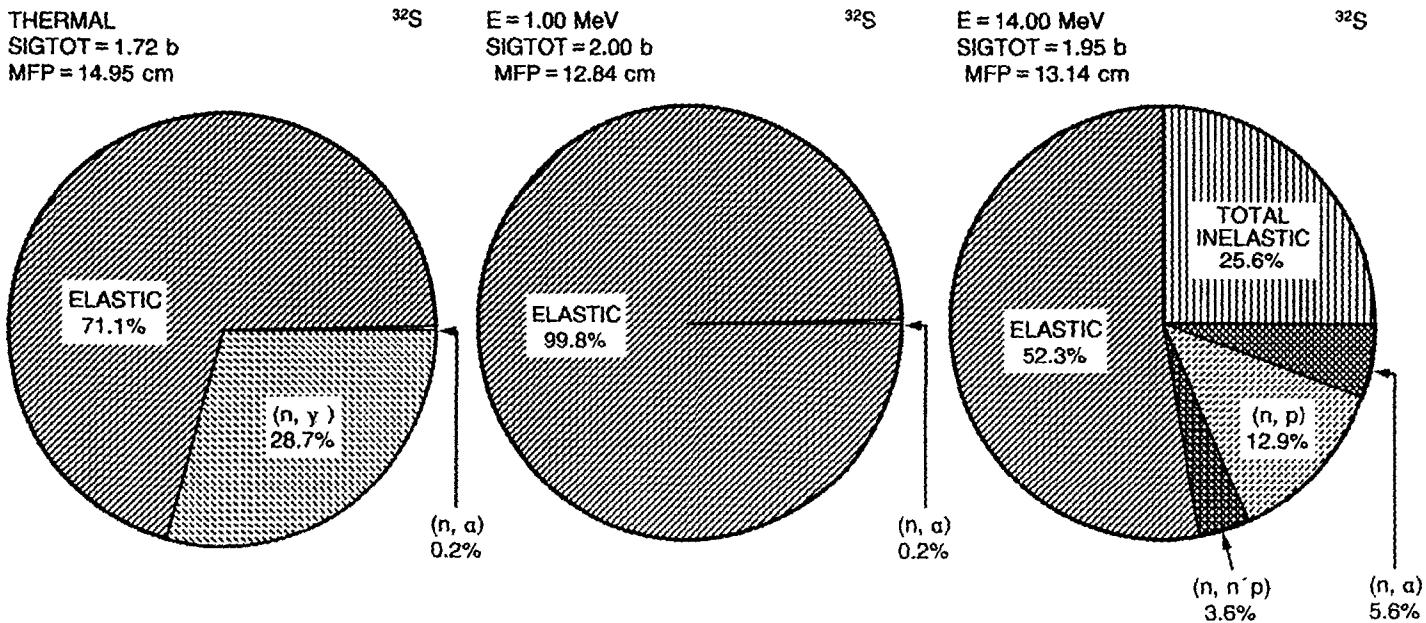

FIG. 6.29. Pie charts of the dominant neutron induced reaction cross-sections for sulphur.

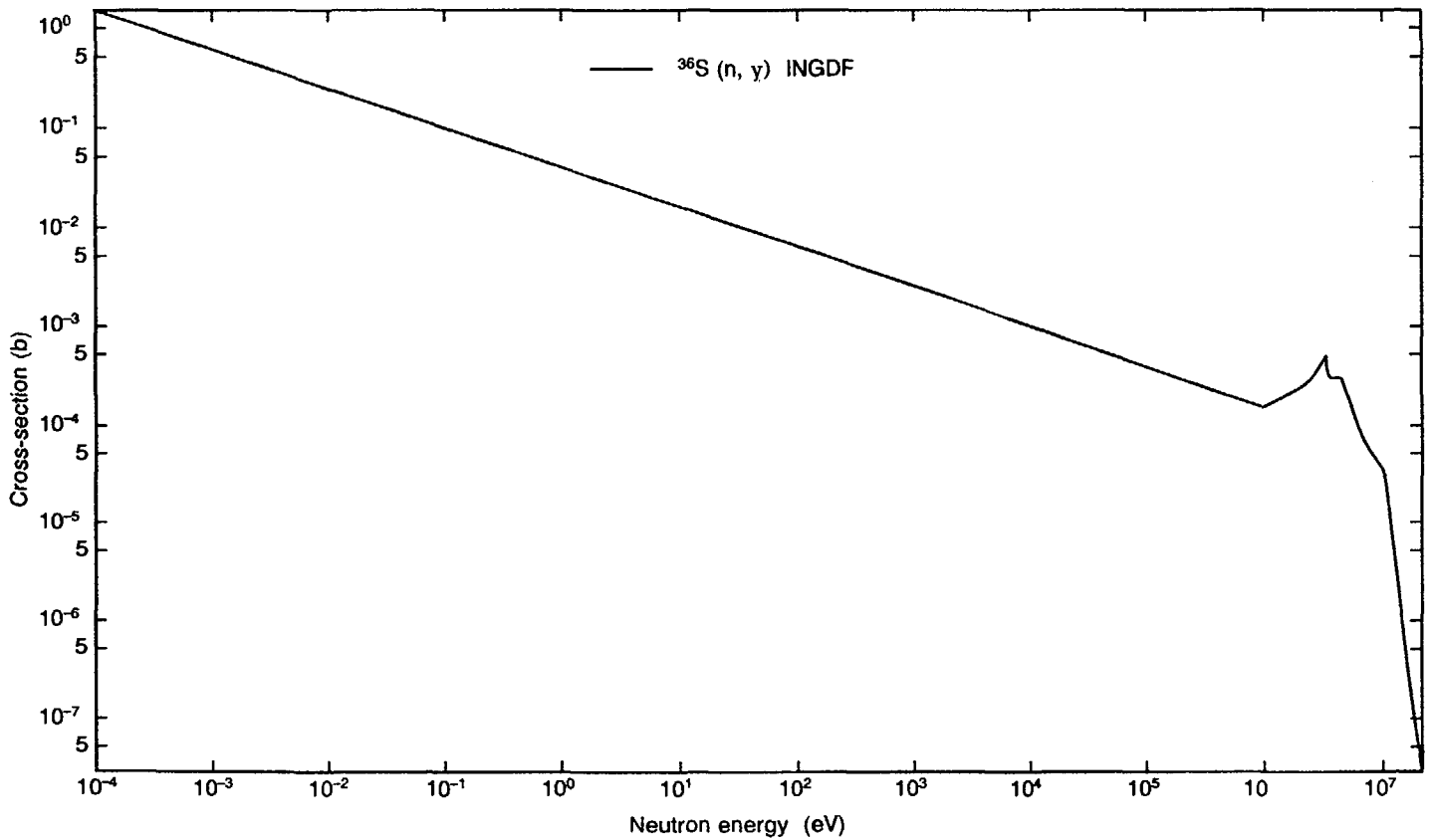

FIG. 6.30. Excitation function for the $^{36}S(n,\gamma)$ reaction. Evaluated data from Ref. [122].

^{36}S (n, γ)

E_n (eV)	σ (b)	E_n (eV)	σ (b)	E_n (eV)	σ (b)
1.00000×10^{-3}	1.37439×10^{-1}	1.00000×10^{-1}	4.93299×10^{-2}	1.00000	2.01501×10^{-2}
1.00000×10^{1}	8.23148×10^{-3}	1.00000×10^{2}	3.36251×10^{-3}	1.00000×10^{3}	1.37364×10^{-3}
1.00000×10^{4}	6.70556×10^{-4}	5.00000×10^{4}	4.41184×10^{-4}	1.00000×10^{5}	2.59714×10^{-4}
5.00000×10^{5}	1.70872×10^{-4}	1.00000×10^{6}	1.80728×10^{-4}	1.50000×10^{6}	2.35556×10^{-4}
2.00000×10^{6}	3.01436×10^{-4}	2.50000×10^{6}	3.87811×10^{-4}	3.00000×10^{6}	4.54127×10^{-4}
3.50000×10^{6}	3.11298×10^{-4}	4.00000×10^{6}	2.84976×10^{-4}	4.50000×10^{6}	2.02395×10^{-4}
5.00000×10^{6}	1.68460×10^{-4}	5.50000×10^{6}	1.27905×10^{-4}	6.00000×10^{6}	9.79906×10^{-5}
6.50000×10^{6}	7.66151×10^{-5}	7.00000×10^{6}	6.34176×10^{-5}	7.50000×10^{6}	5.53512×10^{-5}
8.00000×10^{6}	4.88737×10^{-5}	8.50000×10^{6}	4.35980×10^{-5}	9.00000×10^{6}	3.91268×10^{-5}
9.50000×10^{6}	3.51246×10^{-5}	1.00000×10^{7}	2.55037×10^{-5}	1.10000×10^{7}	1.12134×10^{-5}
1.20000×10^{7}	4.63956×10^{-6}	1.30000×10^{7}	2.05619×10^{-6}	1.40000×10^{7}	9.66475×10^{-7}
1.50000×10^{7}	4.63934×10^{-7}	1.60000×10^{7}	2.35549×10^{-7}	1.70000×10^{7}	1.31875×10^{-7}
1.80000×10^{7}	7.27837×10^{-8}	1.90000×10^{7}	3.92014×10^{-8}		

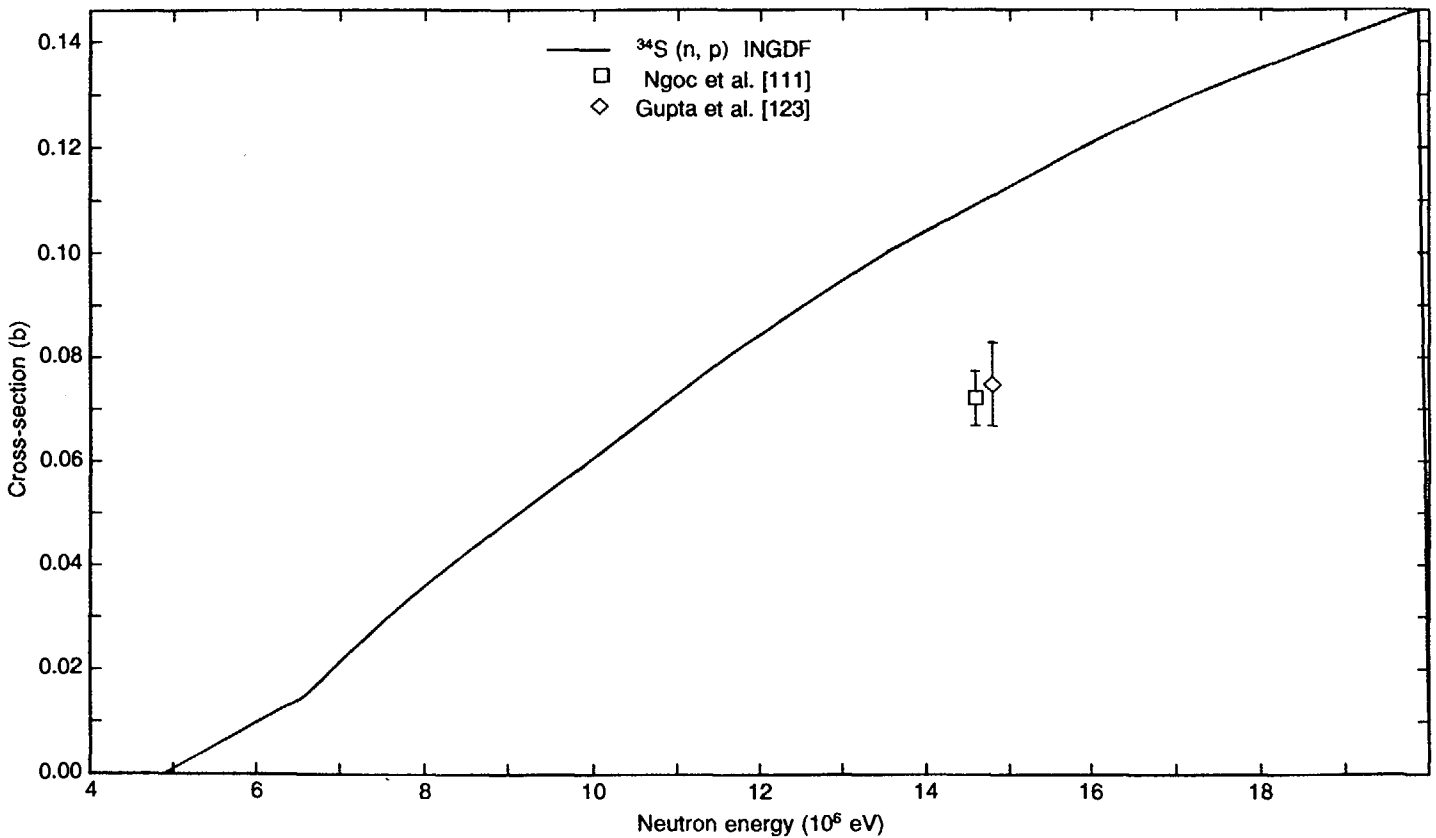

FIG. 6.31. Excitation function for the $^{34}S(n,p)^{34}P$ reaction. Evaluated data from Ref. [122].

$^{34}S(n,p)^{34}P$

E_n (eV)	σ (b)	E_n (eV)	σ (b)	E_n (eV)	σ (b)
4.50000×10^{6}	1.14414×10^{-6}	5.00000×10^{6}	2.22841×10^{-3}	5.50000×10^{6}	6.67761×10^{-3}
6.00000×10^{6}	1.11268×10^{-2}	6.50000×10^{6}	1.69716×10^{-2}	7.00000×10^{6}	2.42120×10^{-2}
7.50000×10^{6}	3.14524×10^{-2}	8.00000×10^{6}	3.84803×10^{-2}	8.50000×10^{6}	4.46343×10^{-2}
9.00000×10^{6}	5.06939×10^{-2}	9.50000×10^{6}	5.67534×10^{-2}	1.00000×10^{7}	6.63543×10^{-2}
1.10000×10^{7}	7.88655×10^{-2}	1.20000×10^{7}	8.98683×10^{-2}	1.30000×10^{7}	9.95896×10^{-2}
1.40000×10^{7}	1.08492×10^{-1}	1.50000×10^{7}	1.16781×10^{-1}	1.60000×10^{7}	1.24464×10^{-1}
1.70000×10^{7}	1.31539×10^{-1}	1.80000×10^{7}	1.38025×10^{-1}	1.90000×10^{7}	1.43920×10^{-1}

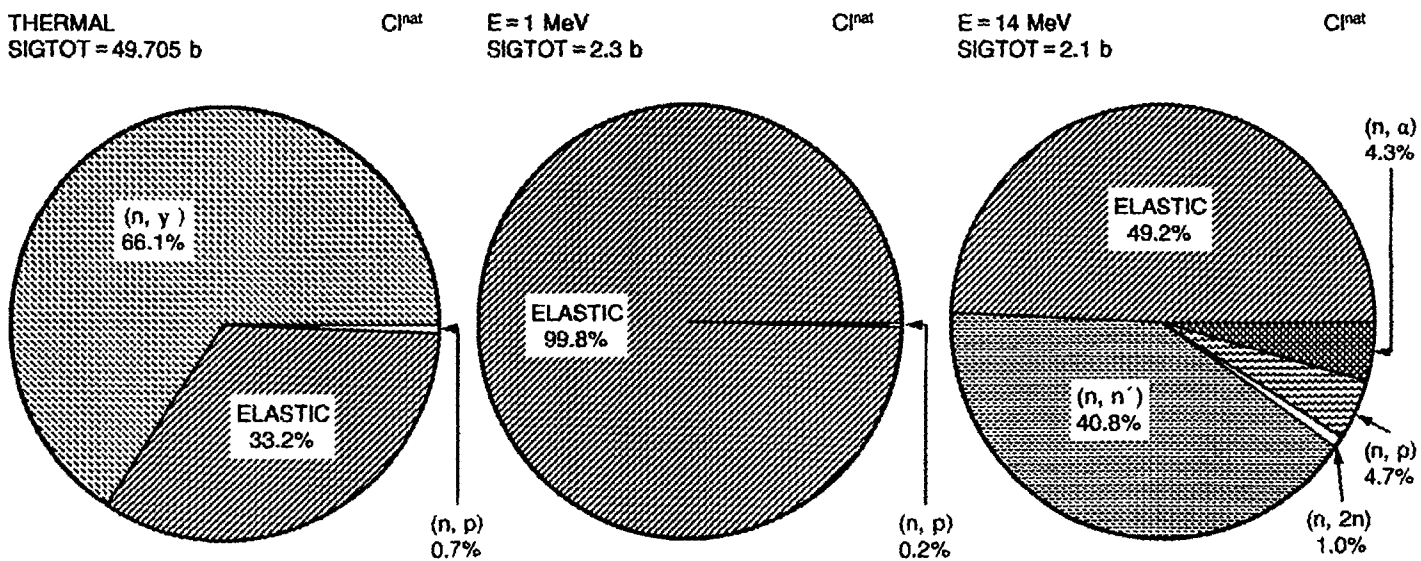

FIG. 6.32. Pie charts of the dominant neutron induced reaction cross-sections for chlorine.

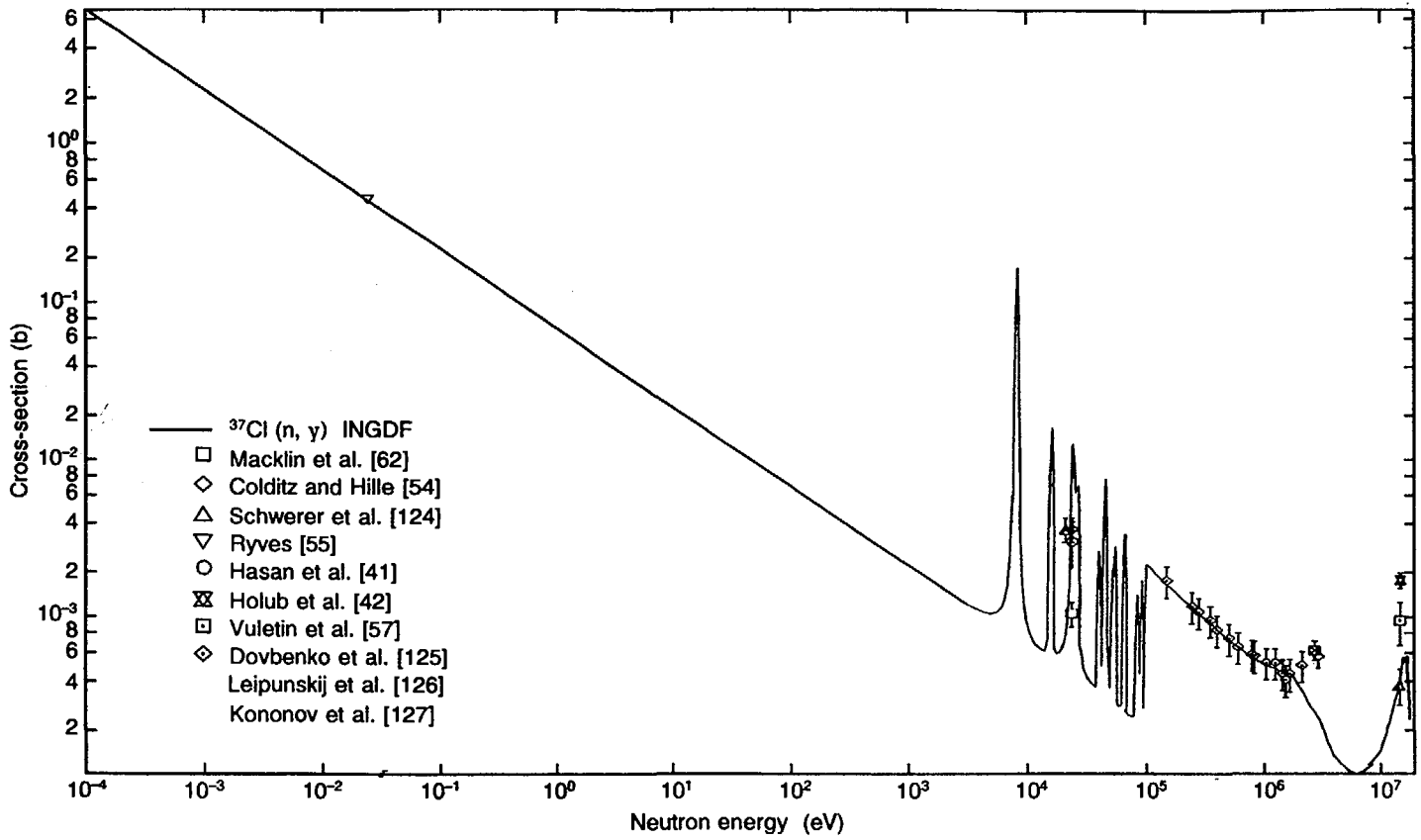

FIG. 6.33. Excitation function for the $^{37}Cl(n,\gamma)^{38}Cl$ reaction. Evaluated data from Ref. [6].

$^{37}Cl\,(n,\gamma)\,^{38}Cl$

E_n (eV)	σ (b)	E_n (eV)	σ (b)	E_n (eV)	σ (b)
1.00000×10^{-3}	3.96216×10^{-1}	1.00000×10^{-1}	1.04708×10^{-1}	1.00000	3.31050×10^{-2}
1.00000×10^{1}	1.04719×10^{-2}	1.00000×10^{2}	3.32153×10^{-3}	1.00000×10^{3}	9.87780×10^{-3}
1.00000×10^{4}	2.41774×10^{-3}	5.00000×10^{4}	9.09488×10^{-4}	1.00000×10^{5}	1.19663×10^{-3}
5.00000×10^{5}	6.18001×10^{-4}	1.00000×10^{6}	4.99251×10^{-4}	1.50000×10^{6}	4.44751×10^{-4}
2.00000×10^{6}	3.40001×10^{-4}	2.50000×10^{6}	2.65001×10^{-4}	3.00000×10^{6}	2.09000×10^{-4}
3.50000×10^{6}	1.57500×10^{-4}	4.00000×10^{6}	1.33750×10^{-4}	4.50000×10^{6}	1.21250×10^{-4}
5.00000×10^{6}	1.13750×10^{-4}	5.50000×10^{6}	1.11250×10^{-4}	6.00000×10^{6}	1.11250×10^{-4}
6.50000×10^{6}	1.13750×10^{-4}	7.00000×10^{6}	1.17000×10^{-4}	7.50000×10^{6}	1.21000×10^{-4}
8.00000×10^{6}	1.26375×10^{-4}	8.50000×10^{6}	1.33125×10^{-4}	9.00000×10^{6}	1.39875×10^{-4}
9.50000×10^{6}	1.46625×10^{-4}	1.00000×10^{7}	1.70000×10^{-4}	1.10000×10^{7}	2.10000×10^{-4}
1.20000×10^{7}	2.62500×10^{-4}	1.30000×10^{7}	3.27501×10^{-4}	1.40000×10^{7}	4.15001×10^{-4}
1.50000×10^{7}	5.25001×10^{-4}	1.60000×10^{7}	5.90001×10^{-4}	1.70000×10^{7}	5.40001×10^{-4}
1.80000×10^{7}	4.00001×10^{-4}	1.90000×10^{7}	2.60000×10^{-4}		

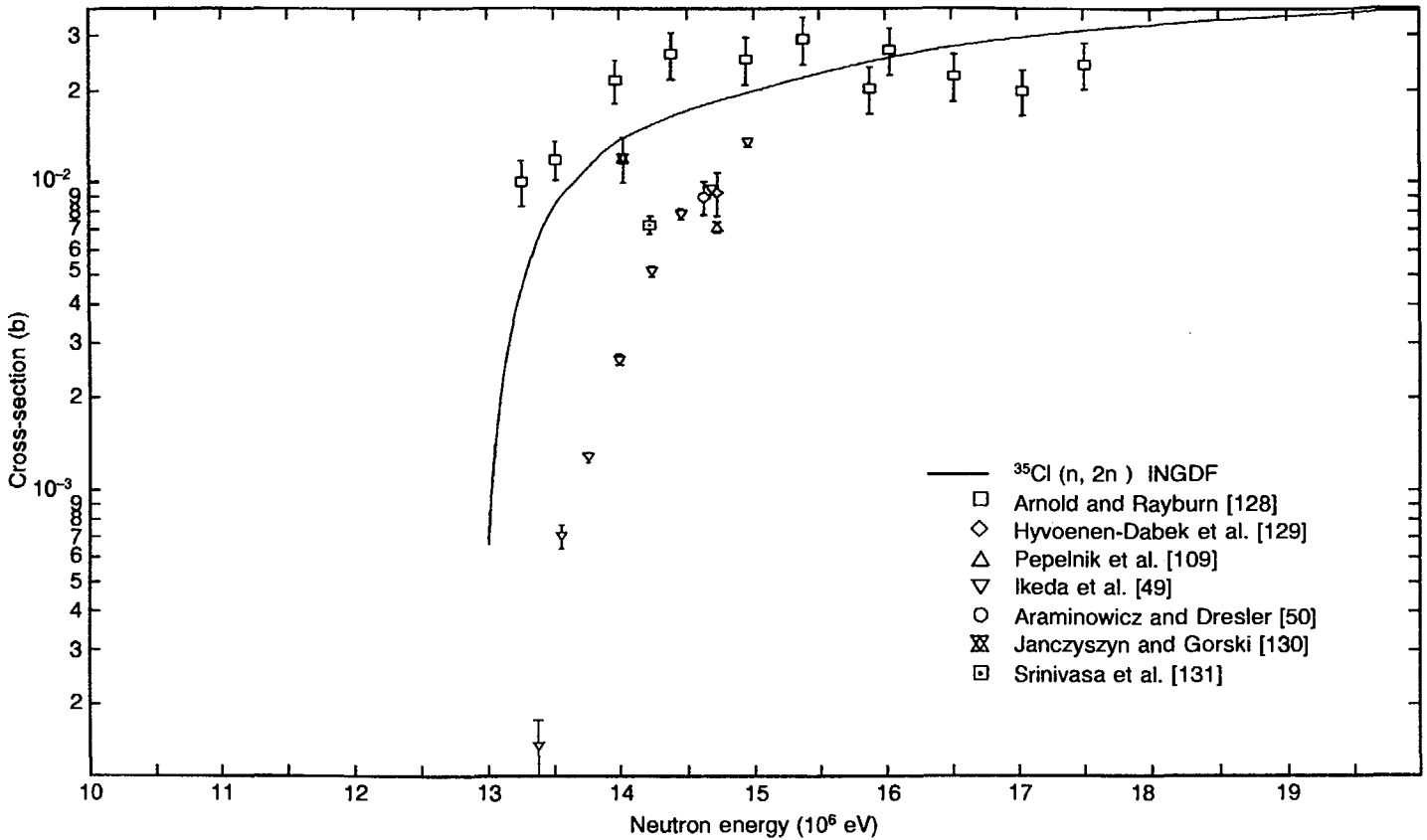

FIG. 6.34. Excitation function for the $^{35}Cl(n,2n)^{34}Cl^{g+m}$ reaction. Evaluated data from Ref. [6].

$^{35}Cl\,(n,2n)^{34}Cl^{g+m}$

E_n (eV)	σ (b)	E_n (eV)	σ (b)	E_n (eV)	σ (b)
1.30000×10^7	7.41648×10^{-3}	1.40000×10^7	1.68445×10^{-2}	1.50000×10^7	2.23865×10^{-2}
1.60000×10^7	2.72600×10^{-2}	1.70000×10^7	3.08947×10^{-2}	1.80000×10^7	3.35215×10^{-2}
1.90000×10^7	3.53312×10^{-2}				

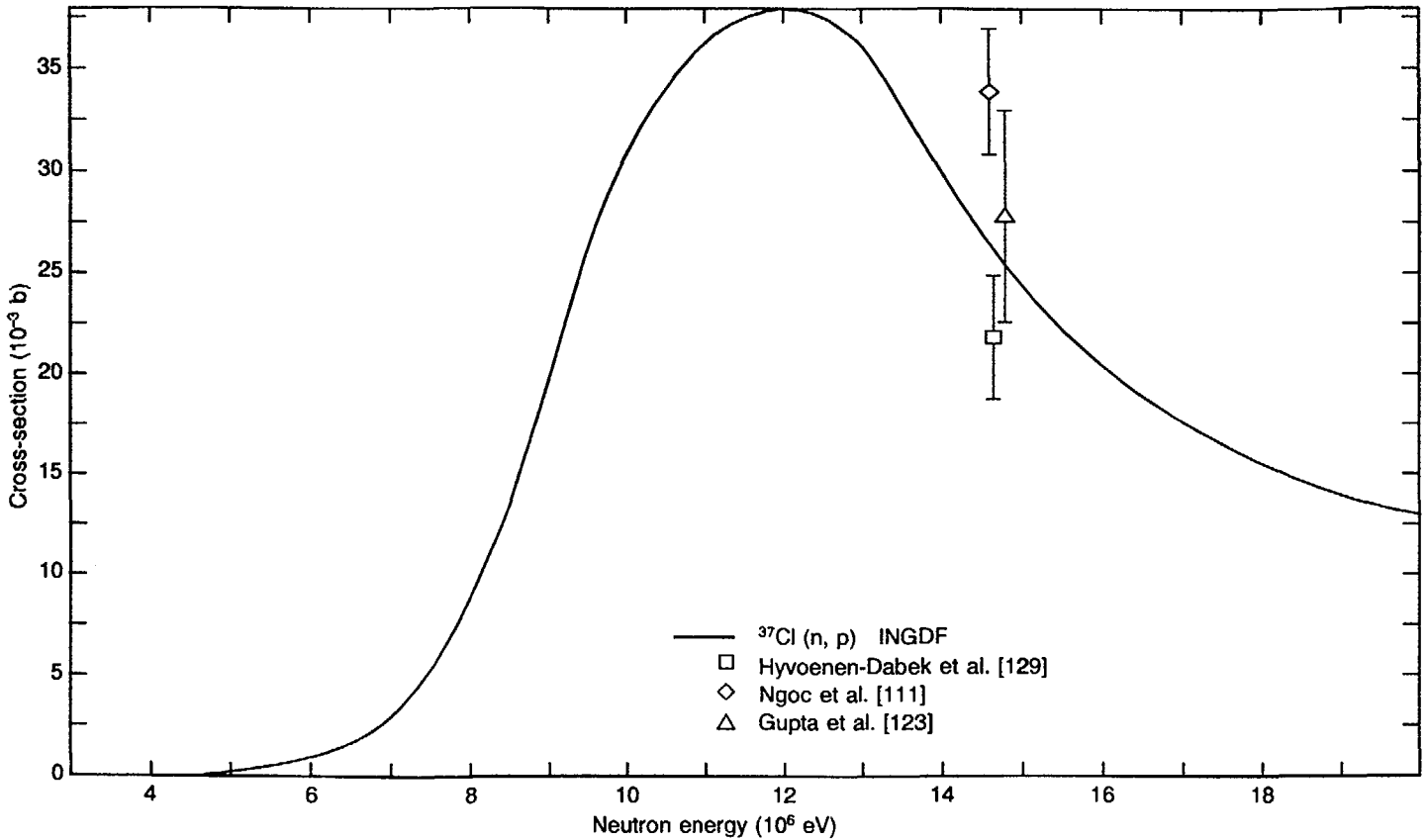

FIG. 6.35. Excitation function for the $^{37}Cl(n,p)^{37}S$ reaction. Evaluated data from Ref. [6].

$^{37}Cl\,(n,p)^{37}S$

E_n (eV)	σ (b)	E_n (eV)	σ (b)	E_n (eV)	σ (b)
4.00000×10^{6}	7.00224×10^{-6}	4.50000×10^{6}	7.15460×10^{-5}	5.00000×10^{6}	2.34185×10^{-4}
5.50000×10^{6}	5.63550×10^{-4}	6.00000×10^{6}	1.16297×10^{-3}	6.50000×10^{6}	2.19100×10^{-3}
7.00000×10^{6}	3.87955×10^{-3}	7.50000×10^{6}	6.54480×10^{-3}	8.00000×10^{6}	1.05708×10^{-2}
8.50000×10^{6}	1.63300×10^{-2}	9.00000×10^{6}	2.30720×10^{-2}	9.50000×10^{6}	2.87785×10^{-2}
1.00000×10^{7}	3.40185×10^{-2}	1.10000×10^{7}	3.74693×10^{-2}	1.20000×10^{7}	3.74465×10^{-2}
1.30000×10^{7}	3.32230×10^{-2}	1.40000×10^{7}	2.73860×10^{-2}	1.50000×10^{7}	2.27562×10^{-2}
1.60000×10^{7}	1.93180×10^{-2}	1.70000×10^{7}	1.68268×10^{-2}	1.80000×10^{7}	1.50445×10^{-2}
1.90000×10^{7}	1.37745×10^{-2}				

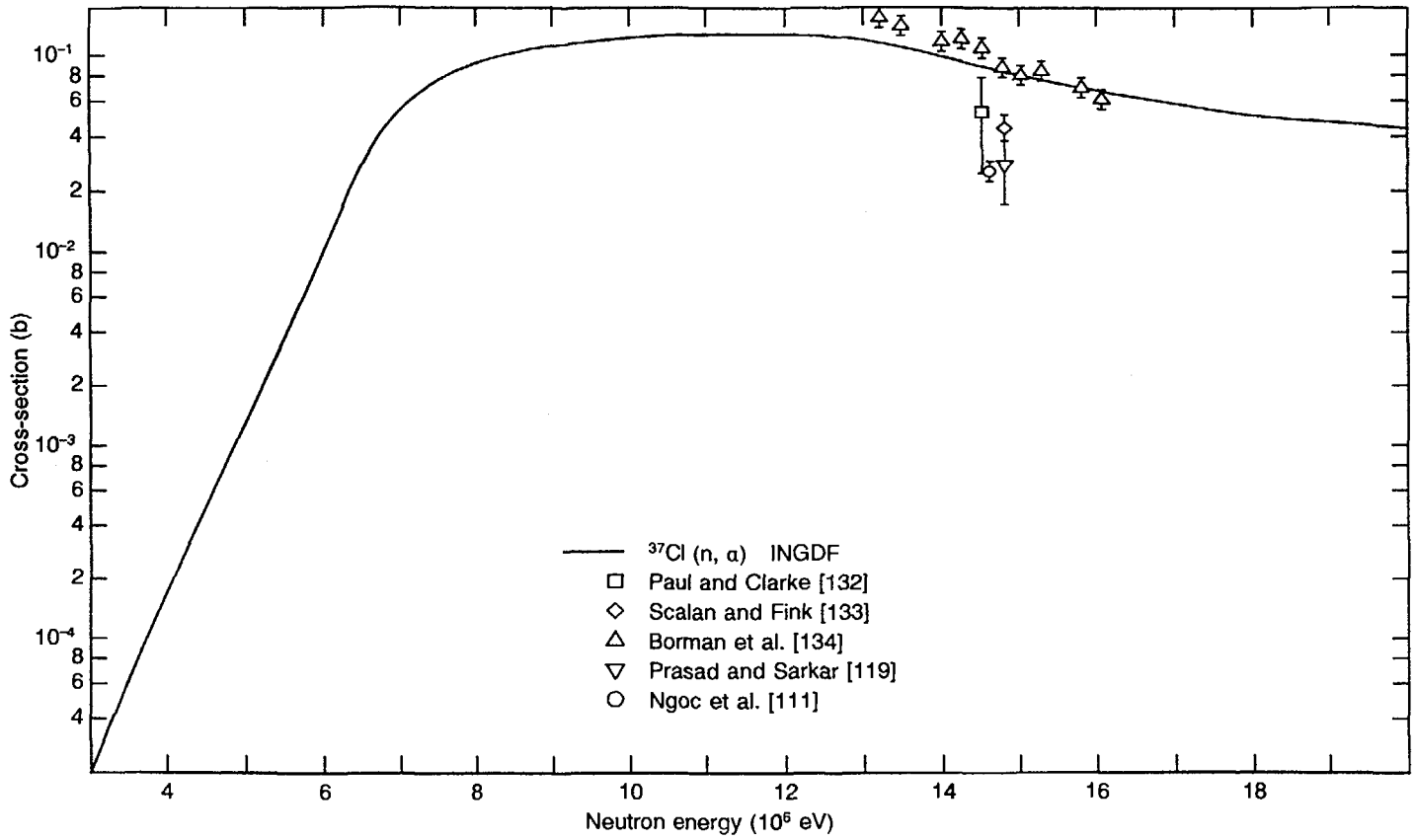

FIG. 6.36. Excitation function for the $^{37}Cl(n,\alpha)^{34}P$ reaction. Evaluated data from Ref. [6].

$^{37}Cl\,(n,\alpha)^{34}P$

E_n (eV)	σ (b)	E_n (eV)	σ (b)	E_n (eV)	σ (b)
1.00000×10^{6}	3.65982×10^{-7}	1.50000×10^{6}	4.63585×10^{-6}	2.00000×10^{6}	9.95951×10^{-6}
2.50000×10^{6}	1.52832×10^{-5}	3.00000×10^{6}	3.61200×10^{-5}	3.50000×10^{6}	1.05648×10^{-4}
4.00000×10^{6}	3.00160×10^{-4}	4.50000×10^{6}	8.38760×10^{-4}	5.00000×10^{6}	2.31710×10^{-3}
5.50000×10^{6}	6.32790×10^{-3}	6.00000×10^{6}	1.69559×10^{-2}	6.50000×10^{6}	3.95570×10^{-2}
7.00000×10^{6}	6.60140×10^{-2}	7.50000×10^{6}	8.57660×10^{-2}	8.00000×10^{6}	9.98260×10^{-2}
8.50000×10^{6}	1.09885×10^{-1}	9.00000×10^{6}	1.17065×10^{-1}	9.50000×10^{6}	1.22140×10^{-1}
1.00000×10^{7}	1.26820×10^{-1}	1.10000×10^{7}	1.29605×10^{-1}	1.20000×10^{7}	1.27532×10^{-1}
1.30000×10^{7}	1.11785×10^{-1}	1.40000×10^{7}	9.02125×10^{-2}	1.50000×10^{7}	7.40838×10^{-2}
1.60000×10^{7}	6.25338×10^{-2}	1.70000×10^{7}	5.43530×10^{-2}	1.80000×10^{7}	4.85835×10^{-2}
1.90000×10^{7}	4.45010×10^{-2}				

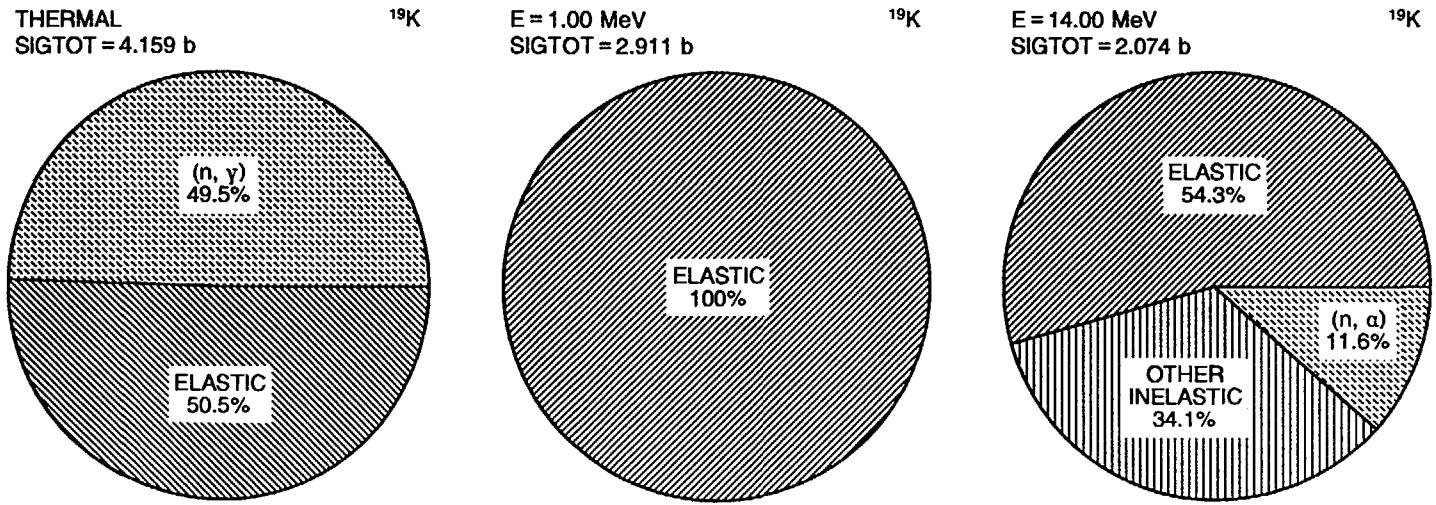

FIG. 6.37. Pie charts of the dominant neutron induced reaction cross-sections for potassium.

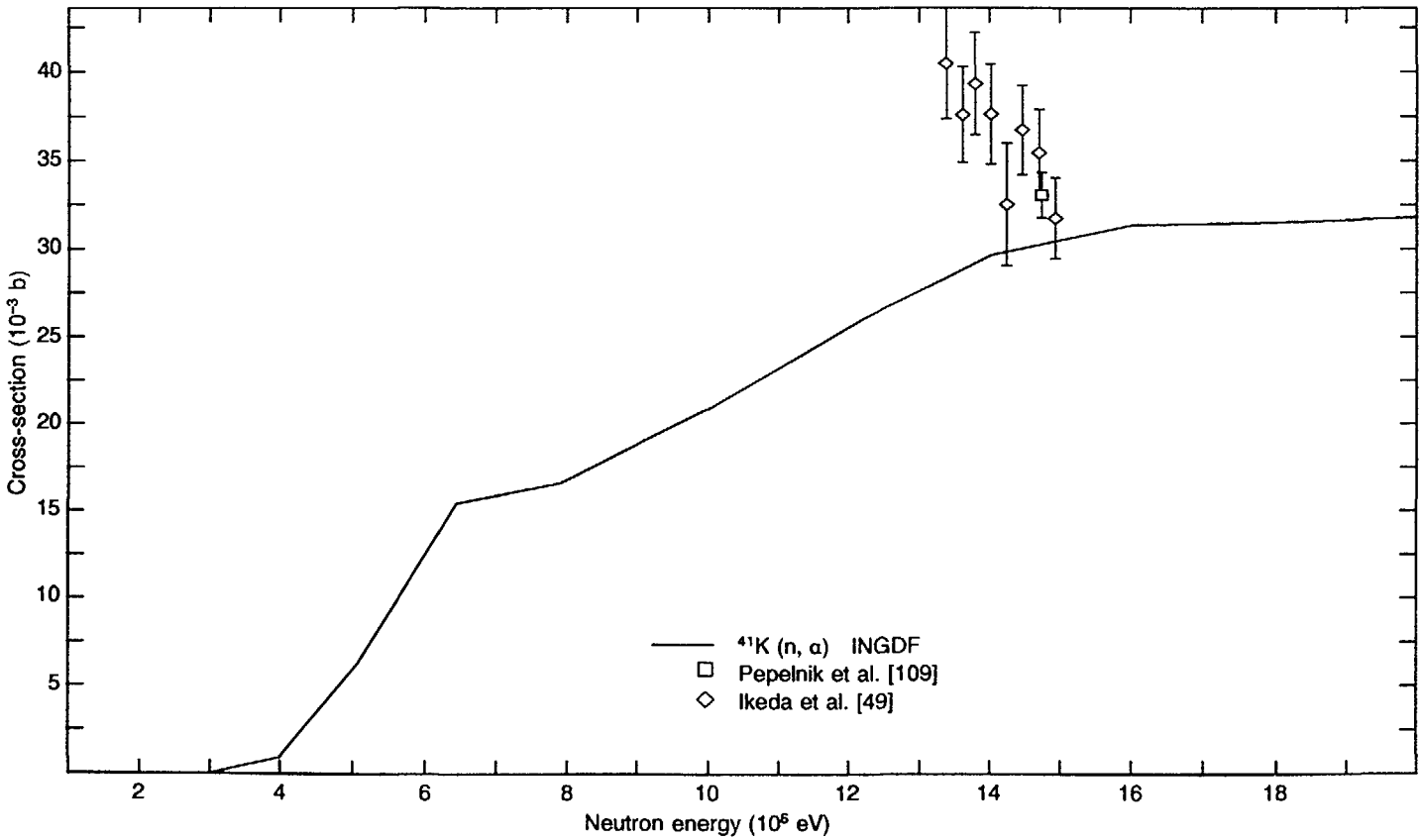

FIG. 6.38. Excitation function for the $^{41}K(n,\alpha)$ reaction.

$^{41}K(n,\alpha)$

E_n (eV)	σ (b)	E_n (eV)	σ (b)	E_n (eV)	σ (b)
1.00000×10^{5}	1.15941×10^{-11}	5.00000×10^{5}	3.96345×10^{-11}	1.00000×10^{6}	7.08084×10^{-11}
1.50000×10^{6}	1.47830×10^{-6}	2.00000×10^{6}	1.17994×10^{-5}	2.50000×10^{6}	2.35935×10^{-5}
3.00000×10^{6}	2.71003×10^{-4}	3.50000×10^{6}	7.54027×10^{-4}	4.00000×10^{6}	2.23645×10^{-3}
4.50000×10^{6}	4.71828×10^{-3}	5.00000×10^{6}	7.63495×10^{-3}	5.50000×10^{6}	1.09864×10^{-2}
6.00000×10^{6}	1.42794×10^{-2}	6.50000×10^{6}	1.56387×10^{-2}	7.00000×10^{6}	1.60604×10^{-2}
7.50000×10^{6}	1.64822×10^{-2}	8.00000×10^{6}	1.72315×10^{-2}	8.50000×10^{6}	1.83084×10^{-2}
9.00000×10^{6}	1.93852×10^{-2}	9.50000×10^{6}	2.04621×10^{-2}	1.00000×10^{7}	2.21376×10^{-2}
1.10000×10^{7}	2.45260×10^{-2}	1.20000×10^{7}	2.67117×10^{-2}	1.30000×10^{7}	2.86836×10^{-2}
1.40000×10^{7}	3.00998×10^{-2}	1.50000×10^{7}	3.09604×10^{-2}	1.60000×10^{7}	3.14098×10^{-2}
1.70000×10^{7}	3.14481×10^{-2}	1.80000×10^{7}	3.15274×10^{-2}	1.90000×10^{7}	3.16478×10^{-2}

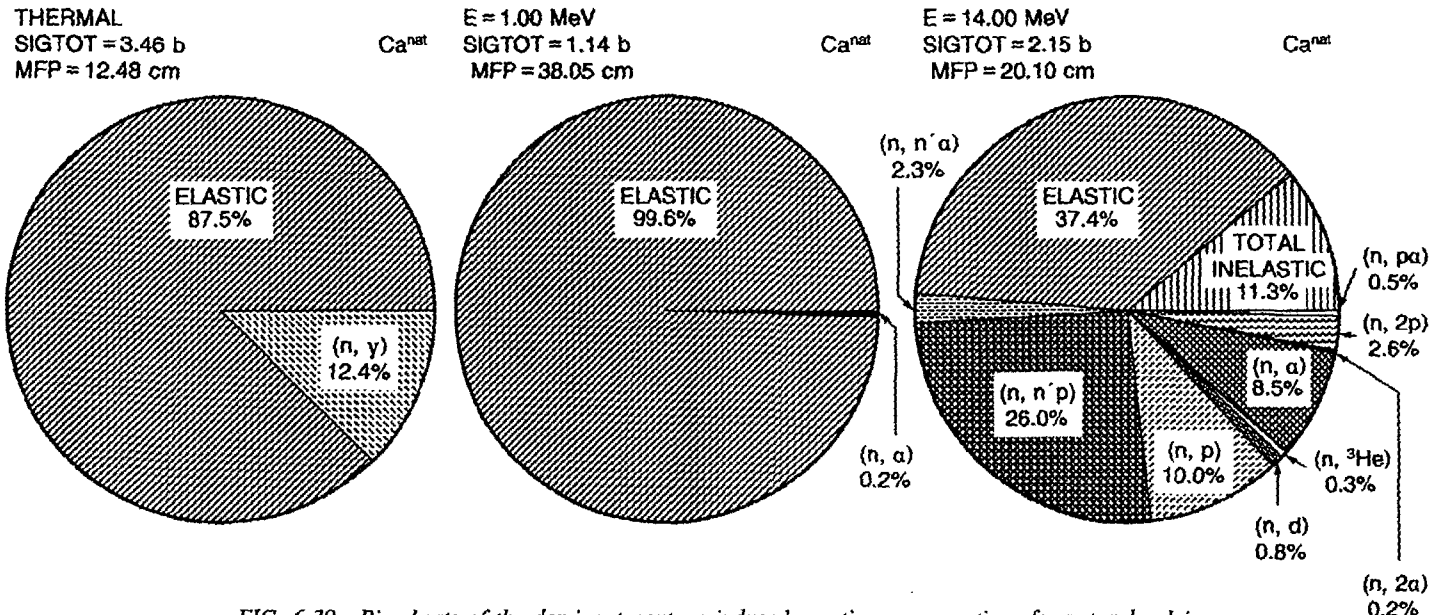

FIG. 6.39. Pie charts of the dominant neutron induced reaction cross-sections for natural calcium.

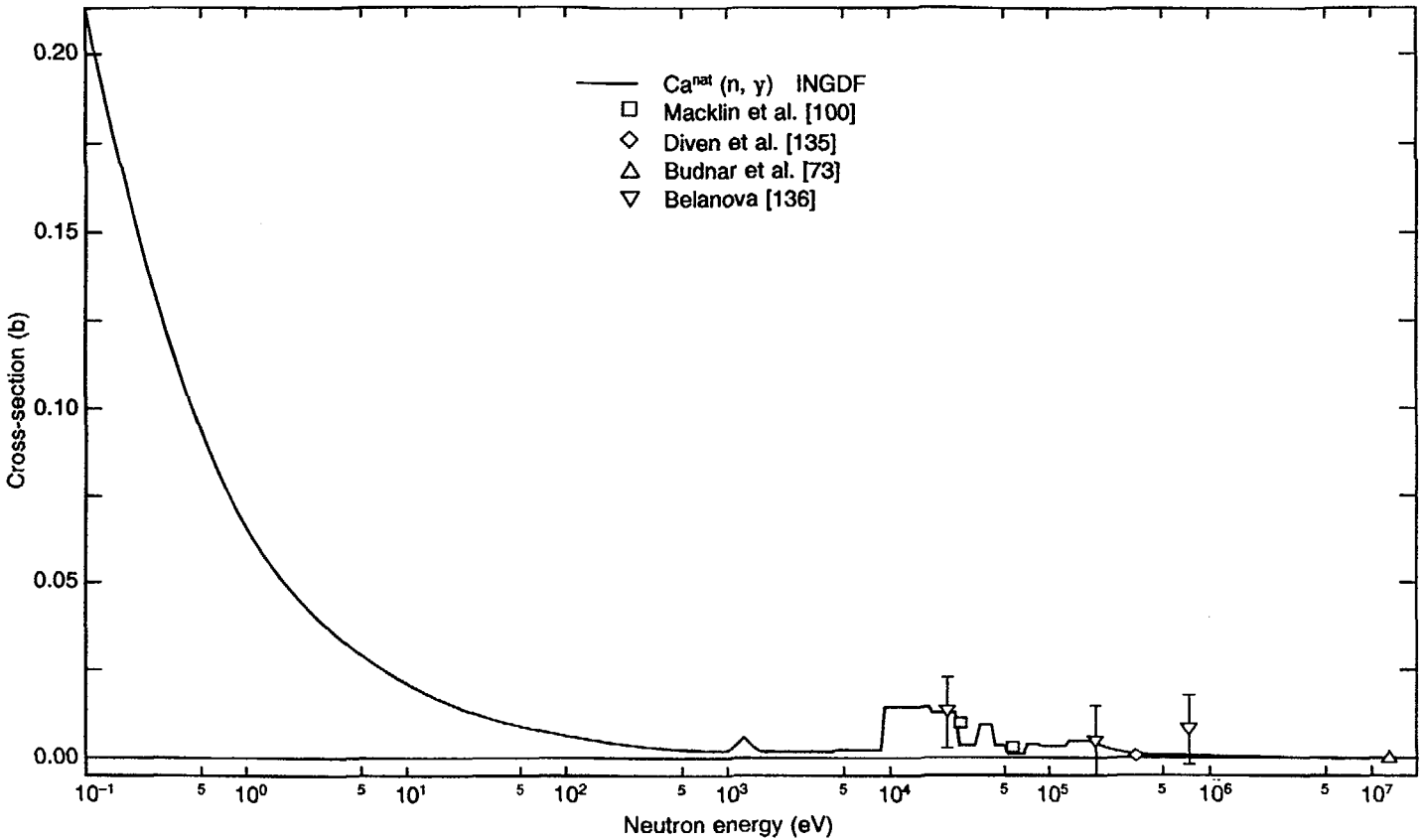

FIG. 6.40. Excitation function for the $Ca^{nat}(n,\gamma)$ reaction. Evaluated data from Ref. [137].

$Ca^{nat}(n,\gamma)$

E_n (eV)	σ (b)	E_n (eV)	σ (b)	E_n (eV)	σ (b)
1.00000×10^{-3}	3.93447×10^{-1}	1.00000×10^{-1}	1.03983×10^{-1}	1.00000	3.28820×10^{-2}
1.00000×10^{1}	1.03983×10^{-2}	1.00000×10^{2}	3.28820×10^{-3}	1.00000×10^{3}	2.21461×10^{-3}
1.00000×10^{4}	1.01750×10^{-2}	5.00000×10^{4}	2.88000×10^{-3}	1.00000×10^{5}	2.83020×10^{-3}
5.00000×10^{5}	4.94818×10^{-4}	1.00000×10^{6}	2.27787×10^{-4}	1.50000×10^{6}	1.86267×10^{-4}
2.00000×10^{6}	1.60426×10^{-4}	2.50000×10^{6}	1.42461×10^{-4}	3.00000×10^{6}	1.29060×10^{-4}
3.50000×10^{6}	1.18597×10^{-4}	4.00000×10^{6}	1.10169×10^{-4}	4.50000×10^{6}	1.03158×10^{-4}
5.00000×10^{6}	1.08182×10^{-4}	5.50000×10^{6}	1.25000×10^{-4}	6.00000×10^{6}	1.42699×10^{-4}
6.50000×10^{6}	1.61260×10^{-4}	7.00000×10^{6}	1.80719×10^{-4}	7.50000×10^{6}	2.00884×10^{-4}
8.00000×10^{6}	2.21857×10^{-4}	8.50000×10^{6}	2.43614×10^{-4}	9.00000×10^{6}	2.66207×10^{-4}
9.50000×10^{6}	2.89361×10^{-4}	1.00000×10^{7}	3.25665×10^{-4}	1.10000×10^{7}	3.76362×10^{-4}
1.20000×10^{7}	4.29659×10^{-4}	1.30000×10^{7}	4.85587×10^{-4}	1.40000×10^{7}	5.19714×10^{-4}
1.50000×10^{7}	5.20001×10^{-4}	1.60000×10^{7}	5.20001×10^{-4}	1.70000×10^{7}	5.20001×10^{-4}
1.80000×10^{7}	5.20001×10^{-4}	1.90000×10^{7}	5.20001×10^{-4}		

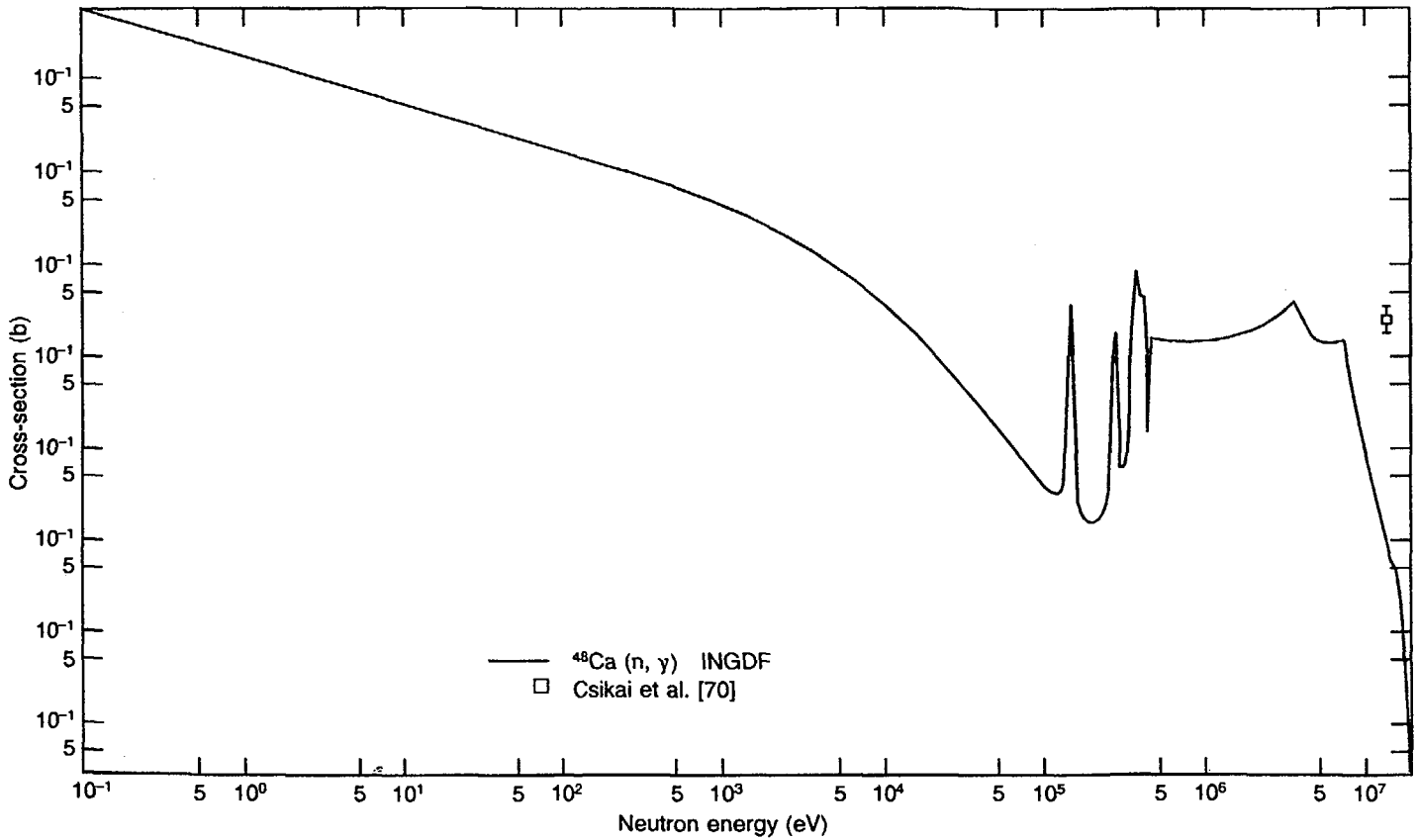

FIG. 6.41. Excitation function for the $^{48}Ca(n,\gamma)$ reaction. Evaluated data from Ref. [138].

$^{48}Ca\ (n, \gamma)$

E_n (eV)	σ (b)	E_n (eV)	σ (b)	E_n (eV)	σ (b)
1.00000×10^{-3}	9.99666×10^{-1}	1.00000×10^{-1}	2.64165×10^{-1}	1.00000	8.34622×10^{-2}
1.00000×10^{1}	2.61714×10^{-2}	1.00000×10^{2}	7.63184×10^{-3}	1.00000×10^{3}	1.33581×10^{-3}
1.00000×10^{4}	1.03340×10^{-4}	5.00000×10^{4}	1.03224×10^{-5}	1.00000×10^{5}	1.46755×10^{-4}
5.00000×10^{5}	1.49090×10^{-4}	1.00000×10^{6}	1.48472×10^{-4}	1.50000×10^{6}	1.68055×10^{-4}
2.00000×10^{6}	2.01303×10^{-4}	2.50000×10^{6}	2.45858×10^{-4}	3.00000×10^{6}	3.02767×10^{-4}
3.50000×10^{6}	3.72366×10^{-4}	4.00000×10^{6}	2.87038×10^{-4}	4.50000×10^{6}	2.06155×10^{-4}
5.00000×10^{6}	1.61517×10^{-4}	5.50000×10^{6}	1.45274×10^{-4}	6.00000×10^{6}	1.42588×10^{-4}
6.50000×10^{6}	1.45211×10^{-4}	7.00000×10^{6}	1.43414×10^{-4}	7.50000×10^{6}	1.47905×10^{-4}
8.00000×10^{6}	1.34307×10^{-4}	8.50000×10^{6}	7.33953×10^{-5}	9.00000×10^{6}	4.22621×10^{-5}
9.50000×10^{6}	2.71205×10^{-5}	1.00000×10^{7}	1.59018×10^{-5}	1.10000×10^{7}	8.27829×10^{-6}
1.20000×10^{7}	4.34143×10^{-6}	1.30000×10^{7}	2.38715×10^{-6}	1.40000×10^{7}	1.38739×10^{-6}
1.50000×10^{7}	8.15194×10^{-7}	1.60000×10^{7}	5.45432×10^{-7}	1.70000×10^{7}	3.52613×10^{-7}

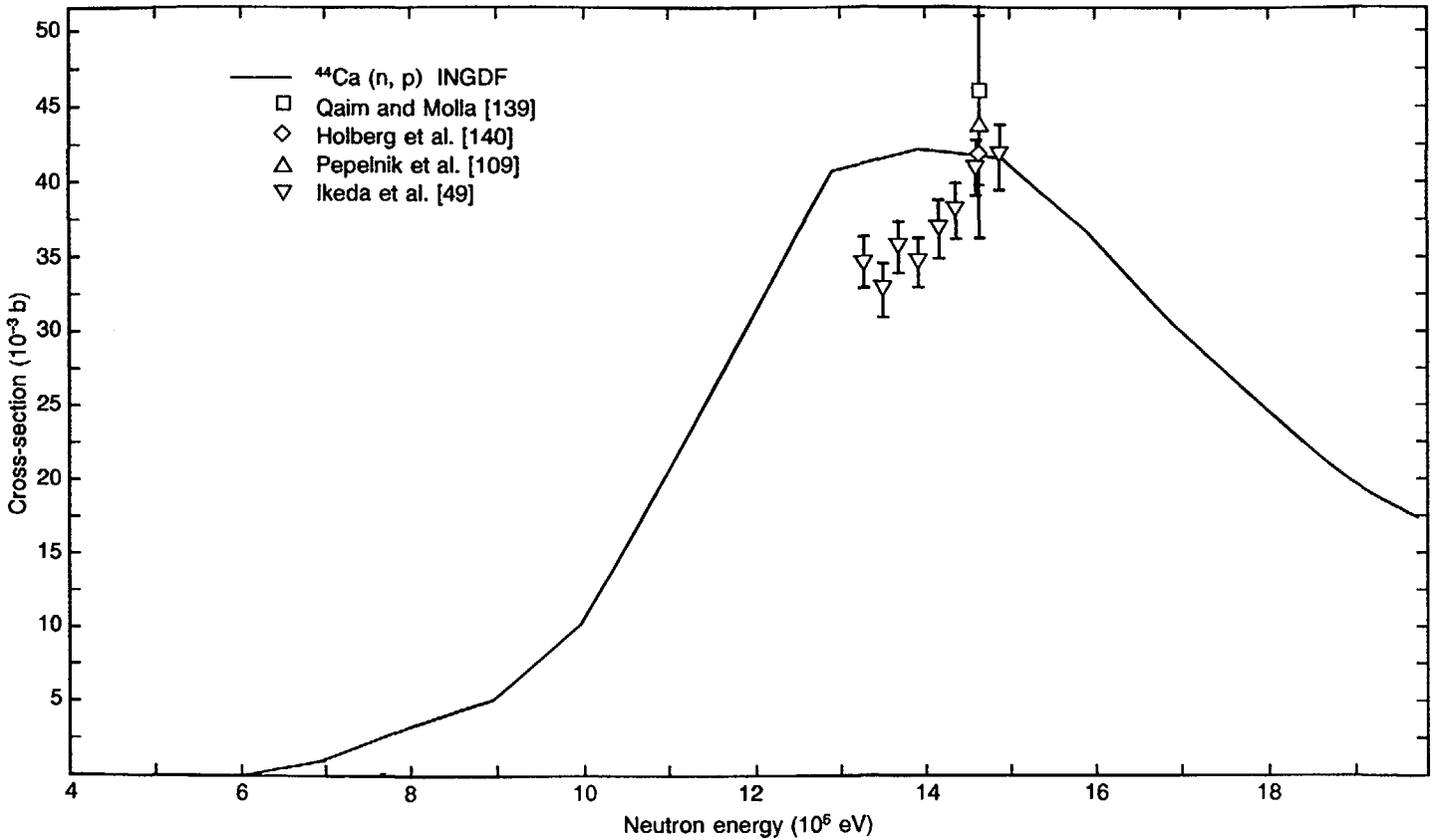

FIG. 6.42. Excitation function for the $^{44}Ca(n,p)^{44}K$ reaction. Evaluated data from Ref. [138].

$^{44}Ca\,(n,p)^{44}K$

E_n (eV)	σ (b)	E_n (eV)	σ (b)	E_n (eV)	σ (b)
5.00000×10^{6}	3.56704×10^{-6}	5.50000×10^{6}	1.07011×10^{-5}	6.00000×10^{6}	2.60595×10^{-4}
6.50000×10^{6}	7.53250×10^{-4}	7.00000×10^{6}	1.54422×10^{-3}	7.50000×10^{6}	2.63352×10^{-3}
8.00000×10^{6}	3.62020×10^{-3}	8.50000×10^{6}	4.50427×10^{-3}	9.00000×10^{6}	6.13760×10^{-3}
9.50000×10^{6}	8.52019×10^{-3}	1.00000×10^{7}	1.45762×10^{-2}	1.10000×10^{7}	2.49806×10^{-2}
1.20000×10^{7}	3.56567×10^{-2}	1.30000×10^{7}	4.15572×10^{-2}	1.40000×10^{7}	4.20727×10^{-2}
1.50000×10^{7}	3.94277×10^{-2}	1.60000×10^{7}	3.40195×10^{-2}	1.70000×10^{7}	2.81702×10^{-2}
1.80000×10^{7}	2.29255×10^{-2}	1.90000×10^{7}	1.88171×10^{-2}		

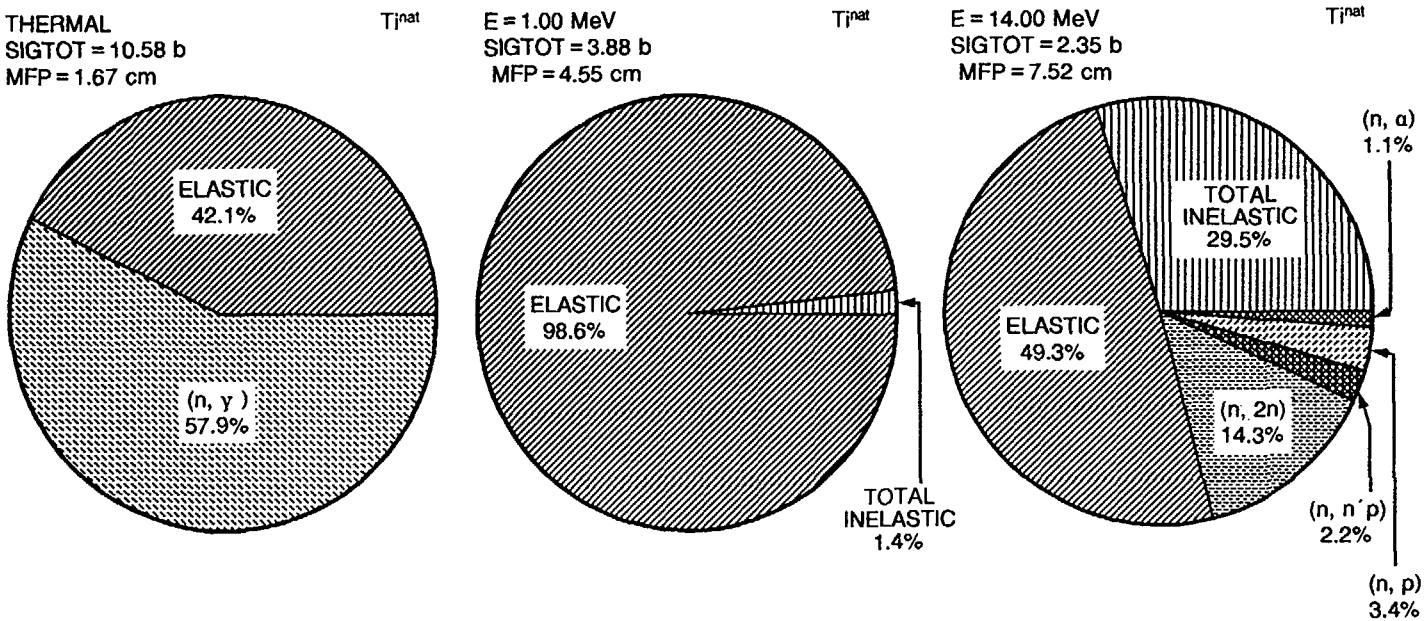

FIG. 6.43. Pie charts of the dominant neutron induced reaction cross-sections for natural titanium.

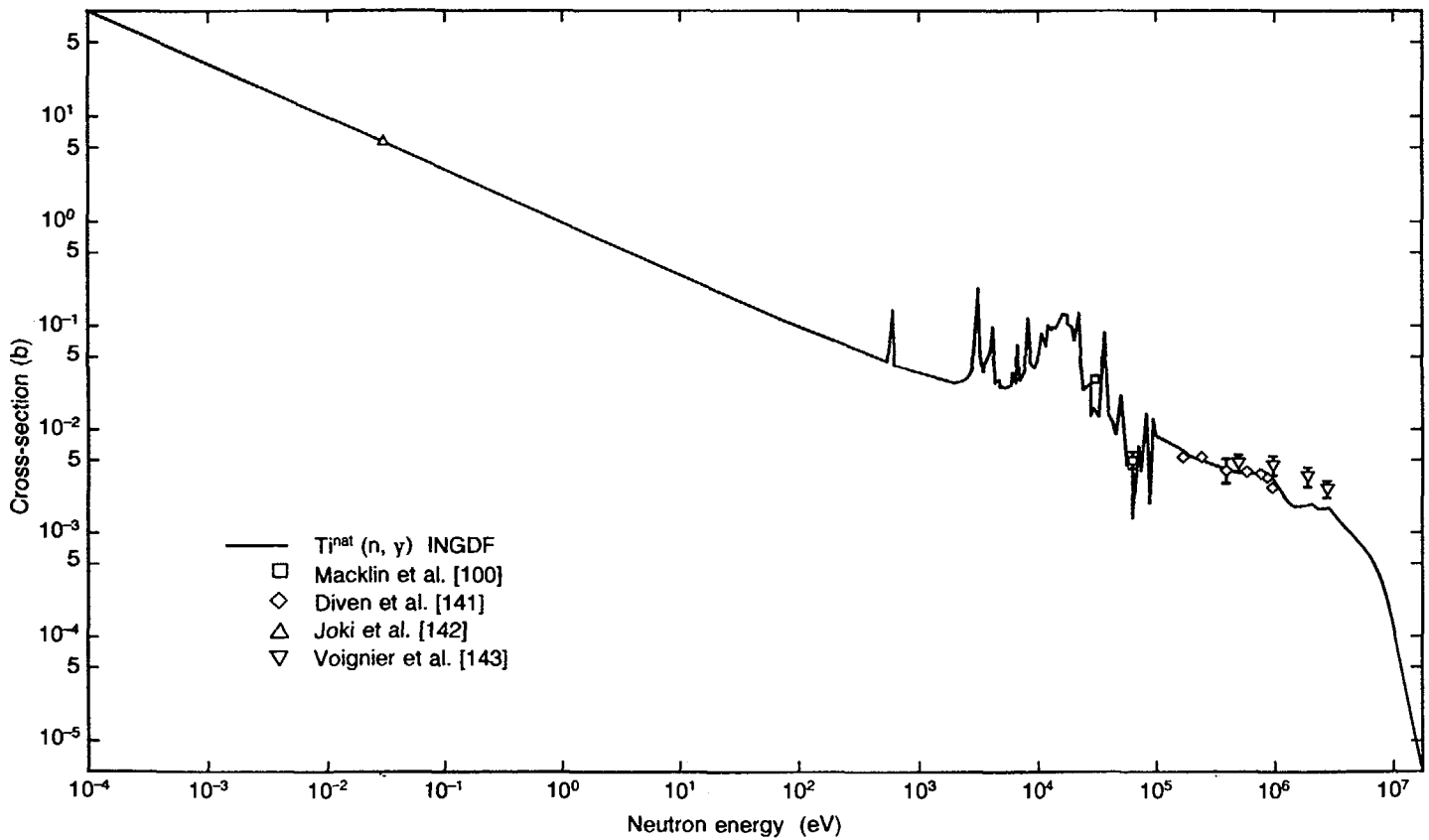

FIG. 6.44. Excitation function for the $Ti^{nat}(n,\gamma)$ reaction. Evaluated data from Ref. [144].

$Ti^{nat}(n,\gamma)$

E_n (eV)	σ (b)	E_n (eV)	σ (b)	E_n (eV)	σ (b)
1.00000×10^{-3}	5.57289	1.00000×10^{-1}	1.47284	1.00000	4.65743×10^{-1}
1.00000×10^{1}	1.47475×10^{-1}	1.00000×10^{2}	5.12575×10^{-2}	1.00000×10^{3}	4.68073×10^{-2}
1.00000×10^{4}	4.91684×10^{-2}	5.00000×10^{4}	6.80634×10^{-3}	1.00000×10^{5}	5.07396×10^{-3}
5.00000×10^{5}	3.80453×10^{-3}	1.00000×10^{6}	2.52878×10^{-3}	1.50000×10^{6}	1.82206×10^{-3}
2.00000×10^{6}	1.85144×10^{-3}	2.50000×10^{6}	1.73485×10^{-3}	3.00000×10^{6}	1.65053×10^{-3}
3.50000×10^{6}	1.38457×10^{-3}	4.00000×10^{6}	1.15128×10^{-3}	4.50000×10^{6}	9.93233×10^{-4}
5.00000×10^{6}	8.69123×10^{-4}	5.50000×10^{6}	7.70186×10^{-4}	6.00000×10^{6}	6.82236×10^{-4}
6.50000×10^{6}	5.96665×10^{-4}	7.00000×10^{6}	5.13360×10^{-4}	7.50000×10^{6}	4.35484×10^{-4}
8.00000×10^{6}	3.65611×10^{-4}	8.50000×10^{6}	3.04954×10^{-4}	9.00000×10^{6}	2.52710×10^{-4}
9.50000×10^{6}	2.09172×10^{-4}	1.00000×10^{7}	1.57316×10^{-4}	1.10000×10^{7}	1.06597×10^{-4}
1.20000×10^{7}	7.15852×10^{-5}	1.30000×10^{7}	4.63764×10^{-5}	1.40000×10^{7}	2.92634×10^{-5}
1.50000×10^{7}	1.89551×10^{-5}	1.60000×10^{7}	1.32208×10^{-5}	1.70000×10^{7}	9.96135×10^{-6}
1.80000×10^{7}	7.64364×10^{-6}	1.90000×10^{7}	5.75409×10^{-6}		

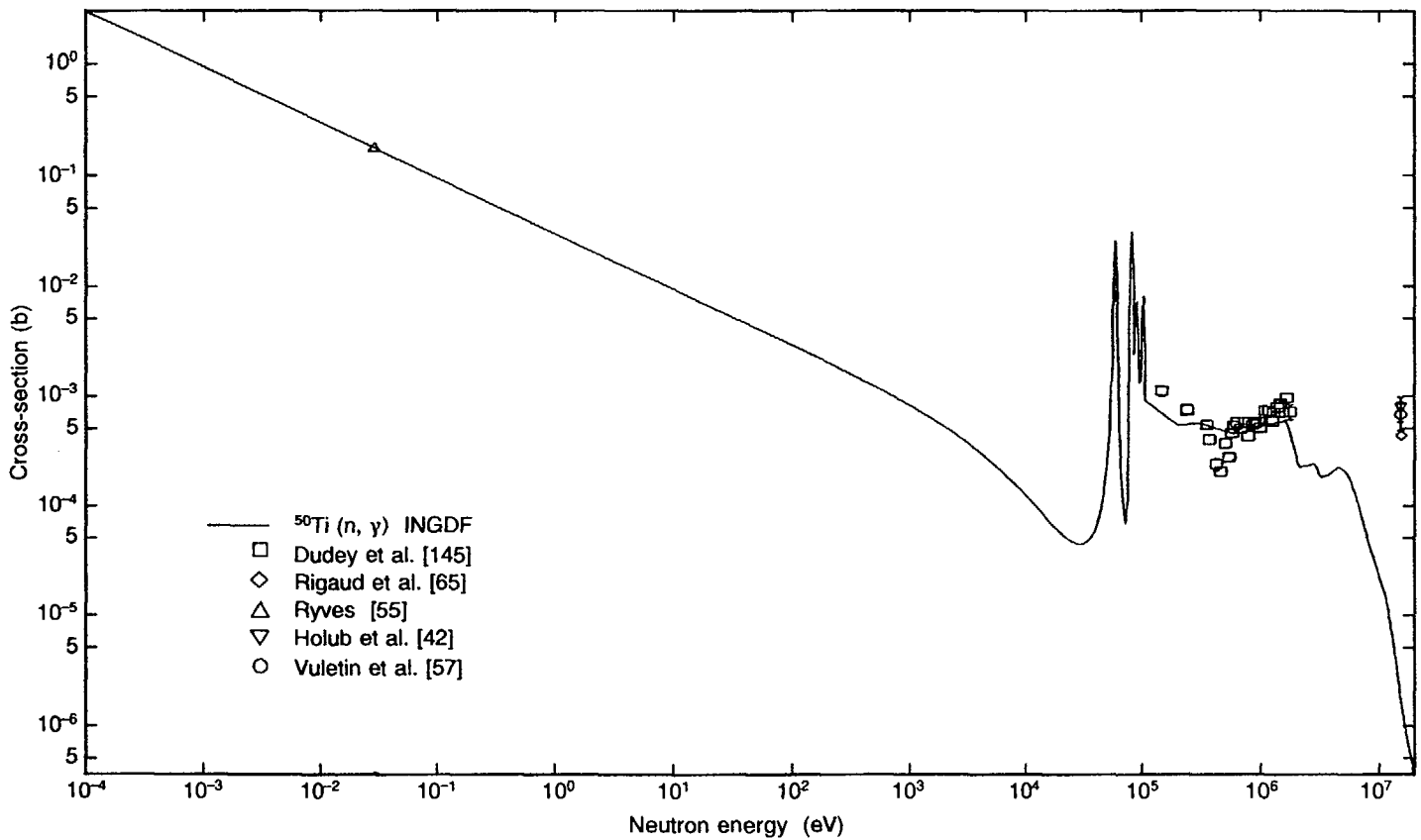

FIG. 6.45. Excitation function for the $^{50}Ti(n,\gamma)^{51}Ti$ reaction. Evaluated data from Ref. [144].

$^{50}Ti\,(n,\gamma)^{51}Ti$

E_n (eV)	σ (b)	E_n (eV)	σ (b)	E_n (eV)	σ (b)
1.00000×10^{-3}	1.63393×10^{-1}	1.00000×10^{-1}	4.31814×10^{-2}	1.00000	1.36478×10^{-2}
1.00000×10^{1}	4.29521×10^{-3}	1.00000×10^{2}	1.29673×10^{-3}	1.00000×10^{3}	2.84388×10^{-4}
1.00000×10^{4}	7.94218×10^{-5}	5.00000×10^{4}	5.86602×10^{-3}	1.00000×10^{5}	5.83425×10^{-4}
5.00000×10^{5}	5.17895×10^{-4}	1.00000×10^{6}	5.80809×10^{-4}	1.50000×10^{6}	4.27294×10^{-4}
2.00000×10^{6}	2.36424×10^{-4}	2.50000×10^{6}	2.30088×10^{-4}	3.00000×10^{6}	1.91968×10^{-4}
3.50000×10^{6}	2.06848×10^{-4}	4.00000×10^{6}	2.25271×10^{-4}	4.50000×10^{6}	2.17287×10^{-4}
5.00000×10^{6}	1.88841×10^{-4}	5.50000×10^{6}	1.49312×10^{-4}	6.00000×10^{6}	1.13060×10^{-4}
6.50000×10^{6}	8.57368×10^{-5}	7.00000×10^{6}	6.61994×10^{-5}	7.50000×10^{6}	5.21435×10^{-5}
8.00000×10^{6}	4.20096×10^{-5}	8.50000×10^{6}	3.44570×10^{-5}	9.00000×10^{6}	2.85663×10^{-5}
9.50000×10^{6}	2.39017×10^{-5}	1.00000×10^{7}	1.86668×10^{-5}	1.10000×10^{7}	1.32251×10^{-5}
1.20000×10^{7}	8.59582×10^{-6}	1.30000×10^{7}	5.05681×10^{-6}	1.40000×10^{7}	2.91695×10^{-6}
1.50000×10^{7}	1.77620×10^{-6}	1.60000×10^{7}	1.17055×10^{-6}	1.70000×10^{7}	8.18386×10^{-7}
1.80000×10^{7}	6.00990×10^{-7}	1.90000×10^{7}	4.38751×10^{-7}		

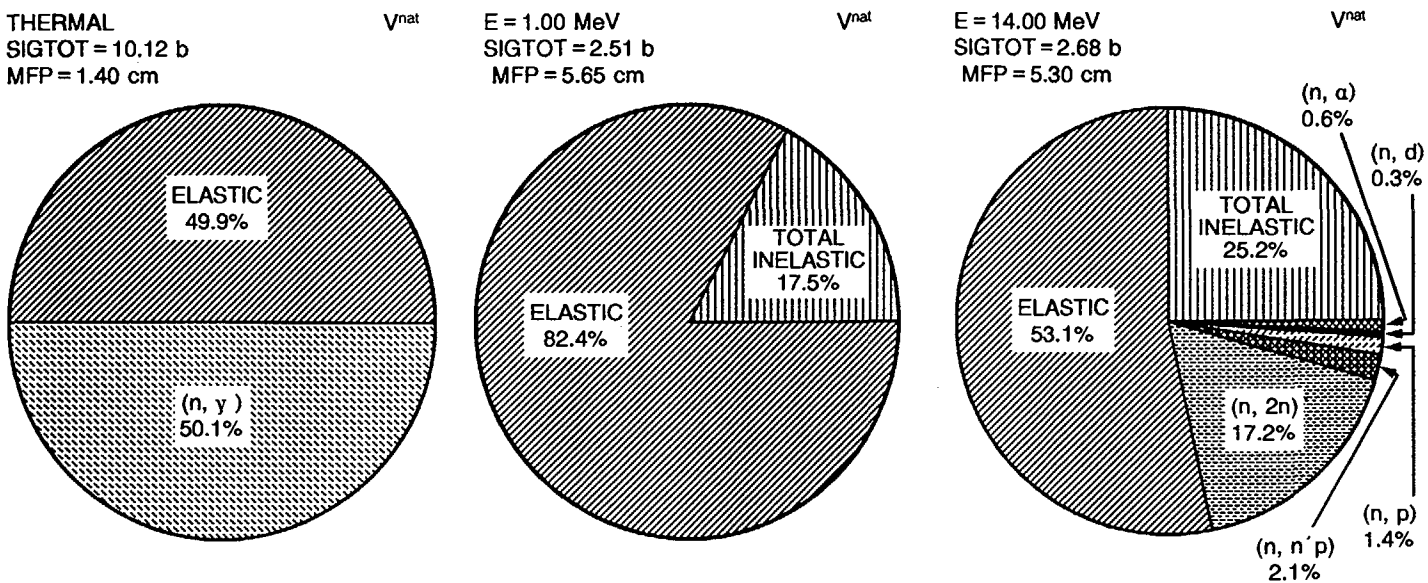

FIG. 6.46. Pie charts of the dominant neutron induced reaction cross-sections for natural vanadium.

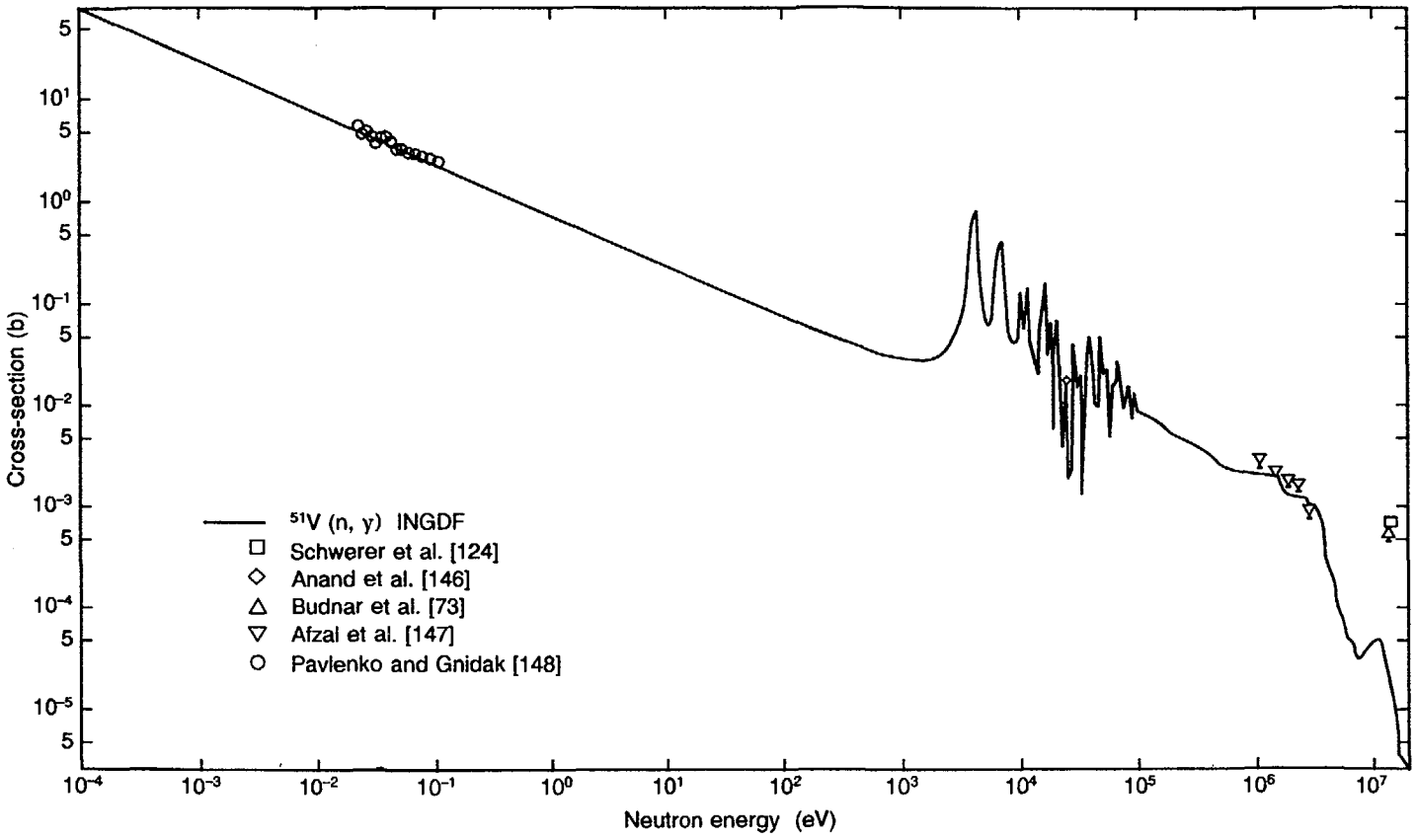

FIG. 6.47. Excitation function for the $^{51}V(n,\gamma)$ reaction. Evaluated data from Ref. [149].

$^{51}V\ (n, \gamma)$

E_n (eV)	σ (b)	E_n (eV)	σ (b)	E_n (eV)	σ (b)
1.00000×10^{-3}	4.48534	1.00000×10^{-1}	1.18545	1.00000	3.75041×10^{-1}
1.00000×10^{1}	1.19186×10^{-1}	1.00000×10^{2}	4.04600×10^{-2}	1.00000×10^{3}	1.52418×10^{-1}
1.00000×10^{4}	3.52505×10^{-2}	5.00000×10^{4}	1.40342×10^{-2}	1.00000×10^{5}	4.63781×10^{-3}
5.00000×10^{5}	2.32983×10^{-3}	1.00000×10^{6}	2.05804×10^{-3}	1.50000×10^{6}	1.70956×10^{-3}
2.00000×10^{6}	1.28432×10^{-3}	2.50000×10^{6}	1.17596×10^{-3}	3.00000×10^{6}	1.00839×10^{-3}
3.50000×10^{6}	5.85357×10^{-4}	4.00000×10^{6}	2.68159×10^{-4}	4.50000×10^{6}	1.62418×10^{-4}
5.00000×10^{6}	9.67624×10^{-5}	5.50000×10^{6}	7.11932×10^{-5}	6.00000×10^{6}	5.32638×10^{-5}
6.50000×10^{6}	4.29743×10^{-5}	7.00000×10^{6}	3.62685×10^{-5}	7.50000×10^{6}	3.31465×10^{-5}
8.00000×10^{6}	3.37893×10^{-5}	8.50000×10^{6}	3.81967×10^{-5}	9.00000×10^{6}	4.14969×10^{-5}
9.50000×10^{6}	4.36897×10^{-5}	1.00000×10^{7}	4.76374×10^{-5}	1.10000×10^{7}	5.00094×10^{-5}
1.20000×10^{7}	4.20251×10^{-5}	1.30000×10^{7}	2.82675×10^{-5}	1.40000×10^{7}	1.90052×10^{-5}
1.50000×10^{7}	1.33393×10^{-5}	1.60000×10^{7}	8.59520×10^{-6}	1.70000×10^{7}	5.24407×10^{-6}
1.80000×10^{7}	3.64516×10^{-6}	1.90000×10^{7}	3.10925×10^{-6}		

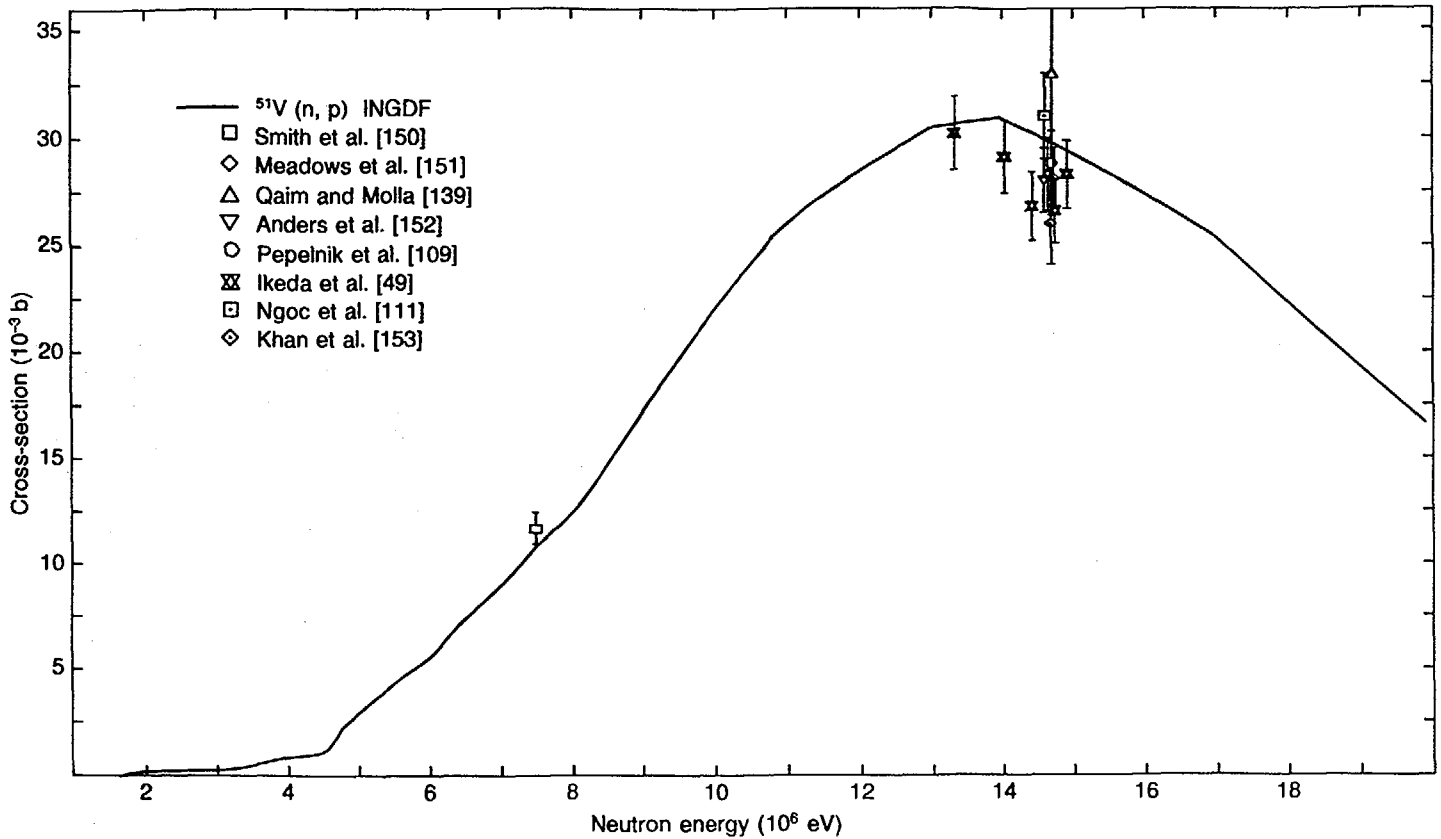

FIG. 6.48. Excitation function for the $^{51}V(n,p)^{51}Ti$ reaction. Evaluated data from Ref. [149].

$^{51}V(n,p)^{51}Ti$

E_n (eV)	σ (b)	E_n (eV)	σ (b)	E_n (eV)	σ (b)
1.50000×10^6	5.84002×10^{-5}	2.00000×10^6	2.33334×10^{-4}	2.50000×10^6	3.00000×10^{-4}
3.00000×10^6	3.66667×10^{-4}	3.50000×10^6	6.00001×10^{-4}	4.00000×10^6	9.50001×10^{-4}
4.50000×10^6	2.05000×10^{-3}	5.00000×10^6	3.62500×10^{-3}	5.50000×10^6	4.87500×10^{-3}
6.00000×10^6	6.37500×10^{-3}	6.50000×10^6	8.12500×10^{-3}	7.00000×10^6	9.87500×10^{-3}
7.50000×10^6	1.16250×10^{-2}	8.00000×10^6	1.36250×10^{-2}	8.50000×10^6	1.58750×10^{-2}
9.00000×10^6	1.82500×10^{-2}	9.50000×10^6	2.07500×10^{-2}	1.00000×10^7	2.40000×10^{-2}
1.10000×10^7	2.72500×10^{-2}	1.20000×10^7	2.95000×10^{-2}	1.30000×10^7	3.07500×10^{-2}
1.40000×10^7	3.02500×10^{-2}	1.50000×10^7	2.85000×10^{-2}	1.60000×10^7	2.65000×10^{-2}
1.70000×10^7	2.40000×10^{-2}	1.80000×10^7	2.10000×10^{-2}	1.90000×10^7	1.80000×10^{-2}

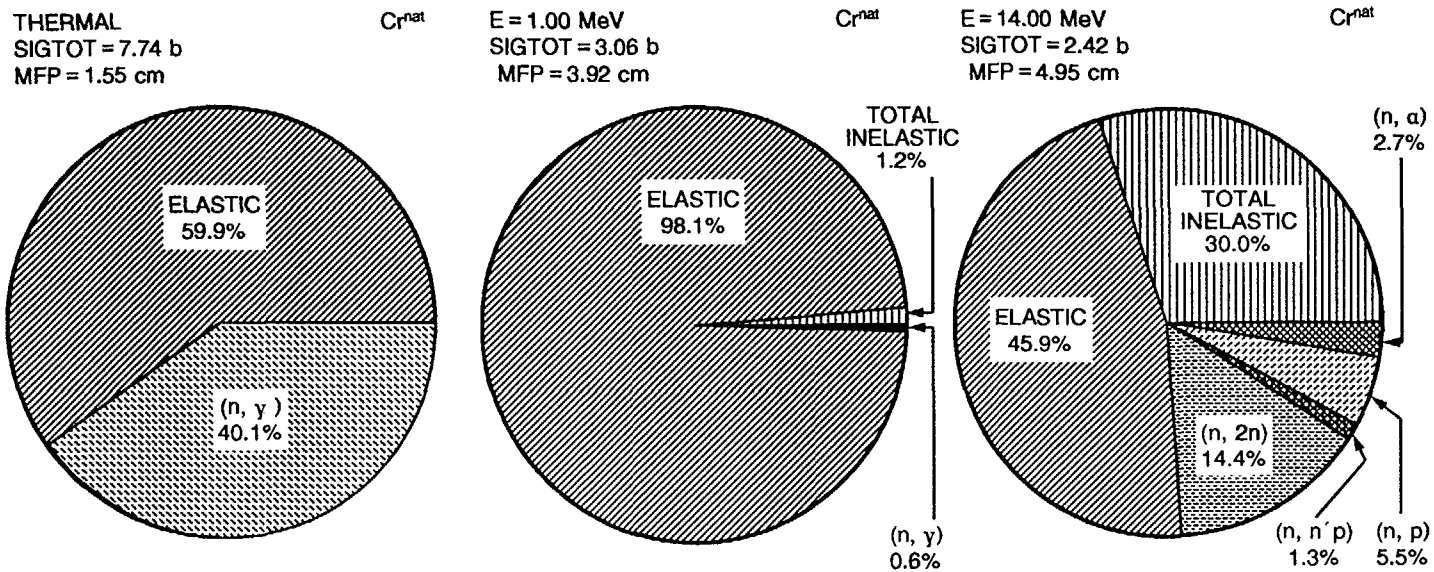

FIG. 6.49. Pie charts of the dominant neutron induced reaction cross-sections for natural chromium.

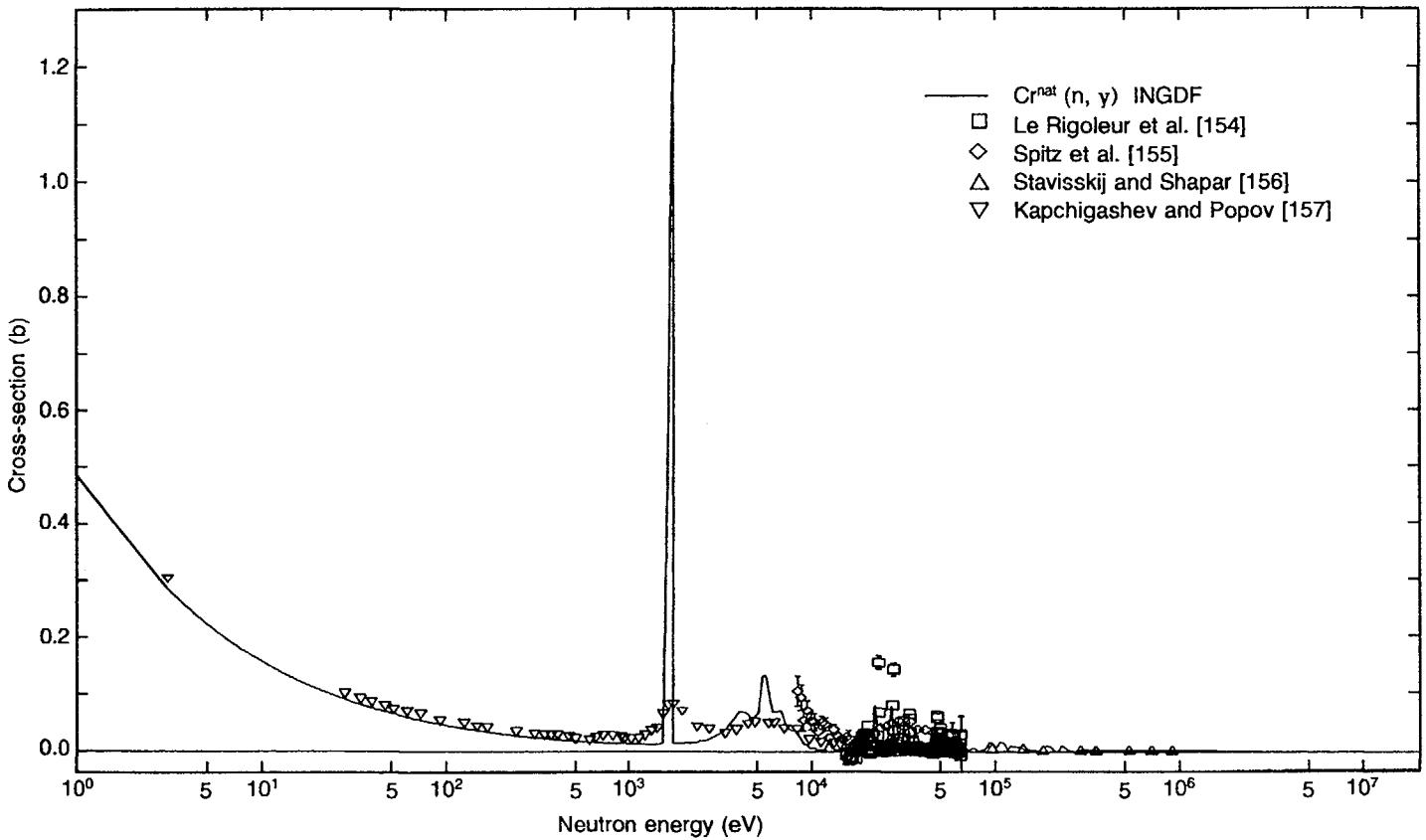

FIG. 6.50. Excitation function for the $Cr^{nat}(n,\gamma)$ reaction. Evaluated data from Ref. [158].

$Cr^{nat}(n,\gamma)$

E_n (eV)	σ (b)	E_n (eV)	σ (b)	E_n (eV)	σ (b)
1.00000×10^{-3}	2.80945	1.00000×10^{-1}	7.42142×10^{-1}	1.00000	2.33667×10^{-1}
1.00000×10^{1}	7.11190×10^{-2}	1.00000×10^{2}	1.96283×10^{-2}	1.00000×10^{3}	5.71540×10^{-2}
1.00000×10^{4}	1.12879×10^{-2}	5.00000×10^{4}	6.32819×10^{-3}	1.00000×10^{5}	4.37341×10^{-3}
5.00000×10^{5}	3.28146×10^{-3}	1.00000×10^{6}	3.29990×10^{-3}	1.50000×10^{6}	2.26503×10^{-3}
2.00000×10^{6}	1.58759×10^{-3}	2.50000×10^{6}	1.44591×10^{-3}	3.00000×10^{6}	1.25874×10^{-3}
3.50000×10^{6}	1.08034×10^{-3}	4.00000×10^{6}	9.27564×10^{-4}	4.50000×10^{6}	7.75592×10^{-4}
5.00000×10^{6}	5.16476×10^{-4}	5.50000×10^{6}	3.63558×10^{-4}	6.00000×10^{6}	2.77523×10^{-4}
6.50000×10^{6}	2.28563×10^{-4}	7.00000×10^{6}	1.94284×10^{-4}	7.50000×10^{6}	1.70016×10^{-4}
8.00000×10^{6}	1.51039×10^{-4}	8.50000×10^{6}	1.36032×10^{-4}	9.00000×10^{6}	1.23286×10^{-4}
9.50000×10^{6}	1.12372×10^{-4}	1.00000×10^{7}	9.85061×10^{-5}	1.10000×10^{7}	8.24367×10^{-5}
1.20000×10^{7}	6.55580×10^{-5}	1.30000×10^{7}	4.58902×10^{-5}	1.40000×10^{7}	2.76768×10^{-5}
1.50000×10^{7}	1.54231×10^{-5}	1.60000×10^{7}	8.51200×10^{-6}	1.70000×10^{7}	4.45421×10^{-6}
1.80000×10^{7}	2.30186×10^{-6}	1.90000×10^{7}	1.26901×10^{-6}		

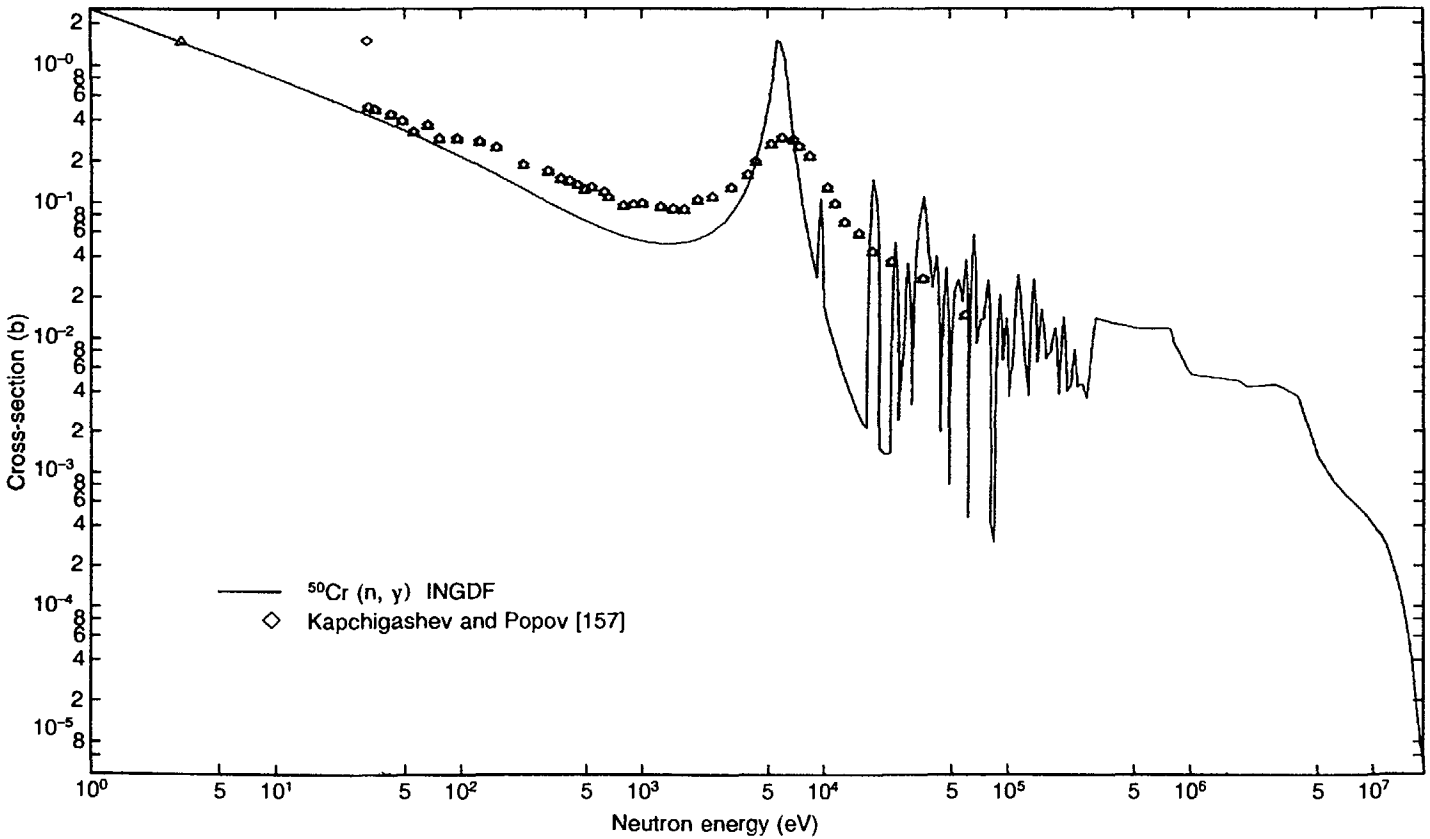

FIG. 6.51. Excitation function for the $^{50}Cr(n,\gamma)^{51}Cr$ reaction. Evaluated data from Ref. [158].

$^{50}Cr\,(n,\gamma)^{51}Cr$

E_n (eV)	σ (b)	E_n (eV)	σ (b)	E_n (eV)	σ (b)
1.00000×10^{-3}	1.45676×10^{1}	1.00000×10^{-1}	3.84623	1.00000	1.20486
1.00000×10^{1}	3.50781×10^{-1}	1.00000×10^{2}	8.17086×10^{-2}	1.00000×10^{3}	2.69965×10^{-1}
1.00000×10^{4}	2.87699×10^{-2}	5.00000×10^{4}	1.69662×10^{-2}	1.00000×10^{5}	1.08387×10^{-2}
5.00000×10^{5}	1.00937×10^{-2}	1.00000×10^{6}	5.27519×10^{-3}	1.50000×10^{6}	4.93036×10^{-3}
2.00000×10^{6}	4.47212×10^{-3}	2.50000×10^{6}	4.56183×10^{-3}	3.00000×10^{6}	4.30356×10^{-3}
3.50000×10^{6}	3.81220×10^{-3}	4.00000×10^{6}	2.57053×10^{-3}	4.50000×10^{6}	1.63307×10^{-3}
5.00000×10^{6}	1.18597×10^{-3}	5.50000×10^{6}	9.74933×10^{-4}	6.00000×10^{6}	8.34825×10^{-4}
6.50000×10^{6}	7.42344×10^{-4}	7.00000×10^{6}	6.70156×10^{-4}	7.50000×10^{6}	6.13635×10^{-4}
8.00000×10^{6}	5.63754×10^{-4}	8.50000×10^{6}	5.19640×10^{-4}	9.00000×10^{6}	4.76877×10^{-4}
9.50000×10^{6}	4.35765×10^{-4}	1.00000×10^{7}	3.82927×10^{-4}	1.10000×10^{7}	3.16221×10^{-4}
1.20000×10^{7}	2.43762×10^{-4}	1.30000×10^{7}	1.78622×10^{-4}	1.40000×10^{7}	1.25608×10^{-4}
1.50000×10^{7}	8.26770×10^{-5}	1.60000×10^{7}	5.12333×10^{-5}	1.70000×10^{7}	2.76376×10^{-5}
1.80000×10^{7}	1.42564×10^{-5}	1.90000×10^{7}	7.95178×10^{-6}		

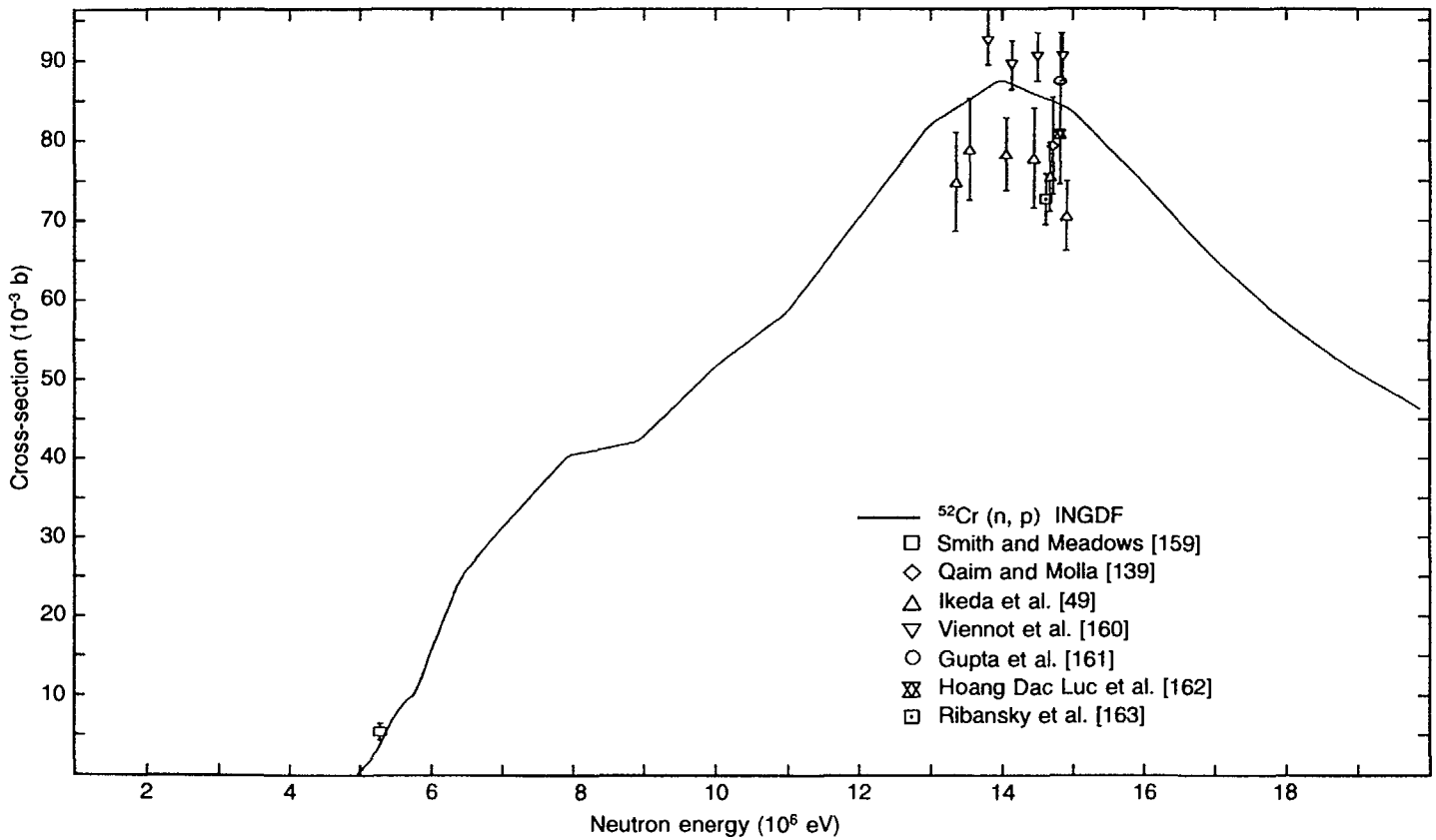

FIG. 6.52. Excitation function for the $^{52}Cr(n,p)^{52}V$ reaction. Evaluated data from Ref. [158].

$^{52}Cr\,(n,p)\,^{52}V$

E_n (eV)	σ (b)	E_n (eV)	σ (b)	E_n (eV)	σ (b)
5.00000×10^{6}	2.60848×10^{-3}	5.50000×10^{6}	9.66834×10^{-3}	6.00000×10^{6}	1.97500×10^{-2}
6.50000×10^{6}	2.82500×10^{-2}	7.00000×10^{6}	3.35000×10^{-2}	7.50000×10^{6}	3.85000×10^{-2}
8.00000×10^{6}	4.14000×10^{-2}	8.50000×10^{6}	4.23113×10^{-2}	9.00000×10^{6}	4.50692×10^{-2}
9.50000×10^{6}	4.95625×10^{-2}	1.00000×10^{7}	5.52768×10^{-2}	1.10000×10^{7}	6.46991×10^{-2}
1.20000×10^{7}	7.66082×10^{-2}	1.30000×10^{7}	8.53925×10^{-2}	1.40000×10^{7}	8.63840×10^{-2}
1.50000×10^{7}	8.01195×10^{-2}	1.60000×10^{7}	7.10015×10^{-2}	1.70000×10^{7}	6.23459×10^{-2}
1.80000×10^{7}	5.52598×10^{-2}	1.90000×10^{7}	4.95868×10^{-2}		

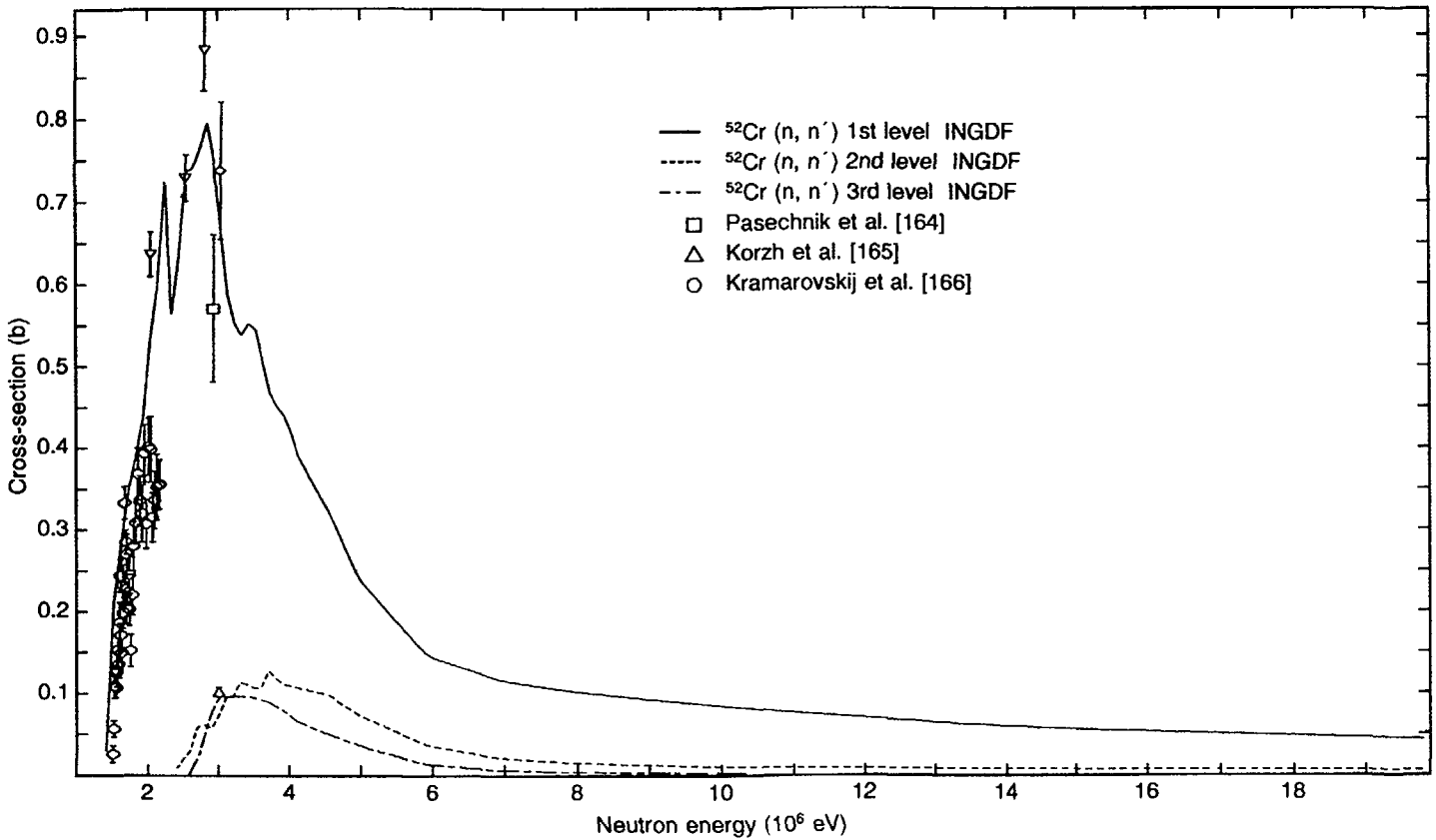

FIG. 6.53. Excitation function for the $^{52}Cr(n,n')$ reaction. Evaluated data from Ref. [158].

^{52}Cr (n, n′), first level (1.434 MeV)

E_n (eV)	σ (b)	E_n (eV)	σ (b)	E_n (eV)	σ (b)
1.00000×10^{6}	5.48928×10^{-3}	1.50000×10^{6}	3.35731×10^{-1}	2.00000×10^{6}	6.11507×10^{-1}
2.50000×10^{6}	7.55861×10^{-1}	3.00000×10^{6}	5.78784×10^{-1}	3.50000×10^{6}	4.80402×10^{-1}
4.00000×10^{6}	3.76254×10^{-1}	4.50000×10^{6}	2.89613×10^{-1}	5.00000×10^{6}	2.15098×10^{-1}
5.50000×10^{6}	1.66456×10^{-1}	6.00000×10^{6}	1.35803×10^{-1}	6.50000×10^{6}	1.21114×10^{-1}
7.00000×10^{6}	1.10487×10^{-1}	7.50000×10^{6}	1.03922×10^{-1}	8.00000×10^{6}	9.82581×10^{-2}
8.50000×10^{6}	9.34963×10^{-2}	9.00000×10^{6}	8.90411×10^{-2}	9.50000×10^{6}	8.48928×10^{-2}
1.00000×10^{7}	7.90434×10^{-2}	1.10000×10^{7}	7.18974×10^{-2}	1.20000×10^{7}	6.56436×10^{-2}
1.30000×10^{7}	6.03872×10^{-2}	1.40000×10^{7}	5.60980×10^{-2}	1.50000×10^{7}	5.26167×10^{-2}
1.60000×10^{7}	4.97171×10^{-2}	1.70000×10^{7}	4.71798×10^{-2}	1.80000×10^{7}	4.48435×10^{-2}
1.90000×10^{7}	4.26331×10^{-2}				

^{52}Cr (n, n′), second level (2.369 MeV)

E_n (eV)	σ (b)	E_n (eV)	σ (b)	E_n (eV)	σ (b)
2.00000×10^{6}	8.89444×10^{-4}	2.50000×10^{6}	4.32596×10^{-2}	3.00000×10^{6}	9.53184×10^{-2}
3.50000×10^{6}	1.12171×10^{-1}	4.00000×10^{6}	1.03289×10^{-1}	4.50000×10^{6}	8.65702×10^{-2}
5.00000×10^{6}	6.22458×10^{-2}	5.50000×10^{6}	4.31532×10^{-2}	6.00000×10^{6}	3.01236×10^{-2}
6.50000×10^{6}	2.25823×10^{-2}	7.00000×10^{6}	1.74313×10^{-2}	7.50000×10^{6}	1.43786×10^{-2}
8.00000×10^{6}	1.21052×10^{-2}	8.50000×10^{6}	1.06112×10^{-2}	9.00000×10^{6}	9.42595×10^{-3}
9.50000×10^{6}	8.54954×10^{-3}	1.00000×10^{7}	7.54305×10^{-3}	1.10000×10^{7}	6.57522×10^{-3}
1.20000×10^{7}	5.87027×10^{-3}	1.30000×10^{7}	5.33160×10^{-3}	1.40000×10^{7}	4.93255×10^{-3}
1.50000×10^{7}	4.64777×10^{-3}	1.60000×10^{7}	4.43583×10^{-3}	1.70000×10^{7}	4.26270×10^{-3}
1.80000×10^{7}	4.11058×10^{-3}	1.90000×10^{7}	3.96672×10^{-3}		

$^{52}Cr(n,n')$, third level (2.6489 MeV)

E_n (eV)	σ (b)	E_n (eV)	σ (b)	E_n (eV)	σ (b)
2.50000×10^{6}	2.77249×10^{-2}	3.00000×10^{6}	9.37599×10^{-2}	3.50000×10^{6}	8.62645×10^{-2}
4.00000×10^{6}	6.10354×10^{-2}	4.50000×10^{6}	4.28591×10^{-2}	5.00000×10^{6}	2.83556×10^{-2}
5.50000×10^{6}	1.64005×10^{-2}	6.00000×10^{6}	8.95229×10^{-3}	6.50000×10^{6}	5.49756×10^{-3}
7.00000×10^{6}	3.29346×10^{-3}	7.50000×10^{6}	2.21684×10^{-3}	8.00000×10^{6}	1.47649×10^{-3}
8.50000×10^{6}	1.04242×10^{-3}	9.00000×10^{6}	7.27851×10^{-4}	9.50000×10^{6}	5.23342×10^{-4}
1.00000×10^{7}	3.21231×10^{-4}	1.10000×10^{7}	1.67967×10^{-4}	1.20000×10^{7}	8.66288×10^{-5}
1.30000×10^{7}	4.08952×10^{-5}	1.40000×10^{7}	1.69913×10^{-5}	1.50000×10^{7}	6.84278×10^{-6}
1.60000×10^{7}	3.09647×10^{-6}	1.70000×10^{7}	1.55972×10^{-6}	1.80000×10^{7}	8.12913×10^{-7}
1.90000×10^{7}	4.77591×10^{-7}				

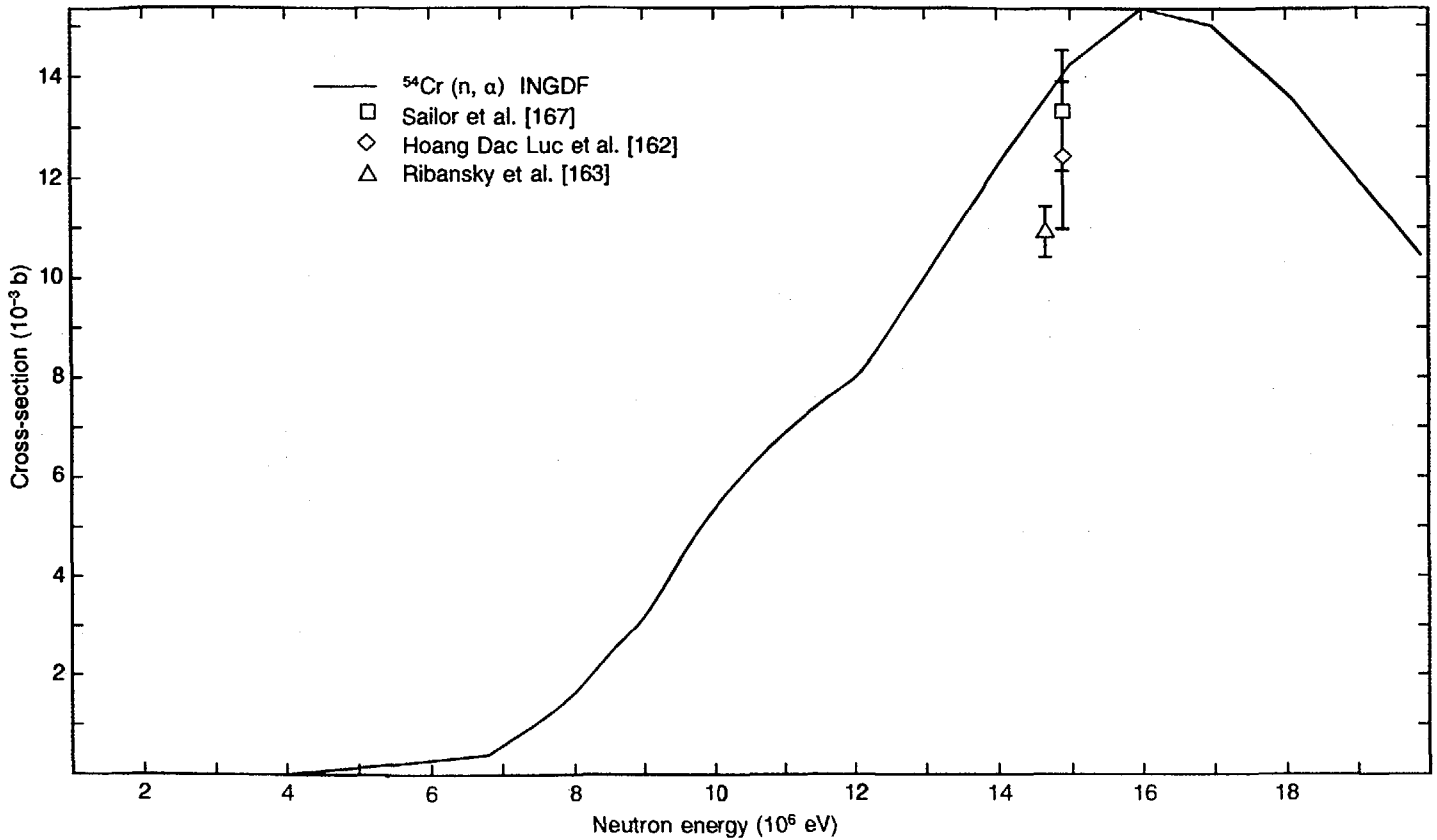

FIG. 6.54. Excitation function for the $^{54}Cr(n,\alpha)^{51}Ti$ reaction. Evaluated data from Ref. [158].

$^{54}Cr\,(n,\alpha)^{51}Ti$

E_n (eV)	σ (b)	E_n (eV)	σ (b)	E_n (eV)	σ (b)
1.50000×10^{6}	6.61037×10^{-9}	2.00000×10^{6}	2.47406×10^{-8}	2.50000×10^{6}	4.30798×10^{-8}
3.00000×10^{6}	6.14189×10^{-8}	3.50000×10^{6}	7.97581×10^{-8}	4.00000×10^{6}	1.37269×10^{-5}
4.50000×10^{6}	4.10028×10^{-5}	5.00000×10^{6}	9.53315×10^{-5}	5.50000×10^{6}	1.76713×10^{-4}
6.00000×10^{6}	2.67471×10^{-4}	6.50000×10^{6}	3.67607×10^{-4}	7.00000×10^{6}	6.94379×10^{-4}
7.50000×10^{6}	1.24779×10^{-3}	8.00000×10^{6}	1.92694×10^{-3}	8.50000×10^{6}	2.73184×10^{-3}
9.00000×10^{6}	3.69340×10^{-3}	9.50000×10^{6}	4.81162×10^{-3}	1.00000×10^{7}	6.11338×10^{-3}
1.10000×10^{7}	7.44293×10^{-3}	1.20000×10^{7}	9.01100×10^{-3}	1.30000×10^{7}	1.11768×10^{-2}
1.40000×10^{7}	1.33899×10^{-2}	1.50000×10^{7}	1.49078×10^{-2}	1.60000×10^{7}	1.52260×10^{-2}
1.70000×10^{7}	1.44192×10^{-2}	1.80000×10^{7}	1.29339×10^{-2}	1.90000×10^{7}	1.12139×10^{-2}

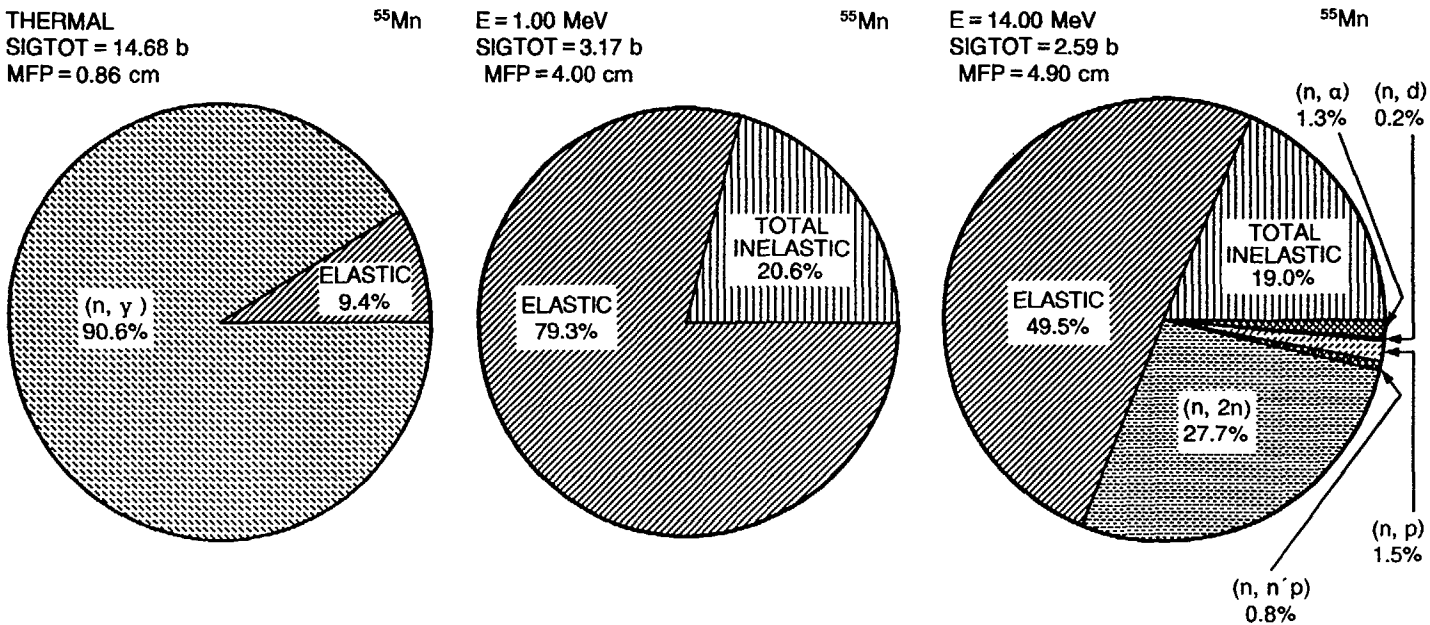

FIG. 6.55. Pie charts of the dominant neutron induced reaction cross-sections for ^{55}Mn.

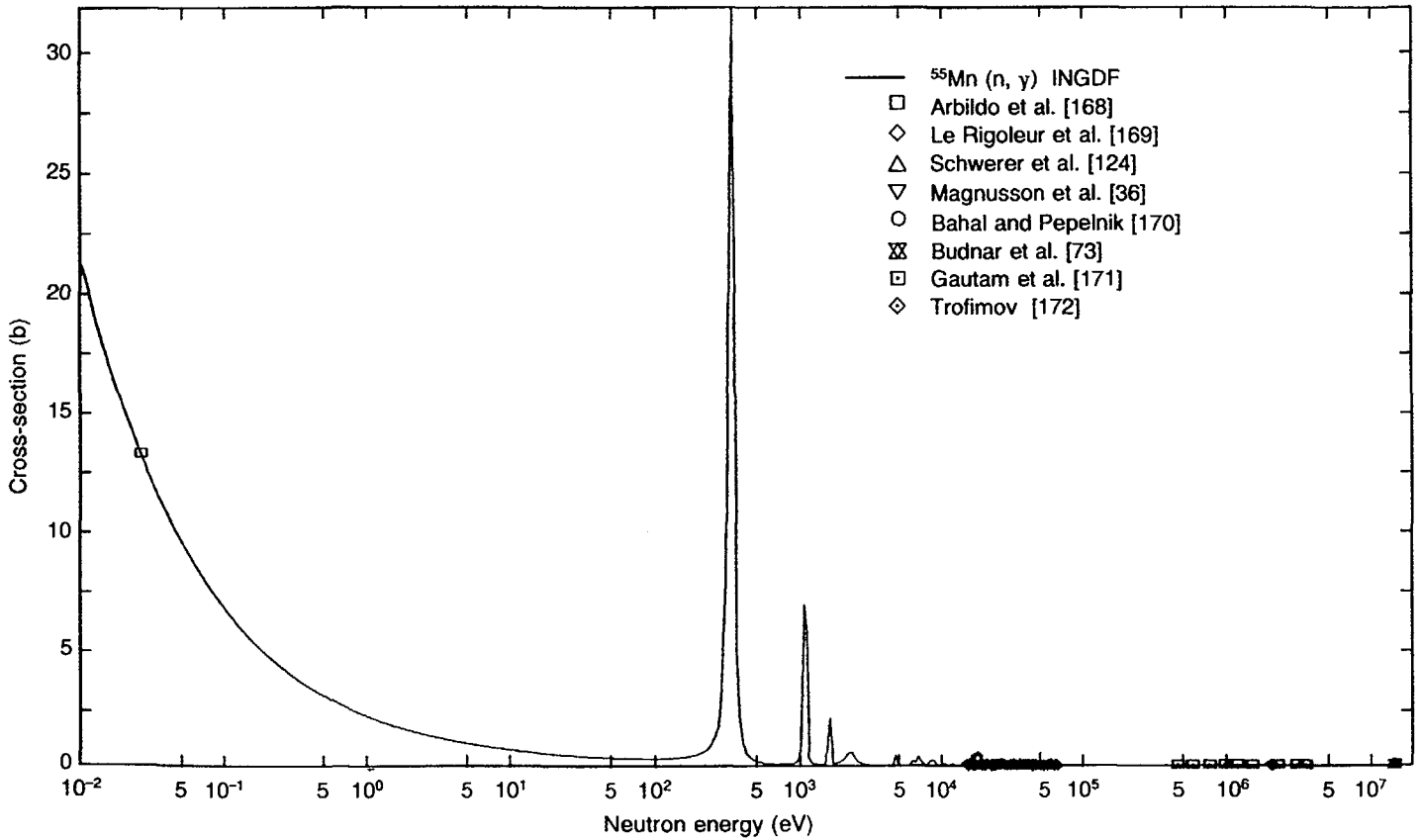

FIG. 6.56. Excitation function for the $^{55}Mn(n,\gamma)$ reaction. Evaluated data from Ref. [173].

^{55}Mn (n, γ)

E_n (eV)	σ (b)	E_n (eV)	σ (b)	E_n (eV)	σ (b)
1.00000×10^{-3}	1.22706×10^{1}	1.00000×10^{-1}	3.24622	1.00000	1.03716
1.00000×10^{1}	3.75629×10^{-1}	1.00000×10^{2}	1.82206	1.00000×10^{3}	2.07318×10^{-1}
1.00000×10^{4}	2.96984×10^{-2}	5.00000×10^{4}	1.63954×10^{-2}	1.00000×10^{5}	6.57751×10^{-3}
5.00000×10^{5}	3.51494×10^{-3}	1.00000×10^{6}	2.38270×10^{-3}	1.50000×10^{6}	1.91300×10^{-3}
2.00000×10^{6}	1.77000×10^{-3}	2.50000×10^{6}	1.66443×10^{-3}	3.00000×10^{6}	1.45466×10^{-3}
3.50000×10^{6}	1.30254×10^{-3}	4.00000×10^{6}	1.18331×10^{-3}	4.50000×10^{6}	1.07854×10^{-3}
5.00000×10^{6}	9.82838×10^{-4}	5.50000×10^{6}	9.01524×10^{-4}	6.00000×10^{6}	8.36166×10^{-4}
6.50000×10^{6}	7.82188×10^{-4}	7.00000×10^{6}	7.40502×10^{-4}	7.50000×10^{6}	7.13502×10^{-4}
8.00000×10^{6}	7.00002×10^{-4}	8.50000×10^{6}	6.94169×10^{-4}	9.00000×10^{6}	6.90502×10^{-4}
9.50000×10^{6}	6.86835×10^{-4}	1.00000×10^{7}	6.83251×10^{-4}	1.10000×10^{7}	6.79752×10^{-4}
1.20000×10^{7}	6.74854×10^{-4}	1.30000×10^{7}	6.68440×10^{-4}	1.40000×10^{7}	6.59412×10^{-4}
1.50000×10^{7}	6.47497×10^{-4}	1.60000×10^{7}	6.26002×10^{-4}	1.70000×10^{7}	5.70386×10^{-4}
1.80000×10^{7}	4.70988×10^{-4}	1.90000×10^{7}	3.30548×10^{-4}		

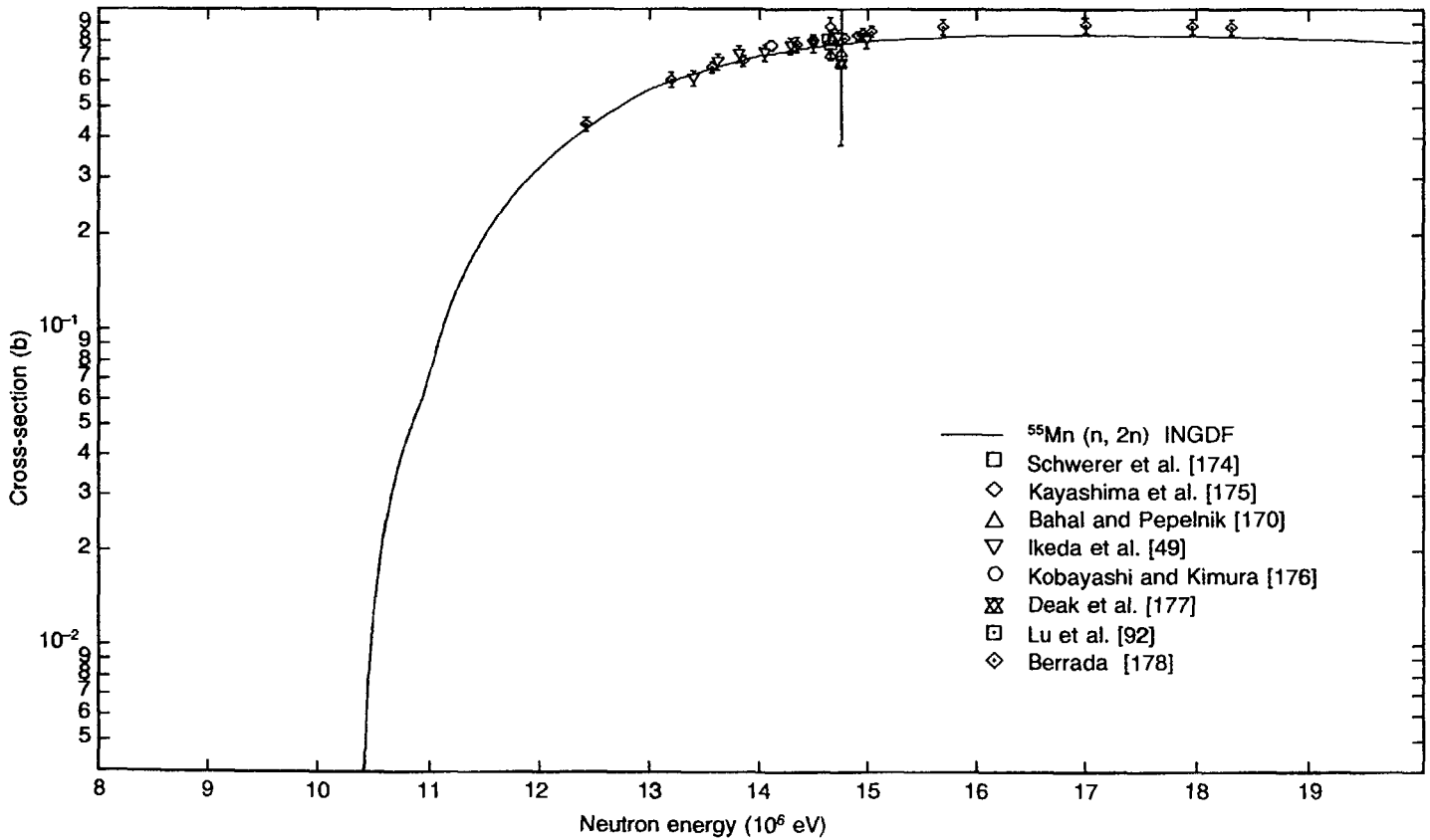

FIG. 6.57. Excitation function for the $^{55}Mn(n,2n)^{54}Mn$ reaction. Evaluated data from Ref. [173].

$^{55}Mn(n,2n)^{54}Mn$

E_n (eV)	σ (b)	E_n (eV)	σ (b)	E_n (eV)	σ (b)
1.00000×10^{7}	1.93965×10^{-2}	1.10000×10^{7}	1.95350×10^{-1}	1.20000×10^{7}	4.46605×10^{-1}
1.30000×10^{7}	6.43900×10^{-1}	1.40000×10^{7}	7.62162×10^{-1}	1.50000×10^{7}	8.13550×10^{-1}
1.60000×10^{7}	8.32125×10^{-1}	1.70000×10^{7}	8.30350×10^{-1}	1.80000×10^{7}	8.17450×10^{-1}
1.90000×10^{7}	7.99575×10^{-1}				

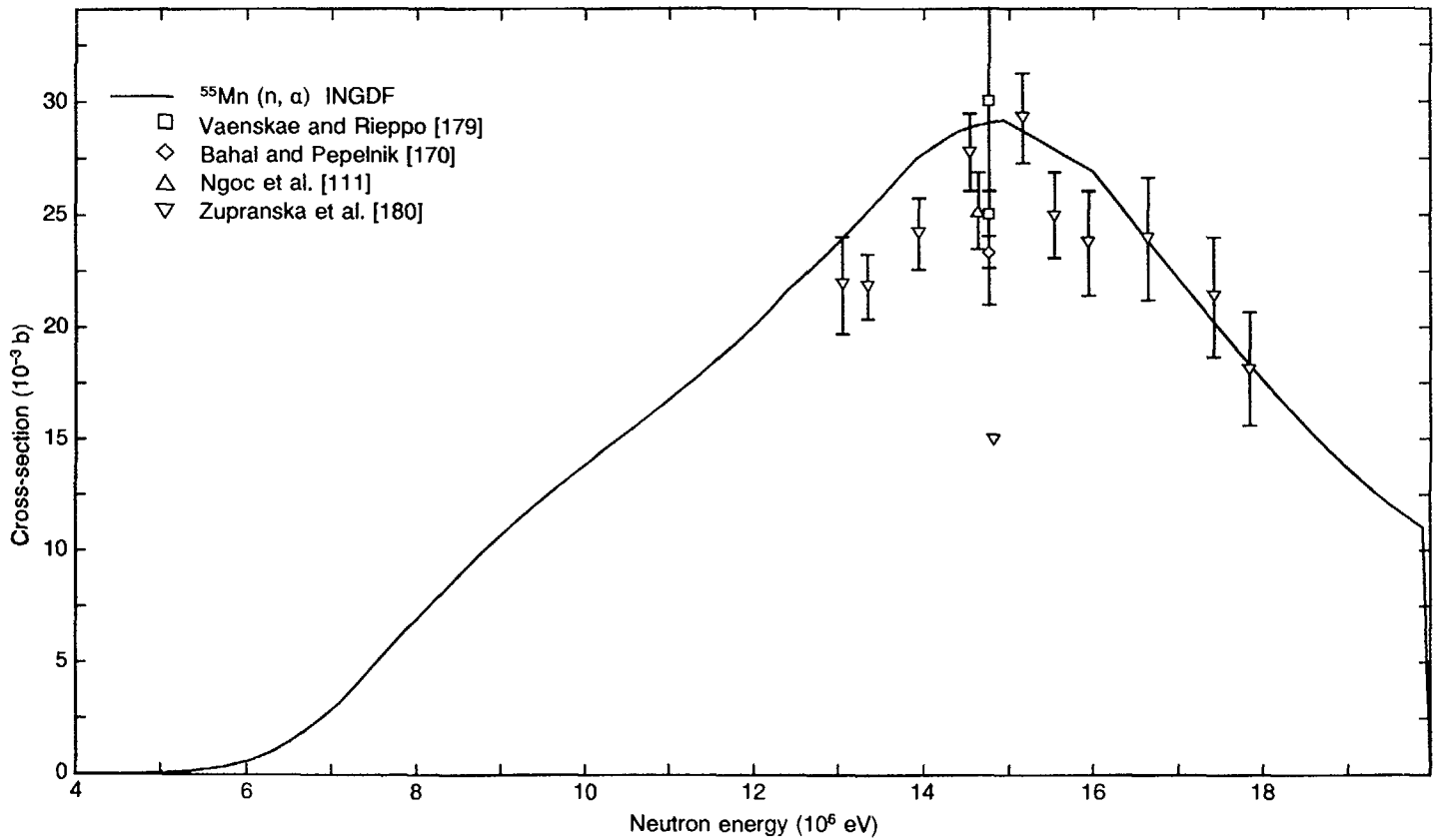

FIG. 6.58. Excitation function for the $^{55}Mn(n,\alpha)^{52}V$ reaction. Evaluated data from Ref. [173].

$^{55}Mn\,(n,\alpha)^{52}V$

E_n (eV)	σ (b)	E_n (eV)	σ (b)	E_n (eV)	σ (b)
5.00000×10^{4}	1.41466×10^{-8}	1.00000×10^{6}	6.54967×10^{-8}	1.50000×10^{6}	1.18812×10^{-7}
2.00000×10^{6}	1.72127×10^{-7}	2.50000×10^{6}	2.25443×10^{-7}	3.00000×10^{6}	2.78758×10^{-7}
3.50000×10^{6}	3.32073×10^{-7}	4.00000×10^{6}	2.70352×10^{-6}	4.50000×10^{6}	1.99562×10^{-5}
5.00000×10^{6}	9.66622×10^{-5}	5.50000×10^{6}	3.42865×10^{-4}	6.00000×10^{6}	9.48086×10^{-4}
6.50000×10^{6}	2.08840×10^{-3}	7.00000×10^{6}	3.79820×10^{-3}	7.50000×10^{6}	5.85460×10^{-3}
8.00000×10^{6}	7.90971×10^{-3}	8.50000×10^{6}	9.80736×10^{-3}	9.00000×10^{6}	1.15375×10^{-2}
9.50000×10^{6}	1.30863×10^{-2}	1.00000×10^{7}	1.52683×10^{-2}	1.10000×10^{7}	1.83466×10^{-2}
1.20000×10^{7}	2.18988×10^{-2}	1.30000×10^{7}	2.57563×10^{-2}	1.40000×10^{7}	2.86555×10^{-2}
1.50000×10^{7}	2.79595×10^{-2}	1.60000×10^{7}	2.44990×10^{-2}	1.70000×10^{7}	1.98966×10^{-2}
1.80000×10^{7}	1.56555×10^{-2}	1.90000×10^{7}	1.22225×10^{-2}		

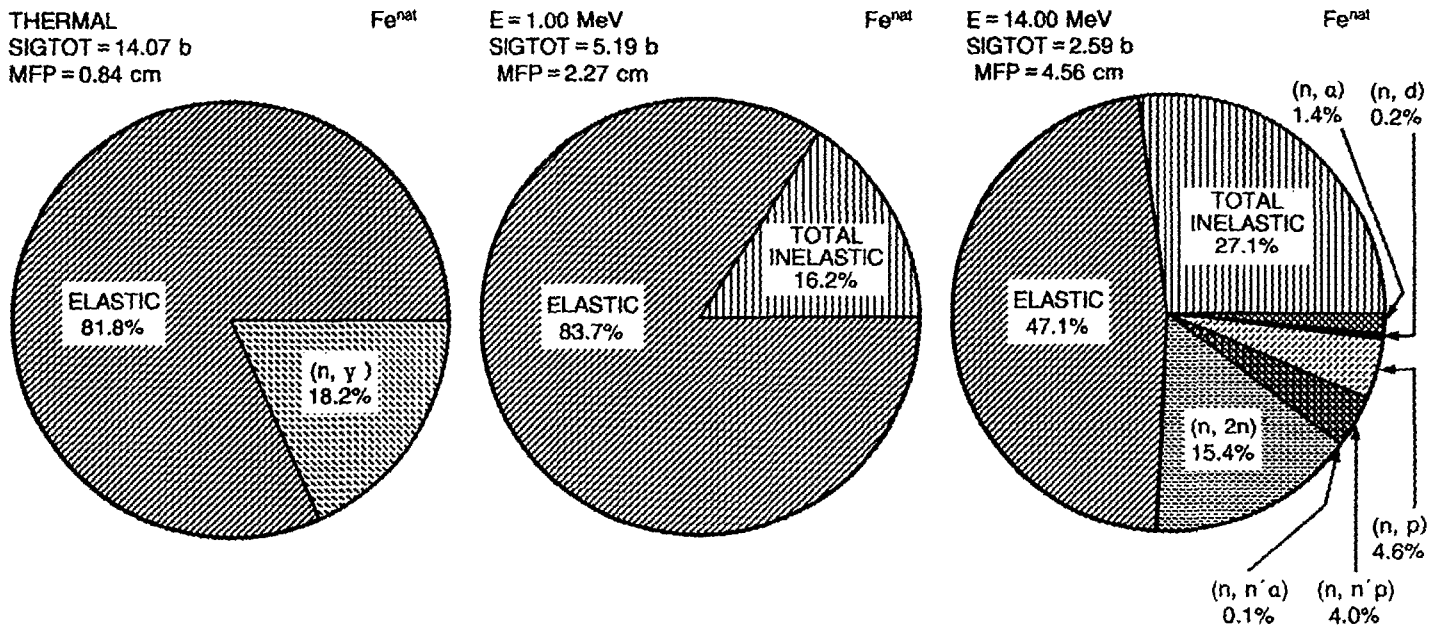

FIG. 6.59. Pie charts of the dominant neutron induced reaction cross-sections for natural iron.

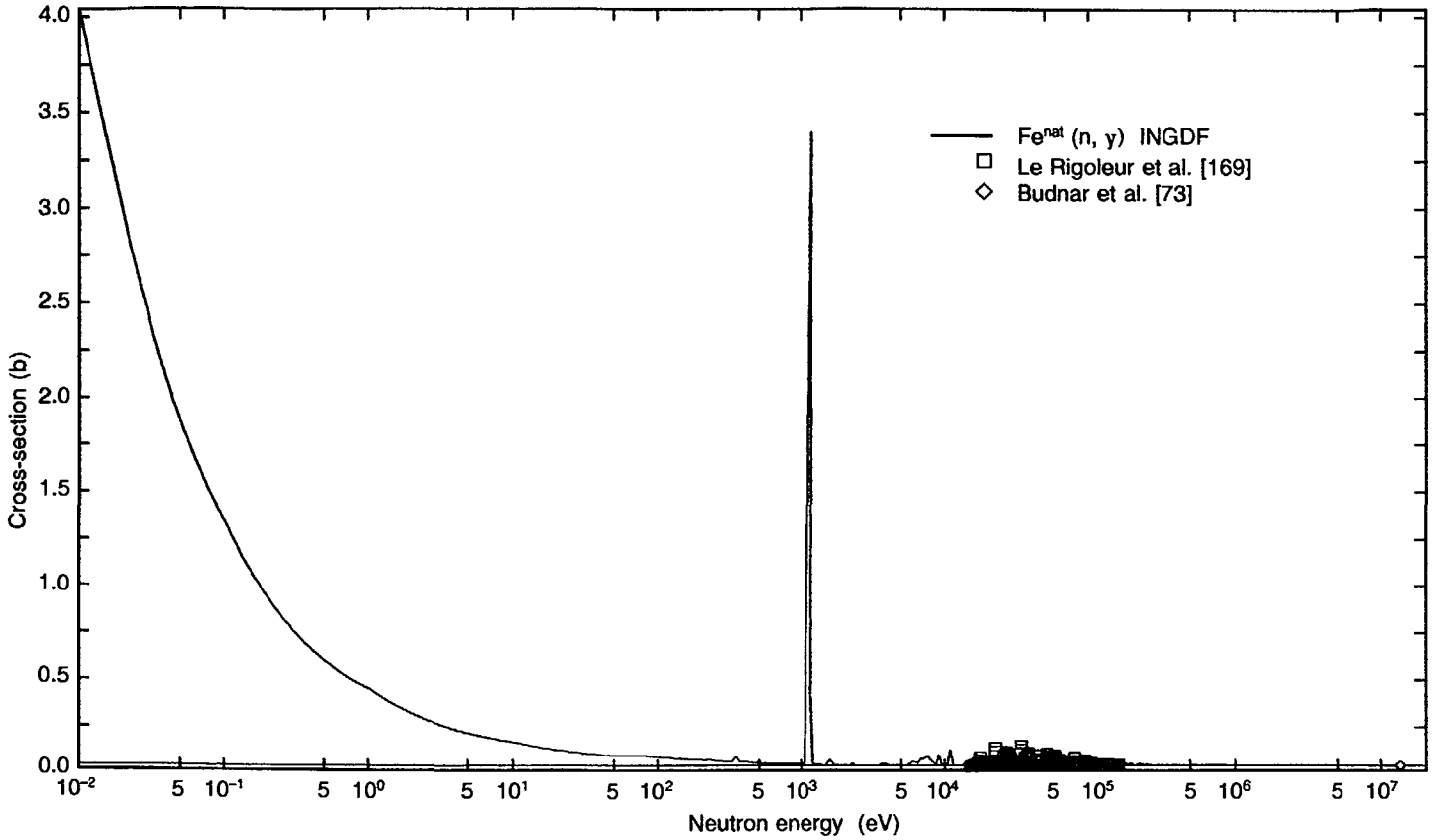

FIG. 6.60. Excitation function for the $Fe^{nat}(n,\gamma)$ reaction. Evaluated data from Ref. [181].

$Fe^{nat}(n,\gamma)$

E_n (eV)	σ (b)	E_n (eV)	σ (b)	E_n (eV)	σ (b)
1.00000×10^{-3}	2.31062	1.00000×10^{-1}	6.00650×10^{-1}	1.00000	1.89052×10^{-1}
1.00000×10^{1}	6.18415×10^{-2}	1.00000×10^{2}	1.85729×10^{-2}	1.00000×10^{3}	3.58320×10^{-2}
1.00000×10^{4}	1.36397×10^{-2}	5.00000×10^{4}	1.38642×10^{-2}	1.00000×10^{5}	6.64105×10^{-3}
5.00000×10^{5}	5.19461×10^{-3}	1.00000×10^{6}	2.73332×10^{-3}	1.50000×10^{6}	2.59118×10^{-3}
2.00000×10^{6}	2.80583×10^{-3}	2.50000×10^{6}	2.58914×10^{-3}	3.00000×10^{6}	2.31933×10^{-3}
3.50000×10^{6}	1.91701×10^{-3}	4.00000×10^{6}	1.64662×10^{-3}	4.50000×10^{6}	1.48943×10^{-3}
5.00000×10^{6}	1.39415×10^{-3}	5.50000×10^{6}	1.30966×10^{-3}	6.00000×10^{6}	1.22006×10^{-3}
6.50000×10^{6}	1.12792×10^{-3}	7.00000×10^{6}	1.03251×10^{-3}	7.50000×10^{6}	9.35911×10^{-4}
8.00000×10^{6}	8.42570×10^{-4}	8.50000×10^{6}	7.53200×10^{-4}	9.00000×10^{6}	6.72197×10^{-4}
9.50000×10^{6}	5.99094×10^{-4}	1.00000×10^{7}	5.04119×10^{-4}	1.10000×10^{7}	3.75137×10^{-4}
1.20000×10^{7}	2.40380×10^{-4}	1.30000×10^{7}	1.36083×10^{-4}	1.40000×10^{7}	7.31316×10^{-5}
1.50000×10^{7}	3.81892×10^{-5}	1.60000×10^{7}	2.04749×10^{-5}	1.70000×10^{7}	1.16419×10^{-5}
1.80000×10^{7}	7.67291×10^{-6}	1.90000×10^{7}	5.88925×10^{-6}		

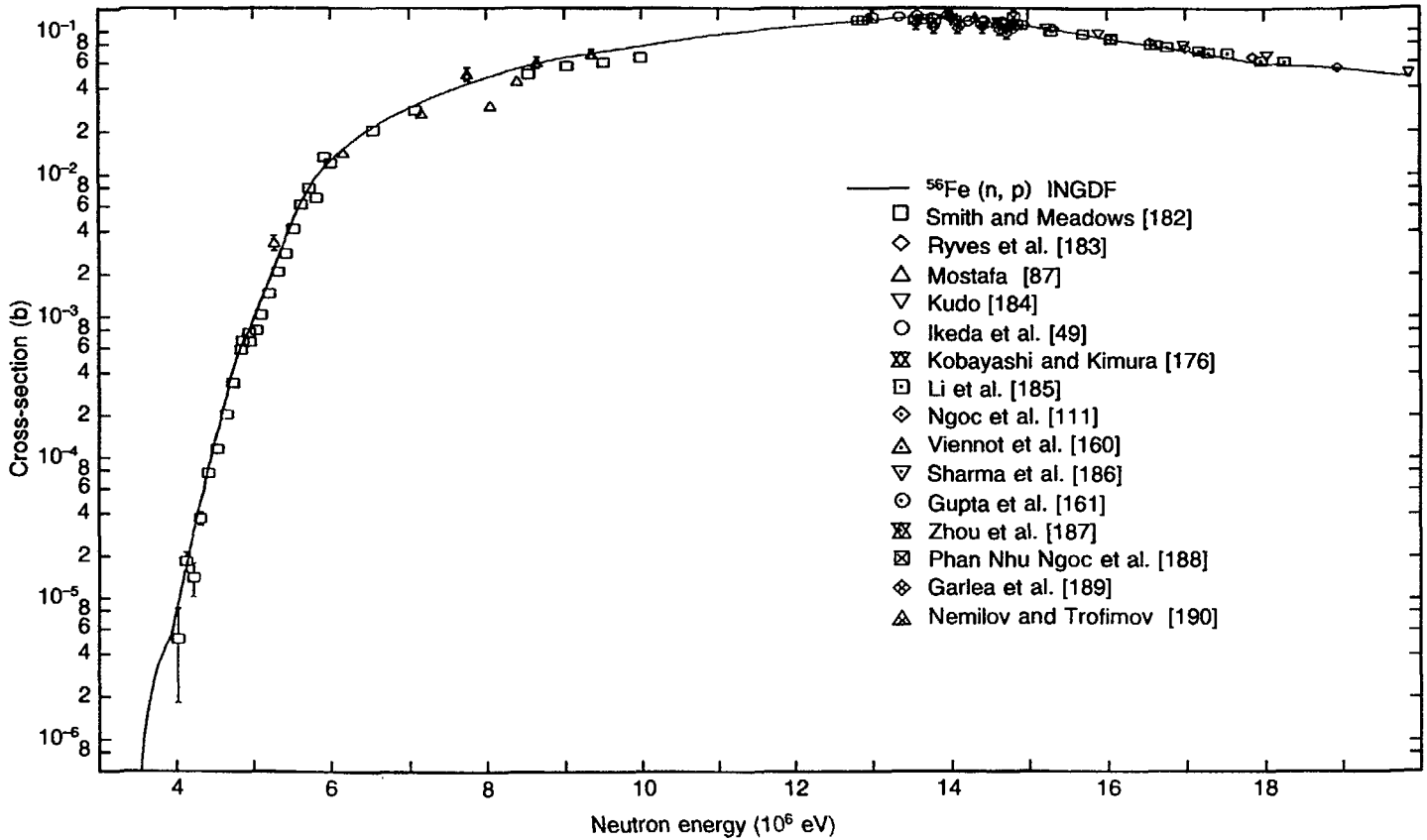

FIG. 6.61. Excitation function for the $^{56}Fe(n,p)^{56}Mn$ reaction. Evaluated data from Ref. [181].

$^{56}Fe\,(n,p)\,^{56}Mn$

E_n (eV)	σ (b)	E_n (eV)	σ (b)	E_n (eV)	σ (b)
3.50000×10^{6}	3.10001×10^{-6}	4.00000×10^{6}	4.43900×10^{-5}	4.50000×10^{6}	4.85801×10^{-4}
5.00000×10^{6}	2.38500×10^{-3}	5.50000×10^{6}	8.50001×10^{-3}	6.00000×10^{6}	1.61500×10^{-2}
6.50000×10^{6}	2.40000×10^{-2}	7.00000×10^{6}	3.22500×10^{-2}	7.50000×10^{6}	4.07500×10^{-2}
8.00000×10^{6}	4.92500×10^{-2}	8.50000×10^{6}	5.77500×10^{-2}	9.00000×10^{6}	6.50000×10^{-2}
9.50000×10^{6}	7.10000×10^{-2}	1.00000×10^{7}	8.20000×10^{-2}	1.10000×10^{7}	9.60000×10^{-2}
1.20000×10^{7}	1.07500×10^{-1}	1.30000×10^{7}	1.15750×10^{-1}	1.40000×10^{7}	1.09000×10^{-1}
1.50000×10^{7}	9.47500×10^{-2}	1.60000×10^{7}	7.75000×10^{-2}	1.70000×10^{7}	6.35000×10^{-2}
1.80000×10^{7}	5.50000×10^{-2}	1.90000×10^{7}	4.90000×10^{-2}		

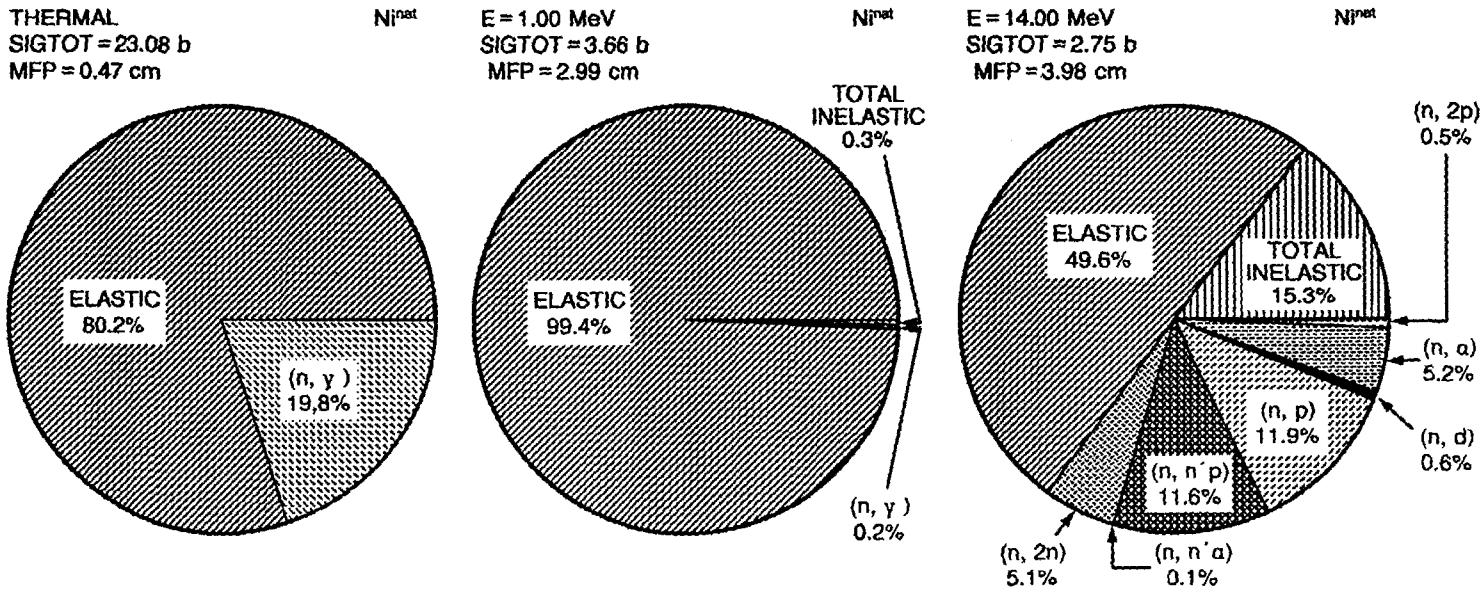

FIG. 6.62. Pie charts of the dominant neutron induced reaction cross-sections for natural nickel.

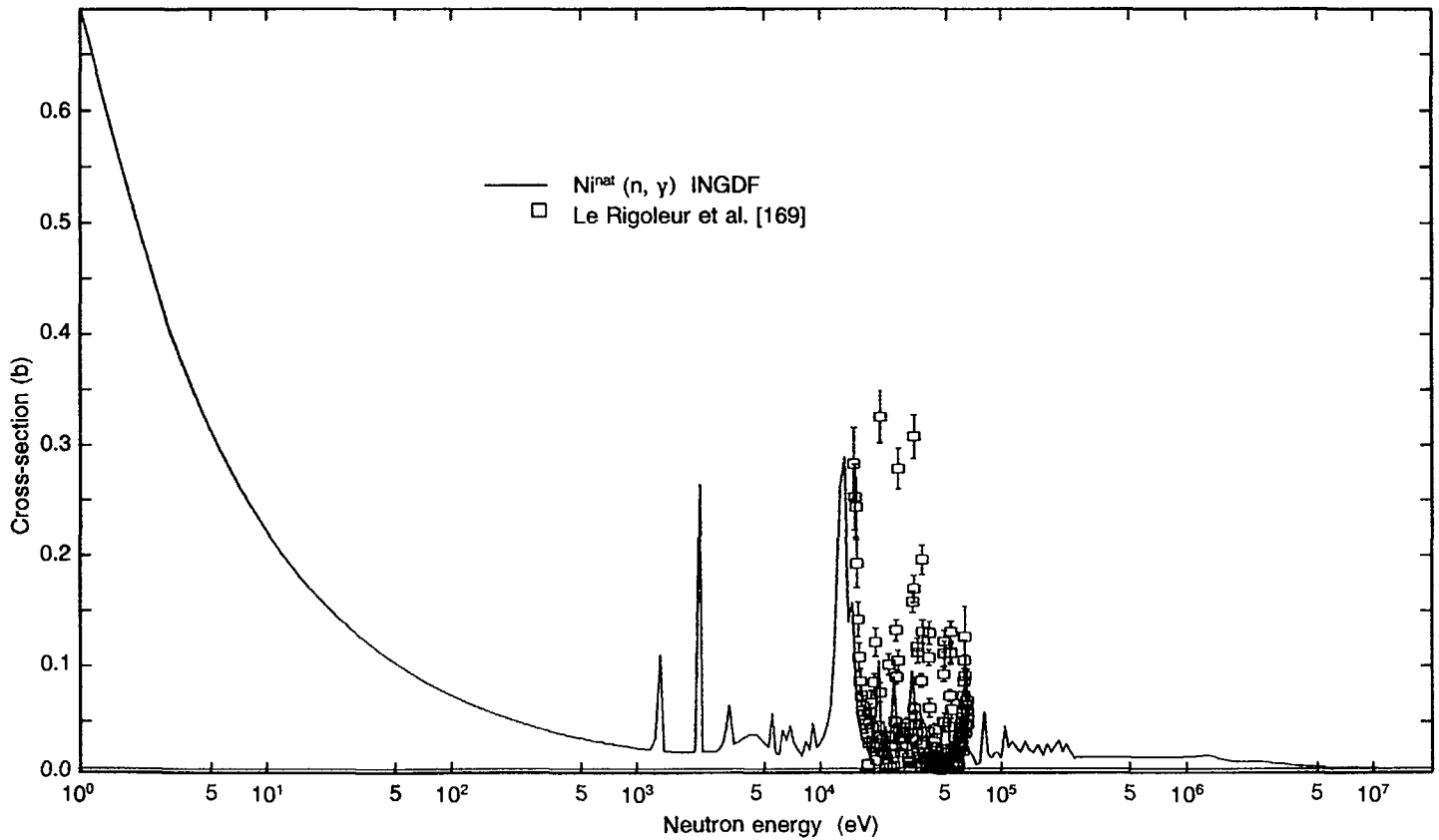

FIG. 6.63. Excitation function for the $Ni^{nat}(n,\gamma)$ reaction. Evaluated data from Ref. [181].

$Ni^{nat}(n,\gamma)$

E_n (eV)	σ (b)	E_n (eV)	σ (b)	E_n (eV)	σ (b)
1.00000×10^{-3}	4.00942	1.00000×10^{-1}	1.05943	1.00000	3.34490×10^{-1}
1.00000×10^{1}	1.04247×10^{-1}	1.00000×10^{2}	3.04679×10^{-2}	1.00000×10^{3}	2.73055×10^{-2}
1.00000×10^{4}	4.63309×10^{-2}	5.00000×10^{4}	1.92046×10^{-2}	1.00000×10^{5}	1.33653×10^{-2}
5.00000×10^{5}	9.81568×10^{-3}	1.00000×10^{6}	1.07666×10^{-2}	1.50000×10^{6}	6.87522×10^{-3}
2.00000×10^{6}	5.85632×10^{-3}	2.50000×10^{6}	5.31716×10^{-3}	3.00000×10^{6}	4.06007×10^{-3}
3.50000×10^{6}	2.92148×10^{-3}	4.00000×10^{6}	2.22708×10^{-3}	4.50000×10^{6}	1.87186×10^{-3}
5.00000×10^{6}	1.59877×10^{-3}	5.50000×10^{6}	1.38377×10^{-3}	6.00000×10^{6}	1.19396×10^{-3}
6.50000×10^{6}	1.02556×10^{-3}	7.00000×10^{6}	8.79084×10^{-4}	7.50000×10^{6}	7.50774×10^{-4}
8.00000×10^{6}	6.41883×10^{-4}	8.50000×10^{6}	5.48761×10^{-4}	9.00000×10^{6}	4.67156×10^{-4}
9.50000×10^{6}	3.95618×10^{-4}	1.00000×10^{7}	3.00670×10^{-4}	1.10000×10^{7}	1.97928×10^{-4}
1.20000×10^{7}	1.23443×10^{-4}	1.30000×10^{7}	7.39243×10^{-5}	1.40000×10^{7}	4.36190×10^{-5}
1.50000×10^{7}	2.51837×10^{-5}	1.60000×10^{7}	1.33389×10^{-5}	1.70000×10^{7}	6.66561×10^{-6}
1.80000×10^{7}	3.37991×10^{-6}	1.90000×10^{7}	1.72464×10^{-6}		

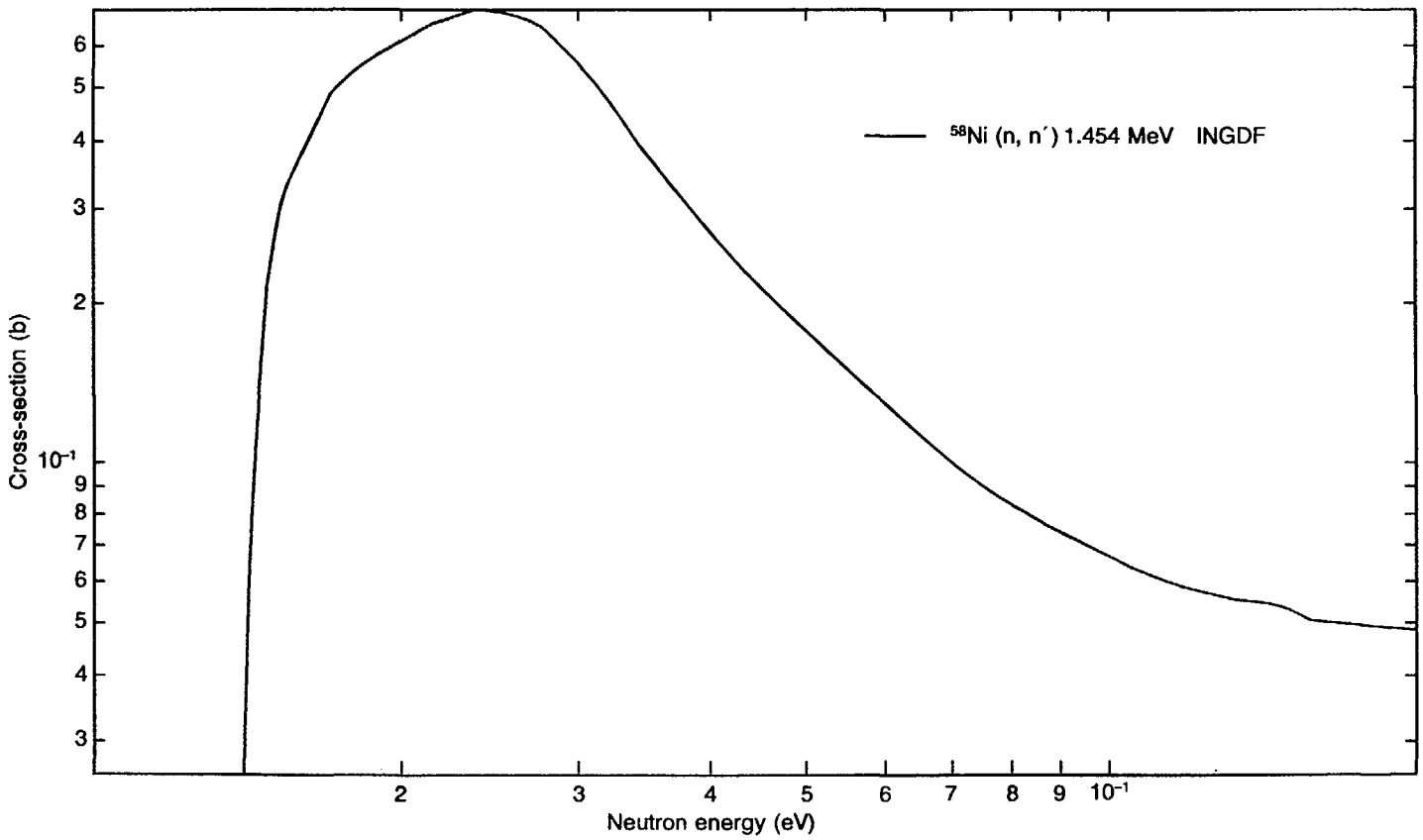

FIG. 6.64. Excitation function for inelastic scattering of ^{58}Ni to the first level (1.4543 MeV). Evaluated data from Ref. [103].

^{58}Ni (n, n′)

E_n (eV)	σ (b)	E_n (eV)	σ (b)	E_n (eV)	σ (b)
1.00000×10^{6}	5.27230×10^{-3}	1.50000×10^{6}	4.63187×10^{-1}	2.00000×10^{6}	6.59380×10^{-1}
2.50000×10^{6}	6.47360×10^{-1}	3.00000×10^{6}	4.72340×10^{-1}	3.50000×10^{6}	3.33775×10^{-1}
4.00000×10^{6}	2.52765×10^{-1}	4.50000×10^{6}	2.00715×10^{-1}	5.00000×10^{6}	1.65150×10^{-1}
5.50000×10^{6}	1.40190×10^{-1}	6.00000×10^{6}	1.21995×10^{-1}	6.50000×10^{6}	1.08150×10^{-1}
7.00000×10^{6}	9.75315×10^{-2}	7.50000×10^{6}	8.93086×10^{-2}	8.00000×10^{6}	8.26285×10^{-2}
8.50000×10^{6}	7.71255×10^{-2}	9.00000×10^{6}	7.26730×10^{-2}	9.50000×10^{6}	6.89800×10^{-2}
1.00000×10^{7}	6.43990×10^{-2}	1.10000×10^{7}	6.01936×10^{-2}	1.20000×10^{7}	5.74966×10^{-2}
1.30000×10^{7}	5.54920×10^{-2}	1.40000×10^{7}	5.41103×10^{-2}	1.50000×10^{7}	5.21180×10^{-2}
1.60000×10^{7}	5.07224×10^{-2}	1.70000×10^{7}	5.00362×10^{-2}	1.80000×10^{7}	4.94170×10^{-2}
1.90000×10^{7}	4.88090×10^{-2}				

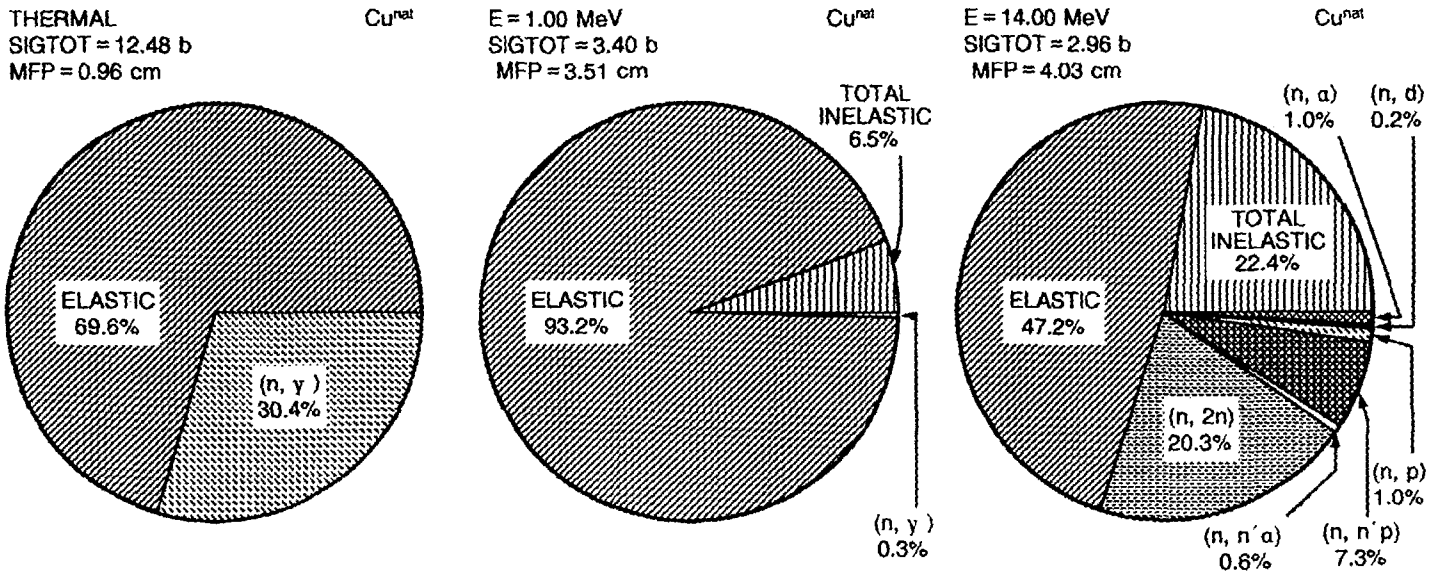

FIG. 6.65. Pie charts of the dominant neutron induced reaction cross-sections for natural copper.

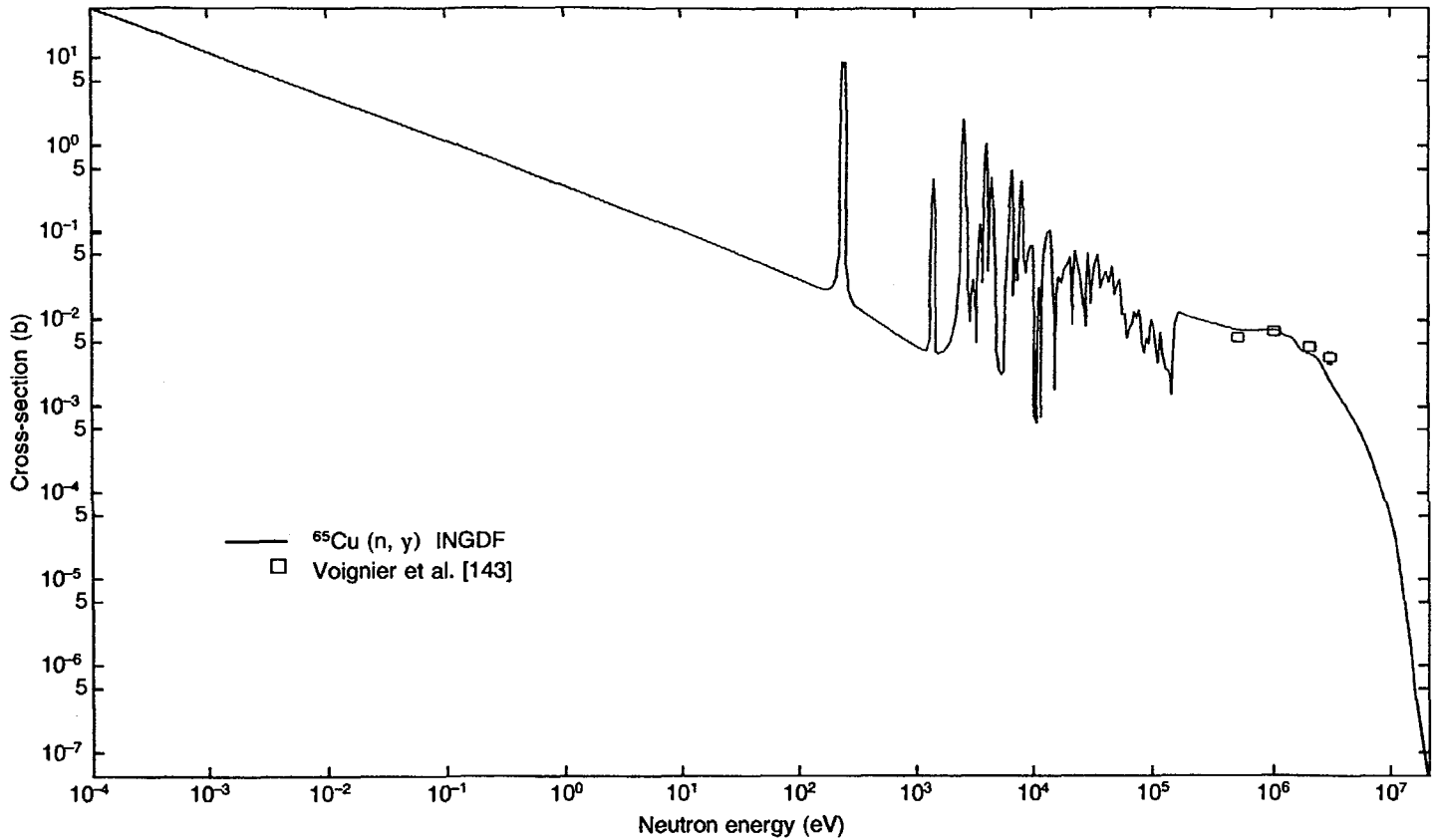

FIG. 6.66. Excitation function for the $^{65}Cu(n,\gamma)^{66}Cu$ reaction. Evaluated data from Ref. [184].

$^{65}Cu\,(n,\gamma)^{66}Cu$

E_n (eV)	σ (b)	E_n (eV)	σ (b)	E_n (eV)	σ (b)
1.00000×10^{-3}	1.98362	1.00000×10^{-1}	5.23915×10^{-1}	1.00000	1.64753×10^{-1}
1.00000×10^{1}	4.95370×10^{-2}	1.00000×10^{2}	2.21671×10^{-1}	1.00000×10^{3}	1.51480×10^{-1}
1.00000×10^{4}	3.76878×10^{-2}	5.00000×10^{4}	1.10954×10^{-2}	1.00000×10^{5}	9.42134×10^{-3}
5.00000×10^{5}	8.52736×10^{-3}	1.00000×10^{6}	7.82756×10^{-3}	1.50000×10^{6}	5.39050×10^{-3}
2.00000×10^{6}	4.29181×10^{-3}	2.50000×10^{6}	2.95793×10^{-3}	3.00000×10^{6}	1.92772×10^{-3}
3.50000×10^{6}	1.40054×10^{-3}	4.00000×10^{6}	1.05228×10^{-3}	4.50000×10^{6}	8.10497×10^{-4}
5.00000×10^{6}	6.25735×10^{-4}	5.50000×10^{6}	4.82429×10^{-4}	6.00000×10^{6}	3.72925×10^{-4}
6.50000×10^{6}	2.88079×10^{-4}	7.00000×10^{6}	2.23039×10^{-4}	7.50000×10^{6}	1.72558×10^{-4}
8.00000×10^{6}	1.33927×10^{-4}	8.50000×10^{6}	1.04015×10^{-4}	9.00000×10^{6}	8.12699×10^{-5}
9.50000×10^{6}	6.37679×10^{-5}	1.00000×10^{7}	4.30928×10^{-5}	1.10000×10^{7}	2.28247×10^{-5}
1.20000×10^{7}	1.10823×10^{-5}	1.30000×10^{7}	5.45980×10^{-6}	1.40000×10^{7}	2.75606×10^{-6}
1.50000×10^{7}	1.38852×10^{-6}	1.60000×10^{7}	6.65343×10^{-7}	1.70000×10^{7}	3.11330×10^{-7}
1.80000×10^{7}	1.52184×10^{-7}	1.90000×10^{7}	7.73650×10^{-8}		

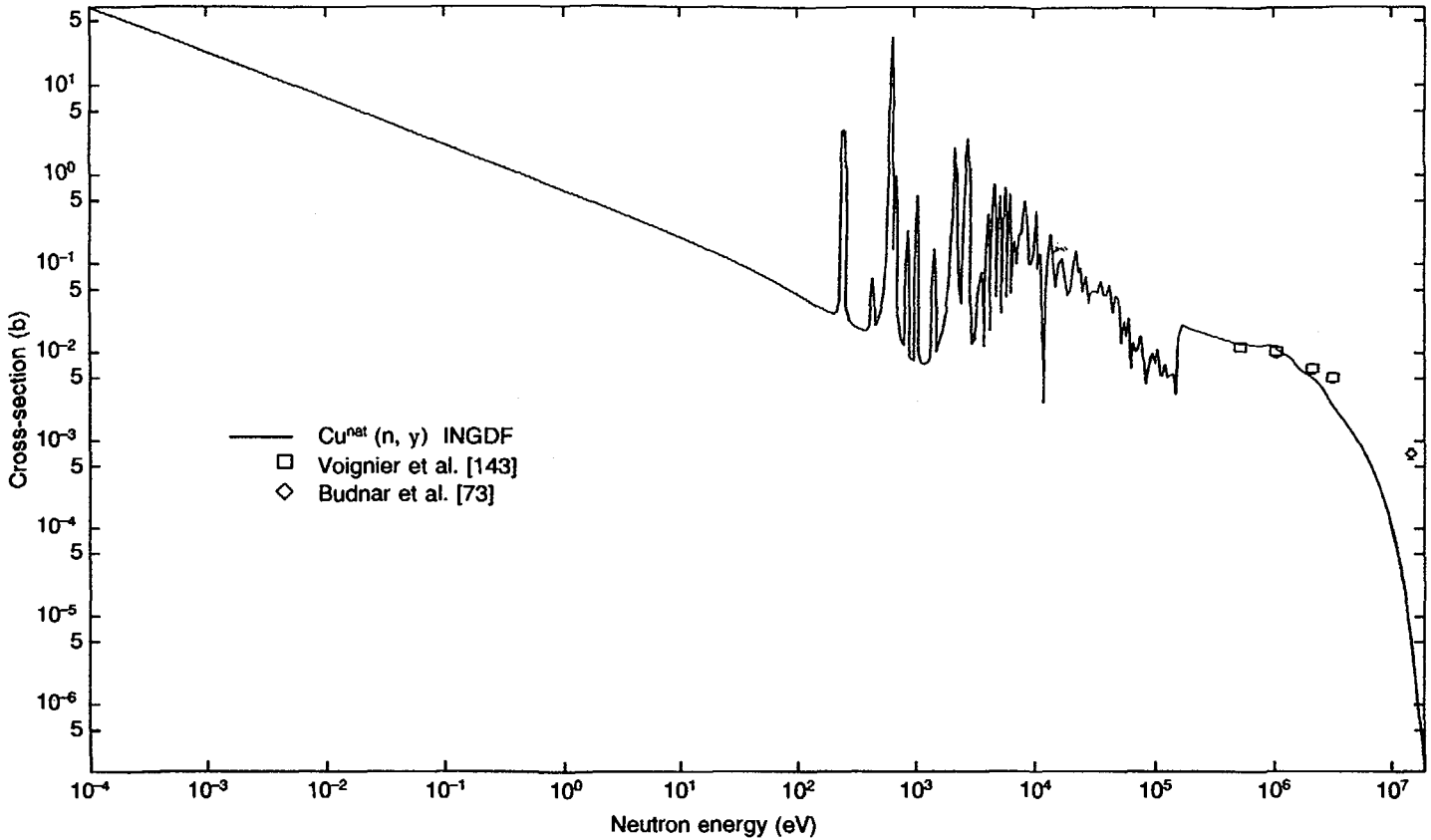

FIG. 6.67. Excitation function for the $Cu^{nat}(n,\gamma)$ reaction. Evaluated data from Ref. [184].

$Cu^{nat}(n,\gamma)$

E_n (eV)	σ (b)	E_n (eV)	σ (b)	E_n (eV)	σ (b)
1.00000×10^{-3}	3.46285	1.00000×10^{-1}	9.13298×10^{-1}	1.00000	2.83301×10^{-1}
1.00000×10^{1}	7.64316×10^{-2}	1.00000×10^{2}	1.07585	1.00000×10^{3}	2.65041×10^{-1}
1.00000×10^{4}	6.13823×10^{-2}	5.00000×10^{4}	1.10311×10^{-2}	1.00000×10^{5}	1.44928×10^{-2}
5.00000×10^{5}	1.25796×10^{-2}	1.00000×10^{6}	9.74843×10^{-3}	1.50000×10^{6}	6.30848×10^{-3}
2.00000×10^{6}	4.83801×10^{-3}	2.50000×10^{6}	3.36034×10^{-3}	3.00000×10^{6}	2.36968×10^{-3}
3.50000×10^{6}	1.84149×10^{-3}	4.00000×10^{6}	1.46142×10^{-3}	4.50000×10^{6}	1.17721×10^{-3}
5.00000×10^{6}	9.45354×10^{-4}	5.50000×10^{6}	7.54765×10^{-4}	6.00000×10^{6}	6.04192×10^{-4}
6.50000×10^{6}	4.83564×10^{-4}	7.00000×10^{6}	3.87610×10^{-4}	7.50000×10^{6}	3.10395×10^{-4}
8.00000×10^{6}	2.47570×10^{-4}	8.50000×10^{6}	1.96224×10^{-4}	9.00000×10^{6}	1.54354×10^{-4}
9.50000×10^{6}	1.20281×10^{-4}	1.00000×10^{7}	8.17850×10^{-5}	1.10000×10^{7}	4.64639×10^{-5}
1.20000×10^{7}	2.51848×10^{-5}	1.30000×10^{7}	1.33692×10^{-5}	1.40000×10^{7}	7.10591×10^{-6}
1.50000×10^{7}	3.72635×10^{-6}	1.60000×10^{7}	1.86483×10^{-6}	1.70000×10^{7}	9.14935×10^{-7}
1.80000×10^{7}	4.76377×10^{-7}	1.90000×10^{7}	2.62960×10^{-7}		

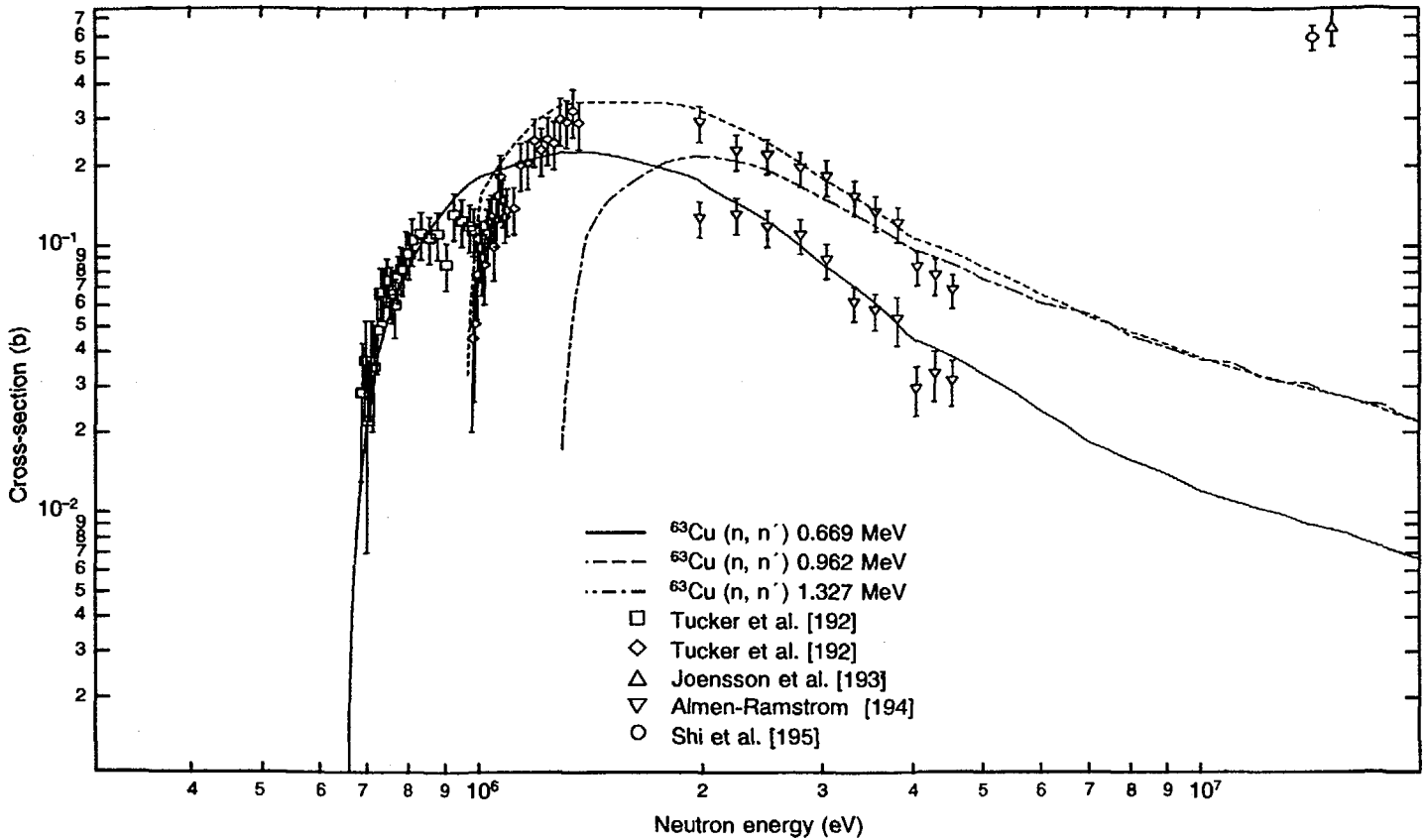

FIG. 6.68. Excitation functions for inelastic scattering of ^{63}Cu to the 0.669, 0.962 and 1.327 MeV levels. Evaluated data from Ref. [184].

^{63}Cu (n, n′), 0.669 MeV level

E_n (eV)	σ (b)	E_n (eV)	σ (b)	E_n (eV)	σ (b)
5.00000×10^{5}	6.15904×10^{-2}	1.00000×10^{6}	2.06771×10^{-1}	1.50000×10^{6}	2.01659×10^{-1}
2.00000×10^{6}	1.52793×10^{-1}	2.50000×10^{6}	1.06051×10^{-1}	3.00000×10^{6}	7.45030×10^{-2}
3.50000×10^{6}	5.40492×10^{-2}	4.00000×10^{6}	4.18184×10^{-2}	4.50000×10^{6}	3.59639×10^{-2}
5.00000×10^{6}	3.07909×10^{-2}	5.50000×10^{6}	2.62996×10^{-2}	6.00000×10^{6}	2.26295×10^{-2}
6.50000×10^{6}	1.97806×10^{-2}	7.00000×10^{6}	1.76941×10^{-2}	7.50000×10^{6}	1.63702×10^{-2}
8.00000×10^{6}	1.52660×10^{-2}	8.50000×10^{6}	1.43816×10^{-2}	9.00000×10^{6}	1.34747×10^{-2}
9.50000×10^{6}	1.25452×10^{-2}	1.00000×10^{7}	1.16149×10^{-2}	1.10000×10^{7}	1.08004×10^{-2}
1.20000×10^{7}	1.01720×10^{-2}	1.30000×10^{7}	9.51051×10^{-3}	1.40000×10^{7}	8.94426×10^{-3}
1.50000×10^{7}	8.57597×10^{-3}	1.60000×10^{7}	8.08404×10^{-3}	1.70000×10^{7}	7.59756×10^{-3}
1.80000×10^{7}	7.24019×10^{-3}	1.90000×10^{7}	6.89136×10^{-3}		

^{63}Cu (n, n′), 0.962 MeV level

E_n (eV)	σ (b)	E_n (eV)	σ (b)	E_n (eV)	σ (b)
5.00000×10^{5}	2.63357×10^{-3}	1.00000×10^{6}	2.70360×10^{-1}	1.50000×10^{6}	3.37766×10^{-1}
2.00000×10^{6}	2.88184×10^{-1}	2.50000×10^{6}	2.13042×10^{-1}	3.00000×10^{6}	1.59176×10^{-1}
3.50000×10^{6}	1.23360×10^{-1}	4.00000×10^{6}	1.01191×10^{-1}	4.50000×10^{6}	8.92366×10^{-2}
5.00000×10^{6}	7.88444×10^{-2}	5.50000×10^{6}	7.00146×10^{-2}	6.00000×10^{6}	6.26499×10^{-2}
6.50000×10^{6}	5.67504×10^{-2}	7.00000×10^{6}	5.21501×10^{-2}	7.50000×10^{6}	4.88489×10^{-2}
8.00000×10^{6}	4.59933×10^{-2}	8.50000×10^{6}	4.35832×10^{-2}	9.00000×10^{6}	4.12607×10^{-2}
9.50000×10^{6}	3.90258×10^{-2}	1.00000×10^{7}	3.64387×10^{-2}	1.10000×10^{7}	3.39123×10^{-2}
1.20000×10^{7}	3.19813×10^{-2}	1.30000×10^{7}	3.02331×10^{-2}	1.40000×10^{7}	2.87502×10^{-2}
1.50000×10^{7}	2.75328×10^{-2}	1.60000×10^{7}	2.62003×10^{-2}	1.70000×10^{7}	2.48837×10^{-2}
1.80000×10^{7}	2.36980×10^{-2}	1.90000×10^{7}	2.25391×10^{-2}		

^{63}Cu (n,n′), 1.327 MeV level

E_n (eV)	σ (b)	E_n (eV)	σ (b)	E_n (eV)	σ (b)
1.00000×10^{6}	2.52227×10^{-2}	1.50000×10^{6}	1.81707×10^{-1}	2.00000×10^{6}	2.08577×10^{-1}
2.50000×10^{6}	1.72955×10^{-1}	3.00000×10^{6}	1.36577×10^{-1}	3.50000×10^{6}	1.09412×10^{-1}
4.00000×10^{6}	9.16482×10^{-2}	4.50000×10^{6}	8.07471×10^{-2}	5.00000×10^{6}	7.16680×10^{-2}
5.50000×10^{6}	6.44110×10^{-2}	6.00000×10^{6}	5.94407×10^{-2}	6.50000×10^{6}	5.67569×10^{-2}
7.00000×10^{6}	5.29463×10^{-2}	7.50000×10^{6}	4.80088×10^{-2}	8.00000×10^{6}	4.44631×10^{-2}
8.50000×10^{6}	4.23090×10^{-2}	9.00000×10^{6}	4.02538×10^{-2}	9.50000×10^{6}	3.82975×10^{-2}
1.00000×10^{7}	3.69423×10^{-2}	1.10000×10^{7}	3.45133×10^{-2}	1.20000×10^{7}	3.16490×10^{-2}
1.30000×10^{7}	3.07469×10^{-2}	1.40000×10^{7}	2.93626×10^{-2}	1.50000×10^{7}	2.75106×10^{-2}
1.60000×10^{7}	2.63037×10^{-2}	1.70000×10^{7}	2.55186×10^{-2}	1.80000×10^{7}	2.43304×10^{-2}
1.90000×10^{7}	2.27544×10^{-2}				

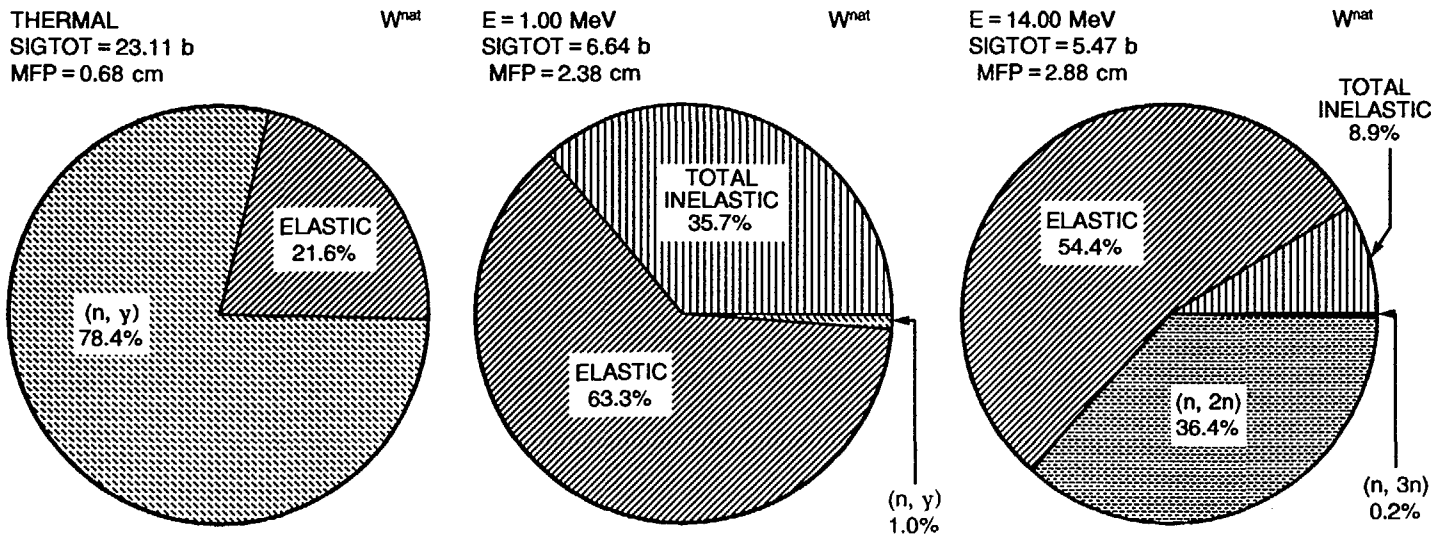

FIG. 6.69. Pie charts of the dominant neutron induced reaction cross-sections for natural tungsten.

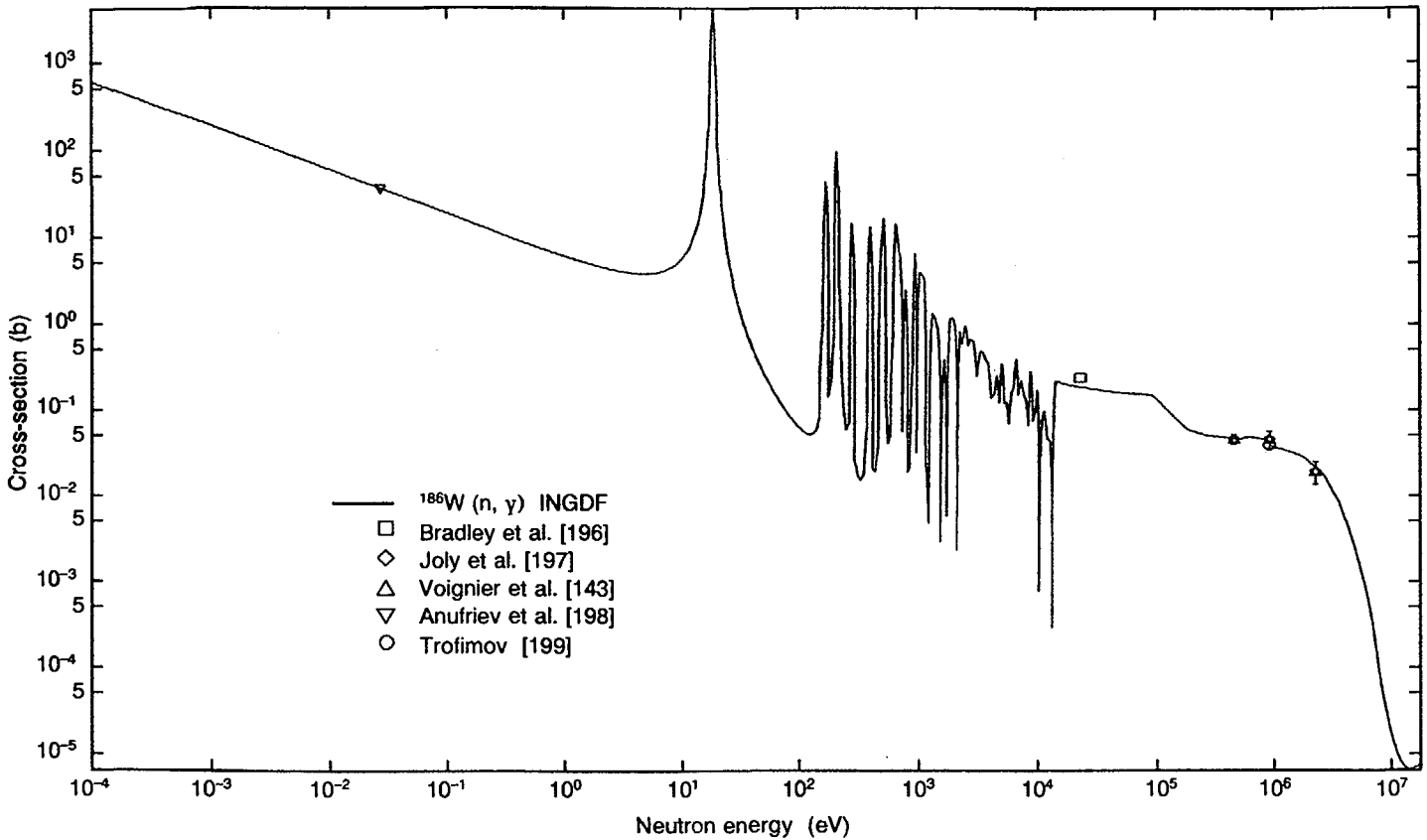

FIG. 6.70. Excitation function for the $^{186}W(n,\gamma)^{187}W$ reaction. Evaluated data from Ref. [193].

$^{186}W(n,\gamma)^{187}W$

E_n (eV)	σ (b)	E_n (eV)	σ (b)	E_n (eV)	σ (b)
1.00000×10^{-3}	3.46832×10^{1}	1.00000×10^{-1}	9.39781	1.00000	4.56016
1.00000×10^{1}	6.60240×10^{1}	1.00000×10^{2}	4.64867	1.00000×10^{3}	3.71841×10^{-1}
1.00000×10^{4}	1.71266×10^{-1}	5.00000×10^{4}	1.60281×10^{-1}	1.00000×10^{5}	6.42219×10^{-2}
5.00000×10^{5}	4.96013×10^{-2}	1.00000×10^{6}	3.86762×10^{-2}	1.50000×10^{6}	3.30526×10^{-2}
2.00000×10^{6}	2.68804×10^{-2}	2.50000×10^{6}	2.10035×10^{-2}	3.00000×10^{6}	1.56125×10^{-2}
3.50000×10^{6}	1.09925×10^{-2}	4.00000×10^{6}	7.53230×10^{-3}	4.50000×10^{6}	4.97848×10^{-3}
5.00000×10^{6}	3.29305×10^{-3}	5.50000×10^{6}	2.16106×10^{-3}	6.00000×10^{6}	1.42863×10^{-3}
6.50000×10^{6}	9.45086×10^{-4}	7.00000×10^{6}	6.09772×10^{-4}	7.50000×10^{6}	3.80772×10^{-4}
8.00000×10^{6}	2.25812×10^{-4}	8.50000×10^{6}	1.25603×10^{-4}	9.00000×10^{6}	7.72230×10^{-5}
9.50000×10^{6}	5.26402×10^{-5}	1.00000×10^{7}	3.15097×10^{-5}	1.10000×10^{7}	1.77734×10^{-5}
1.20000×10^{7}	1.20027×10^{-5}	1.30000×10^{7}	9.09611×10^{-6}	1.40000×10^{7}	7.61816×10^{-6}
1.50000×10^{7}	6.96766×10^{-6}	1.60000×10^{7}	6.76503×10^{-6}	1.70000×10^{7}	6.81251×10^{-6}
1.80000×10^{7}	6.97523×10^{-6}	1.90000×10^{7}	7.18858×10^{-6}		

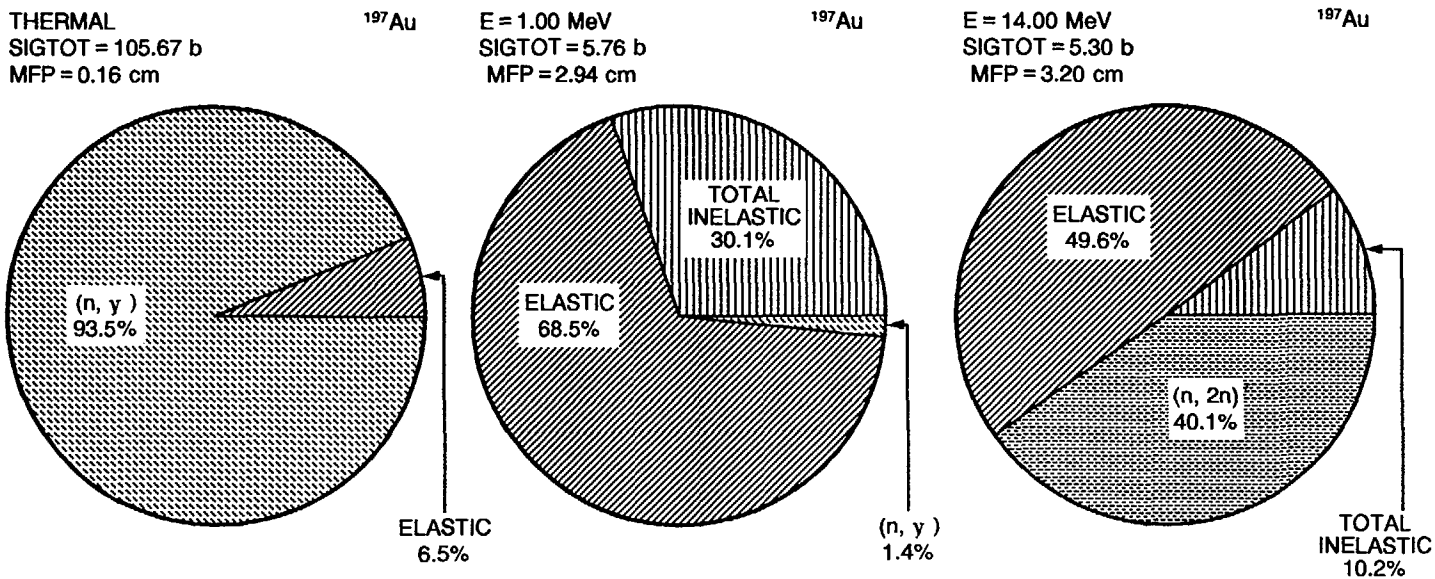

FIG. 6.71. Pie charts of the dominant neutron induced reaction cross-sections for gold.

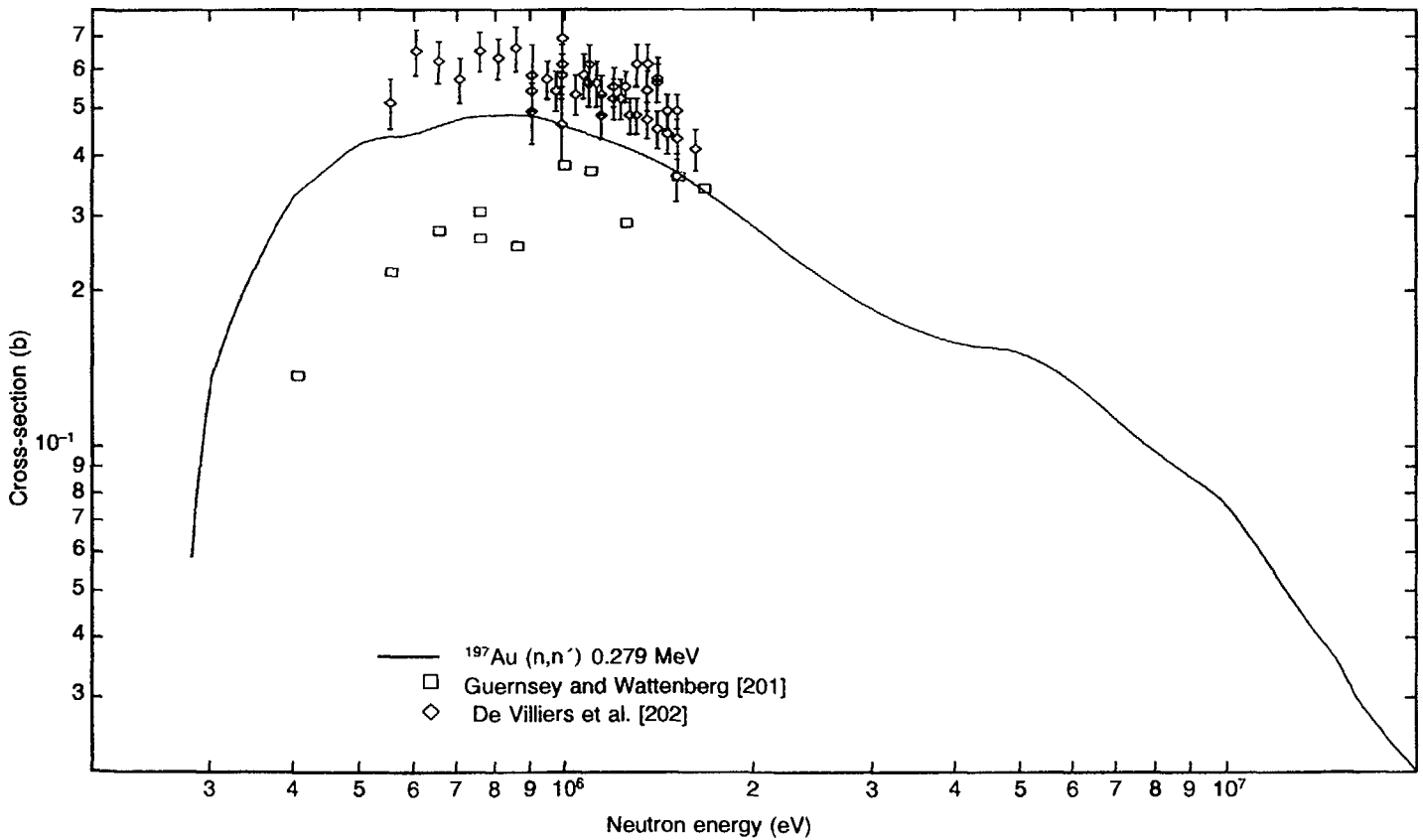

FIG. 6.72. Excitation function for inelastic scattering of ^{197}Au to the 0.279 MeV level. Evaluated data from Ref. [196].

^{197}Au (n, n′)

E_n (eV)	σ (b)	E_n (eV)	σ (b)	E_n (eV)	σ (b)
1.00000×10^{5}	1.49282×10^{-1}	5.00000×10^{5}	4.63107×10^{-1}	1.00000×10^{6}	4.21877×10^{-1}
1.50000×10^{6}	3.29626×10^{-1}	2.00000×10^{6}	2.55248×10^{-1}	2.50000×10^{6}	2.09905×10^{-1}
3.00000×10^{6}	1.83593×10^{-1}	3.50000×10^{6}	1.69081×10^{-1}	4.00000×10^{6}	1.61592×10^{-1}
4.50000×10^{6}	1.58535×10^{-1}	5.00000×10^{6}	1.52160×10^{-1}	5.50000×10^{6}	1.42502×10^{-1}
6.00000×10^{6}	1.31502×10^{-1}	6.50000×10^{6}	1.20087×10^{-1}	7.00000×10^{6}	1.09510×10^{-1}
7.50000×10^{6}	1.01191×10^{-1}	8.00000×10^{6}	9.47958×10^{-2}	8.50000×10^{6}	8.94285×10^{-2}
9.00000×10^{6}	8.47101×10^{-2}	9.50000×10^{6}	8.02761×10^{-2}	1.00000×10^{7}	7.19917×10^{-2}
1.10000×10^{7}	6.02206×10^{-2}	1.20000×10^{7}	5.08209×10^{-2}	1.30000×10^{7}	4.36671×10^{-2}
1.40000×10^{7}	3.83330×10^{-2}	1.50000×10^{7}	3.32560×10^{-2}	1.60000×10^{7}	2.85791×10^{-2}
1.70000×10^{7}	2.56940×10^{-2}	1.80000×10^{7}	2.34325×10^{-2}	1.90000×10^{7}	2.16198×10^{-2}

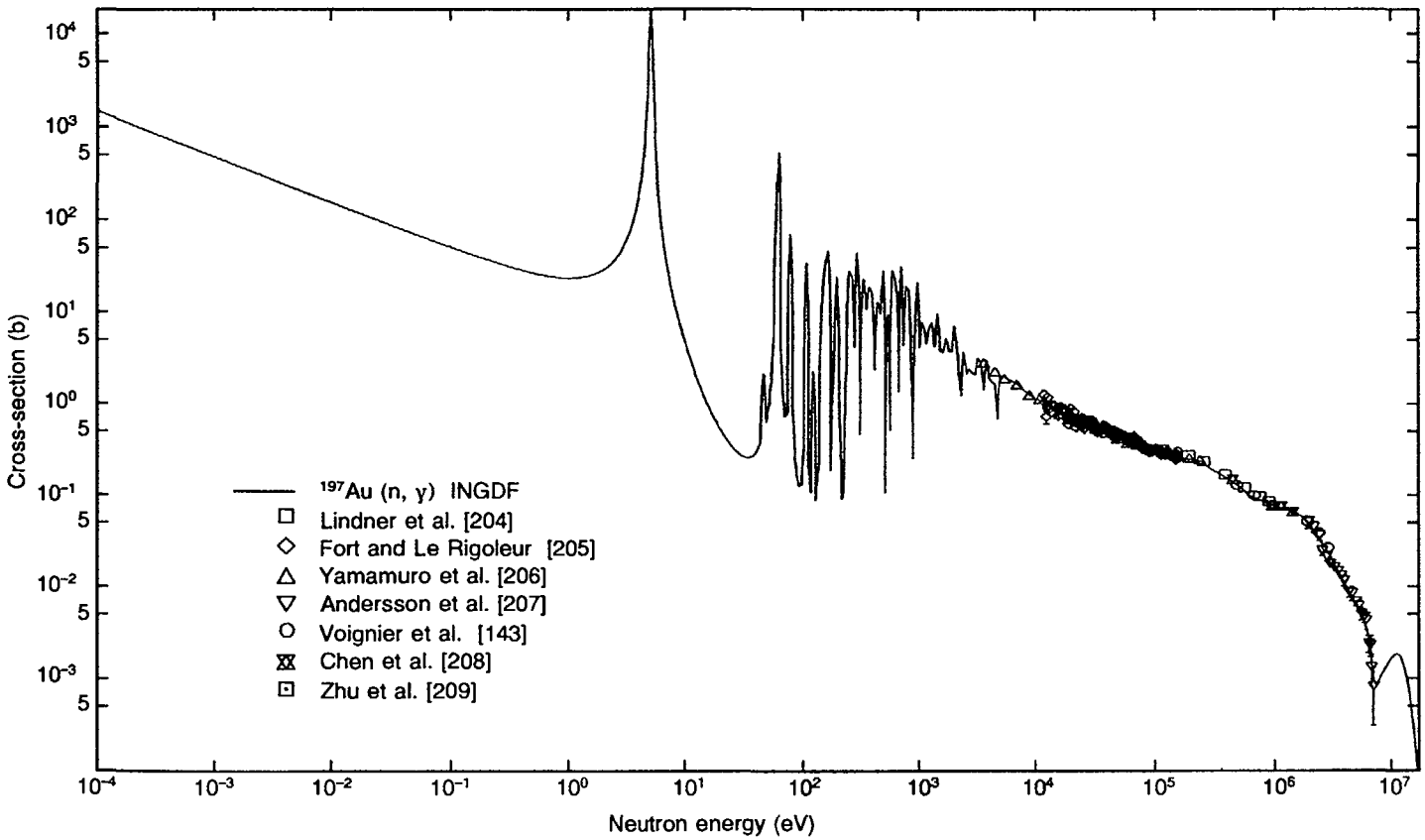

FIG. 6.73. Excitation function for the $^{197}Au(n,\gamma)^{198}Au$ reaction. Evaluated data from Ref. [196].

$^{197}Au\,(n,\gamma)\,^{198}Au$

E_n (eV)	σ (b)	E_n (eV)	σ (b)	E_n (eV)	σ (b)
1.00000×10^{-3}	9.07112×10^{1}	1.00000×10^{-1}	2.87873×10^{1}	1.00000	7.85924×10^{2}
1.00000×10^{1}	2.60141×10^{1}	1.00000×10^{2}	1.33314×10^{1}	1.00000×10^{3}	2.23146
1.00000×10^{4}	6.38357×10^{-1}	5.00000×10^{4}	3.59083×10^{-1}	1.00000×10^{5}	2.07911×10^{-1}
5.00000×10^{5}	9.69509×10^{-2}	1.00000×10^{6}	7.33451×10^{-2}	1.50000×10^{6}	6.12651×10^{-2}
2.00000×10^{6}	4.21400×10^{-2}	2.50000×10^{6}	2.90718×10^{-2}	3.00000×10^{6}	2.08241×10^{-2}
3.50000×10^{6}	1.44615×10^{-2}	4.00000×10^{6}	1.08622×10^{-2}	4.50000×10^{6}	8.41945×10^{-3}
5.00000×10^{6}	6.75819×10^{-3}	5.50000×10^{6}	5.46054×10^{-3}	6.00000×10^{6}	4.14691×10^{-3}
6.50000×10^{6}	2.99490×10^{-3}	7.00000×10^{6}	1.70684×10^{-3}	7.50000×10^{6}	9.08340×10^{-4}
8.00000×10^{6}	8.78249×10^{-4}	8.50000×10^{6}	1.00925×10^{-3}	9.00000×10^{6}	1.16000×10^{-3}
9.50000×10^{6}	1.32000×10^{-3}	1.00000×10^{7}	1.54735×10^{-3}	1.10000×10^{7}	1.77370×10^{-3}
1.20000×10^{7}	1.80220×10^{-3}	1.30000×10^{7}	1.52000×10^{-3}	1.40000×10^{7}	1.12447×10^{-3}
1.50000×10^{7}	7.40353×10^{-4}	1.60000×10^{7}	4.22581×10^{-4}	1.70000×10^{7}	2.58920×10^{-4}
1.80000×10^{7}	1.78466×10^{-4}	1.90000×10^{7}	1.21116×10^{-4}		

REFERENCES

[1] PEISER, H.S., et al., Element by element review of their atomic weights, Pure Appl. Chem. **566** (1984) 695.

[2] WEAST, R.C. (Ed.), Handbook of Chemistry and Physics, CRC Press, Boca Raton, FL (1987–1988).

[3] AHMED, M.R., et al., Atlas of Gamma Ray Spectra from the Inelastic Scattering of Reactor Fast Neutrons, Atomizdat, Moscow (1978).

[4] US NATIONAL NUCLEAR DATA CENTER, Evaluated Nuclear Data File, ENDF/B-6, Brookhaven National Laboratory, Upton, NY (1990).

[5] JAPANESE NUCLEAR DATA CENTRE, Japanese Evaluated Data Library, JENDL-3, Tokai-mura (1990).

[6] RUSSIAN NUCLEAR DATA CENTRE, Activation Data Library, ADL-90, Obninsk (1990).

[7] FISHER, H.M., Nuclear Cross-Section Data Handbook, Rep. LA-11711-M, Los Alamos Scientific Laboratory, Los Alamos, NM (1989).

[8] ROSE, P.F., DUNFORD, C.L. (Eds), ENDF-102 Data Formats and Procedures for the Evaluated Nuclear Data File ENDF-6, Rep. BNL-NCS-44945, US National Nuclear Data Center, Brookhaven National Laboratory, Upton, NY (1990).

[9] MEADOWS, J.W., WHALEN, J.F., Thermal neutron absorption cross-sections by the pulsed source method, Nucl. Sci. Eng. **9** (1961) 132.

[10] COX, A.E., et al., The proton thermal neutron capture cross section, Nucl. Phys. **74** (1965) 497.

[11] TUDORIC-GHEMO, J., Neutron–proton radiative capture at 14.4 MeV, Nucl. Phys., A **92** (1967) 233.

[12] SLAUS, I., et al., Neutron–proton radiative capture at 14.4 MeV, C.R. Congr. Int. Phys. Nucl. Paris **2** (1964) 244.

[13] FRIESENHAHN, S.J., et al., "Measurements of the 6-Li and 10-B partial cross sections from 1 to 1500 keV", Nuclear Cross Sections and Technology, NBS Spec. Publ. 425, National Bureau of Standards, Washington, DC (1975) 232.

[14] VIESTI, G., LISKIEN, H., The 10-B(n, $\alpha\gamma$)7-Li cross sections between 0.1 and 2.2 MeV, Ann. Nucl. Energy **6** (1979) 13.

[15] FU, C.Y., AXTON, E.J., PEREY, F.G., in ENDF/B-6, US National Nuclear Data Center, Brookhaven National Laboratory, Upton, NY (1990).

[16] JURNEY, E.T., MOTS, H., Thermal Neutron Capture in D and O-16, Rep. ANL-6797, Argonne National Laboratory, Argonne, IL (1963).

[17] JURNEY, E.T., et al., Thermal neutron capture cross-section of deuterium, Phys. Rev., C **25** (1980) 2810.

[18] MUGHABGHAB, S.F., et al., Quantitative test of the Lane–Lynn theory of direct radiative capture of thermal neutrons by 12C and 13C, Phys. Rev., C **26** (1982) 2698.

[19] HAOUAT, G., et al., Differential Cross-Sections for Carbon Neutron Elastic and Inelastic Scattering from 8 to 14.5 MeV, Rep. CEA-R-4641, Centre d'études de Bruyères-le-Châtel (1975).

[20] KREGER, W.E., KERN, B.D., C-12(n, p)B-12 cross-section for 14.9 to 17.5 MeV neutrons, Phys. Rev. **113** (1959) 890.

[21] RIMMER, E.M., FISHER, P.S., Resonances in the (n, p) reaction on C-12, Nucl. Phys., A **108** (1968) 567.

[22] ORPHAN, V.J., et al., Gamma ray production cross-sections for the O-16(n, x gamma) reaction from 6.35 to 16.52 MeV neutron energy, Nucl. Sci. Eng. **42** (1970) 352.

[23] KANDA, Y., MURATA, T., in JENDL-3, Japanese Nuclear Data Centre, Tokai-mura (1990).

[24] KANTELE, J., GARDNER, D.G., Some activation cross-sections for 14.7 MeV neutrons, Nucl. Phys. **35** (1962) 353.

[25] PAUL, E.B., CLARKE, R.K., Cross-section measurements of reactions induced by neutrons of the 14.5 MeV energy, Can. J. Phys. **31** (1953) 267.

[26] SEEMAN, K.W., MOORE, W.E., O-16(n, p)N-16 Cross-Section from 12.6 to 16.3 MeV, Rep. KAPL-2214, Knolls Atomic Power Laboratory, Schenectady, NY (1962).

[27] MARTIN, H.C., Cross-sections for the O-16(n, p)N-16 reaction from 12 to 18 MeV, Phys. Rev. **93** (1954) 498.

[28] DE JUREN, J.A., STOOKSBURY, R.W., Measurement of the O-16(n, p)N-16 cross-section at 14.7 MeV, Phys. Rev. **120** (1960) 901.

[29] DE JUREN, J.A., et al., Measurement of the O-16(n, p)N-16 cross-section from 11 to 19 MeV, Phys. Rev. **127** (1962) 1229.

[30] SCHMIDT-HOENOW, M., HERR, W., Activation cross-section of the O-16(n, p)N-16 and O-18(n, α)C-15 reaction for 14 MeV (D–T) neutrons, Radiochim. Acta. **17** (1972) 142.

[31] BORMANN, M., et al:, "Measurements of some fast neutron cross-sections with the activation method", Nuclear Data for Reactors (Proc. Conf. Paris, 1966), Vol. 1, IAEA, Vienna (1967) 225.

[32] SCHANTL, W., personal communication, 1970.

[33] PRASAD, R., SARKAR, D.C., Measurement of (n, p) and (n, α) cross-sections at 14.8 MeV, Nuovo Cimento, A **3** (1971) 467.

[34] MITRA, B., GHOSE, A.M., (n, p) cross-sections of some low Z nuclei for 14.8 MeV neutrons, Nucl. Phys. **83** (1966) 157.

[35] SIGG, R.A., Fast neutron induced reaction cross-sections and their systematics, Diss. Abstr. B **37** (1976) 2237.

[36] MAGNUSSON, G., et al., 14.7 MeV neutron capture cross-section measurements with the activation technique, Phys. Scr. **21** (1980) 21.

[37] YAMAMURO, N., et al., A measurement of the radiation width of the 2.85 keV neutron resonance and the thermal neutron capture cross-section in sodium, Nucl. Sci. Eng. **41** (1970) 445.

[38] MENLOVE, H.O., et al., Neutron radiative capture cross-sections for Na-23, Mn-55, In-115 and Ho-165 in the energy region 1 to 19.4 MeV, Phys. Rev. **163** (1967) 1299.

[39] RYVES, T.B., PERKINS, D.R., Thermal neutron capture cross-section measurements for 13-Na, 27-Al, 37-Cl and 51-V, Nucl. Energy **24** (1970) 419.

[40] CSIKAI, J., et al., Radiative capture cross-sections for 14.7 MeV neutrons, Nucl. Phys., A **95** (1967) 229.

[41] HASAN, S.S., et al., Neutron activation cross-sections at 24 keV, Nuovo Cimento, B **58** (1968) 402.

[42] HOLUB, E., et al., Activation Measurements of Fast Neutron Radiative Capture, Rep. LNS-4-72, Rudjer Bošković Institute, Zagreb (1972).

[43] PLASTINARU, D., et al., Cross-section of Na-23(n, gamma)Na-24m reaction for fast neutrons, Stud. Cercet. Fiz. **25** (1973) 387.

[44] LARSON, D.C., in ENDF/B-6, US National Nuclear Data Center, Brookhaven National Laboratory, Upton, NY (1977).

[45] BARRAL, R.C., et al., High Energy Neutron Cross-Section Validation and Neutron Flux Spectrum Using the Henre Source, Rep. AFWL-TR-68-134, Air Force Weapons Laboratory, Kirtland, NM (1969).

[46] PRESTWOOD, R.J., (n, 2n) cross-sections of Na-23 at 14.1 MeV, Phys. Rev. **98** (1955) 47.

[47] PICARD, J., WILLIAMSON, C.F., The (n, p), (n, α) and (n, 2n) cross-sections for F-19 and Na-23 between 13 and 21 MeV, Phys. Rev. **63** (1965) 673.

[48] LISKIEN, H., PAULSEN, A., Cross-sections for the reactions Cu-36(n, α)Co-60, Ni-60(n, p)Co-60, Ti-46(n, p)Sc-46 and Na-23(n, 2n)Na-22, Nucl. Phys. **63** (1965) 303.

[49] IKEDA, Y., et al., Activation Cross-Section Measurement for Fusion Reactor Structural Materials at Neutron Energy from 13.3 to 15.0 MeV Using FNS Facility, Rep. JAERI-1312, Japan Atomic Energy Research Institute, Tokai-mura (1988).

[50] ARAMINOWICZ, J., DRESLER, J., Investigation of the (N, 2N) Reactions at 14.6 MeV for 42 Nuclides, Rep. INR-1464, Institute of Nuclear Research, Warsaw (1973).

[51] SHANI, G., (N, 2N) Cross-Section Measurement of Light Elements with 15.1 MeV Neutrons, Rep. INIS-MF-3663, IAEA, Vienna (1976).

[52] ADAMSKI, L., et al., Cross-sections for the Na-23(n, 2n)Na-22 reaction, Ann. Nucl. Energy **7** (1980) 397.

[53] MASLOV, G.N., et al., The experimental cross-sections of the nuclear reactions for 14 MeV neutrons, Yad. Konst. **9** (1972) 50.

[54] COLDITZ, J., HILLE, P., Some n, gamma cross-section measurements for fast neutrons, Anz. Oesterr. Akad. Wiss., Math.-Naturwiss. Kl. **105** (1968) 236.

[55] RYVES, T.B., Activation measurements of thermal neutron capture cross-sections and resonance integrals, Nucl. Energy **24** (1970) 35.

[56] PERKIN, J.L., et al., Radiative capture cross-sections for 14.5 MeV neutrons, Proc. Phys. Soc. **72** (1958) 505.

[57] VULETIN, J., et al., Activation cross-sections of (n, gamma) reactions at 14 MeV, Lett. Nuovo Cimento **10** (1974) 1.

[58] HATCHYA, M., ASAMI, T., in JENDL-3, Japanese Nuclear Data Centre, Tokai-mura (1987).

[59] GERALDO, L.P., et al., Activation cross-section measurements near threshold for the Mg-24(n, p)Na-24 and Al-27(n, α)Na-24 reactions, Ann. Nucl. Energy **16** (1989) 293.

[60] OKAZAKI, A., GREEN, R.E., Thermal Neutron Absorption Cross-Sections of Zircaloy-2, Copper and Aluminium, Rep. AECL-3073, At. Energy of Canada Ltd., Chalk River, Ontario (1968).

[61] MALIK, S.S., et al., Factors in the precision of slow neutron capture cross-section measurements using a simple Moxon–Rae detector, Nucl. Instrum. Methods **86** (1970) 83.

[62] MACKLIN, R.L., et al., Neutron activation cross-sections with Sb–Be sources, Phys. Rev. **107** (1957) 504, 584.

[63] SHER, R., MAGURNO, B.A., Brookhaven National Laboratory, Upton, NY, Measurements in a 0.06 eV beam, personal communication, 1962.

[64] FUKETA, T., OTOMO, S., Measurement of Thermal Neutron Absorption Cross-Section with a Pile Oscillator, Rep. JAERI-1009, Japan Atomic Energy Research Institute, Tokai-mura (1960).

[65] RIGAUD, F., et al., Improved activation measurements of (n, gamma) cross-section for 14.6 MeV neutrons, Nucl. Sci. Eng. **55** (1974) 17.

[66] TATTERSAL, R.B., et al., Pile oscillator measurements of resonance absorption integrals, Nucl. Energy, A **12** (1960) 32.

[67] CARRE, J.C., VIDAL, R., Measurements of Cross-Sections and Resonance Integrals by the Oscillation Method, Rep. NEANDC(E)-57, Nuclear Data Committee, OECD Nuclear Energy Agency, Paris (1965).

[68] BRASE, M., BECKURTS, K.H., Measurement of the neutron absorption cross-section in aluminium, Nukleonika **2** (1960) 139.

[69] PETO, G., et al., Radiative capture cross-sections for 3 MeV neutrons, Nucl. Energy **21** (1967) 797.

[70] CSIKAI, J., et al., Radiative capture cross-sections for 14.7 MeV neutrons, Nucl. Phys., A **95** (1967) 229.

[71] CVELBAR, F., et al., Gamma ray spectra and (n, gamma) cross-sections at 14 MeV for Al, S, V, Cr, Mn, Fe, Nucl. Instrum. Methods **44** (1966) 292.

[72] CVELBAR, F., et al., Cross-section and gamma spectrum of Al-27(n, gamma) at 14 MeV, Phys. Lett. **3** (1963) 364.

[73] BUDNAR, M., et al., Prompt Gamma Ray Spectra and Integrated Cross-sections for the Radiative Capture of 14 MeV Neutrons for 28 Natural Targets in the Mass Region 12 to 208, Rep. INDC(YUG)-6, International Nuclear Data Committee, IAEA, Vienna (1979).

[74] YOUNG, P.G., FASTER, D.G., in ENDF/B-6, US National Nuclear Data Center, Brookhaven National Laboratory, Upton, NY (1973).

[75] SMITH, D.L., MEADOWS, J.W., Cross-section measurement of (n, p) reactions for Al-27, Ti-46, 47, 48, Fe-54, 56, Ni-58, Co-59 and Zn-64 from near threshold to 10 MeV, Nucl. Sci. Eng. **58** (1975) 314.

[76] TAHIR, N.A., Study of Al-27(n, p)Mg-27 excitation function by five different techniques, Indian J. Pure Appl. Phys. **23** (1985) 439.

[77] KOBAYASHI, K., KIMURA, I., "Application of a 6-lid thermal 14 MeV neutron converter to the measurement of activation cross-sections", Nuclear Data for Science and Technology (Proc. Int. Conf. Mito, 1988), Saikon Publ., Tokyo (1988) 261.

[78] KUDO, K., et al., "Measurement of Al-27(n, p)Mg-27 activation cross-section", ibid., p. 1021.

[79] AI, C.E., et al., Measurements of Al-27(n, p)Mg-27 and Fe-54(n, p)Mn-54 cross-sections, Nucl. Sci., Taiwan **14** (1977) 1.

[80] CSIKAI, J., et al., Study of the excitation functions of 13-Al-27(n, α), 13-Al-27(n, p) and 14-Si(n, p), Z. Phys., A **325** (1986) 69.

[81] BRADLEY, D.A., et al., "Measurements of (n, p) cross-sections using monoenergetic neutrons from T–D reaction", Fast Neutrons in Science and Technology (Proc. Chiangmai Conf. 1985), Chiangmai University, Chiangmai, Thailand (1985) 19.

[82] GREENWOOD, L.R., Recent Research in Neutron Dosimetry and Damage Analysis for Materials Irradiations, Rep. DOE-ER-0046-21, Department of Energy, Washington, DC (1985).

[83] ANDERSSON, P., et al., Absolute Measurements of some Neutron Activation Cross-Sections in Al-27, In-115 and Au-197 at 14.9 MeV, Rep. LUNF-DG-3021, Lund University, Sweden (1972).

[84] NORDBORG, C., et al., Gamma ray production cross-sections of neutron induced reactions in oxygen, Nucl. Sci. Eng. **66** (1978) 75.

[85] RYVES, T.B., et al., Cross-section measurements of N-14(n, 2n)N-13, F-19(n, 2n)F-18, Fe-54(n, 2n)Fe-53, Al-27(n, p)Mg-27 and Al-27(n, α)Na-24 between 14.7 and 19.0 MeV, J. Phys., G **4** (1978) 1783.

[86] SWINHOE, M.T., UTTLEY, C.A., Measurements of MeV Neutron Cross-Sections by Activation, Rep. AERE-PR/NP-26, UKAEA, Atomic Energy Research Establishment, Harwell (1979).

[87] MOSTAFA, A.B.M.G., Measurements of relative neutron activation cross-sections of Al-27(n, p), Al-27(n, α), Mg-24(n, p) and Fe-56(n, p) reactions in the energy range of 4.5 to 8.35 MeV, Nucl. Sci. Appl., B **9** (1976) 10.

[88] FRIEDMAN, H., Precision measurement of the total cross-section for the reaction Al-27(n, α) relative to the cross-section of Au-197(n, 2n) in the energy range from 13.7 to 14.42 MeV, Z. Phys., A **302** (1981) 271.

[89] KUDO, K., "Cross-section measurements of Fe-56(n, p) and Al-27(n, α) between 14.0 and 19.9 MeV", Nuclear Standard Reference Data (Proc. IAEA Advisory Group Meeting Vienna, 1984), IAEA-TECDOC-335, IAEA, Vienna (1985).

[90] FIRKIN, S., Differential Neutron Cross-Section of Ti-47, 48(n, p) and Al-27(n, α), Rep. AERE-M-3350, UKAEA, Atomic Energy Research Establishment, Harwell (1983).

[91] GARUSKA, U., et al., Cross-Section Measurements of the (n, α) Reaction at 14.6 MeV Neutron Energy, Rep. INR-1773/I/PL, Institute of Nuclear Research, Warsaw (1978).

[92] LU, Han-Lin, et al., Excitation Curves for some Reactions of Al, Ti, V and I, Rep. INDC(CPR)-16, International Nuclear Data Committee, IAEA, Vienna (1989).

[93] GARG, K.C., Cross-sections for the millisecond activities of the reactions Al-27(n, α), Mg-24(n, p) and As-75(n, n′), personal communication, 1975.

[94] CSIKAI, J., "Study of excitation functions around 14 MeV neutron energy", Nuclear Data for Science and Technology (Proc. Conf. Antwerp, 1982), Reidel Publ., Dordrecht (1983) 414.

[95] GARLEA, I., et al., Measurements of the Integral Cross-Sections at 14 MeV for Reactions In-115(n, inl), Au-197(n, 2n), Nb-93(n, 2n), Al-27(n, α), Fe-56(n, p), U-235(n, f), Pu-239(n, f), Np-237(n, f), U-238(n, f), Th-232(n, f), Rep. INDC(ROM)-15, International Nuclear Data Committee, IAEA, Vienna (1983).

[96] ZHOU, Muyao, et al., Shell effect from the cross-section of the (n, 2n) reaction produced by 14.6 MeV neutrons, Chin. J. Nucl. Phys. **9** (1987) 34 (in Chinese).

[97] CHIMOYE, T., et al., Study of the excitation functions of Al-27(n, α), Al-27(n, p) and Si-28(n, p), Z. Phys., A **325** (1986) 69.

[98] CSIKAI, J., et al., Study of the excitation functions of Al-27(n, α), Al-27(n, p) and Si-28(n, p) reactions, Z. Phys., A **325** (1986) 69.

[99] GIBBONS, J.H., et al., Average radiative capture cross-sections for 7 to 170 keV neutrons, Phys. Rev. **122** (1961) 182.

[100] MACKLIN, R.L., et al., Average radiative capture cross-sections for 30 and 65 keV neutrons, Phys. Rev. **129** (1963) 2695.

[101] RIGAUD, F., et al., Radiative neutron capture of Si, Rb, Sr and Y in the dipole giant resonance region, Nucl. Phys., A **154** (1970) 243.

[102] KOESTER, L., et al., Scattering lengths and resonance properties of the interaction of slow neutrons with the isotopes of silicon and sulphur, Z. Phys., A **289** (1979) 399.

[103] LARSON, D.C., in ENDF/B-6, US National Nuclear Data Center, Brookhaven National Laboratory, Upton, NY (1990).

[104] KINNEY, W.E., PEREY, F.G., Neutron Elastic and Inelastic Scattering Cross-sections for Si in the Energy Range 4.19 to 8.56 MeV, Rep. ORNL-4517, Oak Ridge National Laboratory, Oak Ridge, TN (1970).

[105] OBST, A.W., WEIL, J.L., Scattering of 9.8 MeV neutrons from Si and S, Phys. Rev., C **7** (1973) 1076.

[106] CLARKE, L.R., CROSS, W.G., Elastic and inelastic scattering of 14.1 MeV neutrons from C, Mg, Si and S, Nucl. Phys. **53** (1964) 177.

[107] BENVENISTE, J., et al., Spectra of Continuum Gamma Rays Resulting from 14 MeV Neutron Interactions with Several Elements, Rep. UCID-4619, California University, Livermore, CA (1963).

[108] BEZOTOSNIJ, V.M., et al., "Discrete gamma lines in the nonelastic interaction of 14 MeV neutrons with Mg, Si, P, S, Ti and Zn nuclei", Neutron Physics (Proc. Conf. Kiev, 1980), Atominform, Moscow (1980) 221.

[109] PEPELNIK, R., et al., 14 MeV Neutron Activation Cross-Sections, Rep. NEANDC(E)-262U, Nuclear Data Committee, OECD, Nuclear Energy Agency, Paris (1985).

[110] GHOSE, A.M., Al(n, p) and Si(n, p) Cross-sections at 8.4 MeV, Rep. IAEA/TA-1390, IAEA, Vienna (1978).

[111] NGOC, P.N., et al., Investigations of (n, p), (n, α) and (n, 2n) reactions around 14 MeV, personal communication, 1980.

[112] ALEKSANDROV, D.V., et al., Cross-section of (n, p) reaction on Al-27, Si-28, P-31, Cl-35, K-39 and Co-52 at 14.1 MeV neutron energy, At. Ehnerg. **39** (1975) 137.

[113] SHCHEBOLEV, V.T., RAMENDIK, Z.A., Determination of (n, p) and (n, α) cross-sections on Si-28, Si-29 and Si-30 for 14.8 MeV, At. Ehnerg. **43** (1977) 54.

[114] KITAZAWA, H., et al., in JENDL-3, Japanese Nuclear Research Centre, Tokai-mura (1989).

[115] STRAIN, J.E., ROSS, W.J., 14 MeV Neutron Reactions, Rep. ORNL-3672, Oak Ridge National Laboratory, Oak Ridge, TN (1963).

[116] RANAKUMAR, N., et al., Neutron activation cross-sections at 14.4 MeV for Si and Zn isotopes, Nucl. Phys., A **122** (1968) 679.

[117] ROBERTSON, J.C., et al., Some activation cross-sections at 14.78 MeV, J. Nucl. Energy **27** (1973) 531.

[118] PASQUARELLI, A., Measurement of cross-sections for (n, 2n), (n, p) and (n, α) reactions at 14.7 MeV, Nucl. Phys., A **93** (1967) 218.

[119] PRASAD, R., SARKAR, D.C., Measured (n, p) reaction cross-sections and their predicted values at 14.8 MeV, Nuovo Cimento, A **3** (1971) 467.

[120] HERMAN, M., et al., Cross-sections for the Fast Neutron Induced Reactions on Si and Zn Isotopes, Rep. INR-1871/I/PL/A 13, Institute of Nuclear Research, Warsaw (1980).

[121] JANCZYSZYN, J., "Simple measurement of neutron cross-section ratio for reactions leading to the same radionuclide", Nuclear Data for Science and Technology (Proc. Conf. Antwerp, 1982), Reidel Publ., Dordrecht (1983) 869.

[122] NAKAMURA, H., in JENDL-3, Japanese Nuclear Research Centre, Tokai-mura (1987).

[123] GUPTA, J.P., et al., Pre-equilibrium emission effect in (n, p) reaction cross-section at 14.8 MeV, Indian J. Phys. **24** (1985) 637.

[124] SCHWERER, O., et al., Measurement of cross-sections for 14 MeV neutron capture, Nucl. Phys., A **264** (1976) 105.

[125] DOVBENKO, A.G., et al., Radiative capture for fast neutrons by isotopes Cl-37, Rb-87, Ir-193, At. Ehnerg. **23** (1967) 151.

[126] LEIPUNSKIJ, A.I., et al., "Radiative cross-section measurements for fast neutrons", Peaceful Uses of Atomic Energy (Proc. 2nd Int. Conf. Geneva, 1958), United Nations, New York (1958) 2219.

[127] KONONOV, V.N., et al., Radiative capture cross-sections for 25 keV neutrons, At. Ehnerg. **5** (1958) 564.

[128] ARNOLD, D.M., RAYBURN, L.A., personal communication, 1965.

[129] HYVOENEN-DABEK, M., et al., 14 MeV neutron cross-sections on Mg, Cl and Sr, J. Radioanal. Chem. **46** (1978) 357.

[130] JANCZYSZYN, J., GORSKI, L., Cross sections of 14 MeV neutron reactions producing short-lived nuclides, J. Radioanal. Chem. **14** (1973) 201.

[131] SRINIVASA, S.V., et al., personal communication, 1978.

[132] PAUL, E.B., CLARKE, R.L., Cross-section measurements of reactions induced by neutrons of the 14.5 MeV energy, Can. J. Phys. **31** (1953) 267.

[133] SCALAN, R.S., FINK, R.W., Activation cross-sections for reactions of chlorine and copper with 14.8 MeV neutrons, Nucl. Phys. **9** (1958) 334.

[134] BORMAN, N., et al., Excitation Functions of some Fast Neutron Reactions, Rep. NEANDC(E)-76, Nuclear Data Committee, OECD, Nuclear Energy Agency, Paris (1967).

[135] DIVEN, B.C., et al., Radiative capture cross-sections for fast neutrons, Phys. Rev. **120** (1960) 556.

[136] BELANOVA, T.S., Measurement of fast neutron absorption cross-sections, Zh. Ehksp. Teor. Fiz. **34** (1958) 574 (in Russian).

[137] FU, C.Y., HETRICK, D.M., in ENDF/B-6, US National Nuclear Data Center, Brookhaven National Laboratory, Upton, NY (1971).

[138] HATCHYA, M., in JENDL-3, Japanese Nuclear Data Centre, Tokai-mura (1987).

[139] QAIM, S.M., MOLLA, N.I., Nuclear data measurements for FR-wall and structural materials, Nucl. Phys., A **283** (1977) 269.

[140] HOLBERG, P., et al., J. Radioanal. Chem. **42** (1978) 477.

[141] DIVEN, B.C., et al., Radiative capture cross-sections for fast neutrons, Phys. Rev. **120** (1960) 556.

[142] JOKI, E.G., et al., Total slow neutron cross-section measurements of titanium, zirconium and hafnium, Nucl. Sci. Eng. **11** (1961) 298.

[143] VOIGNIER, J., et al., Capture cross-sections and gamma-ray spectra from the interaction of 0.5 to 3.0 MeV neutrons with nuclei in the mass range A = 63 to 209, Nucl. Sci. Eng. **93** (1968) 43.

[144] KOBAYASHI, K., HASHIKURA, H., in JENDL-3, Japanese Nuclear Data Centre, Tokai-mura (1988).

[145] DUDEY, N.D., et al., Fast neutron capture by vanadium and titanium, Nucl. Energy **23** (1969) 443.

[146] ANAND, R.P., et al., Measurement of isotopic neutron capture cross-sections for V-51, Cu-63, Ga-71, Ge-74, As-75, Mo-98, Mo-100, Ru-104, In-115, Te-128, Te-130, Ce-140, Ce-142, Ho-165 at the neutron energy of (25 ± 5) keV, Nuovo Cimento, A **50** (1979) 274.

[147] AFZAL, M., et al., Radiative capture cross-sections of isotopes of Gd, Sm, V and isomeric cross-sections of In and Rh, Ann. Nucl. Energy **13** (1986) 287.

[148] PAVLENKO, E.A., GNIDAK, N.L., "Neutron capture cross-section measurement for hafnium and vanadium isotopes", Neutron Physics (Proc. Conf. Kiev, 1975), Atominform, Moscow (1975) 171.

[149] WATANABE, T., in JENDL-3, Japanese Nuclear Data Centre, Tokai-mura (1988).

[150] SMITH, D.L., et al., Measured activation cross-sections below 10 MeV for the 51-V(n, p)51-T and 51-V(n, α)48-Sc reactions, Ann. Nucl. Energy **11** (1984) 623.

[151] MEADOWS, J.W., et al., Measurement of 14.7 MeV neutron activation cross-sections for fusion, Ann. Nucl. Energy **14** (1987) 489.

[152] ANDERS, B., et al., "Application of a novel 14 MeV neutron activation analysis system for cross-section measurements with short-lived nuclides", Nuclear Data for Science and Technology (Proc. Conf. Antwerp, 1982), Reidel Publ., Dordrecht (1982) 859.

[153] KHAN, N.A., et al., Studies of (n, α) and (n, p) reactions on V-51 with 14.7 MeV neutrons, Nucl. Instrum. Methods. **215** (1983) 193.

[154] LE RIGOLEUR, C., et al., Measurement of Neutron Radiative Capture Cross-Sections of Chromium, Iron and Nickel from 70 keV to 550 keV, Rep. CEA-N-1661, CEA, Centre d'études nucléaires, Paris (1973).

[155] SPITZ, L.M., et al., Neutron capture cross-sections of Cr, Mn, Ni, Nb, Ag, In, Sb and Au in the 8 to 120 keV region, Nucl. Phys., A **130** (1969) 401.

[156] STAVISSKIJ, Yu.Ya., SHAPAR, A.V., Fast neutron capture cross-section of chromium, At. Ehnerg. **12** (1962) 514.

[157] KAPCHIGASHEV, S.P., POPOV, Yu.P., Radiation capture cross-sections for neutrons of energy up to 50 keV for Cr-50, Cr-52, Cr-53, At. Ehnerg. **16** (1964) 256.

[158] ASAMI, T., in JENDL-3, Japanese Nuclear Data Centre, Tokai-mura (1987).

[159] SMITH, D.L., MEADOWS, J.W., Cross-section measurement for the Cr-52(n, p)V-52 reaction near threshold, Nucl. Sci. Eng. **76** (1980) 43.

[160] VIENNOT, M., et al., Cross-section Measurements of (n, p) and (n, np) Reactions on some Metallic Elements in the Region 13.75 to 15 MeV, Rep. MOH-5, Université Mohammed, Morocco (1982).

[161] GUPTA, J.P., et al., Pre-equilibrium emission effect in (n, p) reaction cross-section at 14 MeV, Indian J. Phys. **24** (1985) 637.

[162] HOANG DAC LUC, et al., Determination of some (n, p), (n, np) and (n, α) Reaction Cross-sections Induced by 14.8 MeV Neutrons on Cr and Ti Isotopes, Rep. INDC(VN)-5, International Nuclear Data Committee, IAEA, Vienna (1982).

[163] RIBANSKY, I., et al., Neutron activation cross-sections for Cr isotopes at 14.6 MeV neutron energy, Ann. Nucl. Energy **12** (1985) 577.

[164] PASECHNIK, M.V., et al., Neutron scattering with initial energy of 2.9 MeV by Ti and Cr nuclei, Usp. Fiz. Nauk. **14** (1969) 1874.

[165] KORZH, V.A., et al., "Neutron scattering in the energy range 1.5–3.0 MeV on the even isotopes of Cr, Ni, Zn", Nuclear Data for Science and Technology (Proc. 4th Conf. Kiev, 1975), Atominform, Moscow (1976) 220.

[166] KRAMAROVSKIJ, Ya.M., et al., The excitation functions of neutron inelastic scattering on the isotopes Al-27, Cr-52 and Cr-53, Yad. Konst. **1** (1989) 30.

[167] SAILOR, K., et al., The Cross-sections of (n, 2n), (n, p), (n, α) Reactions for 14.8 MeV Neutrons on Isotopes of C and Zr, Rep. INDC(SEC)-61, International Nuclear Data Committee, IAEA, Vienna (1977).

[168] ARBILDO, A., et al., The Mn/H and B/H thermal absorption cross-section ratio, Ann. Nucl. Energy **13** (1986) 679.

[169] LE RIGOLEUR, C., et al., Absolute Measurements of Neutron Radiative Capture Cross-sections for Na-23, Cr, Mn-55, Fe, Ni, Rh, Ta, Au-197 in the Range 10–600 keV, Rep. CEA-R-4788, CEA, Centre d'études nucléaires, Paris (1976).

[170] BAHAL, B.M., PEPELNIK, R., Cross-section Measurements of Cr, Mn, Fe, Co, Ni for an Accurate Determination of these Elements in Natural and Synthetic Samples using a 14 MeV Neutron Generator, Rep. GKSS-84-E, Gesellschaft für Kernenergieverwertung in Schiffbau und Schiffahrt mbH, Hamburg (1984).

[171] GAUTAM, R.P., et al., Measurement of radiative capture of fast neutrons in Mn-55 and In-115, Indian J. Appl. Phys. **28** (1990) 235.

[172] TROFIMEV, Yu.N., Activation cross-sections for 33 nuclei at the neutron energy 2 MeV, Yad. Konst. **4** (1987).

[173] SHIBATA, K., in ENDF/B-6, US National Nuclear Data Center, Brookhaven National Laboratory, Upton, NY (1988).

[174] SCHWERER, O., et al., Measurements of (n, 2n), (n, p) and (n, α) cross-sections for 14 MeV neutrons, Anz. Oesterr. Akad. Wiss., Math.-Naturwiss. Kl. **113** (1976) 153.

[175] KAYASHIMA, K., et al., Activation cross-section on Ti, Mn, Cu, Zn, Sr, Yt, Cd, In and Te for 14.6 MeV neutrons, Rep. NEANDC(J)-61U, OECD, Nuclear Data Committee, Nuclear Energy Agency, Paris (1979).

[176] KOBAYASHI, K., KIMURA, I., "Application of a 6-lid thermal 14 MeV neutron converter to the measurement of activation cross-sections", Nuclear Data for Science and Technology (Proc. Int. Conf. Mito, 1988), Saikon Publ., Tokyo (1988) 261.

[177] DEAK, F., et al., Experimental investigation of the neutron–gamma competition in 14.7 MeV fast neutron reactions, Acta Phys. Hung. **38** (1975) 209.

[178] BERRADA, M., Measurement and Analysis of 14 MeV Neutron Nuclear Reaction Cross-sections by X and Gamma Spectroscopy, Prog. Rep. for IAEA RC-3311/RI/RB, IAEA, Vienna (1984).

[179] VAENSKAE, R., RIEPPO, R., On the simultaneous use of a Ge(Li) semiconductor and a NaI(Tl) scintillation detector in neutron activation cross-section measurements, Nucl. Instrum. Methods **171** (1980) 281.

[180] ZUPRANSKA, E., et al., Excitation functions for (n, α) reactions in the neutron energy range from 13 to 18 MeV, Acta Phys. Pol. **11** (1980) 853.

[181] IIJIMA, S., YAMAKOSHI, H., in JENDL-3, Japanese Nuclear Data Centre, Tokai-mura (1987).

[182] SMITH, D.L., MEADOWS, J.W., Cross-section measurements of (n, p) reactions for Al-27, Ti-46, 47, 48, Fe-54, 56, Ni-58, Co-59 and Zn-64 from near threshold to 10 MeV, Nucl. Sci. Eng. **58** (1975) 314.

[183] RYVES, T.B., et al., Cross-section measurements of Fe-56(n, p)Mn-56, Cu-63(n, 2n)Cu-62, and Cu-65(n, 2n)Cu-64 between 14 and 19 MeV, Metrologia **14** (1978) 127.

[184] KUDO, K., Absolute measurement of the Fe-56(n, p)Mn-56 cross-section at 14.8 MeV using an on-line monitoring system for the time variation of neutron flux, Nucl. Instrum. Methods **141** (1977) 325.

[185] LI, Chi-Chou, et al., Cross-section Measurement for the Reaction Fe-56(n, p)Mn-56, Rep. INDC(CRP)-16, International Nuclear Data Committee, IAEA, Vienna (1989).

[186] SHARMA, D., et al., "Absolute measurements of Fe-56(n, p)Mn-56 cross-section at 14.7 MeV using a neutron telescope", Nuclear Physics and Solid State Physics (Proc. Conf. Bombay, 1978), Vol. 2, Indian Institute of Technology, Bombay (1978) 349.

[187] ZHOU, Mujao, et al., Shell effect from the cross-section of the (n, 2n) reaction produced by 14.6 MeV neutrons, Chin. J. Nucl. Phys. **9** (1987) 34 (in Chinese).

[188] PHAN NHU NGOC, et al., Neutron Activation Cross-section for Fe-56(n, p) and Rb-87(n, 2n) Reactions, Rep. INDC(VN)-2, International Nuclear Data Committee, IAEA, Vienna (1983).

[189] GARLEA, I., et al., Neutron cross-sections measured at 14.8 MeV, Rep. INDC(BUL)-17, International Nuclear Data Committee, IAEA, Vienna (1986).

[190] NEMILOV, Yu.A., TROFIMOV, Yu.N., Cross-sections of (n, p) reactions on Ni-58, Fe-56 and Zn-64 isotopes at neutron energies 7.6–9.3 MeV, Yad. Fiz. **26** (1978) 25.

[191] YAMAMURO, N., KAWAKITA, T., in JENDL-3, Japanese Nuclear Data Centre, Tokai-mura (1987).

[192] TUCKER, A.B., et al., Inelastic neutron scattering near threshold, Phys. Rev., B **137** (1965) 1181.

[193] JOENSSON, B., et al., High resolution measurements of gamma rays produced by 15 MeV neutrons, Ark. Fys. **39** (1960) 295.

[194] ALMEN-RAMSTROM, E., A Systematic Study of Neutron Inelastic Scattering in the Energy Range 2.0 to 4.5 MeV, Rep. AE-503, Aktiebolaget Atomenergi, Studsvik (1975).

[195] SHI, Xia-Min, et al., Measurement of the induced gamma ray cross-sections by 14.2 MeV neutrons with Fe, Ni and Cu, Chin. J. Nucl. Phys. **4** (1982) 120.

[196] BRADLEY, T., et al., "Stellar nucleosynthesis and the 24-keV neutron capture cross-sections of some heavy nuclei", Nuclear Data for Science and Technology (Proc. Conf. Knoxville, 1979), NBS Spec. Publ. 594, National Bureau of Standards, Washington, DC (1980) 344.

[197] JOLY, S., et al., Measurement of Fast Neutron Capture Cross-sections Using a NaI Spectrometer, Rep. CEA-R-5089, CEA, Centre d'études nucléaires, Grenoble (1981).

[198] ANUFRIEV, V.A., et al., Neutron resonances of W-186 in the energy range up to 300 eV, At. Ehnerg. **50** (1981) 67.

[199] TROFIMOV, Yu.N., "Neutron radiation capture cross-sections for nuclei of medium and large masses at the neutron energy 1 MeV", Neutron Physics (Proc. Conf. Kiev, 1987), Vol. 3, Atominform, Moscow (1988) 331.

[200] WATANABE, T., ASAMI, T., in JENDL-3, Japanese Nuclear Data Centre, Tokai-mura (1987).

[201] GUERNSEY, J.B., WATTENBERG, A., Excitation of some low lying levels by inelastic neutron scattering, Phys. Rev. **101** (1956) 1516.

[202] DE VILLIERS, J.A.M., et al., Neutron scattering from Au, Hg and Tl, Z. Phys. **183** (1965) 323.

[203] YOUNG, P.G., in ENDF/B-6, US National Nuclear Data Center, Brookhaven National Laboratory, Upton, NY (1984).

[204] LINDNER, M., et al., Neutron capture cross-sections from 0.1 to 3 MeV by activation measurements, Nucl. Sci. Eng. **59** (1976) 381.

[205] FORT, E., LE RIGOLEUR, C., "Capture cross-section of Au-197 between 10 keV and 500 keV", Nuclear Data (Proc. 2nd Conf. Washington, 1975), NBS Spec. Publ. 425, National Bureau of Standards, Washington, DC (1975) 957.

[206] YAMAMURO, N., et al., keV-neutron capture in cesium-133, gold-197, and tantalum-181, J. Nucl. Sci. Technol. **20** (1983) 797.

[207] ANDERSSON, P., et al., Cross-sections for 79-Au-197(n, γ)79-Au-198 and 49-In-115(n, γ)49-In-116m in the neutron energy region 2.0–7.7 MeV, Nucl. Phys., A **443** (1985) 404.

[208] CHEN, Ying, et al., Measurements of Au-197 neutron radiative capture cross-sections between 100 and 1500 keV, Chin. J. Nucl. Phys. **3** (1981) 52.

[209] ZHU, Sheng-Yun, et al., Measurement of the neutron radiative capture cross-section of Au-197 at 30 keV, Chin. J. Nucl. Phys. **6** (1984) 23.

Chapter 7

NEUTRON SOURCE AVERAGED CROSS-SECTIONS

The neutron source averaged cross-sections are the effective values of reaction cross-sections for a given neutron source spectrum. They are defined as follows:

$$\langle \sigma \rangle = \frac{\int_{E_1}^{E_2} \sigma(E) \cdot S(E)\, \mathrm{d}E}{\int_{E_1}^{E_2} S(E)\, \mathrm{d}E}$$

where

E_1 and E_2 are the limits of the energy interval,
$\sigma(E)$ is an energy dependent cross-section,
$S(E)$ is the energy spectrum of the neutron field.

The energy limits are set so that the whole energy interval considered is represented by one group. In our case, $E_1 = 1.00 - 6$ eV and $E_2 = 2.00 + 7$ eV, thus covering the whole energy interval of evaluated cross-section and neutron field data. The spectrum averaged cross-sections were calculated here for the ^{252}Cf, Am–Be and Pu–Be neutron source spectra. The data are given in Table 7.1.

TABLE 7.1. NEUTRON SOURCE AVERAGED CROSS-SECTIONS FOR THE ^{252}Cf, Am–Be AND Pu–Be NEUTRON SPECTRA

Isotope (element) and nuclear reaction	Average cross-section values in neutron source spectra (b)		
	^{252}Cf	Am–Be	Pu–Be
$^{6}C^{nat}$			
Total	2.34917	1.86341	1.79577
Elastic	2.33339	1.75046	1.67888
Inelastic, 1st level	1.38327×10^{-2}	9.35102×10^{-2}	9.57092×10^{-2}
Inelastic, 2nd level	8.88179×10^{-5}	7.64632×10^{-4}	7.1511×10^{-4}
Inelastic, 3rd level	4.3943×10^{-5}	2.22724×10^{-5}	2.78065×10^{-6}
n,γ	1.02581×10^{-5}	3.58064×10^{-5}	3.7648×10^{-5}
$^{8}O^{16}$			
n,n'α	9.07293×10^{-6}	—	—
n,n', 1st level	5.63907×10^{-4}	5.07882×10^{-3}	5.74804×10^{-3}
n,n', 2nd level	3.79245×10^{-3}	3.59613×10^{-2}	4.03246×10^{-2}
n,n', 3rd level	6.50758×10^{-4}	6.96594×10^{-3}	7.37386×10^{-3}
n,n', 4th level	2.98479×10^{-4}	3.25986×10^{-3}	3.47452×10^{-3}
n,n', 5th level	8.87158×10^{-5}	2.90704×10^{-4}	2.168×10^{-4}
n,γ	2.85527×10^{-8}	1.97144×10^{-8}	1.79353×10^{-8}
n,p	4.16875×10^{-5}	2.1855×10^{-7}	—
n,d	8.50834×10^{-6}	1.83347×10^{-7}	1.48903×10^{-8}
n,α	9.021×10^{-3}	4.55304×10^{-2}	4.77497×10^{-2}
$^{11}Na^{23}$			
Total	3.17222	2.36511	2.31177
Elastic	2.64591	1.57811	1.50013
n,2n	1.22624×10^{-5}	—	—
n,γ	2.71062×10^{-4}	2.16286×10^{-4}	1.98618×10^{-4}
n,p	1.94978×10^{-3}	1.43295×10^{-2}	1.47435×10^{-2}
n,α	9.8057×10^{-4}	8.84447×10^{-3}	9.14166×10^{-3}
$^{12}Mg^{nat}$			
Total	3.39349	2.46243	2.30908
Elastic	3.09939	1.82023	1.65196
n,γ	6.68971×10^{-4}	4.13538×10^{-4}	4.04794×10^{-4}
n,p	1.81105×10^{-3}	1.64382×10^{-2}	1.77506×10^{-2}
$^{12}Mg^{24}$			
n,p	2.33417×10^{-3}	2.09489×10^{-2}	2.26967×10^{-2}

TABLE 7.1. (cont.)

Isotope (element) and nuclear reaction	Average cross-section values in neutron source spectra (b)		
	^{252}Cf	Am–Be	Pu–Be
$^{12}Mg^{26}$			
n,γ	2.4164×10^{-4}	1.55745×10^{-4}	1.60477×10^{-4}
$^{13}Al^{27}$			
Total	3.15756	2.50755	2.44309
Elastic	2.85703	1.86657	1.78546
n,γ	2.8967×10^{-4}	2.19242×10^{-4}	1.74557×10^{-4}
n,p	5.13838×10^{-3}	2.84592×10^{-2}	2.94049×10^{-2}
n,α	1.05927×10^{-3}	9.66164×10^{-3}	1.02465×10^{-2}
$^{14}Si^{nat}$			
Total	3.06642	2.45314	2.40693
Elastic	2.82714	1.80787	1.74188
n,n′, 1st level	8.58011×10^{-3}	8.92146×10^{-3}	9.36421×10^{-3}
n,γ	1.06073×10^{-3}	7.97579×10^{-4}	7.34551×10^{-4}
n,p	9.23377×10^{-3}	6.77667×10^{-2}	7.24658×10^{-2}
$^{14}Si^{28}$			
n,p	8.09692×10^{-3}	6.0807×10^{-2}	6.44257×10^{-2}
$^{14}Si^{29}$			
n,p	3.75342×10^{-3}	2.34594×10^{-2}	2.41902×10^{-2}
$^{14}Si^{30}$			
n,α	2.16483×10^{-4}	1.83997×10^{-3}	1.7894×10^{-3}
$^{15}P^{31}$			
Total	2.53264	2.56053	2.55128
Elastic	3.62973×10^{-1}	1.84178×10^{-1}	1.08388×10^{-1}
n,γ	1.17592×10^{-4}	7.30582×10^{-5}	4.16962×10^{-5}
n,α	3.2382×10^{-3}	2.4171×10^{-2}	2.52383×10^{-2}
$^{16}S^{nat}$			
Total	2.66662	2.59945	2.58527
Elastic	2.35009	1.6726	1.63885
n,γ	1.17392×10^{-3}	8.70306×10^{-4}	8.26937×10^{-4}
n,p	7.26197×10^{-2}	2.13412×10^{-1}	2.16836×10^{-1}
$^{16}S^{34}$			
Total	2.15963	2.01784	2.05262
Elastic	2.61289×10^{-1}	1.30165×10^{-1}	7.63275×10^{-2}
n,p	1.1081×10^{-3}	8.73145×10^{-3}	9.15319×10^{-3}

TABLE 7.1. (cont.)

Isotope (element) and nuclear reaction	Average cross-section values in neutron source spectra (b)		
	^{252}Cf	Am–Be	Pu–Be
$^{16}S^{36}$			
n,γ	2.40109×10^{-4}	2.17337×10^{-4}	2.17278×10^{-4}
$^{17}Cl^{nat}$			
Total	2.65499	2.70456	2.72668
Elastic	2.33998	2.00074	2.00338
n,2n	6.22466×10^{-6}	—	—
n,γ	1.00903×10^{-4}	9.16012×10^{-5}	4.88915×10^{-5}
n,p	2.84625×10^{-2}	6.67419×10^{-2}	6.84004×10^{-2}
n,α	1.5224×10^{-2}	5.89817×10^{-2}	5.98931×10^{-2}
$^{17}Cl^{37}$			
n,γ	4.83615×10^{-4}	2.73403×10^{-4}	2.42141×10^{-4}
n,p	2.86543×10^{-4}	2.59493×10^{-3}	2.67008×10^{-3}
n,α	2.34315×10^{-3}	1.99722×10^{-2}	2.15754×10^{-2}
$^{17}Cl^{35}$			
n,2n	4.03876×10^{-6}	—	—
$^{19}K^{41}$			
Total	2.28233	2.33913	2.31035
Elastic	3.61×10^{-2}	3.32833×10^{-2}	1.58811×10^{-2}
n,α	1.13696×10^{-3}	6.31616×10^{-3}	6.44519×10^{-3}
$^{20}Ca^{nat}$			
Total	2.82678	3.12587	3.15899
Elastic	2.60136	2.3647	2.38518
n,γ	5.67124×10^{-4}	3.80996×10^{-4}	2.84828×10^{-4}
n,p	1.20021×10^{-1}	3.74648×10^{-1}	3.81868×10^{-1}
$^{20}Ca^{44}$			
Total	2.75893	2.91247	2.87435
Elastic	3.53978×10^{-1}	1.95685×10^{-1}	1.12087×10^{-1}
n,p	1.14208×10^{-4}	8.67883×10^{-4}	8.68807×10^{-4}
$^{20}Ca^{48}$			
Total	2.05356	1.99963	2.01322
Elastic	2.6358×10^{-1}	1.34434×10^{-1}	7.85489×10^{-2}
n,γ	1.90413×10^{-4}	1.95428×10^{-4}	1.98671×10^{-4}

TABLE 7.1. (cont.)

Isotope (element) and nuclear reaction	Average cross-section values in neutron source spectra (b)		
	^{252}Cf	Am–Be	Pu–Be
$^{22}Ti^{nat}$			
Total	3.13308	3.42005	3.35016
Elastic	2.44799	2.29566	2.18976
n,γ	2.66369×10^{-3}	1.66324×10^{-3}	1.46002×10^{-3}
$^{22}Ti^{50}$			
Total	3.63275	3.58323	3.56951
Elastic	3.18459	2.65283	2.60913
n,γ	4.2916×10^{-4}	2.57092×10^{-4}	2.27377×10^{-4}
$^{23}V^{51}$			
Total	3.81592	3.76504	3.68855
Elastic	3.15463	2.76411	2.65947
n,γ	2.04674×10^{-3}	1.05296×10^{-3}	8.48189×10^{-4}
n,p	7.18383×10^{-4}	4.10888×10^{-3}	4.24095×10^{-3}
$^{24}Cr^{nat}$			
Total	4.54448	4.72518	4.79055
Elastic	2.82887×10^{-1}	1.90933×10^{-1}	1.06647×10^{-1}
n,γ	2.42561×10^{-3}	1.26132×10^{-3}	1.1396×10^{-3}
$^{24}Cr^{50}$			
Total	5.40156	5.80540	5.84875
Elastic	3.35918×10^{-1}	2.34335×10^{-1}	1.30065×10^{-1}
n,γ	6.2119×10^{-3}	3.4584×10^{-3}	3.15709×10^{-3}
$^{24}Cr^{52}$			
Total	4.75511	4.85182	4.91265
Elastic	2.9602×10^{-1}	1.96066×10^{-1}	1.09375×10^{-1}
n,n′, 1st level	2.56015×10^{-1}	2.75785×10^{-1}	2.94432×10^{-1}
n,n′, 2nd level	2.2762×10^{-2}	4.7214×10^{-2}	4.78388×10^{-2}
n,n′, 3rd level	1.60005×10^{-2}	2.97415×10^{-2}	3.04566×10^{-2}
n,p	1.35841×10^{-3}	1.01297×10^{-2}	1.06795×10^{-2}
$^{24}Cr^{54}$			
Total	3.39177	3.54477	3.49186
Elastic	2.11223×10^{-1}	1.43313×10^{-1}	7.77731×10^{-2}
n,α	5.72362×10^{-5}	4.6939×10^{-4}	4.78639×10^{-4}

TABLE 7.1. (cont.)

Isotope (element) and nuclear reaction	Average cross-section values in neutron source spectra (b)		
	^{252}Cf	Am–Be	Pu–Be
$^{25}Mn^{55}$			
Total	3.65296	3.68051	3.62544
Elastic	2.73509	2.42436	2.33744
n,2n	4.63632×10^{-4}	1.6267×10^{-4}	2.32729×10^{-5}
n,γ	2.8127×10^{-3}	1.8283×10^{-3}	1.58058×10^{-3}
n,α	1.84549×10^{-4}	1.59575×10^{-3}	1.68913×10^{-3}
$^{26}Fe^{nat}$			
Total	2.61392	3.19684	2.99326
Elastic	2.12495×10^{-1}	1.56634×10^{-1}	8.19507×10^{-2}
n,γ	3.45347×10^{-3}	2.23729×10^{-3}	2.05146×10^{-3}
$^{26}Fe^{54}$			
Total	5.66122	5.3749	5.74385
Elastic	2.60485×10^{-1}	1.74084×10^{-1}	1.01095×10^{-1}
n,γ	6.51404×10^{-4}	5.14538×10^{-4}	2.83095×10^{-4}
n,α	1.16274×10^{-3}	8.74121×10^{-3}	9.20171×10^{-3}
$^{26}Fe^{56}$			
Total	5.43008	5.68059	5.47385
Elastic	2.56661×10^{-1}	1.88227×10^{-1}	9.8407×10^{-2}
n,p	1.44946×10^{-3}	1.1348×10^{-2}	1.19227×10^{-2}
$^{28}Ni^{nat}$			
Total	3.69224	3.74165	3.63366
Elastic	3.21216	2.68836	2.55466
n,γ	7.61108×10^{-3}	3.92664×10^{-3}	3.58015×10^{-3}
$^{28}Ni^{58}$			
Total	3.73539	3.69208	3.58029
Elastic	3.189	2.5124	2.37184
n,n′, 1st level	2.47053×10^{-1}	2.27594×10^{-1}	2.44771×10^{-1}
n,n′, 2nd level	2.32484×10^{-2}	4.96867×10^{-2}	5.04711×10^{-2}
n,n′, 3rd level	2.7878×10^{-2}	6.06318×10^{-2}	6.10498×10^{-2}
n,n′, 4th level	1.73019×10^{-2}	4.00406×10^{-2}	3.98962×10^{-2}
n,n′, 5th level	6.57288×10^{-3}	1.55026×10^{-2}	1.53656×10^{-2}
$^{29}Cu^{nat}$			
Total	3.67337	3.73391	3.65108
Elastic	2.85361	2.36463	2.23978
n,γ	7.67903×10^{-3}	3.42434×10^{-3}	2.96803×10^{-3}

TABLE 7.1. (cont.)

Isotope (element) and nuclear reaction	Average cross-section values in neutron source spectra (b)		
	^{252}Cf	Am–Be	Pu–Be
$^{29}Cu^{63}$			
Total	8.5018	8.51697	8.61649
Elastic	1.83395×10^{-1}	1.54856×10^{-1}	7.91143×10^{-2}
n,n′, 1st level	1.03589×10^{-1}	5.28941×10^{-2}	5.64136×10^{-2}
n,n′, 2nd level	1.58019×10^{-1}	1.05049×10^{-1}	1.12005×10^{-1}
n,n′, 3rd level	8.52973×10^{-2}	8.1254×10^{-2}	8.62981×10^{-2}
n,n′, 4th level	6.44678×10^{-2}	4.99633×10^{-2}	5.41008×10^{-2}
n,n′, 5th level	4.06266×10^{-2}	3.4224×10^{-2}	3.72592×10^{-2}
$^{29}Cu^{65}$			
Total	9.01429	8.87077	9.11663
Elastic	1.95356×10^{-1}	1.62422×10^{-1}	8.46425×10^{-2}
n,γ	5.67698×10^{-3}	2.48776×10^{-3}	2.20115×10^{-3}
$^{74}W^{nat}$			
Total	6.71793	6.1272	6.08072
Elastic	4.1948	3.417	3.30413
n,γ	4.39496×10^{-2}	1.93121×10^{-2}	1.67535×10^{-2}
$^{74}W^{186}$			
Total	6.68998	6.16471	6.11615
Elastic	4.22238	3.49828	3.37952
n,γ	3.41417×10^{-2}	1.60199×10^{-2}	1.39928×10^{-2}
$^{79}Au^{197}$			
Total	6.63685	6.53462	6.47239
Elastic	4.60666	4.10341	3.98646
n,n′, 1st level	1.13358×10^{-1}	3.65666×10^{-2}	3.04234×10^{-2}
n,n′, 2nd level	1.38035×10^{-1}	3.91882×10^{-2}	3.64581×10^{-2}
n,n′, 3rd level	2.86667×10^{-1}	1.77604×10^{-1}	1.79225×10^{-1}
n,n′, 4th level	3.81361×10^{-2}	1.07743×10^{-2}	1.14464×10^{-2}
n,n′, 5th level	9.05304×10^{-2}	2.44451×10^{-2}	2.53664×10^{-2}
n,γ	7.41763×10^{-2}	3.49555×10^{-2}	2.79475×10^{-2}

LIST OF AUTHORS

Chapter 1

J. Schweitzer — Schlumberger-Doll Research, Ridgefield, Connecticut, United States of America

C.G. Clayton — Editor of the Journal Nuclear Geophysics, United Kingdom

Chapter 2

J.K. Tuli — National Nuclear Data Center, Brookhaven National Laboratory, Upton, New York, United States of America

Chapter 3

M.A. Lone
R.A. Leavitt
D.A. Harrison
— Atomic Energy of Canada Limited, Chalk River Nuclear Laboratories, Chalk River, Ontario, Canada

Chapter 4

P. Ekstroem
L. Spanier
— Department of Physics, Lund University, Lund, Sweden

Chapters 5 to 7

N.P. Kocherov — Division of Physical and Chemical Sciences, Department of Research and Isotopes, International Atomic Energy Agency, Vienna

HOW TO ORDER IAEA PUBLICATIONS

An exclusive sales agent for IAEA publications, to whom all orders and inquiries should be addressed, has been appointed for the following countries:

CANADA UNITED STATES OF AMERICA	UNIPUB, 4611-F Assembly Drive, Lanham, MD 20706-4391, USA

In the following countries IAEA publications may be purchased from the sales agents or booksellers listed or through major local booksellers. Payment can be made in local currency or with UNESCO coupons.

ARGENTINA	Comisión Nacional de Energía Atómica, Avenida del Libertador 8250, RA-1429 Buenos Aires
AUSTRALIA	Hunter Publications, 58 A Gipps Street, Collingwood, Victoria 3066
BELGIUM	Service Courrier UNESCO, 202, Avenue du Roi, B-1060 Brussels
CHILE	Comisión Chilena de Energía Nuclear, Venta de Publicaciones, Amunategui 95, Casilla 188-D, Santiago
CHINA	IAEA Publications in Chinese: China Nuclear Energy Industry Corporation, Translation Section, P.O. Box 2103, Beijing IAEA Publications other than in Chinese: China National Publications Import & Export Corporation, Deutsche Abteilung, P.O. Box 88, Beijing
FRANCE	Office International de Documentation et Librairie, 48, rue Gay-Lussac, F-75240 Paris Cedex 05
HUNGARY	Librotrade Ltd., Book Import, P.O. Box 126, H-1656 Budapest
INDIA	Oxford Book and Stationery Co., 17, Park Street, Calcutta-700 016 Oxford Book and Stationery Co., Scindia House, New Delhi-110 001
ISRAEL	YOZMOT Literature Ltd., P.O. Box 56055, IL-61560 Tel Aviv
ITALY	Libreria Scientifica Dott. Lucio di Biasio "AEIOU", Via Coronelli 6, I-20146 Milan
JAPAN	Maruzen Company, Ltd, P.O. Box 5050, 100-31 Tokyo International
PAKISTAN	Mirza Book Agency, 65, Shahrah Quaid-e-Azam, P.O. Box 729, Lahore 3
POLAND	Ars Polona, Foreign Trade Enterprise, Krakowskie Przedmieście 7, PL-00-068 Warsaw
ROMANIA	Ilexim, P.O. Box 136-137, Bucharest
RUSSIAN FEDERATION	Mezhdunarodnaya Kniga, Sovinkniga-EA, Dimitrova 39, SU-113 095 Moscow
SLOVAK REPUBLIC	Alfa, Publishers, Hurbanovo námestie 3, 815 89 Bratislava
SOUTH AFRICA	Van Schaik Bookstore (Pty) Ltd, P.O. Box 724, Pretoria 0001
SPAIN	Díaz de Santos, Lagasca 95, E-28006 Madrid Díaz de Santos, Balmes 417, E-08022 Barcelona
SWEDEN	AB Fritzes Kungl. Hovbokhandel, Fredsgatan 2, P.O. Box 16356, S-103 27 Stockholm
UNITED KINGDOM	HMSO, Publications Centre, Agency Section, 51 Nine Elms Lane, London SW8 5DR
YUGOSLAVIA	Jugoslovenska Knjiga, Terazije 27, P.O. Box 36, YU-11001 Belgrade

Orders from countries where sales agents have not yet been appointed and requests for information should be addressed directly to:

Division of Publications
International Atomic Energy Agency
Wagramerstrasse 5, P.O. Box 100, A-1400 Vienna, Austria

92-05214

ISBN 92-0-102393-6
ISSN 0074-1914